THERMOELECTRIC MATERIALS EVALUATION PROGRAM SUMMARY TECHNICAL REPORT

APRIL 1979

MMM–2331–0602

by
J. D. HINDERMAN
PROGRAM MANAGER
3M COMPANY

DISCLAIMER

MMM-2331-0602
DoE R and D Report

THERMOELECTRIC MATERIALS EVALUATION PROGRAM

SUMMARY TECHNICAL REPORT

APRIL 1979

by

J. D. Hinderman

Program Manager

Prepared Under
Contract EY-76-C-02-2331
for the
Power Systems Branch
Advanced Systems and Materials
Production Division, Department of Energy

MINNESOTA MINING AND MANUFACTURING COMPANY

Industrial Electrical Products Division

St. Paul, Minnesota 55101

LEGAL NOTICE

This report was prepared as an account of Government sponsored work. Neither the United States, nor DoE, nor any person acting on behalf of DoE:

a. Makes any warranty or representation, expressed or implied, with respect to the accuracy, completeness, or usefulness of the information contained in this report, or that the use of any information, apparatus, method, or process disclosed in this report may not infringe privately owned rights; or

b. Assumes any liabilities with respect to the use of, or for damages resulting from the use of, any information, apparatus, method, or process disclosed in this report.

As used in the above, "person acting on behalf of DoE" includes any employee or contractor of DoE, or employee of such contractor, to the extent that such employee or contractor of DoE, or employee of such contractor prepares, disseminates, or provides access to, any information pursuant to his employment or contract with DoE, or his employment with such contractor.

TABLE OF CONTENTS

INTRODUCTION

This Summary Technical Report was prepared under Contract EY-76-C-02-2331 with the United States Department of Energy and covers the performance period which extends from January 1, 1976, to September 30, 1978. This report contains a summary by task in the first section. The remaining sections of the document contain topical reports on various evaluations which were conducted during the reporting period.

HIGHLIGHTS

TASK 1.0 - N-TYPE MATERIAL DEVELOPMENT

1.2 MATERIAL SYNTHESIS - GADOLINIUM-SELENIDE COMPOSITIONS

Gadolinium-selenide compositions were synthesized and cast into a geometry suitable for electrical (S and ρ) characterization, and further processing.

The synthesis samples prepared during this period were related to process experiments which had the following objectives:

- Control Seebeck coefficient by precise control of the ratio of selenium to gadolinium.
- Elimination of macroscopic defects in fabricated elements.
- Optimization of thermoelectric composition.
- Control formation of second-phase material on grain boundary.

During the period the effect of gadolinium preparation method was evaluated. Gadolinium-selenide was synthesized from gadolinium prepared by two different methods; namely, (1) gadolinium prepared in tungsten crucibles and (2) standard distilled gadolinium metal. Subsequent listing of elements prepared from these synthesized batches indicated the standard distilled gadolinium is preferred.

Numerous batches have been synthesized during this period containing other rare-earth selenides. The objective of these studies is to improve the performance and stability of the gadolinium-selenide system. These include neodymium doping of various compositions and pure neodymium selenide.

A cast sample of neodymium-selenide had previously been prepared as part of the alloying series reported in Technical Task Report No. 45 with a Seebeck coefficient of 145 μV/°C at 500°C and an extraneous resistance of 16%. To obtain data on the operating characteristics of this material, this cast element was tested ingradient in the performance mapping fixture with gadolinium foil pressure engaged between the tungsten-sputtered leg surface and the tantalum gimbal at the hot end and silver foil pressure engaged to the silver-sputtered leg surface and Armco iron calorimeter at the cold end. This test operated for 260 hours at 800°C/200°C, and then for an additional 820 hours at 850°/150°C. During this testing, the Seebeck coefficient remained constant at 133.5 ± 0.1 mΩ-cm. The extraneous resistance of the element operating ingradient, including contact resistance, was 23%.

A small number of batches of yttrium doped gadolinium-selenide were prepared during this period for electrical and chemical evaluation.

1.3 MATERIAL ANALYSES

1.3.1 Chemical, Crystal Structure, and Metallurgical Analyses

Chemical analyses are being performed on raw materials, on atmosphere for control of the synthesis process, on element contact structure, on doping studies, and on isothermal chemical compatibility experiments as required.

Milestone Report No. 51 entitled "Converter Materials Chemical Compatibility and Outgassing Requirements Assessed for GDS" was prepared during this period. It is contained as Attachment 13 to this report.

The role of oxygen in the neodymium-selenide and gadolinium-selenide was examined by Auger surface analysis. Data reduction and analysis of the measurements show that the surface contains an average of 6% oxygen which is much greater than in the bulk material and the distribution of oxygen on the surface is very inhomogeneous, varying from about 1/2% to as much as 30% in some regions. This supports the hypothesis of localized oxygen regions presumably along grain boundaries leading to high resistivity in the material. An additional support for this hypothesis came from neutron activation results obtained on a sample pressed and sintered after air exposure. This material was observed to have a bulk oxygen content of 700 parts per million and an extraneous resistance of 157%, whereas a sample pressed and sintered from the same material but without any exposure to air, had a bulk oxygen content of only 230 parts per million and an extraneous resistance only half as great. Neutron activation analysis also confirmed that a sample hot pressed in the RF induction furnace had a very high oxygen content of 2,100 parts per million, which is consistent with the high extraneous resistance and liquid phase sintering observed in this material.

During this reporting period, Scanning Electron Microscope (S.E.M.) analysis has been done to characterize observed phases found in gadolinium-selenide ingots and pellets.

The white particles appearing randomly in sintered samples of batch 2633 were found from the S.E.M. analysis to be a tungsten-rich material. The particles were associated with cracks in the gadolinium-selenide.

Further analysis showed that:

a. Only trace amounts of tungsten-rich particles appeared in ingot material.

b. Tungsten-rich particles were evident in all sintered compacts examined, even though they were normally too small to see in the optical microscope, and only occasionally gave evidence of being associated with cracks.

It is concluded that the white material was probably tungsten carbide eroded from the ball mill during powder processing. However, no evidence of cobalt (the binder in tungsten-carbide) was found, suggesting that cobalt must be soluble in gadolinium-selenide and diluted to the extent that it is not observable by S.E.M. analysis.

In Top Summary Report No. 117, several phases identified in the gadolinium-selenium-type system were tabulated and remarked upon. Further work has elucidated the black phase of composition approximately $GdSe_{1.5}$ and of orthorhombic crystal structure. A crystal model was built to demonstrate the crystal structure arrangement of the orthorhombic phase. It is essentially a molecular structure made up of double molecules $(Gd_2Se_3)_2$ arranged in layers. Closer examination of the structure leaves rather doubtful the layer-like nature, but it is essentially anisotropic in contrast with the cubic structure which appears more ionic and locally isotropic.

Samples of various compositions and heat treatments have been examined to study the nature of this alloy phase. It seems clear from results thus far that compositions near $GdSe_{1.49}$ are stable as a phase mixture of cubic and orthorhombic phases at 900°C. It seems further clear that oxidation of the sample increases

the proportion of orthorhombic phase so that samples exhibiting optically detectable oxide skins are stable as single-phase orthorhombic at 900°C. It has been observed that the cubic → orthorhombic transformation appears to be initated at free surfaces in the presence of oxygen. A possible mechanism may be the formation of a fairly dense surface layer of Gd_2O_3 and/or Gd_2SeO_3, with the free selenium liberated diffusing into the $GdSe_{1.49}$ to raise the Se/Gd ratio in the vicinity of the surface. Since layers of $GdSe_2$ have been observed adjacent to Gd_2SeO_2, this appears plausible. If one assumes that the cubic → orthorhombic transformation is initially nucleated by a martensitic transformation at constant composition, this would explain the role of oxygen and why the process begins at free surfaces where $GdSe_{1.50+}$ material would be present.

Because of the interest in replacing the gadolinium contacting foil on the N-leg hot end with nickel, the nickel/gadolinium-selenide interface was evaluated.

The nickel/gadolinium-selenide interface was examined after testing under extreme conditions with the following observations:

- Nickel-bonded N-legs showed no reaction between the nickel and the gadolinium-selenide although traces of a reaction were observed at the nickel-tantalum interface. This reaction did not seem to be deleterious to the joint, but should be followed in the event that contact resistance changes occur.

- Another N-leg sample with no gimbal was examined after running ingradient. No unusual features were observed.

A sample from M-12, which had suffered exposure to water, was examined. The gadolinium-selenide was found to have reacted to form the oxyselenide Gd_2SeO_2; this was confirmed by x-ray diffraction.

1.3.2 Thermoelectric Properties

An ongoing activity during this period was the measurement of Seebeck coefficient and resistivity for numerous N- and P-elements.

The laser pulse thermal diffusivity apparatus has been reconditioned and used to obtain additional thermal diffusivity measurements of the gadolinium-selenide material.

The new measurements are in good agreement with the previous data at 500°C and 700°C. There is a discrepancy observed at 250°C which indicates that measurement uncertainty between the original and new measurements may be greater than the estimated 5% uncertainty.

In addition to the diffusivity measurements performed on the standard material, some experimental materials were measured in a preliminary attempt at thermal conductivity characterization. The experimental samples consisted of an yttrium alloy with $GdSe_x$ and of samples of $GdSe_x$ subjected to high temperature heat treatment. The qualitative conclusion from this preliminary data on these experimental materials is that the yttrium-doped material has approximately the same thermal diffusivity as the standard $GdSe_x$ material, while the heat treatment increased the thermal diffusivity of both the yttrium-doped and standard materials.

1.4 MATERIAL PROCESSING

1.4.1 Pressing and Sintering Studies

Pressing and Sintering Experiments:

Cold pressing/sintering studies continue with the objective of forming high density, mechanically strong thermoelectric leg structures while at the same time reducing extraneous resistance to form elements with electrical properties on or near the 10% current standard material trend line. Elements have been formed with approximately a 30% extraneous resistance value.

The major variables studied in this pressing/sintering program include:

- Material used - HTR and RQC reacted ingot material
- Particle size - from 45μ to 5μ and mixtures thereof
- Element geometry - 0.11" - 0.500" diameter
- Pressing pressure - related to geometry - 2,000 to 68,000 psi
- Atmosphere control:
    1. LabVac box: "as is" to implementing the DoE Ames gas purification system.
    2. Transporting green pressed legs from the LavBac to the Astro Furnace.

3. Astro furnace atmosphere: "as is" to use of gas purifier.

- Sintering Cycle

  1. Heat-up rate
  2. Soak temperature
  3. Soak time

- Particle reduction techniques
- Homogeneity of starting materials
- Purified kerosene "wet"/air grinding
- Effects of lubricants
- Hot pressing

During this reporting period experiments have been performed to evaluate several parameters including wet vs. dry grinding, material scale-up, oxygen reduction, sintering cycle effects on density variations in sample and several others. Details of these experiments are contained in Top Summary Reports Nos. 95-127.

Hot Pressing Experiments:

During this period hot pressing experiments were initiated. Several elements were pressed but the Seebeck and resistivity for the hot pressed elements have been uniformly high; probably due to oxidation of the gadolinium-selenide during some stage of the hot press operation.

Thus, extreme caution must be exercised to maintain a good atmosphere during hot-pressing.

1.5 ELEMENT CONTACTING

Contacting Foil Series:

A series of N-leg tests (ATT 407-412) was initiated in the six-station test fixture during February 1976 to determine the effect of hot end contacting methods on performance. Three different hot end contacting configurations were used with two tests of each type (Gd Foil/W Sputter, Pt Foil/W Sputter, No Foil/W Sputter).

It appeared that the Gd foil/W Sputter combination was superior to the other combinations in that the extraneous resistance remained lower during the test. There were observed changes in Seebeck during the test which were probably due to the Gd foil.

N-Leg Contact Pressure Series (ATT 401-406):

A series of N-leg tests (ATT 401-406) was initiated in June 1976 to evaluate the effect of contact pressure on N-leg performance. These tests operated in an argon gas atmosphere in the temperature interval 850°C/125°C. These short-term tests were terminated after 600 hours. A total of six N-legs were tested at three different contact pressures (150, 200 and 300 psia). The tests were run initially in vacuum and backfilled with argon cover gas to 1 psia. No trend was observed in operating leg properties when the fixture was backfilled. It is clear that contact pressure has a very significant influence on contact resistance. The legs operated at 150 and 200 psia had clearly unacceptable performance, the contact resistance was high and variable, whereas the legs operated at 300 psi had significantly lower and stabler resistance.

N-Leg Grinding/Sputtering Series (ATT 431-436):

During this reporting period, the effect on electrical properties of various processing steps in the overall sputtering operation was examined. A series of six N-leg tests (ATT 431-436) were initiated during July 1976 to evaluate the effect that sputtering and grinding has on N-leg thermoelectric and structural performance.

Two legs of each of the following end configurations were tested:

1. sputtered (W hot/Ag cold) and ground
2. sputtered and unground
3. unsputtered and unground

Initially, the thermoelectric performance appeared to be best for the sputtered/unground samples followed by the sputtered/ground and unsputtered/unground. There were oxygen contamination problems in the test which ultimately caused the degradation of all of the elements and made interpretation of test results difficult. It did appear, however, that there was a potential degradation mechanism induced by the grinding-to-length operation.

The development of the Pb-Ag bonded cold-end contact for N-legs was developed during this reporting period. A large group of elements (191) were successfully bonded to Pb-Ag contacts for use in the GDS module.

Measurements of the resistances of the bonded elements showed a mean cold end contact resistance of 0.5 mΩ with a standard deviation of 0.3.

Ingradient Contacting Measurements:

A series of ingradient tests were performed to measure the effect of the gadolinium foil Gd_2Se_3 interface on thermal and electrical contact impedances. These experiments were conducted in a modified radiant heated test fixture with fixed contact probes rather than in the helium glovebox with moveable probes. The hot end measurement probe contact was made by a thermocouple passing through the center of the hot end gimbal to contact the gadolinium on top of the N-leg. The difference between calculated and measured Seebeck voltage was used as a measure of thermal impedance. The relative electrical contact resistance was measured by the potential difference between voltage probes formed by the hot end thermocouple and a second thermocouple pressed against the side of the leg within 50 mils of the top of the leg. The current probes in this four-probe AC technique were the hot end gimbal and the hardware. The Seebeck coefficient drop produced by the foil varied from element to element with an average of 5.6μv/°C which corresponds to a thermal drop of about 16°C. The initial electrical resistance across the gadolinium foil also varied from element to element with an average of 7.5 mΩ; this reading includes material resistance as well as contact resistance since the probe could not be spaced as close to the top of the element as in the moveable probe tests in the helium glovebox.

Replacement of Gd by Ni at Hot Contact:

Replacement of the gadolinium hot-end foil by a nickel hot-end foil offers several advantages:

- Nickel has much better oxidation resistance
- Thermal expansion of nickel is comparable to Gd_3Se_3
- Nickel is ductile at operating temperatures
- Gadolinium foil has an oxide coat which prevents low resistance room temperature contacts
- Gadolinium reacts with Gd_2Se_3 even through the tungsten sputter coat; nickel does not.

In addition, replacement of the tungsten sputter coat with a nickel sputter coat has been found to yield lower contact resistances; for nickel sputtercoated Gd_2Se_3 elements against a gold foil, contact resistances as low as 0.6 mΩ were obtained instead of the 1-3 mΩ typical of tungsten sputter to gold. In further experiments with nickel sputter coats, a thick nickel sputter coat was produced by a 6-hour sputtering cycle. Even this thick coating was strongly adherent with no tendency to spall off. The contact resistance for this thick nickel sputter-coated Gd_2Se_3 leg against a gold contact was only 0.35mΩ.

The ingradient performance of the nickel sputter coat/nickel foil combination was measured by operating an element in standard module hot end and cold end hardware in a purified helium glovebox.

The room temperature resistance in module hardware was about a factor of 10 lower for the nickel sputter coat/nickel foil combination than for the tungsten sputter coat/tungsten foil combination; the low room temperature contact resistance of 1.2 mΩ obtained in module hardware confirmed the low contact resistance predicted by measurements in the standard gold foil room temperature contact resistance test. The contact resistance of the nickel sputter coat/nickel foil remained fairly constant during heat up, then decreased to a value of only 0.6 mΩ within eighteen hours. This is significantly better than the 3-4 mΩ contact resistance measured for the tungsten sputter coat/gadolinium foil contact at thirty hours.

1.7 INGRADIENT COMPATIBILITY AND LIFE TESTING

Numerous N-legs were placed on test during this reporting period to evaluate contacting methods, state-of-the-art pressing/sintering methods, element size, etc. These tests are more completely described in Top Summary Reports Nos. 95-127 and in the report entitled "Summary of Data Generated in the Selenide Thermoelectric Development Program" (3M No. 2331-0537, August 22, 1978).

1.9 MECHANICAL PROPERTIES CHARACTERIZATION

Many N-legs were compression tested during this period to characterize the strength as a function of various processing parameters.

Four N-legs were tested at room temperature for compression strength in the Dillon test apparatus to evaluate the effect of end porosity on basic element strength. The non-porous elements indicated a strength of approximately 50,000 psi, whereas the elements with porous ends exhibited strength of from 15,000 to 40,000 psi. Thus, the end porosity does appear to have an effect on element strength.

TASK 2.0 - TPM-217 P-TYPE CHARACTERIZATION

2.2 and 2.3 MATERIAL PREPARATION AND ANALYSIS

Periodic processing of P-type batches continues in order to provide P-material for processing studies and couple and module development. This processing involves synthesis, casting and analysis. The analysis includes atomic absorption analysis, emission spectrographic analysis and electrical characterization.

2.4 MATERIAL PROCESSING

A new 32-element partitioning mold to produce 0.260-inch diameter elements for M-11 and GDS was tested during this reporting period. No problems were encountered with the new 0.260-inch diameter mold. The rejection rate from geometric and physical tolerances was only 20% for the new mold.

The bond strengths of elements produced in 32-element partitioning runs 529-532 were evaluated by pull testing using the arrangement shown in Technical Task Report No. 46. The average strength of the W-Re foil/element bonds in each of the four runs was superior to the 20 lbs. break strength reported in Technical Task Report No. 46 for elements fabricated with an 8-element partitioning mold.

An experiment on the effect of the surface preparation of W-Re foils on bond strength was performed in partitioning run No. 533. The vapor honing of W-Re foils is not completely satisfactory in that the surface finish is non-uniform. Sand blasting has been found to produce a much more uniform, and more easily reproducible, surface finish. The replacement of vapor-honed foils by sand-blasted foils was evaluated by comparing the bond strengths of elements produced with the different foils in the same partitioning run, run No. 533. Both foils were found to be stronger than the nominal 20 lbs. reported in Technical Task Report No. 46, and no significant difference in strength was observed. This indicates that sand-blasted foils can be substituted for vapor-honed foils without affecting mechanical properties.

2.5 ELEMENT CONTACTING

Quality Control Apparatus:

To increase the electrical measurement capabilities, a second Quality Control test fixture was placed in operation during this reporting period. This fixture is a duplication of the one currently in operation (described in Technical Task Report No. 46). The fixtures share a common vacuum system, but each fixture can be operated independently because of the valving arrangement.

Both fixtures were checked for vacuum integrity and electrical performance by retesting two partitioned and bonded P-legs. The needed computer software was developed to operate the tests simultaneously. This additional fixture increases the electrical QC measurement capabilities to twenty elements per week.

A P-leg which had initially fallen outside the thermoelectric property QC specification was placed on test in a 12-station fixture (ATT 393). The purpose of this test was to determine if operation of a rejected P-leg ingradient would cause the properties to improve. After 290 hours, the properties had improved so that the values were $S = 271\ \mu v/°C$ (rel. to Pt) and $\rho = 9.8\ m\Omega\text{-cm}$ at 800°C/250°C. These values are within the thermoelectric specification. Thus, legs outside the specification were found acceptable after a specified run-in period.

2.6 THERMODYNAMIC STABILITY

The series of sealed tube free-evaporation experiments, described in Technical Task Report No. 46 was continued during this period. This work was initiated to supplement the mass spectrometer vapor pressure determination. The importance of this type of experiment lies in the fact that the rate of material loss in an operating

generator approximates a Langmuir free evaporation process rather than a Knudsen cell equilibrium process. As reported in Technical Task Report No. 46, a test facility consisting of an ion pumped quartz sample tube connected to a partial pressure analyzer has been constructed.

The effects of gettering and tube geometry on these measurements was evaluated to ensure the basic accuracy of the measurements.

Additional data was obtained on the effect of argon gas pressure on selenium weight loss from P-elements. The data indicates that a simple inverse relation between weight loss rate and inert gas pressure is seen to be a good representation of the experimental data in the region 0.1 torr to 2.5 torr. It is concluded that the sublimation rate of selenium from TPM-217 can be significantly reduced by inert gas pressure.

During this reporting period the development of a baffle made of a solid material occurred. The sublimation rate of P-type TPM-217 can be suppressed by reducing the mean free path of the vapor species. For example, it has been demonstrated by weight loss measurements at different inert gas pressures that the selenium sublimation rate is inversely proportional to the selenium mean free path in the inert gas.

Instead of reducing the mean free path by an inert cover gas, an alternative is to surround the element directly with a solid material baffle. Baffling can be produced by insulations, wrappings, sleeves, or coatings. The characteristics required for a good baffle are:

- Compatibility with thermoelectric and other converter materials
- Low outgassing rates
- Good insulator
- Stability (chemical and mechanical)
- Close tolerance fit to element
- Short mean free path

The properties of conventional insulations are being examined to determine their suitability as baffles. The mean free path of vapor species in Fiberfrax HiFi Paper, Fiberfrax H-Blanket, and Min-K 1800 were estimated by observation and scanning electron microscopes. From these data on mean free paths, it appears that the baffling effect of Min-K is potentially 170 times better than that of Fiberfrax insulations. To achieve the potential benefits of Min-K baffle, two methods were used. The first was a tight fitting Min-K sleeve and the second was to utilize pulverized Min-K in a slurry to form a fill for an astroquartz fiber wrap of the element.

The first method was used on modules M-13 and M-15B, but the mechanical problems were extensive enough to make the utilization of this method impractical.

The second method was ultimately selected as the reference baffling method for the P-material. A description of this method and the results is contained in the Topical section at the end of the task description section of this report.

2.8 ISOTHERMAL CHEMICAL COMPATIBILITY

A comprehensive program was completed during this reporting period to study chemical reactions, outgassing and compatibility of converter materials.

The details of this program are contained in Attachments XIII and XVIII of this report.

2.9 INGRADIENT COMPATIBILITY AND INGRADIENT LIFE TESTING

Long-Term Ingradient Testing:

Numerous long-term partitioned and non-partitioned P-leg tests have been operational during this reporting period. These tests are reported in detail in Top Summary Reports Nos. 95-127 and a summary of results is contained in a document which was published during this period. This document is entitled "Summary of Data Generated in the Selenide Thermoelectric Development Program" (3M No. 2331-0537, August 22, 1978).

Computer System Upgrading:

A computer program which handles life test data was written to aid in life test analysis. The program retrieves data from disc storage and outputs it to paper tape to be read and plotted by the Wang system. This new program (PLOT) replaces a portion of a data output program (LDOUT) presently in use. The new features of the PLOT program are:

1. The program retrieves data over any selected interval in the test.

2. The program outputs the time of a test and any two of six parameters of a test; the previous version output all six parameters.

3. The data is conditioned by rejecting data outside of upper and lower limits.

4. The mean, standard deviation, and number of data points for each test is determined.

5. Data is retrieved from the entire disc; previously only data from the date the disc was put in the system to the present date could be retrieved. When a new disc is started, the data from the last disc is copied onto the new disc; thus, data from about the previous three months are available for analysis.

The new features of this computer program improved the analysis of long-term life tests. This program is also set up for use with a graphic plotter which has been connected to the computer system.

Test Fixturing:

A problem was detected in the current control and measuring circuit of the 12-station test fixtures. The problem was caused by wiring the current control and measuring circuit to the ground side of the load current circuit which produced two sources of error--a ground loop error, and parallel paths error. This was corrected by rewiring the circuit.

The DC power supply had a finite resistance to ground which caused the ground loop. Since the cold end of all of the fixtures are connected to ground, a partially grounded power supply can cause currents to flow through the circuit which are not read by the series current shunt. The result of this extraneous current flow is that Seebeck coefficient and resistivity readings are approximately 4% low.

The errors due to a parallel current path caused erroneous current readings both above and below the true readings. The current control rheostats and the shunts were wired on the common ground side of the fixtures. The errors involved can be as much as 100% in the measured current.

A new load current circuit was designed and put into operation in February. The circuit is capable of controlling the load current on a leg from about 0.5 amps to 8 amps with better than 0.1 amp precision across most of the range. This circuit replaces the load current circuit previously used which was designed to operate below 2.5 amps. The new circuit consists of a one ohm 100-watt resistor in series with a half ohm 50-watt variable resistor in series with a pair of 10 ohm 100-watt variable resistors which are mechanically in tandem and can operate either in parallel (for high current conditions) or series (for low current conditions).

2.10 PERFORMANCE MAPPING

The cold end of one bell jar test fixture was modified to permit operation to as low as 125°C. It was anticipated that the equilibration time at the lower cold junction temperatures would make this a long experiment. Simultaneously with the performance mapping determination of the cold junction equilibrium, an experiment was performed in the resistivity fixture with an element with a copper bond on one end to determine the equilibrium second-phase copper line in the region between 250°/100°C. The Seebeck coefficient and resistivity both decreased with decreasing temperature as expected, indicating an increase in carrier concentration.

A standard non-partitioned P-element was operated with a hot junction of 800°C and cold junctions of 250°C and 200°C. During 240 hours of operation in the temperature interval 800°/200°C, ρ gradually decreased 5.6%. Post-test examination revealed creep of the P-material at the hot end shortened the leg by 5.6%. Recalculation of final ρ and $\bar{K}$ parameter with the final L/A returned these values to good agreement with initial test parameters. This test illustrates the importance of the partition in reducing P-material creep and achieving stable electrical properties for long-term operation of unbaffled elements.

2.11 HIGH TEMPERATURE TESTING

Short-term tests were run to evaluate the effects of atmosphere, contact pressure, and temperature on the performance of the P-element at temperatures above 800°C.

Some of the results of these tests included the following observations:

1. A factor of 10 reduction in sublimation weight loss by using an argon cover gas

2. A factor of two increase in sublimation weight loss as a result of an 80% increase in current.

These results may have been influenced by the oxygen effects in these tests, however, so the conclusions are only tentative at this time.

TASK 3.0 - COUPLE DEVELOPMENT

3.3 DESIGN AND DEVELOPMENT OF TPM-217/GADOLINIUM-SELENIDE RARE EARTH CHALCOGENIDE COUPLE

The effort continues to utilize chemical, physical, and thermoelectric data which have been obtained on TPM-217 and gadolinium-selenide to develop effective couples appropriate to RTG operation.

During this period several couples were placed on test. The results are summarized in Top Summary Reports Nos. 95-127 and in a report published during this period entitled "Summary of Data Generated in the Selenide Thermoelectric Development Program" (3M No. 2331-0537, August 22, 1978).

3.4 DESIGN AND DEVELOPMENT OF TPM-217/3N-PbTe COUPLES

Couple test ATT 275 was initiated in October, 1972, to evaluate the performance of a P-TPM-217/3N-PbTe couple which utilized a ball-socket cold end and pivoting hot end. The design characteristics for this test were described in Top Summary Report No. 56. The test had operated for a total of 35,670 hours at the end of the reporting period.

3.6 ADVANCED GENERATOR CONCEPTS

HARDWARE DEVELOPMENT

Follower Friction Testing:

The frictional force has been measured for a number of follower/rail combinations. These measurements were obtained using the apparatus described in Technical Task Report No. 45.

A number of general conclusions drawn as a result of the friction force testing are:

1. The roughness of the mating surface has an influence on the observed frictional force.

2. With an electroless nickel rail, a rhodium plate on the followers reduced friction (this may not have been true on a long-term test because of the tendency of the rhodium plate to scrape off).

3. With an electroless nickel rail, chromium copper followers exhibit less friction than ETP followers.

4. With a rhodium plated follower, electroless nickel had superior friction characteristics as compared to a sulfamate nickel plate.

5. The presence of the MoS_2 interfacial material significantly reduces friction.

Follower/Rail Thermal Resistance Testing:

There is a trade-off between low friction and low thermal resistance for the sliding follower/rail surfaces. That is, the physical properties which produce low friction tend to produce high thermal resistance and vice versa. Hardness is a typical example. Thus, it is necessary to compare both friction and thermal resistance for candidate interfaces to obtain the optimum pair.

Numerous tests have been run on the thermal resistance of various combinations of material and test conditions. This work has been summarized in a topical report entitled "Thermal Resistance for Flat Copper Follower Cold End Hardware" (Attachment XX).

Testing on the thermal resistance is summarized in the Topical report section of this document.

Thermal Cycling Tests:

A series of tests to characterize the effects of heating and cooling rates on the performance of N-legs using high mobility hardware has been done. Originally, the test series was to be done by heating sputtered/ground and sputtered/unground legs to 850°C at three heating rates: 100°C/hour, 500°C/hour, and 2000°C/hour. The information derived may be used to define generator fueling and defueling techniques as well as other thermal cycles to which a generator would be subjected. The test conditions are summarized below.

- High mobility hardware
- Heating rates: 2000°C/hour, 500°C/hour, and 100°C/hour to 850°C
- Cooling rate: same as heating rate
- Argon atmosphere
- Fiberfrax insulation
- Standard sputtered and ground N-legs and sputtered and unground N-legs

The worst case condition was run first, ground/sputtered legs at a heating and cooling rate of 2000°C/hour. The legs did not crack and displayed normal electrical properties. Four more ground/sputtered legs were run, two at the rate of 2000°C/hour and two at the rate of 500°C/hour; all tests produced similar results. The six legs of this test series were from batch N-2585. To insure that these results are not peculiar to a specific batch of elements, two elements from a second batch will be tested at the rate of 2000°C/hour.

With the successful thermal cycling via the worst case condition and the subsequent follow-up tests described in the preceding paragraph the test conditions which had not yet been checked were eliminated from the series.

The tests indicate that the initial fueling of a flight generator should be no problem because the maximum heating rate of the proposed flight RTG is about 400°C/hour.

Dynamic Testing and Analysis:

A significant amount of dynamic testing and analysis has occurred during this reporting period. These activities are summarized in Attachments XI, XV and XVII of this report.

TASK 4.0 - Module Development

Modules M-6 through M-20 were placed on test during this reporting period. Modules M-19 and M-20 were on test at the end of the reporting period so no significant data was obtained from the latter two modules. A summary of test conditions and overall performance for the other modules is contained in Table A.

A report was published during this period which summarized the results of module testing. This report is entitled "Summary of Data Base Applicable to Galileo Mission" (3M No. 2331-0529, June 7, 1978).

Task 5.0 - Liaison with Jet Propulsion Laboratory (JPL) and Material Supply

Technical staff members have been in contact with JPL personnel regarding their test program on numerous occasions during this reporting period.

A number of N- and P-elements were shipped to JPL during this period.

Task 6.0 - Liaison with GGA

A number of N- and P-elements were shipped to Gulf General Atomics during this period.

Task 7.0 - Special Evaluation Projects

7.2 MAGNESIUM ALLOY INVESTIGATION

It has been determined that the magnesium oxide crucible which we have on hand is the best crucible to use to synthesize these materials. A clean reaction to produce magnesium-tin-germanium-silicide has been initiated.

Task 9.0 - Program Management

Work under this task included technical direction and overall coordination of activities associated with the program and liaison with DoE.

Top Summary Reports Nos. 95 through 127 were published during this period. Numerous topical reports were also published during this period; some of them have been referenced in the previous task descriptions.

TOPICAL REPORTING - INTRODUCTION

The following section contains topical reports on work performed during the reporting period. This section is numbered from 1 to 17 in the Technology Status section which is followed by a total of twenty (20) attachments. A list of the topics contained in the Technology Status section and the following attachments is contained in the following Table of Contents.

TOPICAL REPORTING TABLE OF CONTENTS

TECHNOLOGY STATUS

Hot and Cold End ΔT's:

A summary of recent thermal resistance data for the cold end hardware is shown in Table I. The sliding flat-faced follower which was utilized in GDS-I and earlier modules, was found to exhibit considerable variation in performance, although the best readings were adequate to meet the design goal of 7°C/W for SIG/Galileo. The mean value of thermal resistance was 10.5°C/W with a standard deviation of ± 5.2. The variation was contributed primarily by distortion of parts during assembly operations. The required degree of control over dimensions does not appear to be practical at this time. Therefore, following the completion of GDS-I, we accelerated the development of a multi-conductor bonded follower, an approach which we started looking at in 1975. We have looked at two different versions of this system, (1) follower bonded to side of rail, and (2) follower bonded to top of rail. Couple and six-couple module tests have shown that either version of this follower system, which is very similar to the flat-faced sliding follower in configuration, yields thermal resistances at or below the design figure of 7°C/W. The first version was difficult to fabricate by an ultrasonic method and even with a soldering approach the control of solder flow was difficult (creating problems with excessive follower stiffness).

At the present time, it appears that the soldering approach has the most promise and tooling has been developed to accomplish this. The six-couple data points shown in Table I (Sept. '78, and Oct. 20, 1978) indicate that the scale-up from one-couple to six-couple segments has been accomplished (the design goal of 7°C/W(t) has been exceeded). A recent data point on module M-21 indicates that acceptable thermal resistances can be achieved in an eighteen-couple module which is the common test format. This scale-up was accomplished with modifications to the bonding tooling which permits more reliable bonds between the follower and the current strap subassemblies of the cold frame segment assembly. Cold frame segment assemblies for all modules and

converters after M-20 will be fabricated using the modified tooling approach. Techniques are being developed to evaluate the thermal performance of a cold frame segment assembly without having to utilize and instrument an entire thermoelectric module. This is a heat flow test which will be capable of being utilized for a batch sampling evaluation technique for cold frame segments for the flight system. This will serve as a QC technique for evaluating subsequent assemblies and will be backed up with other NDT data including radiography.

As a parallel effort to the soldered cold-end approach, we have been working on a development effort using ultrasonic bonding to provide the necessary layer-to-layer bonds within the follower and between the follower and the rail. This approach has been used successfully in single couples; however, some difficulty is being experienced in obtaining bonded six-couple cold arrays from ultrasonic bonding vendors. We are working with Sonobond Co. on developing the tooling for making six-couple arrays using ultrasonic techniques. At this time, however, the solder bonded approach which was developed in-house, is the reference design approach and the ultrasonic bonding technology development will be carried along on a low level as an alternate approach.

The ΔT exhibited at the hot end between the current strap and POCO graphite on GDS-I has been reduced by introducing a platinium foil between the alumina hot end insulator and POCO graphite. The GDS-I current straps exhibited temperature drops from 50-100°C between the alumina and POCO. This ΔT has been reduced to approximately 20 to 25°C by the introduction of a platinum foil between the alumina and POCO graphite surfaces. The design goal was 25°C, therefore, we have exceeded the design requirements. This change is being introduced into all modules and converters after module M-17.

In summary, the hot and cold end thermal resistance goals have been met. The remaining effort in this area consists of developing a QC method for routinely evaluating thermal resistance characteristics of the bonded cold frame segment.

Hardware Mobility

Hardware mobility (the ability to accommodate motions within the converter, caused by either thermal expansion or P-leg sublimation) is an important requirement for the converter.

In recent module testing, a source of degradation has been a reduction in contact pressure on the P-legs which causes an increase in contact resistance. This follower "hang-up" effect has been caused by excessive friction between the sliding follower and the rail. Recent design changes have been incorporated which eliminate the sliding interface and replaces it with a bonded compliant follower system. This reduces the follower friction as well as reducing the thermal resistance of the cold end.

It is necessary to understand the force-displacement characteristics of the new cold end hardware so that the effect of thermal expansion, creep and tolerance variations on contact pressure can be determined. A summary of the forces on a thermoelectric element is given by a force balance on the thermoelectric leg and surrounding insulation (Figure 1).

$$F_{ToT} = F_s - F_F = F_L + F_I = \sigma_L A_L + \sigma_I A_I \qquad (1)$$

$$F_L = \frac{1}{A_L} F_s - F_F - \sigma_I A_I \qquad (2)$$

where $F_s = F_{si} - K (L-L_i)$

where F_s = Spring Force

F_{si} = Initial Spring Force (Nominal Compression)

F_F = Effective Spring/Friction Force of Follower

F_L = Net Force on Leg

F_I = Net Force on Insulation Surrounding Leg

σ_I = Stress on Insulation as a Result of Compression

σ_L = Net Stress or Contact Pressure on Thermoelectric Leg

K = Spring Constant of Follower Spring

L = Length of Follower Spring

L_i = Initial Length of Follower Spring (Nominal Compression)

A_I = Cross-sectional Area of Thermal Insulation Associated with one Thermoelectric Leg

A_L = Cross-sectional Area of Thermoelectric Leg

Now the stress on the insulation as a function of compression was measured using a special enclosing fixture and an Instron mechanical test machine. These data are shown plotted in Figure 2 and a least squares curve fit to the data is given by:

$$\sigma_I = a_1 + a_2 \varepsilon_I + a_3 \varepsilon_I^2 + a_4 \varepsilon_I^3 + a_5 \varepsilon_I^4 \qquad (4)$$

where $\varepsilon_I = 1 - L_{I/L_o}$ (5)

where L_I = Length of Insulation (Between Hot and Cold Straps)

L_o = Unstressed Insulation Thickness

The measurements of the force-displacement characteristics of the follower were obtained in a spring test device (Figure 3). A typical force-displacement curve is shown in Figure 4. The spring character-

istics of the follower spring are obtained from QC measurements which are routinely performed on the spring. All of the components of the force balance described in equation 2 are thus combined and the results are shown in Figure 5 as a function of follower deflection. Follower deflection will either occur from thermal expansion or P-element creep sublimation. The actual compression of the follower spring at assembly is a function of the tolerance stack-up of components in the N or P-leg stack. The effects for the extreme tolerance stack-up conditions are shown in Figures 6 and 7.

It can be seen that the minimum value for N-leg contact pressure at 10 mils deflection is about 200 psi and the minimum value for contact pressure on the P-leg at 30 mils deflection is about 30 psi. These values should be the maximum amount as a result of thermal expansion and/or creep/sublimation. Measurements have shown that this will still be an acceptable amount of contact pressure for each of the elements.

In addition to the mobility characteristics described above, it has been observed during the post-test analysis of M-7 that an excessive amount of load relaxation of N and P-leg springs occurred. It is unknown at this time what the mechanism for this load relaxation is, but the amount of relaxation was significantly greater than literature data had indicated for the temperatures and stress levels involved. As a result, a test matrix has been defined to evaluate the effects of temperature, stress level, spring material and set and environment on spring load relaxation. In addition, a thorough chemical and metallographic analysis of the M-7 springs is being performed. The results of these tests and analyses will be available in time to affect the spring design for SN-1. The schedule for these activities along with the interaction with the SN-1 schedule is shown in the schedule section of this document.

In summary, it can be concluded that the mobility of the couple hardware has been well characterized and has been demonstrated to be adequate with the exception of spring load relaxation. A program to achieve a solution to the spring load relaxation problem has been identified and is consistent with the schedule for SN-1.

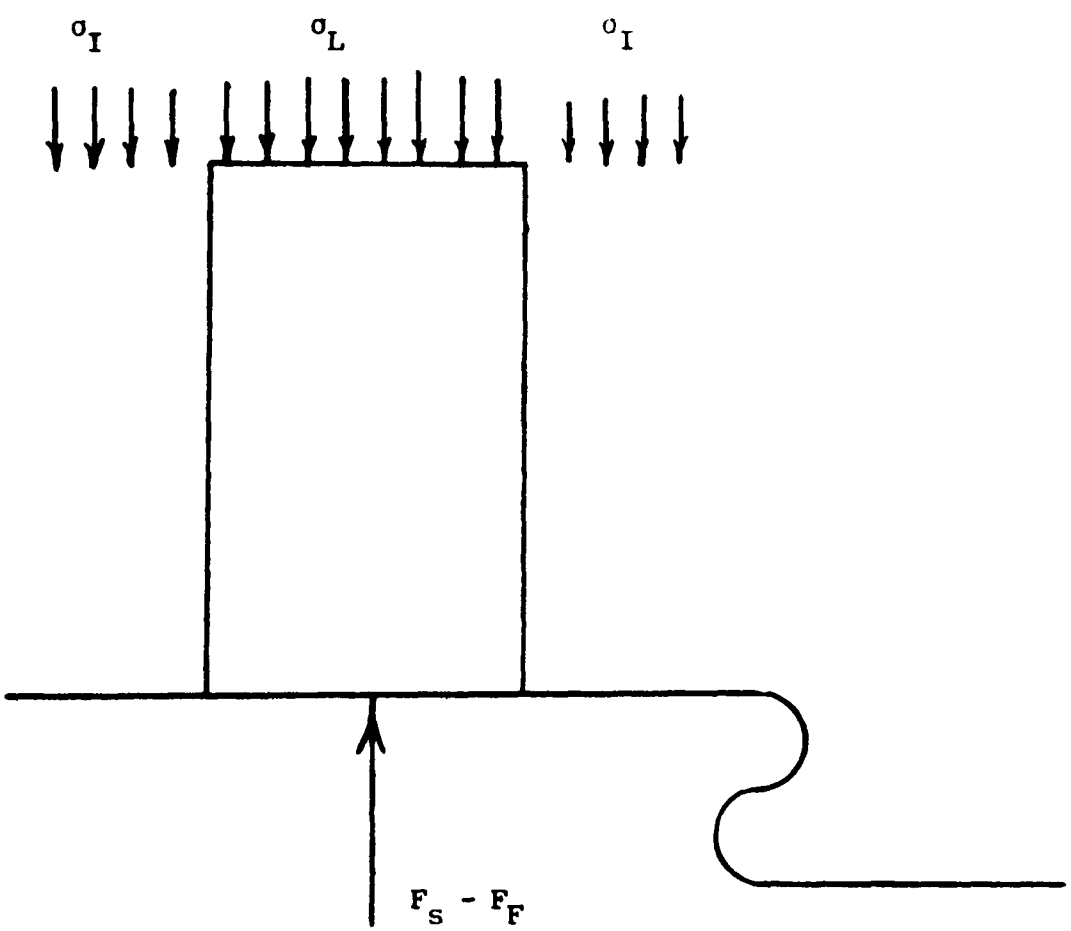

FIGURE 1

Force Balance on Leg and
Surrounding Insulation

FIGURE 2

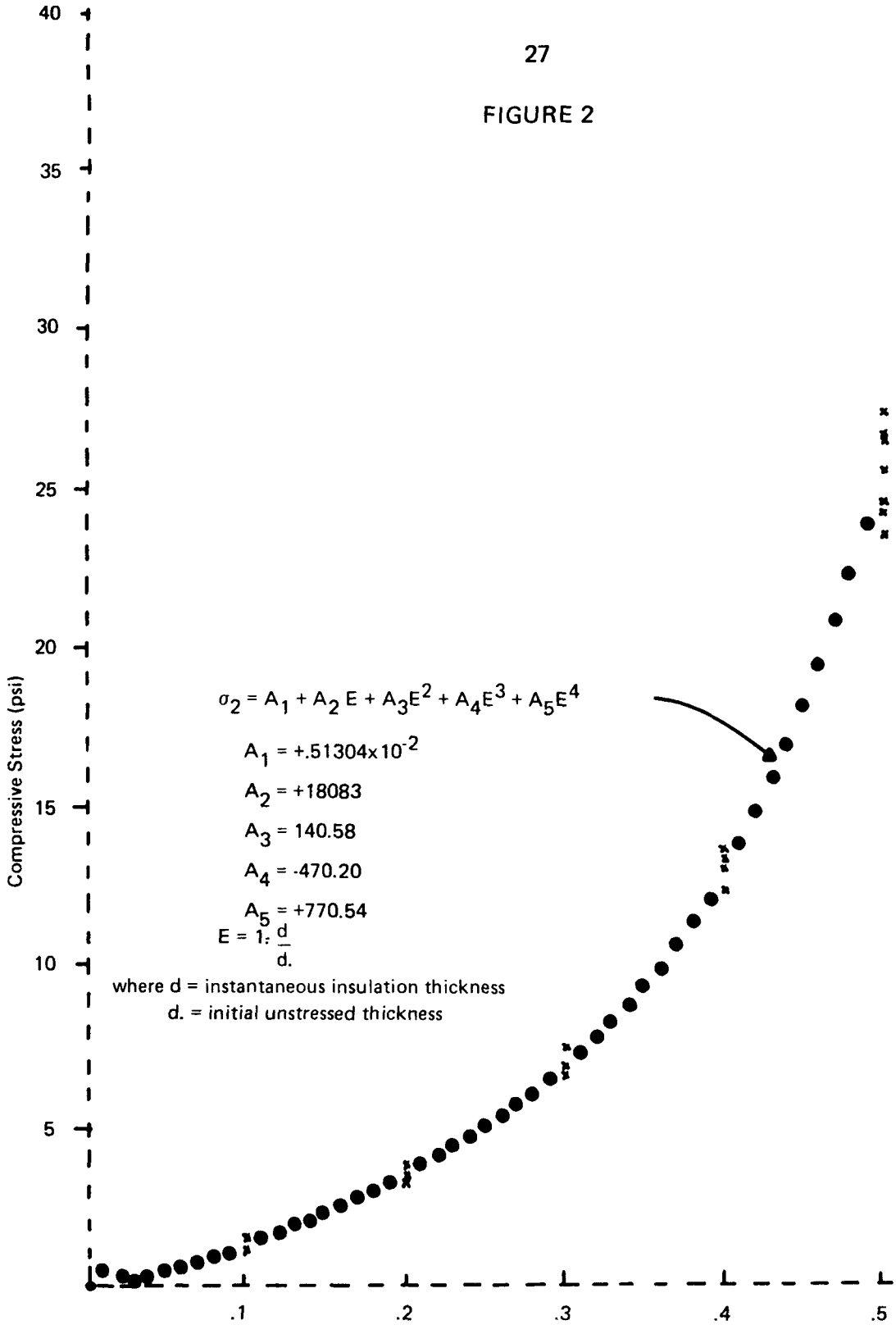

Stress vs. Strain Data
Layered Hi-Fi 660 Paper
1" Thick Test Sections Nominally
4th Order Polynomial Fit

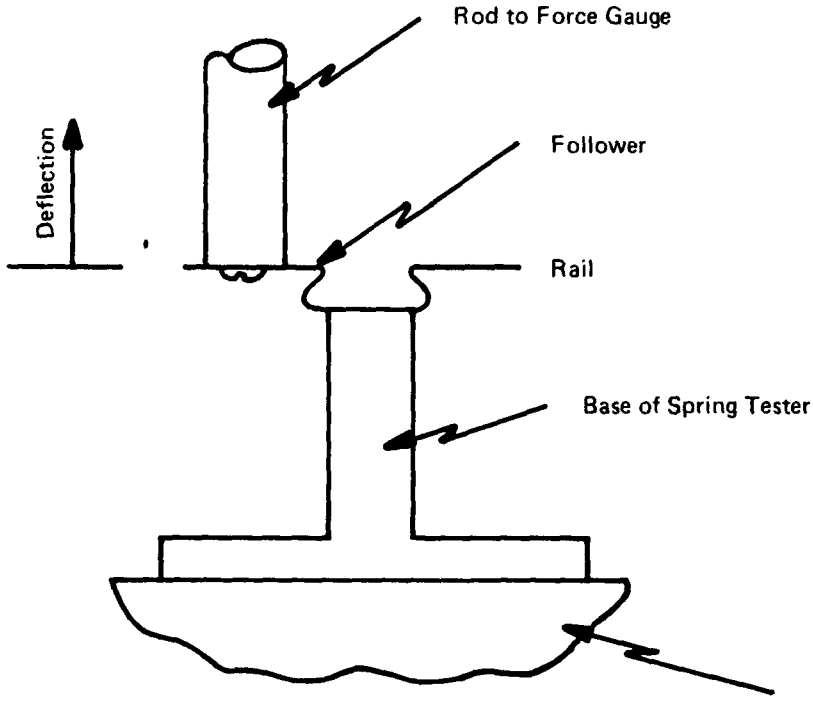

FIGURE 3

Follower Force-Displacement
Measurement Device

Figure 4. Complete Cold End Assembly Force Vs. Deflection

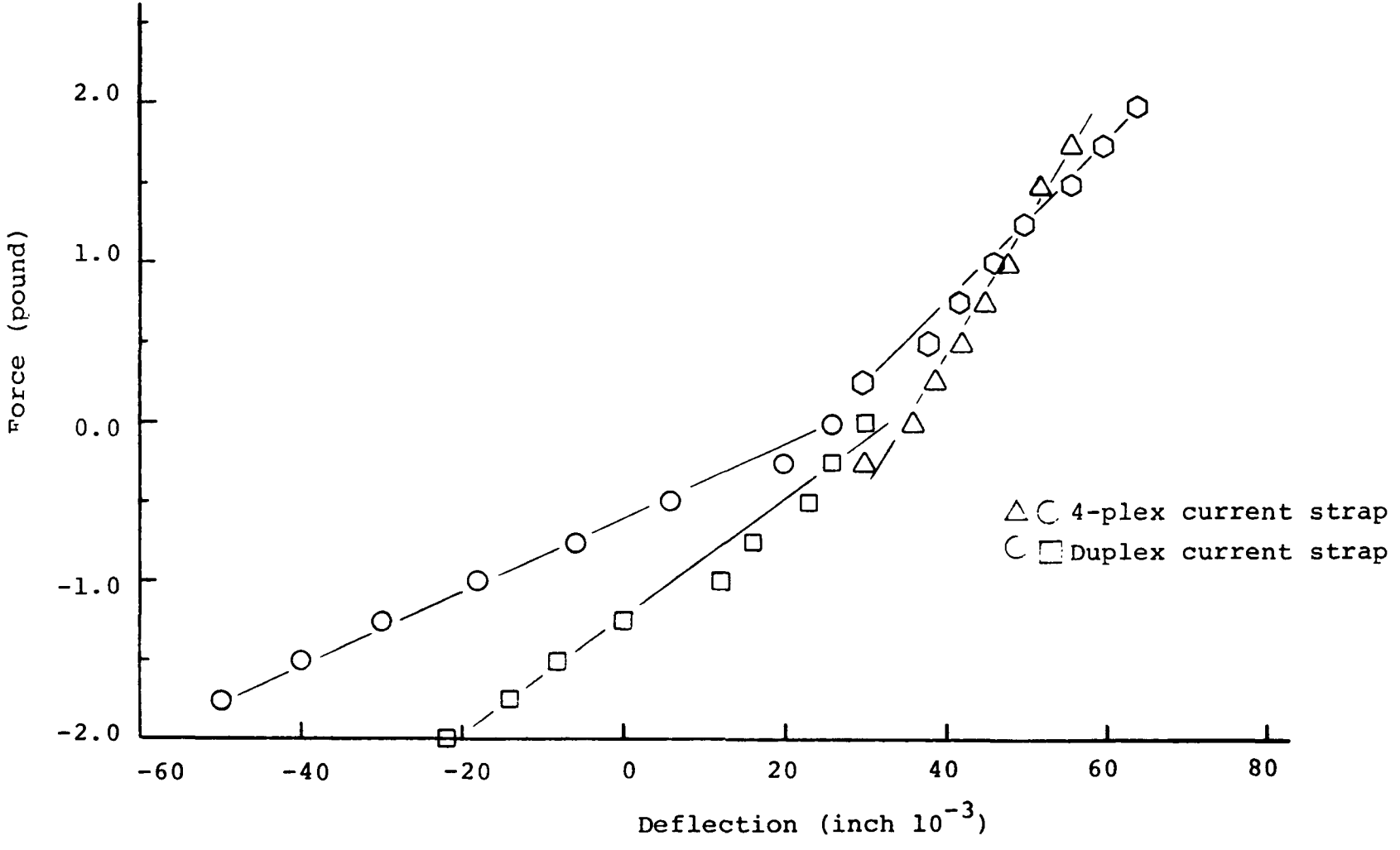

Figure 5. Individual Components of Force Balance on Thermoelectric Leg

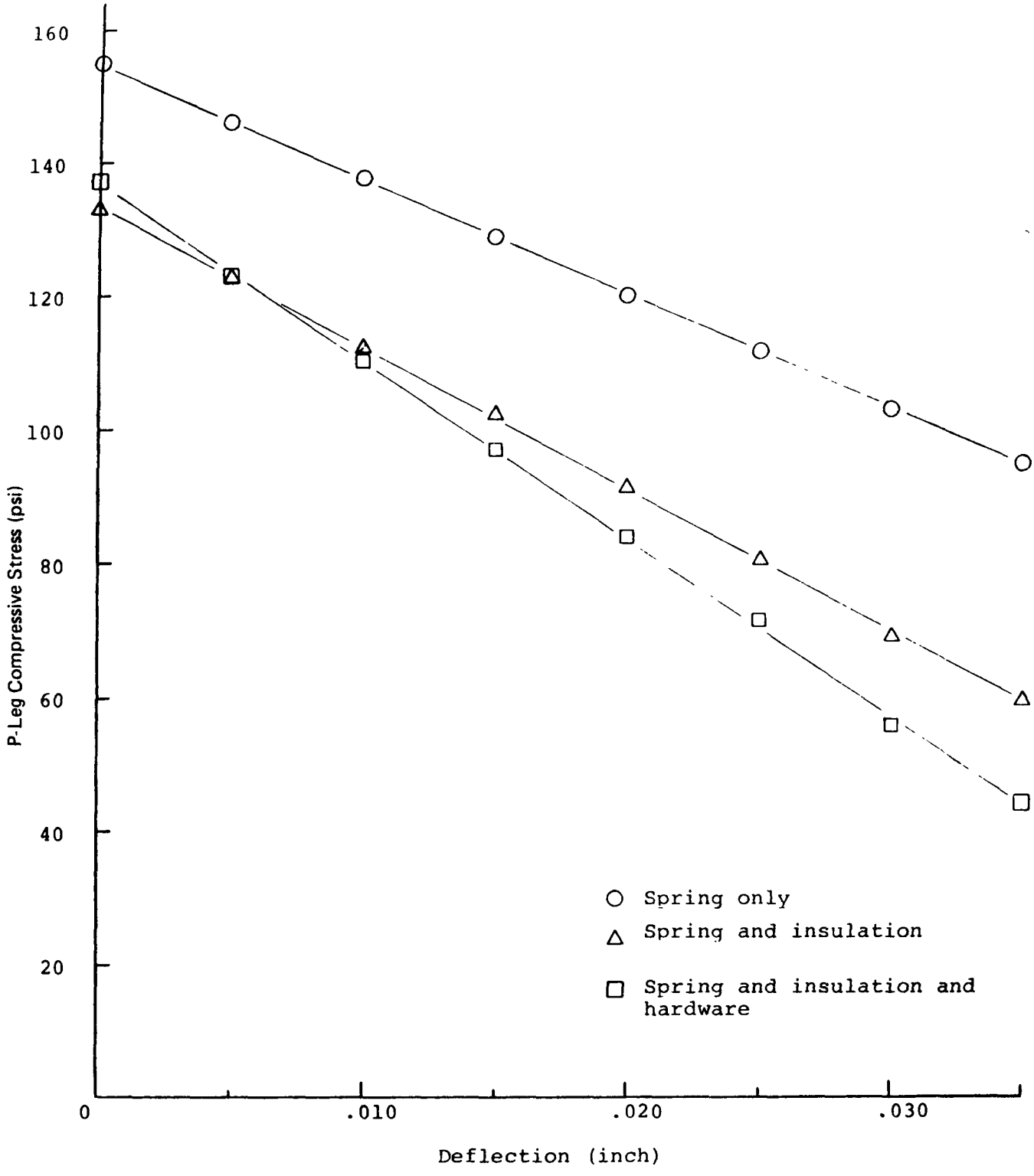

Figure 6 N-Leg Compressive Stress Vs. Deflection

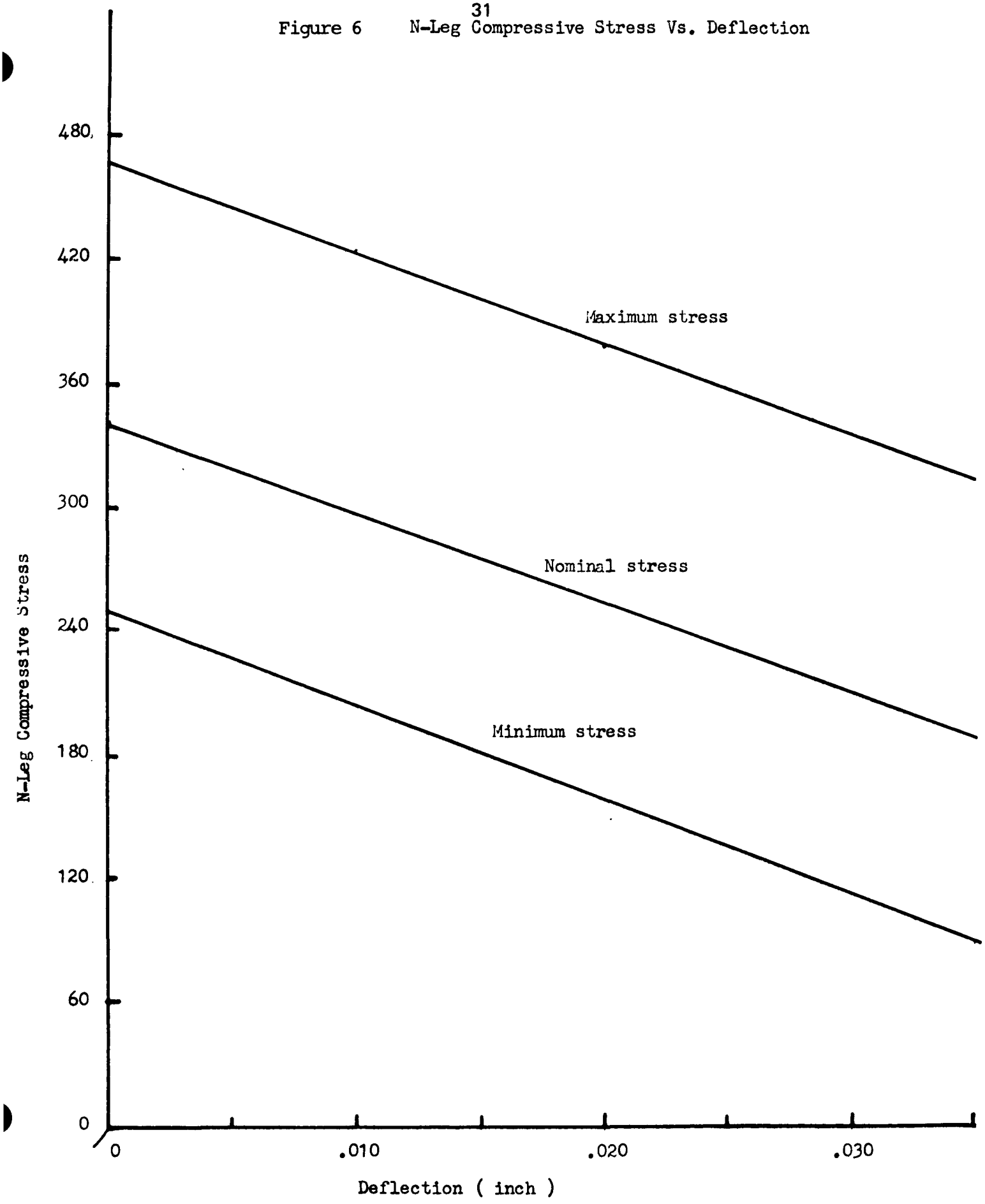

Figure 7 P-Leg Compressive Stress Vs. Deflection

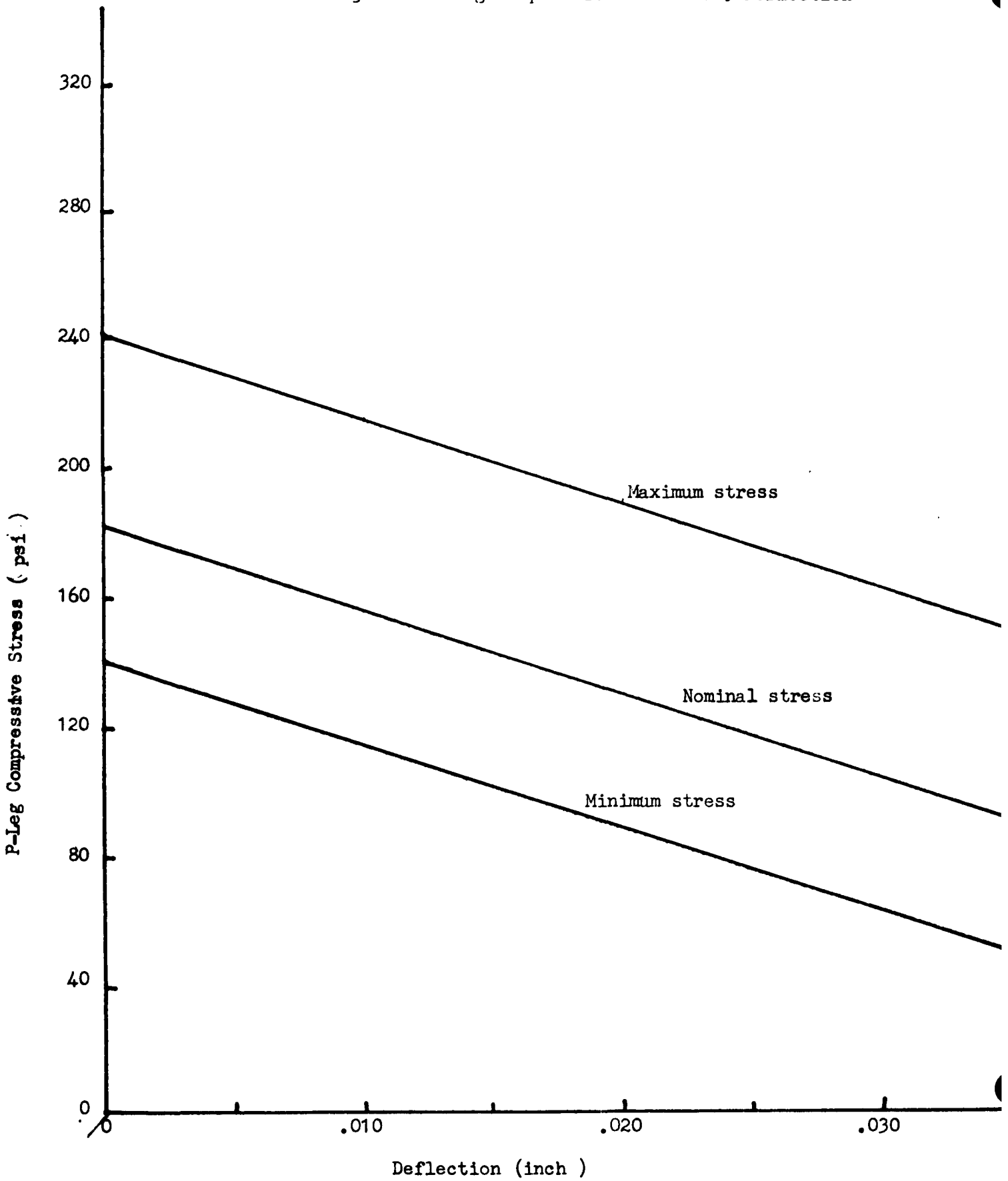

TABLE I.

IMPROVEMENTS IN COLD END HARDWARE
THERMAL RESISTANCES (GOAL OF 7° C/W(T))

CONFIGURATION	THERMAL RESISTANCE (°C/W) MEAN	STD. DEVIATION	DATA POINTS
FLAT FACED SLIDING FOLLOWER, Cr-Cu AND ETP SANDWICH	10.5	± 5.2	47
SLIDING FOLLOWER, ETP SINGLE MATERIAL	7.3*	± 0.5	3
MULTIPLE LAYER FOLLOWER, BONDED TO SIDE OF RAIL (SINGLE COUPLE TESTS)	6.4*	± 2.5	8
MULTIPLE LAYER FOLLOWER, BONDED TO SIDE OF RAIL, SIX COUPLE MODULE (JUNE 1978)	5.4	± 3.3	4
MULTI-LAYER FOLLOWER, BONDED TO TOP OF RAIL (SINGLE COUPLE TESTS IN MAY AND JULY, 1978)	5.0	± 1.7	4
MULTI-LAYER FOLLOWER, BONDED TO TOP OF RAIL (SIX COUPLE MODULE IN SEPT. 1978)	16.5	± 2.3	6
MULTI-LAYER FOLLOWER, BONDED TO TOP OF RAIL (SIX COUPLE MODULE, OCT. 4, 1978)	11.3	± 1.2	4
MULTI-LAYER FOLLOWER, BONDED TO TOP OF RAIL (SINGLE COUPLE TEST, OCT. 17, 1978)	5.2	± 2.1	2
MULTI-LAYER FOLLOWER, BONDED TO TOP OF RAIL (SIX COUPLE MODULE, OCT. 20, 1978)	5.8	± 1.5	4
EIGHTEEN COUPLE MODULE, M-21 (DEC. 8, 1978)	7.2	± 0.8	10

* THESE DATA ARE FROM FOLLOWER TO RAIL RATHER THAN CURRENT STRAP TO RAIL AND WOULD BE EXPECTED TO BE 0.5 C/W LESS THAN THE REFERENCE DESIGN VALUES.

P-Leg Sublimation Suppression

The design goal for the SIG/Galileo program is to reduce the weight loss per element to less than the assigned value of 50 mg in 50,000 hours. Weight loss rates meeting this goal have been demonstrated in accelerated testing of legs with experimental astroquartz fiber/submicron particle baffles. The baffle configuration selected from this research program for more extensive testing for the flight system consisted of an astroquartz fiber yarn wrap impregnated with a Min-K/water slurry, with a stepped foil hot end cap to seal the end of the leg; a weight loss rate of 27 mg/50,000 hours was obtained with this configuration.

The justification for the selection of 50 mg/50,000 hours as the criterion for the allowable sublimation per P-leg is based on three factors. These are:

(1) Observations in M-5 of the effects of Se deposition on the cold end hardware and current straps.

(2) Seated tube depositions on copper cold end parts.

(3) Observations of legs that had lost greater than 50 mg in module testing.

It was observed in M-5 that approximately 50 mg per P-leg was lost during 9,000 hours. There were no deleterious effects (cold end shorting, whisker growth, etc) as a result of the deposition on these parts. The hardware which is currently used is somewhat different from that used in M-5 but the effects with the legs are clearly the same.

A series of tests have been run in which 10 mil copper parts (thickness of cold current straps) have been exposed to selenium environments at the cold end temperature. This supplied essentially an infinite source of Se at the vapor pressures appropriate to converter operation. In this case a reaction of 12% of the copper material occurred. In the case of a contraint of 50 mg/element the source term is limited and only 3% of the copper available would react.

A summary of observations for the P-legs in M-7 is contained in Table II. There is a correlation between degree of copper migration and weight loss. Even the copper migration associated with the high weight loss elements had not been responsible for any observable degradation. The level below about 80 mg appears to be superior to levels higher than 100 mg. Thus, the selection of 50 mg appears to be reasonable from this criteria as well.

All of the above criteria indicate a significant margin in terms of the selection of the 50 mg criteria. Additional accelerated testing will be performed with actual flight system hardware to further substantiate this criterion.

At the present time, the production process for legs with this sublimation suppression configuration is being scaled to allow manufacturing wrapped elements reproducibly in quantities suf-

ficiently large for qualification testing for SIG/Galileo. Early difficulties in controlling wrap spacing and tension have been overcome by improved product controls and special wrapping techniques developed in the program. Supplies of stepped foil hot end caps have recently become available from vendors. It is now necessary to determine the reproducibility of this process for reducing sublimation.

The configuration selected is shown in Attachment I which consists of drawings SG17-10316, SG17-10314 and SG17-10089-P1. The nominal thickness of wrapping applied is 0.025" over the entire length of the element except for the shouldered portion of the cap. The wrap application and vacuum processing are governed by MSI 2008 (Attachement II) and checked by measurements of wrap thickness and density as specified in QA STD 2022 (Attachment III).

Weight loss performance of the wrapped P-leg has shown some variability but much promise for surpassing the design goal of 50 mg in 50,000 hours at 850/150°C and il/a = 8. A capped and wrapped element operating for over 1400 hours displayed the extrapolated rate of 27 mg for 50,000 hours. The basic difficulty encountered is one of proper testing - not the sublimation suppression technique employed. Reduced load pressure is responsible for a runaway high loss mode which must be corrected in future testing. High P-leg contact resistances and high weight losses have occurred in module testing and are attributed to loss of contact pressure. Recent six station results on partitioned/non-partitioned legs also showed the effect of contact pressure loss. Loss of load pressure was determined by a tenfold increase in measured electrical resistance and post-test measured loss rates correlated to the fraction of ingradient time spent in this condition. The correlation, as plotted in Figure 8, is very good for the partitioned and non-partitioned subsets. Loss of proper compressive loading on the wrapped element is evidenced by: (1) the large increase in measured electrical resistance; (2) the ability to temporarily reduce the electrical resistance through a 5°C cold end thermal cycle or increased air pressure to the test station bellows assembly which provides the compressive force; (3) the very reproducible 20 psi measured compressive load required to make good electrical contact on post-test analysis of all legs. This end surface loss mechanism has not only been present in ingradient testing and modules but has also been seen in some of the isothermal accelerated tests. Warpage of fixture members and loss of spring force through aging of the first isothermal test fixture led to high resistances and erratic and inreliable weight loss measurements. After making repairs to the fixture and increasing spring force, the resistance dropped and the weight loss became more reproducible. Comparing a set of four pre-repair measurements with a set of 5 post-repair measurements on legs of the same type, yielded an average factor of 10 increase in loss rate due to load loss. This increase in loss rate with low load pressure by an order of magnitude is more than sufficient to explain the higher than predicted loss rates seen in modules and ingradient tests. Presumably the low load pressure state allows a high conductance path between wrap and cap to bypass

the wrap effectiveness. Further tests are planned to deliberately produce low and/or uneven loading to delineate the parameters controlling this loss mode. In addition, by mid-February a six-station loaded with wrapped, capped P-legs will have completed 1000 hours ingradient with force transducers on the individual legs to measure directly the load pressure on the legs.

Wrapped legs were first introduced into modules 15, 18, 19 and 20. These legs have a different hot end foil geometry than for the flight design because of vendors inability to deliver the optimum stepped foil caps on time and, therefore, are expected to exhibit higher weight losses in operation. However, these tests should give an indication of the reproducibility of the sublimation suppression method and the test results will be correlated with short-term laboratory tests comparing directly the effectiveness of different end foil geometries. The standard short-term laboratory test for comparison of different wrap and end foil configurations consists of isothermal operation at 940°C in a vacuum of 10^{-6} torr with weight loss accelerated by current. The laboratory testing in progress indicates that the weight loss rate should be a factor of 3 lower using the optimum stepped foil hot end cap geometry, instead of the configuration in modules 15, 18, 19, and 20 (Table III). In addition to the isothermal testing, the loss rate of a small set of wrapped P-legs of the type used in modules 15, 18, 19 and 20 has been measured in a thermal gradient at accelerated conditions of temperature and current in a vacuum test fixture with independent leg test stations (Table IV). Using this data and the factor of three rate reduction for the stepped foil cap measured in the laboratory isothermal testing, the weight loss rate projected for the stepped foil cap configuration under flight conditions is 40 $\pm$ 20 mg/50,000 hours. The weight loss rate measured for the two-couples in module M-15 which were of the same type as those used in modules 18, 19, and 20 was higher than that in the controlled ingradient tests. Since contact pressure was lost in this M-15 module with GDS-type hardware, the higher sublimation rate is attributed to sublimation from the ends of the leg under the foil which are normally protected under full contact conditions. The cold end hardware for the flight system has been designed to maintain better contact, so the end surface weight loss which occurred in M-15 is not expected in the flight design; consequently, the projected weight loss rate remains 40 $\pm$ 20 mg/50,000 hours.

Because of vendor fabrication difficulties with the stepped cap it was originally intended to introduce this feature in modules M-25 through M-29 to prevent significant schedule impact. As the result of a September technical directive from DoE, however, and because of increased significance of the data base, it was decided to incorporate the stepped cap into all modules after M-20. This has resulted in the schedule slippage of module M-21 to early December.

The stepped cap significantly reduces the weight loss of the wrapped leg, but it also increases the difficulty of fabricating the P-leg with a partition. The first legs produced in quantity

with the stepped foil cap are non-partitioned. These legs will be used in Module M-21 as well as in isothermal and ingradient evaluations. Laboratory isothermal accelerated testing indicates that the weight loss rate penalty for using non-partitioned legs in these tests is less than a factor or two (Table V). A mold to produce stepped cap legs with the conventional partitioning at acceptable yields is being developed to provide legs for the M-22 module in January.

Another perspective on the effectiveness of the baffling technique is obtained by comparing directly under accelerated isothermal test conditions wrapped and non-wrapped legs, as in Table VI. The ratio of the weight loss of non-wrapped to a wrapped leg is defined as the baffling factor. Although this baffling factor is not used directly in ingradient life calculations, it still furnishes an interesting measure of the effectiveness of the wrap. As shown in Table IV, baffling factors over 700 have been obtained in isothermal testing.

Work is underway to provide direct measurements which support the description of physical mechanisms that make the capped, wrapped P-leg scheme so effective at suppressing sublimation. A program of scanning electron microscopy (SEM) is underway to look at (1) samples of dired slurry alone for comparison, (2) the dried and processed inner wrap surface - which would be in contact with the P-material, (3) the dried and processed outer wrap surface and (4) the post-test inner wrap surface from the hot end of a leg operated ingradient. The information of interest will be characteristic pore size and the distribution of voids which could be potential high conductance paths. In order to be an effective sublimation barrier the wrap must uniformly present a surface with pore sizes much lower than the estimated 0.3 micron mean free path of selenium. Recent results confirm earlier work in revealing a uniform distribution of particles with a measured pore size of 0.05 micron on dried MIN-K/H_2O slurry. Figure 9 shows a 20,000X SEM magnification of a representative section of dried slurry; no voids of any significance can be seen.

Measurement of electrical performance in the standard ingradient QC fixture shows that wrapping for sublimation suppression will not materially degrade the thermoelectric properties of P-elements. A representative group of 39 partitioned legs without wrap averaged 264 μv/°C and 10.5 mΩ-cm while twelve wrapped legs produced 260 μv/°C and 10.6 mΩ-cm, at 800/250°C.

The question of wrap compatibility with the balance of module materials in an operating environment has a less clear answer at this point but some information exists and more is being gathered. From use of a residual gas analyzer on the isothermal test stations, it can be stated (see Table VII) that no major additions to the environment were contributed by the wrapped P-leg when compared to a blank run. Time-of-flight mass spectrometry is underway with both wrap material and wrapped P-elements to 1000°C to identify any volatile species; some information should be available by December 29, 1978. Chemical extraction is being

used to determine the amount of starch oil binder present in the astroquartz as received from the manufacturer. Analyses of the water used in the Min-K slurry shows only minor impurity levels compared to those in other parts of the insulation system.

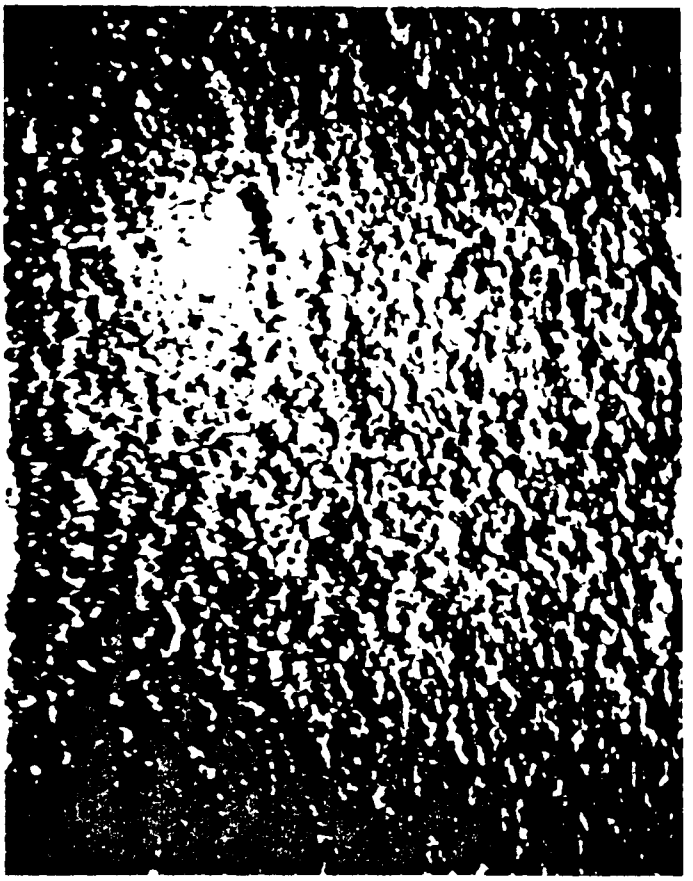

FIGURE 9

20,000X SEM magnification of dried MIN-K/H_2O slurry.

TABLE II
CORRELATION OF P-LEG WEIGHT LOSS AND OBSERVED COPPER MIGRATION EFFECTS

LEG NO.	WT. LOSS	COPPER MIGRATION		
		BEADS	WHISKERS > (50 mil)	BOND SEPARATION
20	59	MODERATE - ONE SIDE	NO	NO
16	78	UNIFORM	NO	NO
8	82	HEAVY-UNIFORM	NO	NO
2	96	NO	NO	YES
18	106	LIGHT-NON UNIFORM	YES	NO
6	109	LIGHT-NON UNIFORM	NO	YES
12	128	NO	NO	YES-COLUMNS
14	129	HEAVY-ONE SIDE	NO	PARTIALLY
10	142	HEAVY-ONE SIDE	NO	YES
4	156	HEAVY-ONE SIDE	NO	YES

Figure 8. Dependence of Weight Loss Rate on Operating Time at Low Load

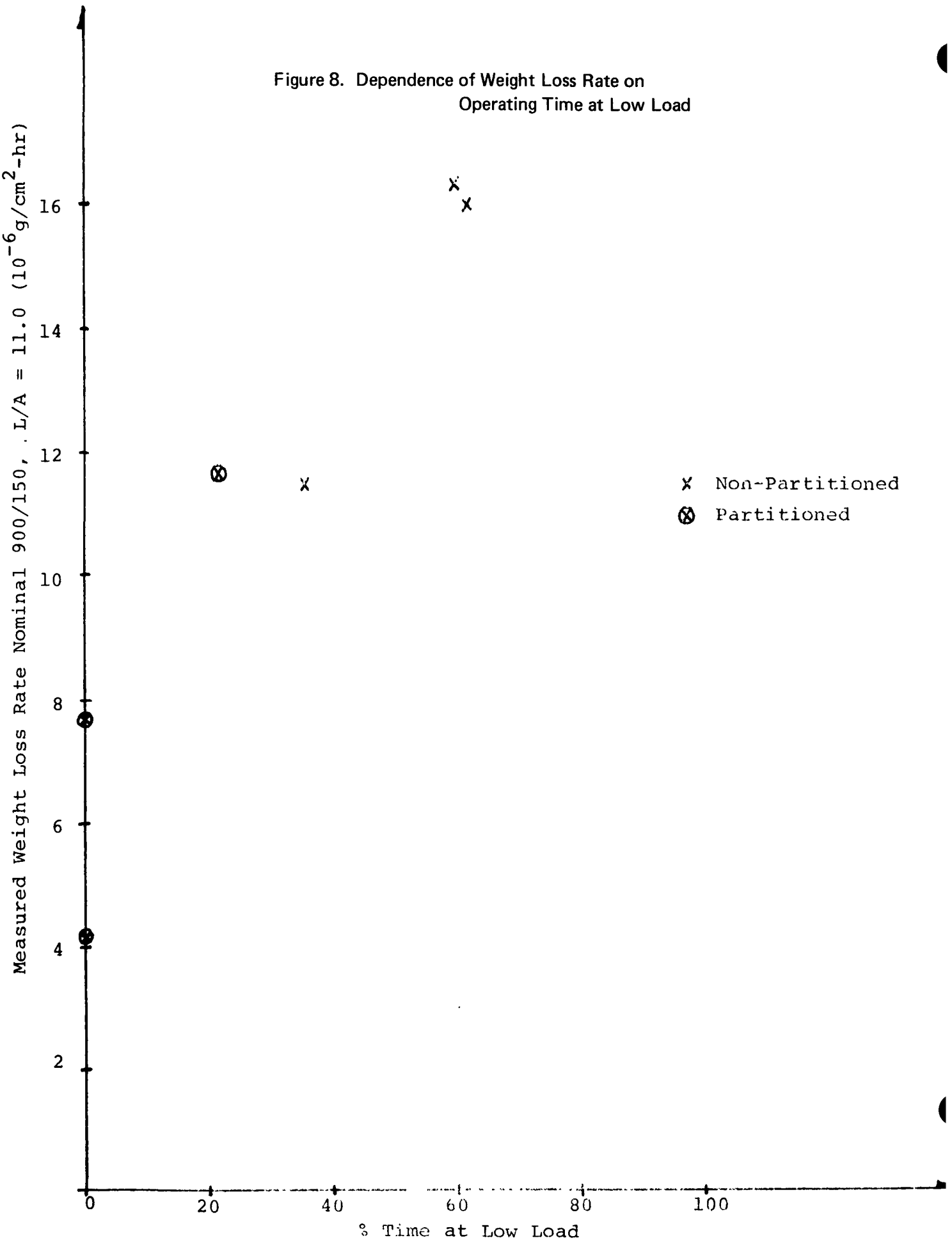

TABLE III

EVALUATION OF WRAP REPRODUCIBILITY
IN ACCELERATED ISOTHERMAL TESTING

Configuration	Number of Legs Tested	Loss Rate in Accelerated Isothermal Testing Under Identical Conditions (10^{-3} gm/cm^2-hr)
Thick Foil, Min-K/H_2O Slurry Astroquartz Wrap (As in M-15C, M-18, M-19, M-20)	8	0.41 ± 0.14
Stepped Cap, Min-K/H_2O Slurry Astroquartz Wrap	6	0.13 ± 0.05

Conclusions:

- Stepped cap more reproducible than thick foil.
- Factor of 3 lower loss with stepped cap.

TABLE IV

PERFORMANCE OF THICK FOIL, MIN-K/H_2O
SLURRY ASTROQUARTZ WRAP LEGS
(M-15C, M-18, M-19, M-20 TYPE)
IN THE TEMPERATURE GRADIENT 900/150°C

Test No.	$\lambda L/A$ (amp/cm)	Measured Weight Loss Rate, Accelerated* Conditions (10^{-6} gm/cm^2-hr)
571	11	4.2
572	11	7.6
573	11	11.8
AVERAGE		7.9

*These tests were accelerated by using both higher hot junction temperatures and higher currents than for the flight design; the combined acceleration factor was 5.

TABLE V

Comparative Weight Loss Rates of Partitioned and Non-Partitioned P-Legs

Condition:

6 Station Fixture

900/150

il/A = 11

Ion Pump Vacuum

Acceleration Factor of 5

	Weight Loss Rate (10^{-3} gm/cm^2-hr)
Partitioned Legs	7.9 $\pm$ 3.8
Non-Partitioned Legs	14.6 $\pm$ 2.7

TABLE VI

Effectiveness of Baffle in Sublimation Suppression in Isothermal Testing at 940°C with High Current Acceleration

Wrap/End Foil Configuration	iL/A (amp/cm)	Rate (10^{-3} gm/cm^2-hr)	Ratio: (Wrapped/Control
Control, No wrap	17.8	103	1
Thick Foil/Min-K/ H_2O Slurry, Astro-quartz Wrap	22	0.41 $\pm$ 0.14	250
Stepped Cap/Min-K/ H_2O Slurry, Astro-quartz Wrap	22	0.13 $\pm$ 0.05	790

TABLE VII

Partial Pressure Comparison of Wrapped Leg Versus Blank Run in Isothermal Test Station

	Condition	Mass No.	Partial Pressure ($\times 10^{-8}$ Torr) Blank	Wrapped Leg
1.	15 minutes after initiating pump-down, T = ambient	44	2.5	2.5
		41	--	1.3
		26	3.5	3.7
		18	53	42
2.	T = 500°C and increasing	44	2.5	10
		26	3	11
		18	39	89
3.	T = 940°C and start soaking	44	29	50
		41	5	18
		39	4	18
		26	16	41
		18	∿100	150
4.	T = 940°C, 10-15 minutes after start soak	44	8	18
		41	3	10
		39	3	9
		26	9	22
		18	68	110
5.	T = 940°C, switch from tube pump to ion pump, approx. one hour after (4)	44	6	10
		41	3	8
		39	2	7
		26	7	13
		18	42	41
6.	T = 940°C, 16 hours after (5)	44	1.6	2.7
		41	3.4	5.2
		39	2.2	3.7
		26	3.3	6.3
		18	4.0	7.6
7.	T = ambient, 5 hours after (6)	44	--	--
		43	0.4	0.3
		41	1.4	0.4
		39	0.3	0.1
		26	0.3	0.2
		18	0.6	0.8

Thermodynamic Stability

Two types of experiments have been performed to increase our knowledge of the thermodynamic stability of the TPM-217 system. One type of experiment involves the measurement of the effusion of ions from a Knudsen cell using a mass spectrometer. Since the aperture of the Knudsen cell is much smaller than the surface area of the sample, this measurement determines equilibrium partial pressures. The second type of experiment involves the measurement of the weight loss of a sample during free evaporation. This is the case which is closest to generator operating conditions, and can be most directly scaled to predict weight loss in module. In addition, the effect of a wrap or baffle is knetic rather than thermodynamic, and requires free evaporation type experiments (either isothermal or ingradient). That is why the current emphasis is on these free evaporation experiments. For completeness, Attachment IV summarizes the Knudsen cell equilibrium experiments.

N-Leg Material Process Improvements to Reduce Extraneous Resistance

Considerable confusion has existed over the use of the term extraneous resistance. The 12-1/2% extraneous resistance used to describe the performance of the SIG/Galileo converter refers to the total extraneous resistance including that of the N and P-elements and all the contacts and current straps.

At the present time, the gadolinium-selenide material extraneous resistance is approximately 40% and the total contact extraneous resistance for the couple is 15% for a total of 55% extraneous resistance. The probability is relatively low that this will be significantly improved in time for SN-1. However, the probability remains reasonably high that 12-1/2% total extraneous resistance, including contacts, will be achieved in time for SN-2.

Reductions in contact resistances are anticipated which may reduce the contact resistance to 10% or less. While some batches of pressed and sintered N-legs have been characterized at 25% extraneous resistance, selected N-elements have exhibited extraneous resistances in the range of 0%. The program to reproducibly fabricate pressed and sintered elements at 0% by early 1979 for introduction into SN-2 is centered on processing changes to permit high sintered densities at lower sintering temperatures.

The rationale for reducing extraneous resistance by processing is based on both experimental and theoretical data as follows. Scaleup during 1977 resulted in batches of 100 N-legs being produced simultaneously. Unfortunately, the large ingots used were inhomogeneous, with a translucent, high resistance material in the interior. Chemical analysis has shown the composition of this material to be $GdSe_{1.50}$ while powder x-ray diffraction has given the same crystal structure as the normal conductive $GdSe_{1.49}$ material. The significant facts are that this material has both a lower melting point than the $GdSe_{1.49}$ composition and

a much higher resistivity. Sintering of powder produced by grinding this compositionally inhomogeneous ingot results in melting of the high resistance phase with liquid sintering and location of the high resistance composition on grain boundaries. The solution to this problem is to sinter at temperatures below the melting point of the high resistance material, thereby avoiding liquid phase sintering. The attendant difficulty is that sintering is less complete at lower temperatures, requiring a higher surface area powder to achieve high sintered densities. N-legs are presently made with densities from 97% to 98%. A lower temperature sintering process does yield lower extraneous resistance at a given density than the standard process. However, the density achieved in the lower temperature sintering is on the order of 93%, whereas higher densities (97% - 98%) at the lower temperature sintering are necessary to yield 0% extraneous resistance legs. Since the present particle size is relatively coarse for good conventional sintering, reduction of particle size in an additional grinding step should produce a more sinterable powder for high density sintering at lower temperatures. A grinding technique has been demonstrated which increases surface area by a factor of 2 to 3; the first experiment was not complete since oxidation of the powder prevented satisfactory sintering but if oxidation can be prevented the procedure should be successful. Amplification of the grinding/sintering experimental data supporting this is contained in Attachment V.

A second technique being investigated to reduce extraneous resistance is to sinter at reduced temperatures to closed porosity, then sinter to 99% density in a gas isostatic hot press. A fixture for this experimental process is scheduled for completion in January.

A third approach to increasing the power output of the N-leg is to use the present $GdSe_x$ N-material in a segmented leg with a PbTe cold segment. The advantage to this approach is that a 10% increase in power is obtained at any given gadolinium-selenide material extraneous resistance, and the technology for the lead-telluride exists and is proven. We have operated our P-material in the presence of lead-telluride in life tests without degradation due to cross contamination. Segmented lead-telluride legs have been used successfully in previous SNAP programs. The interface between gadolinium-selenide and lead-telluride would be transition metals compatible with both materials. We have placed elements of this type on test and obtained the performance indicated in Table VIII. It is anticipated that segmented legs will be introduced into module M-24, and a six-couple module has been placed on test. We feel that there is very low risk associated with this approach since there is considerable knowledge on both the gadolinium-selenide and lead-telluride performances and the combination of our P-type and lead-telluride as a couple. The combination of lead-telluride with gadolinium-selenide would be beneficial with even 0% gadolinium-selenide material, since the performance of $GdSe_x$ is not optimum in the 150-400°C interval.

TABLE VIII
MEASURED PERFORMANCE TO DATE
OF SEGMENTED Gd Se_x - Pb Te

SEGMENTED LEG TEST	HOT JUNCTION	COLD JUNCTION	S($\mu V/_{OC}$)	ρ (MΩ-CM)	K($MW/_{CM\ C}$)	P (WATTS)
PM057	800	150	200	4.90	11.4	215
PM062	800	152	190	4.75	12.4	204

* POWER NORMALIZED TO A 336 COUPLE CONVERTER OPERATING AT 850/150 AT 30V WITH MEASURED N-LEG $\frac{-}{S.}$ $\frac{-}{\rho}$ $\frac{-}{K.}$

N-Leg Cracking

In the recent disassembly of M-7 and GDS-I, a number of N-legs were observed to be cracked. As a result, concern has been expressed about the potential impact on mission performance. Even though N-legs in these converters were observed to be cracked, this cracking did not cause failure or even significant degradation. Degradation in these converters occurred as a result of P-leg resistance increase. This fact can easily be observed because individual elements were instrumented.

The ability of N-legs to resist significant dynamic loads has recently been demonstrated in single-couple vibration tests. A recent test demonstrated the ability of N-legs, which have been operated in the nominal temperature gradient, to survive a dynamic load of 23 g's. This type of testing will continue to further demonstrate the ability of N-legs to survive mission dynamic loads.

To more completely understand all of the stresses which are present within the N-leg, an analytical evaluation will be performed which will include the superposition of all thermally and mechanically induced stresses. A finite element stress analysis of the N-leg will be performed to evaluate more completely the effect of axial and radial temperature gradients on thermal stresses. This work is being performed for us by a 3M analytical support group (ES and T) using existing finite element computer programs.

For the near term, there is a hardware change which has been implemented which has the potential of significantly reducing the cracking. This is the use of a molybdenum gimbal instead of a tantalum gimbal. This has been shown to have less of a tendency to form a high temperature bond with the hot current strap, thereby retaining greater mobility. In a recent six-couple test (ATT 583), molybdenum gimbals were used and none of the N-legs were cracked during the 1100-hour duration of the test.

The processing experiments designed to decrease the extraneous resistance of the N-leg are also expected to increase the homogeneity of the material and consequently its strength. In particular, sintering more finely ground particles at a lower temperature should produce a uniform fine grained structure of higher strength. Isostatic pressing should also lead to strength increases by healing defects and possible microcracks.

To summarize, the following points bear on an understanding of the impact of N-leg cracking on the Galileo mission:

1. N-leg cracking has not caused module failure or significant degradation.

2. N-legs have survived several dynamic loads.

3. A modified hot end gimbal has shown significant potential to reduce mechanically induced stresses and cracking.

4. N-leg material processing changes have the potential of increasing basic material strength.

Dynamic Evaluation of Converter

The SIG/Galileo converter has been designed and will be tested to comply with the Galileo Project Detail Specification for RTG Design and Test Requirements (JPL Spec. ES512280).

The primary test environments for the converter will be those associated with random vibration and shock. Random test environments will continually be defined based on communication with Teledyne Energy Systems on the damping or amplification of the generator input. At the present time the random environments are used directly from the above spec.

Two types of vibration testing are occurring using converter hardware. These are single couple and 18-couple tests. These are operated at temperature and in an inert environment.

The demonstration of the ability of the SIG converter to survive the dynamic environments associated with the Galileo mission will be accomplished with a combination of analytical and experimental evaluations. Simplified analyses of the converter have shown a resonance to occur at approximately 170 Hz in a direction perpendicular to the generator axis. The resonant frequency is lower although still not characterized in a direction parallel to the axis. Component experiments are currently being fabricated to more accurately evaluate the resonant frequencies and damping coefficients for motions perpendicular and parallel to the generator axis. The experimentally measured spring rates, masses and damping coefficients will be included in a detailed dynamic model of the converter. This model is being constructed by an analytical support group within 3M (ES and T) which have existing dynamic modeling computer routines.

In addition to the analytical characterization described above, an ongoing effort to evaluate the converter experimentally has been proceeding.

The vibration module M-12 was subjected to a random vibration test environment. Converter performance was stable (i.e. there was no measurable degradation) during the 2g sine-sweeps (10 minutes) and during four minutes of random vibration, three of which were at greater than 0.5x of specifications. The failure that cut the test short was a failure of the housing and not of the converter.

The converter housing has been modified to alleviate the signal distortion problem and eliminate the possibility of recurring loss of atmosphere in future tests.

In addition to eighteen-couple module vibration testing, there have been seven single-couple vibration tests which have been exposed to a sinusoidal vibration at frequencies from 10 to 60 Hz. Most of these tests were conducted with a sliding follower configuration, but the most recent couple test utilized a compliant cold end hardware configuration of the type utilized in the Galileo reference design.

This couple was exposed to a sinusoidal vibration along three mutually perpendicular axes at 10, 20, 30, 40, 50, and 60 Hz. A ten-minute dwell occurred at each frequency for each axis. The amplitude was held constant as the frequency was changed. The maximum g-level was about 23 g's which is significantly greater than the 15 g (rms) level associated with vibration. There was no significant resistance degradation (changes less than 1%) during the test and, after disassembly, there was no observable degradation as a result of vibration.

Thus, the conclusion is that the compliant follower hardware which has the hot current strap and P-leg pinned to the hot frame (Galileo reference design) has the ability to withstand vibration environments with intensities greater than that which will be experienced during launch. To ensure the validity of this preliminary conclusion, additional testing must be performed with a complete generator and additional tests will also be run with 18-couple modules and single-couple modules. These tests are planned for this fiscal year.

Data Base and Degradation Modes

There has been considerable discussion about the data packages which were recently distributed. These data should be viewed as tests of some of the components which will be part of the flight converter. Since none of the modules or couples on test are of the flight design, it is necessary to separate out the performance of components such as the P-element, since the P-element will be changed very little in the flight design. In particular, it should be emphasized that P-leg Seebeck has been quite stable which is indicative that no chemical changes are occurring which would affect thermoelectric properties. The increase in resistances of the P-legs in some of the tests was caused by reduction in load pressure, indicating the need for reducing the friction in the follower. This lead to the design and incorporation of the bonded multi-layer follower system which was described in the section on cold end ΔT's.

The follower friction mechanism which was described at the recent Critical Action Conference was recently reinforced during the post-test disassembly of module M-7. This module had experienced a degradation due to P-leg resistance increase as have most modules which have the sliding follower. During diassembly of M-7 it became obvious that there was follower friction hang-up; most of the P-legs could be removed while the pile was under compression without any subsequent motion of the followers. Subsequent

evaluation of the springs in M-7 indicated that load relaxation has occurred. Thus, it was clear that hardware mobility which included follower friction as well as spring load relaxation was the cause of high P-leg resistance in M-7. To provide additional evidence to support this mechanistic explanation for the observed P-leg behavior, additional modules of a more recent vintage will be terminated and evaluated.

N-element Seebeck and resistivity has been affected in recent modules by the presence of the gadolinium electrode. This phenomenon was also described at the recent Critical Action Conference. The electrode has recently been changed to nickel to eliminate that problem. Thus, every module after M-18 will utilize nickel electrodes on the N-leg hot junction.

In addition to the component and single couple tests which have already been described, the majority of the data base for Galileo will be provided by a combination of three types of information. These include:

(1) Accelerated development tests.

(2) Accelerated tests of flight design to identify test conditions for reliability testing.

(3) Reliability tests which consist of 24 identical six-couple modules of flight design all operating at the same accelerated test condition.

A summary of the module test program is contained in Table IX. The accelerated development test series consists of M-21 through M-24 (M-A through M-F) and FM-1 and FM-2. The purpose of these modules is to identify the P-leg and N-leg configuration for SN-1 and SN-2 respectively.

The accelerated test series consists of a series of ten modules (five of which are M-25 through M-29). An additional five eighteen-couple modules must be added to this test series to complete the matrix. The test matrix consists of a statistically designed test series for a quadratic response which has test parameters which are summarized in Table X. The results of this test series will define a test condition which will accelerate degradation by a factor of 12. In this way the reliability test series will yield information predicting power degradation and P-leg weight loss for the 50,000 hour mission in approximately 4000 hours.

In summary, there is currently a limited data base on the flight design for Galileo. There is an extensive accelerated test program which will provide some data base information as early as the first quarter of 1979. Additional data will be obtained on accelerated testing until a reliability statement will be able to be made in the second quarter of 1980.

TABLE IX

Module Test Program

Module	T_h (°C)	I (amps)	Purpose	Planned Duration (hours)
M-21(A)	913	12	Development (Unpartitioned P-leg)	1000
M-22(B)	913	12	Development (Partitioned P-leg)	1000
M-23(C)	913	12	Development (N-leg Processing Change)	1000
M_23(E)	913	12	Development (Segmented N-Leg)	1000
M-23(F)	913	12	Development (Segmented N-Leg)	Indefinite
M-24(D)	913	12	Development (N-Leg Processing Change)	Indefinite
M-25	Defined by Accelerated Test Matrix		Accelerated Test	2500
M-26			" " " "	2500
M-27			" " " "	2500
M-28			" " " "	2500
M-29			" " " "	2500
M-30	850	8	Vibration Test	200
FM-1	913	12	Long Term Development	Indefinite
FM-2	913	12	Long Term Development	Indefinite
FM-3	850	8	Long Term	Indefinite
FM-4 7	Defined by Accelerated Tests		Reliability	4000
FM-8 11			Reliability	8000
FM-12 16			JPL Tests	--

TABLE X

Values of Independent Stress Variables for Accelerated Test Series

Variable	Range				
T_h (°C)	976	950	913	876	850
T_c (°C)	175	165	150	135	125
I(amps)	16	14.4	12	9.6	8

ATTACHMENTS

ATTACHMENT I

Wrapped P-Leg Assembly, SG17-10316

ITEM	BM	DRWG. NO.	REQ.	MAT'L.	COM'L	NAME
0	x	SG17-10316	0			P-Leg Assembly, Wrapped
1		SG17-10314	1			Capped P-Leg
2		SG17-10089-P1	1			Contacting Disc
3		C-1033	AR			Quartz Yarn

ISSUE	DATE AND CHANGE RECORD	BY	REV.	CH.
1	November 14, 1978	D. Brauer		

USED ON	TITLE
	P-Leg Assembly, Wrapped

PIONEERING LABORATORY
ELECTRICAL PRODUCTS GROUP
ST. PAUL, MINNESOTA

3M COMPANY

SHEET 1 OF 1 SHEETS

BM SG17-10316

FORM 16091-PWO

(3) WITH MIN-K/H_2O SLURRY (APPLY PER MSI #2008, SECTION 8.1.4)

(1)

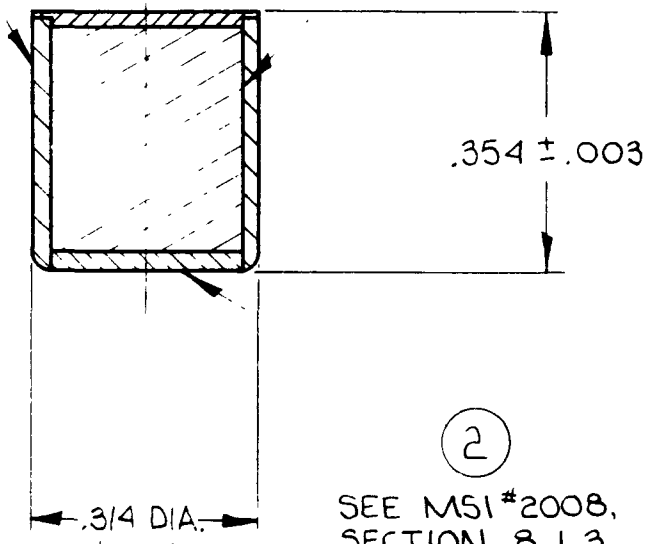

(2) SEE MSI #2008, SECTION 8.1.3 FOR BONDING PROCEDURE

REV	DATE	DESCRIPTION	BY	MF
1	11-14-78		db	

MATERIAL: SEE DETAIL DRAWINGS

FINISH:

UNLESS OTHERWISE SPECIFIED:
DIMENSIONS ARE IN INCHES
TOLERANCES
.0 ± 1 | .000 ± .005
00 ± .02 | ANGULAR DIM. ± 2°
- BREAK SHARP EDGES
- MACH. RADII (INSIDE) _____
- SURFACE ROUGHNESS ✓ MAX.

SCALE: 4X

WEIGHT (lbs.):

DR. BRAUER	11-14-78	I-2
CH.		
APPROVALS		
ENG. K [illegible]	[illegible]	
QC.		
MFG [illegible]		
MAT'L.		
PROG.		
SYS. [illegible]	11/20/78	
[illegible]	[illegible]	

PIONEERING LABORATORY
ELECTRICAL PRODUCTS GROUP
ST. PAUL, MINNESOTA
3M COMPANY

P-LEG ASS'Y WRAPPED

A | SG17-10316 | SHEET

BRUNING 40-22

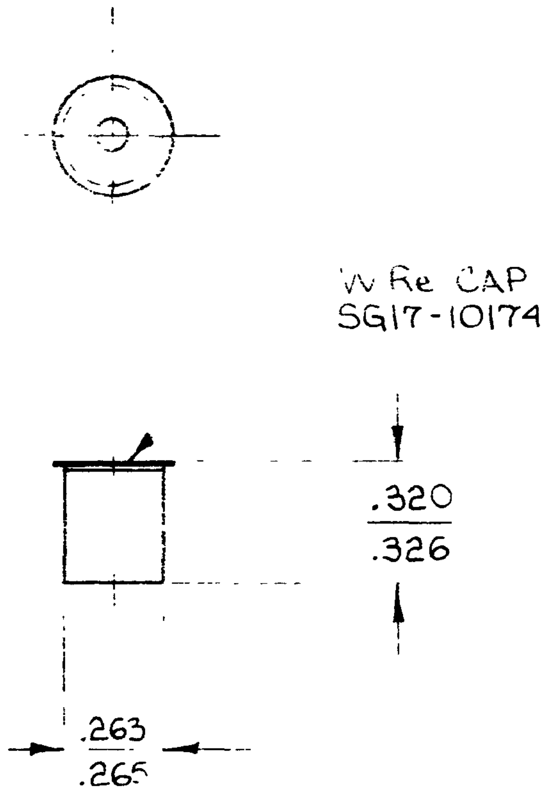

SEE MSI # 2008
SECTION 8.1.1 & 8.1.2
FOR PROCESSING AND
SPECIFICATIONS OF P-LEG

REV	DATE	DESCRIPTION	BY	MF
1	10-17-78		JB	

MATERIAL	FINISH
Cu-Ag-Se	

UNLESS OTHERWISE SPECIFIED:
DIMENSIONS ARE IN INCHES
TOLERANCES

.0 ± .1	.000 ± .005
.00 ± .02	ANGULAR DIM. ± 2°

- BREAK SHARP EDGES
- MACH. RADII (INSIDE) ______
- SURFACE ROUGHNESS ✓ MAX.

SCALE 2X

WEIGHT (lbs.)

DR.	BRAUER	10-17-78
CH.		
APPROVALS		
ENG.	[illegible signature]	[illegible]
QC.	[illegible signature]	[illegible]
MFG.	[illegible signature]	[illegible]
MAT'L.		
PROG.	[illegible signature]	
SYS.	[illegible signature]	11-10-78
REL.	[illegible signature]	11-[illegible]-78

PIONEERING LABORATORY
ELECTRICAL PRODUCTS GROUP
ST. PAUL, MINNESOTA
3M COMPANY

CAPPED P-LEG

A SG17-10314 SHEET

BRUNING 40-22

I-3

P NO.	DIAMETER	THICKNESS
P1	.265 DIA.	.032±.001
P2	.342 DIA.	.032±.001
P3	.265 DIA.	.010±.001

REV	DATE	DESCRIPTION	BY	MF
C	7-24-78	REVISED PER ECN # 0053	db	
B	1-16-78	REVISED PER ECN # 0027	Dwa	
A	10-25-77		Dwa	

MATERIAL: ETP COPPER CDA-110

FINISH:

UNLESS OTHERWISE SPECIFIED:
DIMENSIONS ARE IN INCHES
TOLERANCES
.0 ± .1 | .000 ± .005
.00 ± .02 | ANGULAR DIM. ± 2°
- BREAK SHARP EDGES
- MACH. RADII (INSIDE) _____
- SURFACE ROUGHNESS ✓ MAX.

SCALE: N/A

WEIGHT(lbs.):

APPROVALS		
DR.	Dwa	10-25-77
CH.		
ENG.	J. D. Hutchinson	11-10-77
QC.	W. A. Wald	11-14-77
MFG.	Brockman	11-14-77
MAR	R B Duncan	11-15-77
PEG	R. L. Ryall	11-17-77
REL	R. L. Ryall	12/8/78

PIONEERING LABORATORY
ELECTRICAL PRODUCTS GROUP
ST. PAUL, MINNESOTA
3M COMPANY

CONTACTING DISC

A | SG17-10089 | SHEET

I-4

BRUNING 40-22 33978

SUGGESTED SOURCE:
J.P. STEVENS & CO., INC.
1185 AVE. OF THE AMERICAS
NEW YORK, N.Y. 10036

ASTROQUARTZ
99.90% SILICA (SiO_2) YARN
60 STRAND, 7 MICRON DIA. STRAND
CONTINUOUS FILAMENT
WITH STARCH OIL BINDER
.5 TWIST PER INCH

REV	DATE	DESCRIPTION	BY	MF
A	1-4-78		DW	

MATERIAL: AS NOTED

FINISH:

UNLESS OTHERWISE SPECIFIED
DIMENSIONS ARE IN INCHES
TOLERANCES
0 ± 1 | 000 ± 005
00 ± 02 | ANGULAR DIM ± 2°
- BREAK SHARP EDGES
- MACH RADII (INSIDE)
- SURFACE ROUGHNESS ✓ MAX

SCALE: N/A

WEIGHT (lbs):

DR	Dwa	1-4-78
CH		
APPROVALS		
ENG	[signature]	1-24-78
QC	[signature]	1-30-78
MFG	[signature]	1-[illegible]-78
PE	[signature]	1-24-78
Mkt'l	RB Emerson	1/31/78
REL	[signature]	12/8/78

PIONEERING LABORATORY
ELECTRICAL PRODUCTS GROUP
ST. PAUL, MINNESOTA
3M COMPANY

QUARTZ YARN

A | C-1033 | SHEET

5-1

MATERIAL LIST			
ITEM	QUANTITY	NAME	MATERIAL

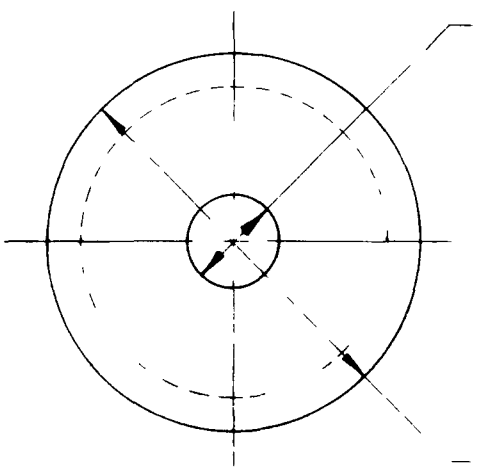

NOTE
3M PIONEERING LAB QUALITY CONTROL INSPECTION
RESISTIVITY PER Q.A. STD #4001
HARDNESS PER Q.A. STD #4002, E.S. #1009

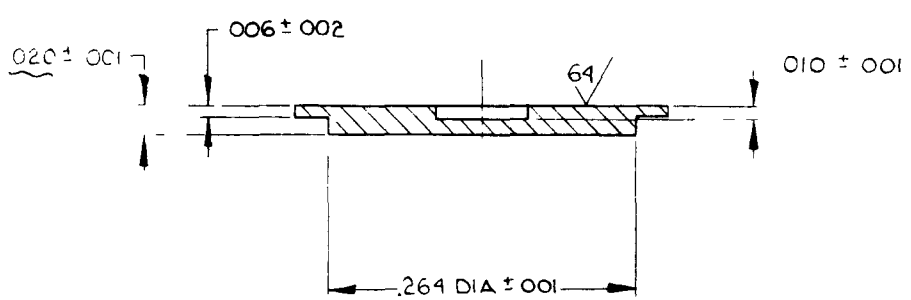

REV	DATE	DESCRIPTION	BY	MF
C	12-6-78	REVISED MAT'L & DIM. PER ECN #0089		
B	11-13-78	ADDED FINISH NOTE & Q.C. NOTE PER ECN #0080		
A	10-18-78	.020 DIM WAS .024"; .014 WAS .015, PER ECN #0074		
2	8 23 78	.320 DIA WAS .292"; .264 DIA. WAS .242		
1	6-30-78			

MATERIAL: TUNGSTEN-RHENIUM ALLOY W-25Re

FINISH:

UNLESS OTHERWISE SPECIFIED DIMENSIONS ARE IN INCHES
TOLERANCES
0 ± 1 | .000 ± .005
.00 ± .02 | ANGULAR DIM ± 2°
- BREAK SHARP EDGES
- MACH RADII (INSIDE) _____
- SURFACE ROUGHNESS ✓ MAX

SCALE: 10/1

WEIGHT (lbs):

APPROVALS		
DR	BRAUER	6-30-78
CH		
ENG	R. P. Brauer	8-10-78
QC	D. A. Wold	8/11/78
MFG	[illegible]	8-11-78
MAT'L	P. B. Brauer	8/23/78
PROG	[illegible]	[illegible]
SYS	[illegible]	8-11-78
REL	[illegible]	12/1/78

PIONEERING LABORATORY
ELECTRICAL PRODUCTS GROUP
ST. PAUL, MINNESOTA
3M COMPANY

STEPPED P-LEG CAP

ACTUAL SIZE

B | SG17-10174 | SHEET

BRUNING 40-22 33978

ATTACHMENT II

Process and Process Control Specifications of
Bonded Partitioned P-Elements, MSI-2008

3M COMPANY

ELECTRICAL PRODUCTS GROUP
PIONEERING LABORATORY

MANUFACTURING STANDARD INSTRUCTIONS

Issue Date 10/17/75 MSI 2008

Revised 8/7/78 Page 1 of 75

TITLE: PROCESS AND PROCESS CONTROL SPECIFICATIONS OF BONDED PARTITIONED P-ELEMENTS

APPLICABLE DOCUMENTS

This standard describes the product process and quality control procedures for the fabrication of partitioned bonded P-type TPM-217 thermoelectric contacted leg structures. The principle steps in the fabrication of TPM-217 thermoelectric bonded leg structures are:

- The synthesis and fabrication of TPM-217 pellet material.
- The bonding of tungsten-rhenium partitioning foils and hot end electrode foils.
- The ingradient bonding of copper cold end electrode contacts.
- Wrapping of bonded elements.

The processing procedures for these steps are described in Section I, indexed as 8.1.1, 8.1.2, 8.1.3 and 8.1.4 respectively. The corresponding quality control procedures and acceptance criteria are described in Section II.

R.B. Emmons 8/7/78
L.J. Thompson 8/7/78

Originator	Engineer	Materials	Quality / Product Control	Program
R.M. Semmelbeck 8/7/78	J.C. Hallman 10/10/78	J. Huck 8/8/78	R.B. Emmons 10/20/78	R.L. Pigel 10-20-78

FORM 18807-PWO

8.1.4 TPM-217 SUBLIMATION SUPPRESSION WRAPPING

SUMMARY OF METHOD:

The TPM-217 element with W-Re partitions and copper cold end electrode is wrapped on a coil winding apparatus with astroquartz yarn and Min-K 1800/water slurry.

APPARATUS AND MATERIALS:

Materials:

1. Astroquartz yarn - style 900 1/0/.5Z.
   - Starch oil binder.
2. Min-K 1800 slurry.
   - Formulation:
     1) 52.5 g. Min-K 1800 ground through a No. 10 sieve.
     2) 5 g. quartz wool.
     3) 110 ml. water.
     4) Mix components together in blender - mix until uniform - fluid consistency obtained - then mix another 10 minutes.

Equipment:

1. Hamilton Beach mixer or Oster blender.
2. No. 10 mesh sieve w/pan.
3. Bobifil ER-10 coil winder.
4. Amacoil Model P1 dereeler - tensioner.
5. Leg holding jig.
6. Tape.
7. Razor blade.
8. Small artist's brush.
9. Cotton swabs.
10. Tweezers with flat, curved jaws matching wrapping leg diameter.

PROCEDURE:

1. Clamp leg in jig with sufficient pressure to prevent rotation of jig with respect to leg. Only spindle and live center should rotate. Leg to be properly centered so that off axis motion does not exceed 0.030". When thick hot end legs are used the thick foil should be properly seated in the recessed face of the appropriate spindle jig half.

2. Adjust yarn guide pulley limits so that pulley travel matches length of leg to be wrapped.

3. Set pitch for minimum value (0.04).

4. Set spindle speed control at 4.

5. Set tensioner at 0.10.

6. Tape yarn end to one side of jig.

7. Take enough turns to start the yarn around the leg until it has wrapped over itself several times. Spindle should be rotated by hand during this step.

8. If slurry has thickened since last use, remix until original consistency is obtained. Addition of water should not be necessary.

9. Dampen the brush with water - then use it to apply a coating of slurry to the entire leg surface.

10. Reset counter on winder. Preset counter according to:

Counter Preset for Various Leg Geometries
(Assumptions: 1.0×10^4 turns/cm^2)

Leg Winding Length (")	0.025" Thick		0.030" Thick	
	Turns	Counter	Turns	Counter
.280	450	225	542	271
.285	460	230	552	276
.290	468	234	561	280
.295	475	238	571	285
.300	485	243	581	290
.305	492	246	590	295
.310	500	250	600	300

11. Reset counter and continue rotation in manual mode - removing excess slurry from leg until a smooth surface just revealing the outer yarn turns is evident.

12. Cut starting end of yarn where it passes from jig to leg.

13. Unclamp leg allowing it to drop into a gloved hand. If necessary, gently pry it from the jig faces using a properly formed tweezers to hold the leg.

14. If any turns have wrapped over the faces of the leg, carefully trim them off with sharp razor blade and smooth the cut ends around leg with cotton swab. Adjust number of turns and/or winding travel limits to correct this condition on subsequent legs.

15. Clean the leg faces with damp and dry cotton swabs to remove all residual traces of slurry.

16. Allow wraps to air dry overnight (at least 15 hours).

17. Load the air-dried, wrapped TPM-217 elements into an Al_2O_3 tray for vacuum processing. Place wrapped elements and Al_2O_3 tray into a quartz tube and connect to high temperature vacuum station:

    - Evacuate furnace tube to $\leq 3 \times 10^{-6}$ torr.
    - Slowly heat the quartz tube to 150° $\pm$ 20°C (rate should be such that pressure inside tube never exceeds 3×10^{-5} torr).
    - Maintain 150° $\pm$ 20°C at a pressure of $\leq 5 \times 10^{-7}$ torr for two (2) $\pm$ 0.2 hours.
    - Furnace cool-down while under vacuum.

19. Submit processed legs for inspection as described by QA STD 2022.

20. Store in bonded stock under an inert atmosphere until ready for assembly into modules.

ATTACHMENT III

P-Leg Assembly Wrapped Elements
QA-STD-2022

FORM 16118-PWO

3M COMPANY

ELECTRICAL PRODUCTS GROUP
PIONEERING LABORATORY

QUALITY ASSURANCE STANDARD INSTRUCTION

Issue Date 9-7-78 QA-STD 2022

Revised Page 1 of 2

TITLE: P-LEG ASSEMBLY: WRAPPED ELEMENTS

APPLICABLE DOCUMENTS

MSI 2008 P-LEG ASSEMBLY PROCESSING PROCEDURE; Process and Process Control Specification of Bonded Partition P-Elements

1.0 PURPOSE AND SCOPE

To provide general instructions for inspecting P-leg assemblies (wrapped).

This procedure applies specifically to the dimensional and weight characteristics.

The inspection sample shall represent a specific lot or batch.

2.0 GENERAL

Engineering specifications are used to determine the acceptance and rejection points.

3.0 EQUIPMENT REQUIRED

- Ex-Cell-O Contour Projector
- Torbal balance Model ET-1 or equivalent
- Tweezer

4.0 PROCEDURE

4.1 PRIOR TO INSPECTION

P-legs (wrapped) will be processed per MSI 2008 - 8.1.4

4.2 INSPECTION - 100% Inspection

NOTE: P-legs are to be handled with a tweezer only, and handled gently.

4.2.1 Dimensionally Check:

Wrapped diameter with the Ex-Cell-O Comparator. Measure the diameter at the top, middle, and near the bottom (before the wrap tapers down). Record the average.

Originator	Dept. Mgr.	Q. C. Sup'r.	Materials	Product Control
9/8/78	R. D. Lyle 9-8-78	Wardell 9/8/78	Skench 9/8/78	RB Emerson 9/8/78

Title:	QA-STD 2022
	Page 2 of 2

4.2.2 Weight:

Measure and record

4.2.3 Wrap Length:

Measure to see if there is any amount of the P-leg unwrapped with the Ex-Cell-O Comparator; record. Subtract this measurement from the bonded length to determine the wrapped length, and record.

4.2.4 Wrap Thickness - .020 to .030 inches.

Determine the wrap thickness by subtracting the orginal diameter (which is the average of the top and bottom diameter) from the wrapped diameter. Record data.

4.2.5 Wrap Density - Greater than or equal to 0.90 g/cc:

Determine the wrap density by the following formula; record value.

$$W.D. = \frac{(\text{Weight Wrapped}) - (\text{Weight Original})}{\pi/4 \left[(\text{dia. wrapped})^2 - (\text{dia. Original})^2\right] (\text{Length wrap}) (2.54^3)}$$

4.2.6 Turns Density - Greater than or equal to 1.0×10^4 turns/cm^2

Determine the turn density by the following formula; record value

$$T.D. = \frac{\text{No. Turns}}{(\text{length of wrap}) \times (\text{wrap thickness}) \times (2.54^2)}$$

4.3 DISPOSITION OF INSPECTED LEGS

Any legs failing to meet the acceptance criteria will be taken from the lot, rejected and tagged as such.

Any legs meeting the acceptance criteria will be tagged QC approved.

4.4 POST INSPECTION

P-legs will be immediately stored in an inert atmosphere in bonded stock.

ATTACHMENT IV

Knudsen Cell Equilibrium Experiments

A. INTRODUCTION

Two types of experiments were performed to increase knowledge of the thermodynamic stability of the TPM-217 system. One type of experiment involved the measurement of the effusion of ions from a Knudsen cell using a mass spectrometer. Since the aperture of the Knudsen cell is much smaller than the surface area of the sample, this measurement determines equilibrium partial pressures. The second type of experiment involved the measurement of the weight loss of a sample during free evaporation. In this case, which is closer to generator operating conditions, kinetic effects can reduce the weight loss significantly below that calculated from equilibrium partial pressures, particularly for baffled legs.

In this section, the Knudsen cell mass spectrometer measurements leading to the determination of the fourth power dependence of selenium partial pressure on composition and Knudsen cell data on partitioned and non-partitioned elements are summarized.

B. EXPERIMENTAL RESULTS

The addition of a selenium atom to the copper selenide lattice creates two vacancies of positively charged copper ions and two mobile holes:

$$1/2\ Se \rightarrow 2V_{Cu}{}^{+} + 2h \qquad (1)$$

The proportionality between excess selenium and hole concentration has been verified by doping studies in which elements with a systematic variation of excess selenium (y) have been prepared. The resistivity of these samples was inversely proportional to y and the Seebeck coefficient was proportional to $-\ell$ ny, which is the behavior predicted from equation (1).

The observed doping mechanism also implies a specific relation between Se_2 partial pressure and carrier concentration if the additional assumption* is made that the high degree of disorder of copper ions in even the ideal stoichiometry of Cu_2Se renders the chemical potential of the copper ions independent of small deviations in the Se/Cu ratio. The difference in chemical potential between two equilibrium states at different partial pressures (P_1 and P_2) of selenium is given by

$$1/2\ \Delta\mu Se_2 = 2\ \Delta\mu V_{Cu}{}^{+} + 2\Delta\mu h \qquad (2)$$

---

* J. Bruck Wagner and Carl Wagner, J. Chem. Phys., 26 (1702 (1958).

The difference in chemical potential of the selenium gas in the two states is the logarithm of their partial pressure ratio:

$$\Delta\mu_{Se_2} = kT \ln P_2/P_1 \tag{3}$$

The chemical potential of the holes is directly proportional to the logarithm of the hole concentration, which is in turn directly porportional to the excess selenium in the extrinsic region with no other acceptors present:

$$\Delta\mu_h = kT \ln \frac{[h_1]}{[h_2]} = kT \ln \left(\frac{Y_2}{Y_1}\right) \tag{4}$$

Under Wagner's assumption, $\Delta\mu_{Cu^+}$ is negligible because of the high intrinsic defect concentration, so this leads to a fourth power dependence of selenium partial pressure on excess selenium concentration

$$P_2 = P_1 \left(\frac{Y_2}{Y_1}\right)^4 \tag{5}$$

This equation has been investigated using a mass spectrometer to measure the ion current, 1^+, of mass specie evolving from a Knudsen cell at temperature, T(^oC), after the gas molecules have been ionized by an electron beam and the resulting ionized molecules accelerated down the time-of-flight chamber of the Bendix mass spectrometer. The equilibrium partial pressure of any given mass specie, i, evolving from the solid sample in the Knudsen cell is given by

$$P_i = K_i \, I + T\,(i) \tag{6}$$

where

P_i is the equilibrium partial pressure of mass specie i,

K_i is the proportionality constant for specie i, (a function of the mass spectrometer characteristics and Knudsen cell aperture size)

I+T (i) is the product of the ion current for specie i and the absolute temperature T(^oK) of the Knudsen cell.

Since the partial pressure of selenium in the Knudsen cell is directly proportional to the beam current measured in the mass spectrometer, the equation to be experimentally verified is

$$I+T\,(Se_2) \propto Y^4 \tag{7}$$

The Bendix time-of-flight mass spectrometer was used to measure the I+T values for the volatile constituents effusing from the graphite Knudsen cell for three samples covering the composition range $.029 \leq Y \leq .081$ where Y specifies the excess selenium content in a given sample according to the formula $Cu_{1.97}Ag_{.03}Se_{1+y}$. These samples are described in Table I. I+T values were recorded as a function of time and temperature for any volatile species evolving from each sample in the Knudsen cell. The only volatiles observed from these samples were Se_2, Se, Ag, and Cu with the Se_2 predominant. The $I+T(Se_2)$ values for Se_2 gas are plotted in Figure 1 as the logarithm of $I+T(Se_2)$ versus the reciprocal of the absolute temperature ($1/T°K$) of the sample in the Knudsen cell. It is assumed that the straight lines shown are the best fit of the data and points on these lines will be used for further calculations.

In order to verify equation (7), it was written in the form $\log I+T(Se_2) \propto n \log y$ (8)

The method of least squares was applied to the $I+T(Se_2)$ and y data to evaluate the value of n in the above equation. According to equation (7), n should have a value of 4. To avoid errors due to excitation of intrinsic carriers at high temperatures and low excess selenium levels, which would modify equation (4), only $I+T(Se_2)$ values at 800°C will be considered for the least squares calculation. The data are listed in Table II.

TABLE II. Measured $I+T(Se_2)$ Values at 800°C on the Calibration Samples.

Sample Designation	y as Prepared	Measured $I+T(Se_2)$ at 800°C
SAC-43	0.0081	6.90×10^{-8} amps °K
SAC-44	0.0045	4.75×10^{-9} amps °K
SAC-45	0.0029	1.35×10^{-9} amps °K

TABLE I. Calibration Samples for Knudsen Cell Effusion/Mass Spectrometric Studies

Sample Designation	Excess Se y as Prepared	Sample Condition	Weight of Sample used in Mas Spectrometer Run
SAC-43 17169-11B Section C, 0.18 at.% excess Se	0.0081	Cylinder ~ .75 long x .20 dia.	1.01266 grams
SAC-44 17144-56A Section C, 0.10 at.% excess Se	0.0045	"	1.01258 grams
SAC-45 17144-56B Section C, 0.065 at.% excess Se	0.0029	"	1.02325 grams

FIGURE 1.

Se_2 Ion Current (I+) x Temperature (T°K) vs 1/T °K

Slug Samples of $Cu_{1.97}Ag_{0.03}Se_{1+Y}$

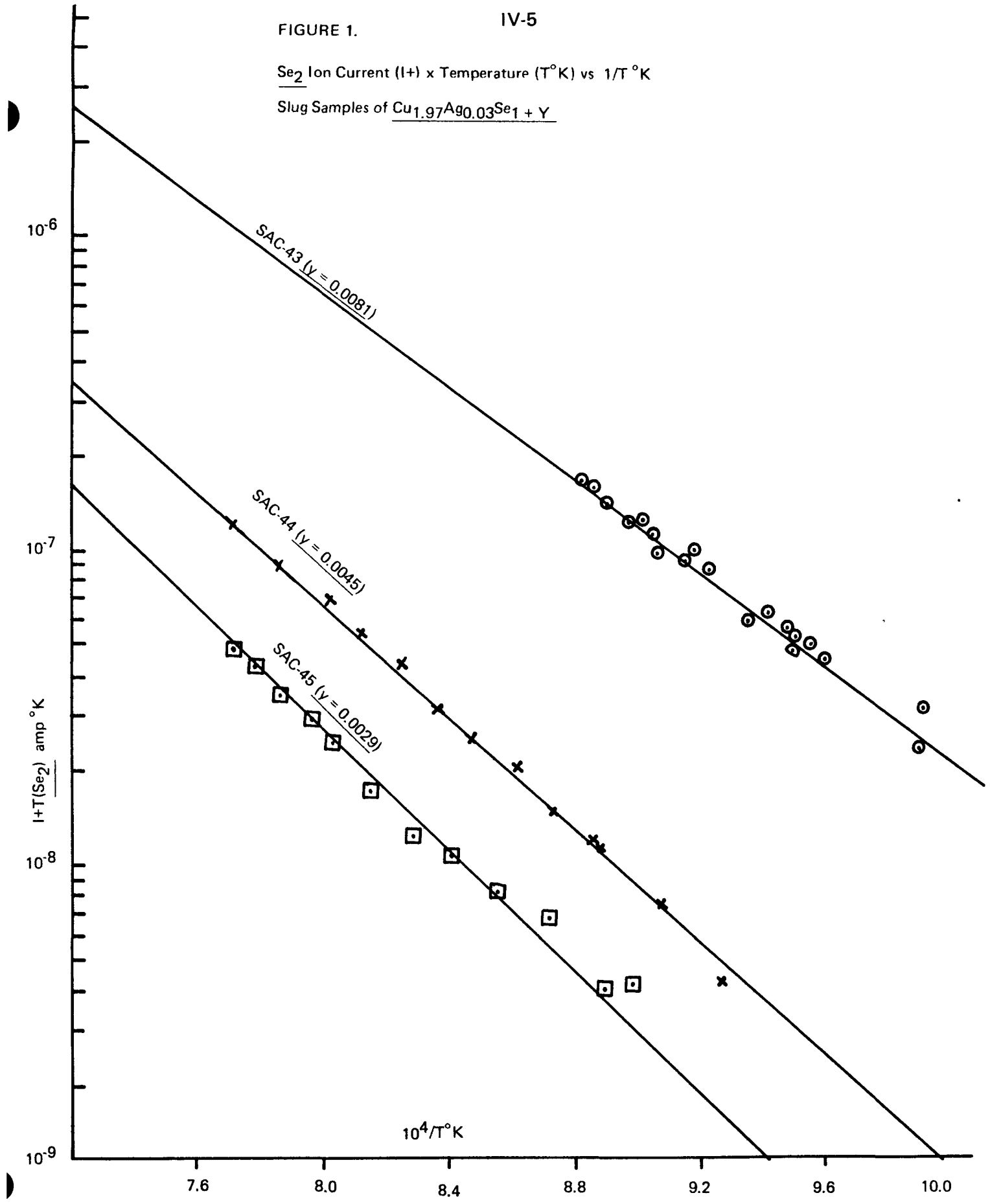

FIGURE 2. Dependence of Se_2 ion current (I+) x temperature (T°K) on Composition (y) in $Cu_{1.97}Ag_{.03}Se_{1+y}$

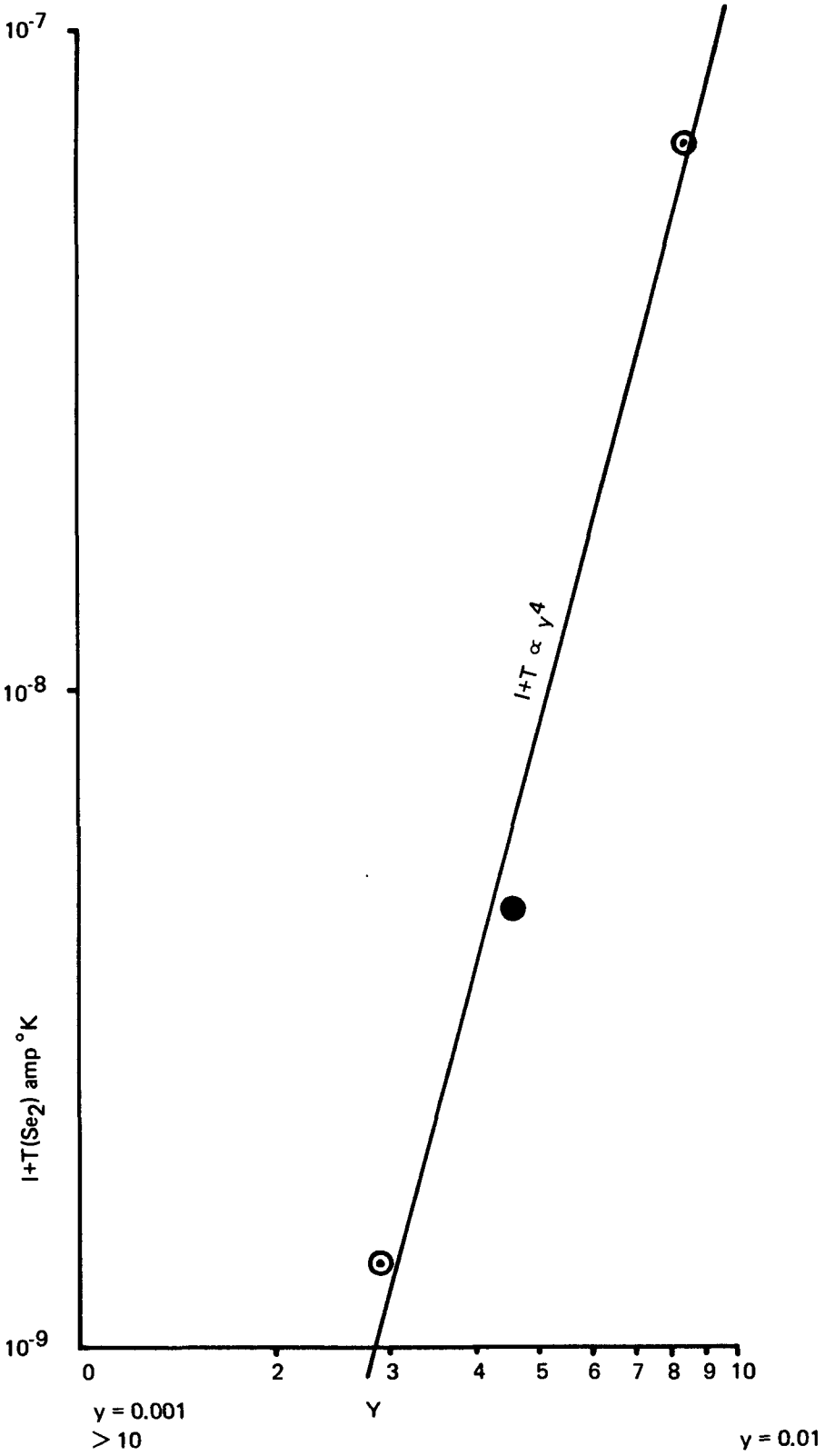

A least squares calculation using the $1+T(Se_2)$ and y data for samples SAC-43, SAC-44, and SAC-45 in Table II gives the value n = 3.9, which is in excellent agreement with the predicted value of 4 in equation (7). A curve fit of the data in Table II using the fourth power relation is given in Figure 2.

The fourth power dependence of vapor pressure on excess selenium was checked by a second, independent method. Instead of preparing a series of samples at different compositions, the composition of a single sample was altered directly in the Knudsen cell by volatilization of Se_2. A series of four runs was made on sample SAC-43 and the data on $1+T(Se_2)$ and temperature, T, are plotted in Figure 3 as log $1+T(Se_2)$ versus $1/T°K$. The composition for Run 1 was the composition of the sample as prepared for which the excess selenium content is described by y = 0.0081.

At the end of Run 1, the sample was held at 1000°C in the Knudsen cell for sufficient time so that the excess selenium content would decrease to a new value due to the volatilization of selenium from the sample. The amount of selenium lost is directly proportional to the time integral of $1+T(Se_2)$. Since the change in excess selenium is also proportional to the amount of selenium lost, we have for the difference in excess selenium between Runs 1 and 2:

$$Y_1 - Y_2 = \int_{t_1}^{t_2} K_\ell \frac{1+T(Se_2)}{T^{1/2}} dt \qquad (9)$$

where K_ℓ is the unknown proportionality constant.

FIGURE 3.

Se_2 Ion Current (I+) x Temperature (T°K) vs. $1/T°K$

Slug Sample of $Cu_{1.97}Ag_{0.03}Se_{1.008}$

SAC-43 (y = 0.0081)

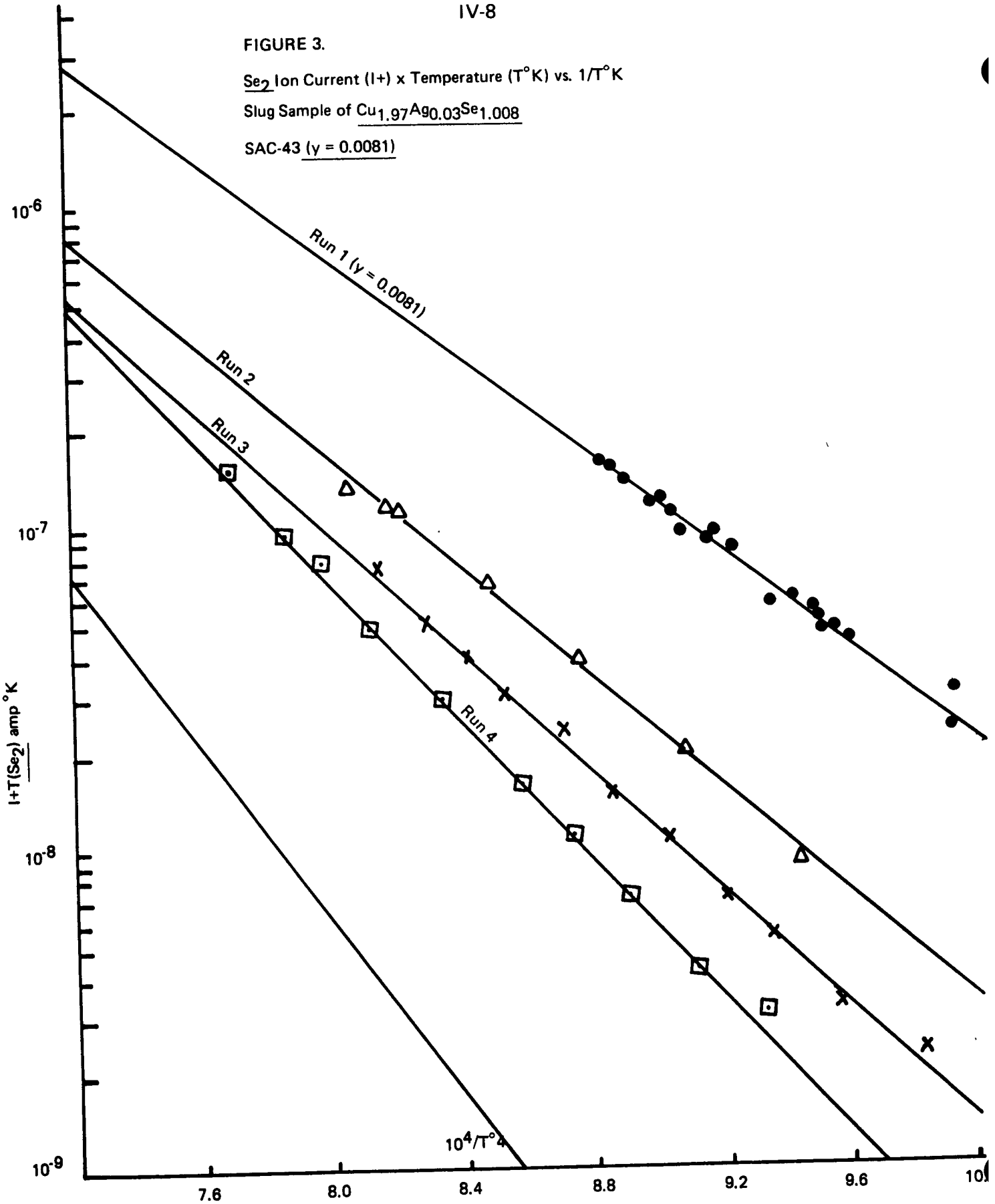

FIGURE 3: Dependence of Se_2 Partial Pressure on Carrier Concentration and Temperature

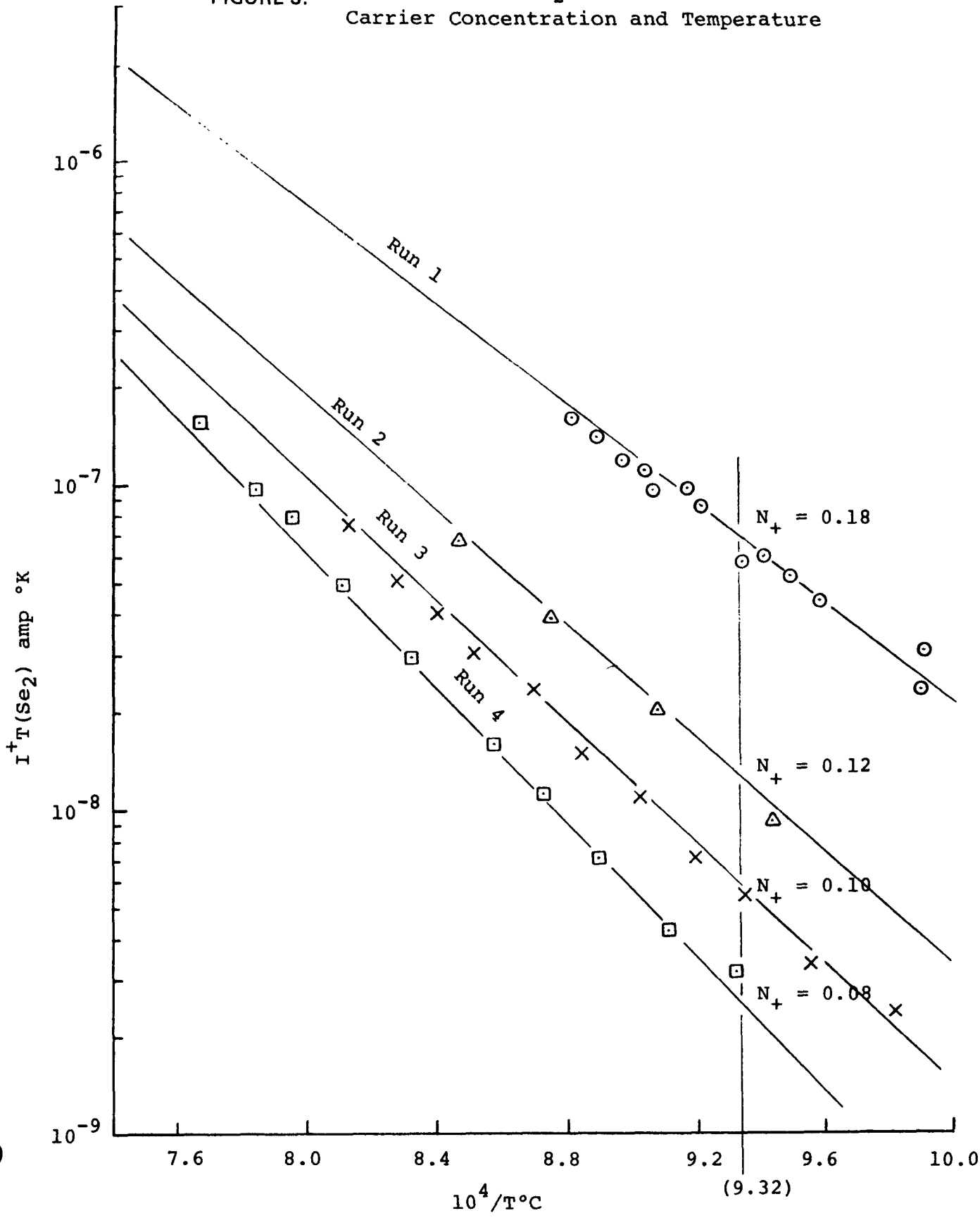

After each run, the excess selenium was decreased by holding the Knudsen cell containing the sample at elevated temperature and monitoring the amount of selenium lost with the mass spectrometer as indicated above.

The values of $I+T(Se_2)$ at 800°C can be used as a measure of the y values for the various runs by assuming a power log relation:

$$\frac{Y_2}{Y_1} = \frac{[I+T(Se_2)]_2}{[I+T(Se_2)]_1}^{1/n} \qquad (10)$$

The object is to use the data in Figure 3 to determine both n and K_ℓ .

Using equations 9 and 10, we can relate n and K_ℓ for Runs 1 and 2 by the equation:

$$1 - \frac{[I+T(Se_2)]_2}{[I+T(Se_2)]_1}^{1/n} = \frac{K_\ell}{Y_1} \int_{t_1}^{t_2} \frac{I+T(Se_2)}{T^{1/2}}\, dt \qquad (11)$$

To similar equations hold for the Runs 1 and 3, and Runs 1 and 4, which provides three equations to determine the two unknowns, K_ℓ and n. The data taken from Figure 3 which were used to determine n and K_ℓ are given in Table III. The values of

$$\int_{t_1}^{t_2} \frac{I+T(Se_2)}{T^{1/2}}\, dt$$

were obtained by graphical integration of I+, T, and t data.

TABLE III. Calculated Parameters from SAC-43 Multiple Run Used to Determine n and K_ℓ Values

Run	$I+T(Se_2)$ at 800°C (amps °K)	$[I+T(Se_2)]_r$ / $[I+T(Se_2)]_1$	$\int_{t_1}^{t_r} \frac{I+T(Se_2)\,dt}{T^{1/2}}$ (amps (°K) $^{1/2}$ sec)
r = 1	6.90×10^{-8}	–	–
r = 2	1.34×10^{-8}	0.1942	1.482×10^{-4}
r = 3	6.15×10^{-9}	0.08913	2.052×10^{-4}
4 = 4	2.70×10^{-9}	0.03913	2.472×10^{-4}

Three equations of the form of equation (11) were obtained from the data in Table III which were used to determine the best values of n and K_ℓ / Y_1. To carry out the calculations, various values of n were assumed ranging from 3.8 to 4.8 and corresponding average values of K_ℓ / Y_1 and percent average deviation of K_ℓ / Y_1 were calculated. A value of n = 4.3 gave a minimum percent average deviation in K_ℓ / Y_1 of 0.9%. We feel that this value for n is within our experimental error of the predicted value of 4 and therefore verifies the predicted value.

If the value of n is taken as 4, the value of the constant

$\frac{K_{\ell}}{Y_1}$ is found to be

$$\frac{K_{\ell}}{Y_1} = 2242 \text{ amps}^{-1} \cdot (^{\circ}\text{K})^{-1/2} \cdot \text{sec}^{-1}$$

Table IV compares the compositions (y in $cu_{1.97}Ag_{0.03}Se_{1+y}$) of runs 1, 2, 3, and 4 as obtained from the $[I+T(Se_2)]/[I+T(Se_2)]$ ratio (equation 10 with n = 4) with the values obtained through using the integrated material loss (equation 9 with $K_{\ell}/Y_1 = 2242$). It is clear from this table that the two methods of calculating composition are in excellent agreement.

TABLE IV

Run	y from I+T Ratio	y from integral
r = 1	.00810*	.00810*
r = 2	.00538	.00541
r = 3	.00426	.00437
r = 4	.00360	.00361

The conclusion drawn from this Knudsen cell work is that the dependence of equilibrium selenium partial pressure on the fourth power (equation 7) of the excess selenium (y) has been established by two independent Knudsen cell mass spectrometer techniques.

* As fabricated initial composition.

The initial Knudsen cell mass spectrometer vapor pressure studies summarized here showed that the vapor pressure increases as the fourth power of the excess selenium content. The lowest selenium partial pressure occurs at the lowest attainable excess selenium content in the single phase region, which occurs at the boundary of the single phase region. If a specimen is prepared with less selenium than this limit, a second phase of essentially free metal is formed, while the selenium content of the $Cu_{1.97}Ag_{.03}Se_{1+y}$ phase remains the same as at the boundary of the single phase region.

Knudsen cell mass spectrometer vapor pressure measurements were made on samples prepared at this limiting, "two phase" composition. Figure 4 exhibits this data together with vapor pressure data obtained for several samples with a fixed excess selenium level prepared in the same time period.

The data is Figure 4 has been converted from the experimentally observed parameters of ion beam current times temperature (I+T) to Se_2 partial pressure using the proportionality constant derived from the correlation between integrated beam current, change in partial pressure, and Knudsen cell orifice as calibrated by silver effusion.

Comparison of the Partial Pressures of Copper and Silver over $Cu_{1.97}Ag_{0.03}Se_{1+y}$ with the Partial Pressures of Pure Copper and Silver

Mass spectrometer measurement of I+T values for copper and silver were made concurrently with those for selenium on the Knudsen cell volatilization studies on the samples listed in Table V. The data are plotted in Figure 5 for the measurements on copper vapor, and in Figure 6 for the measurements on silver vapor. Measurements for pure copper metal are also shown in Figure 4, and measurements on pure silver metal are shown in Figure 6; this data was used to determine the proportionality factor for converting beam current (I+T) into vapor pressure for copper and silver. Evidently, the vapor pressures for copper and silver over $Cu_{1.97}Ag_{0.03}Se_{1+y}$ are not very sensitive to changes in the excess selenium content, y, as opposed to the I+T values for selenium which are quite sensitive.

The data for copper vapor pressure at different selenium contents, y, (Figure 5) are consistent with a single copper vapor pressure curve having the same slope and value as that of pure copper.

The silver vapor pressure data (Figure 6) also shows only minor variations with excess selenium content, y, in $Cu_{1.97}Ag_{0.03}Se_{1+y}$, but are lower than the pure silver vapor pressure curve by a factor of about 25.

Figure 4. Selenium Vapor Pressure for $Cu_{1.97}Ag_{.03}Se_{1+y}$
Comparison of Two-Phase Composition with High Excess Selenium Composition

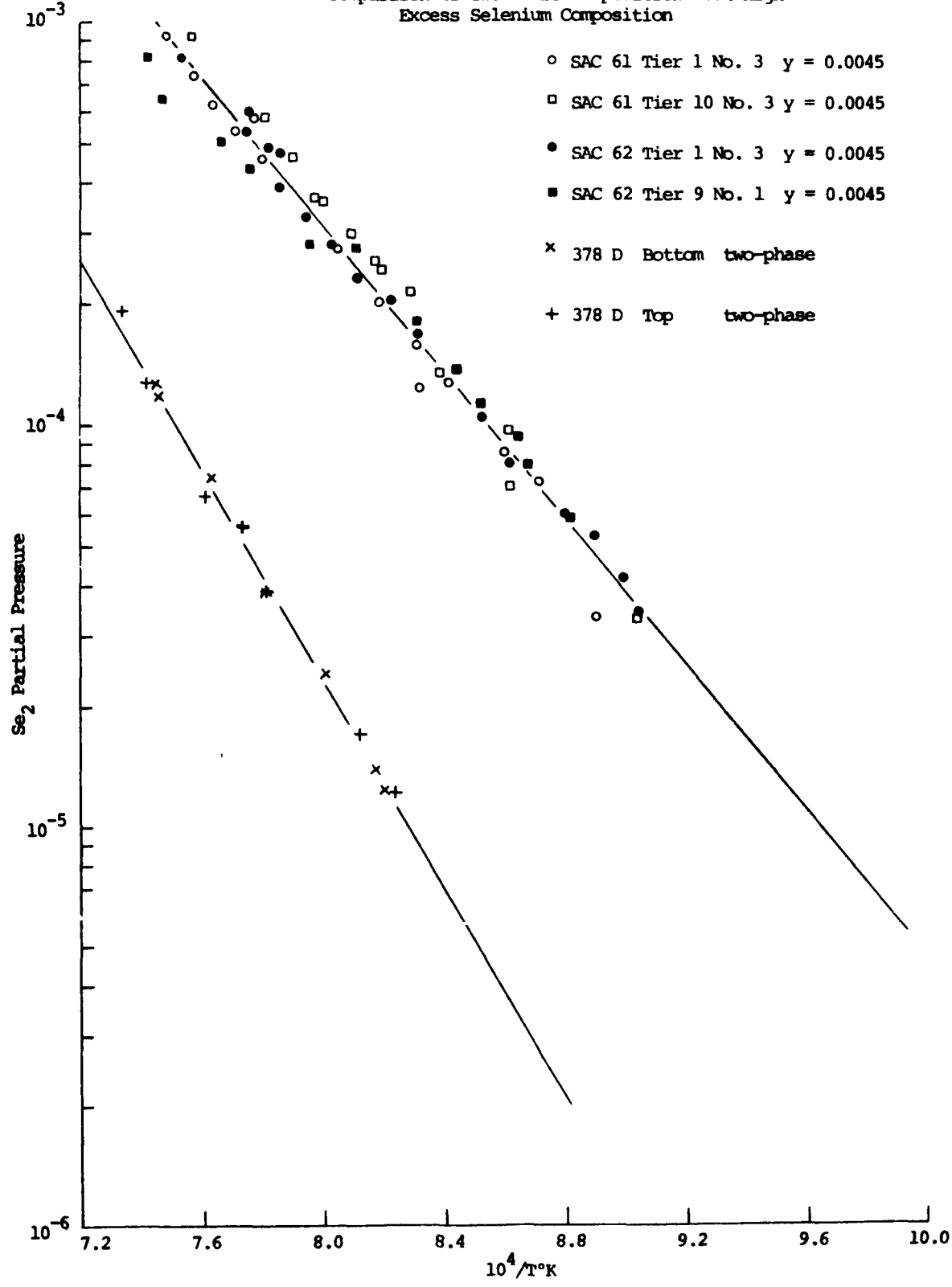

Figure 5. Copper Vapor Pressure for Pure Copper and for $Cu_{1.47}Ag_{.03}Se_{1+y}$

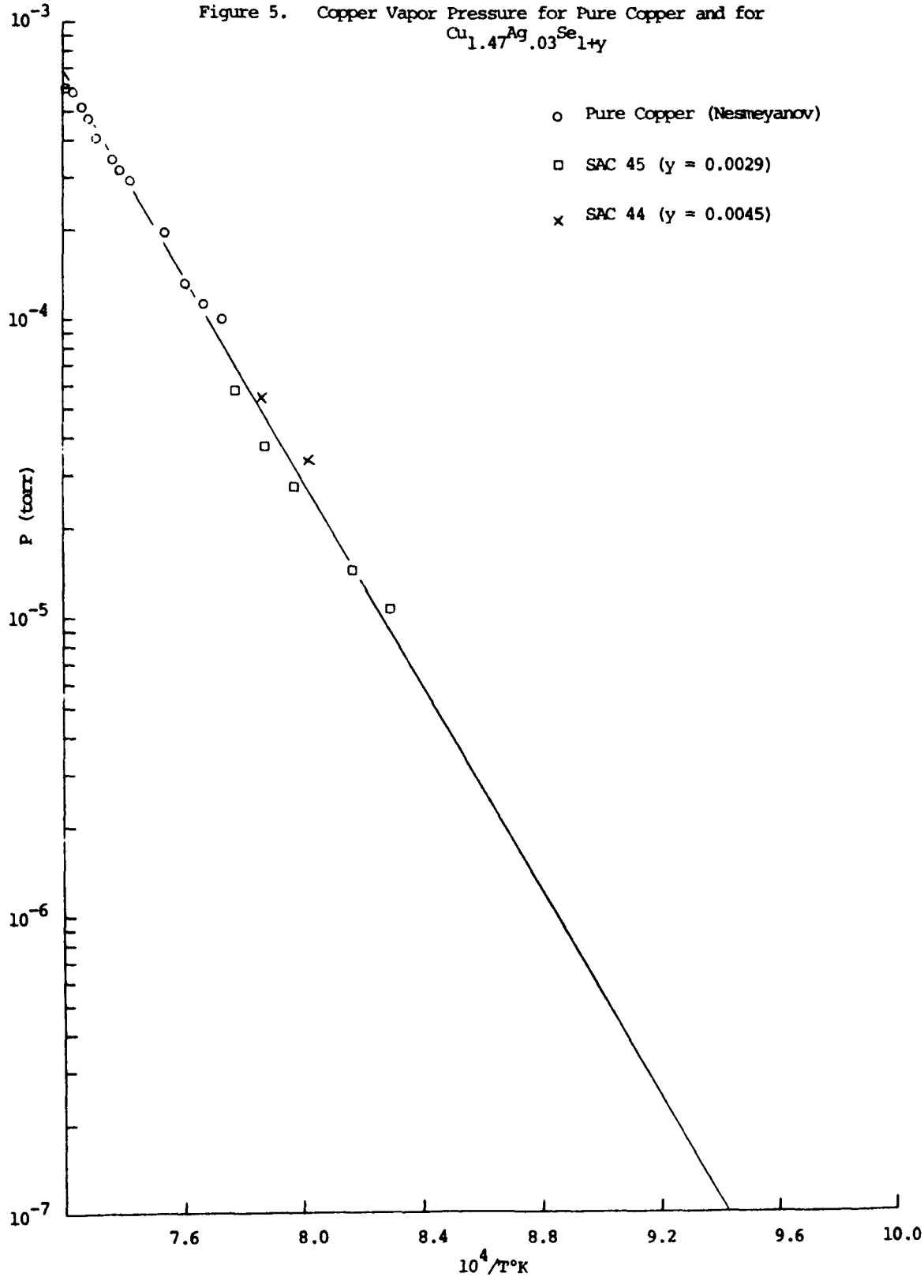

Figure 6. Silver Vapor Pressure for Pure Silver and for $Cu_{1.97}Ag_{.03}Se_{1+y}$

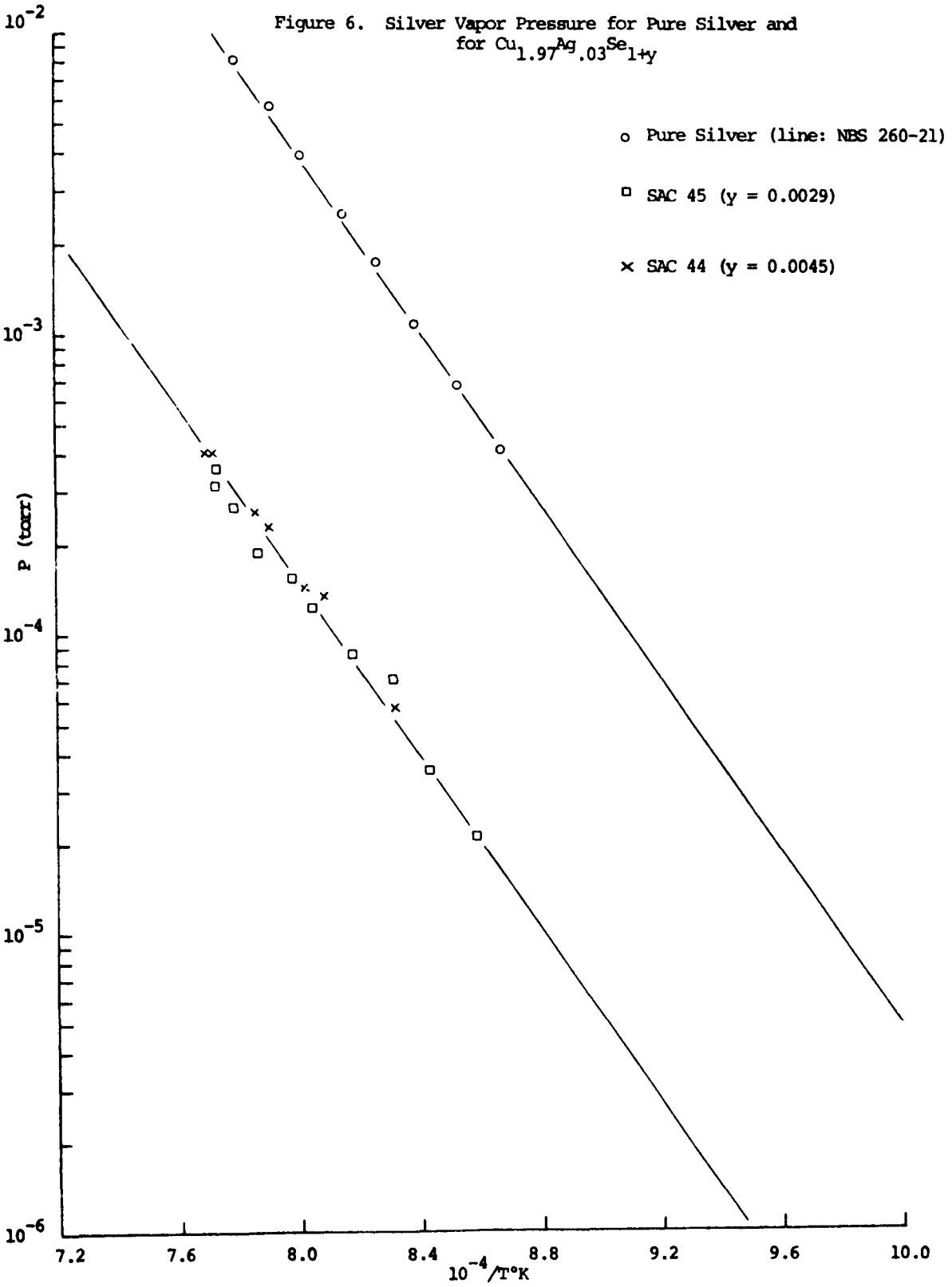

ATTACHMENT IV–A

Accelerated Testing for P-Leg Lifetime Projection

The expected lifetime of wrapped P-legs is projected by extrapolation of measured leg ingradient performance under conditions close to design operating conditions. To speed up the acquisition of data, moderate departures from design temperatures and current are used to provide a moderate acceleration of the testing. This attachment summarizes the data base for the two principal accelerating variables, temperature and current, as they affect P-leg sublimation. In considering these mechanisms, it should be born in mind that since the technique is to extrapolate lifetime using only moderate acceleration conditions, the precision required for the model is much less rigorous than would be the case for calculation of lifetime from more fundamental data.

Effect of Temperature

The effect of temperature on accelerating P-leg sublimation is straightforward and well documented. What is required is the dependence of weight loss rate on sublimation. Both 3M and Gulf Atomics have measured the vapor pressure of P-legs using the Knudsen cell/mass spectrometer technique. The results were similar: selenium is lost primarily as the specie Se_2, with a thermal activation of the form

$$P_{Se_2} \propto \exp\left[\frac{-29,700}{T}\right]$$

The free evaporation weight loss rate has also been measured by 3M, Gulf Atomics, and JPL. The temperature dependence of the free evaporation weight loss determined by JPL* is

$$R \propto \exp\left[\frac{-27,200}{T}\right]$$

which is in reasonably good agreement with the independent Knudsen cell partial pressure measurements. For operation at 900°C instead of the nominal 850°C, the acceleration is about 3 based on either isothermal Se_2 partial pressure or direct isothermal weight loss measurements. This lends a high degree of confidence to the use

of moderate temperature acceleration factors for projecting ingradient lifetime performance.

* G. Stapher, "Selenide Isotope Systems Design Review," JPL, Pasadena, CA, May 24-27, 1977.

Effect of Current

Before discussing some of the more technical aspects of this mechanism, three (3) simple facts should be clearly stated:

1) The weight loss rate can be accelerated by current
2) This effect was predicted and described before it was measured
3) The relative acceleration factors used for lifetime projections from ingradient measurements are very modest, on the order of 3, not several orders of magnitude.

The model for the acceleration of weight loss rate has two basic components. The first principle is that the rate of weight loss increases as the fourth power of the hole concentration. As described in Attachment IV, the fourth power dependence of Se_2 partial pressure on hole concentration was derived from Knudsen cell partial pressure measurements. The assumption is then, that for any position (x) in the leg, the rate of Se_2 loss (R) is proportional to the hole concentration (N). is proportional to the hole concentration (N).

$$R(x) \quad \propto \quad N(x)^4$$

The second principle is that the hole concentration N (x) is itself a function of current. The approximate form for this current dependence is.

$$N(x) = N(0) + B\, {}^{iL}/_{A}\, \left(\frac{Tm}{773}\right)^{2/3} x,$$

which was derived essentially from the doping model of Wagner**. This variation of hole concentration with current has been observed by measuring the change of Seebeck coefficient and resistivity with applied current, as in Figures IV a-1 and IV a-2.

Combining these two relations leads to the current acceleration effect on weight loss.

** See J. B. Wagner, C. Wagner "Investigations on Cuprous Sulfide," J. Chem. Phys. 26 , 1602 (1957).

Also:

G. Lorenz, C. Wagner, "Investigations on Cuprous Selenide and Copper Tellurides," J. Chem. Phys. 26, 1607 (1957)

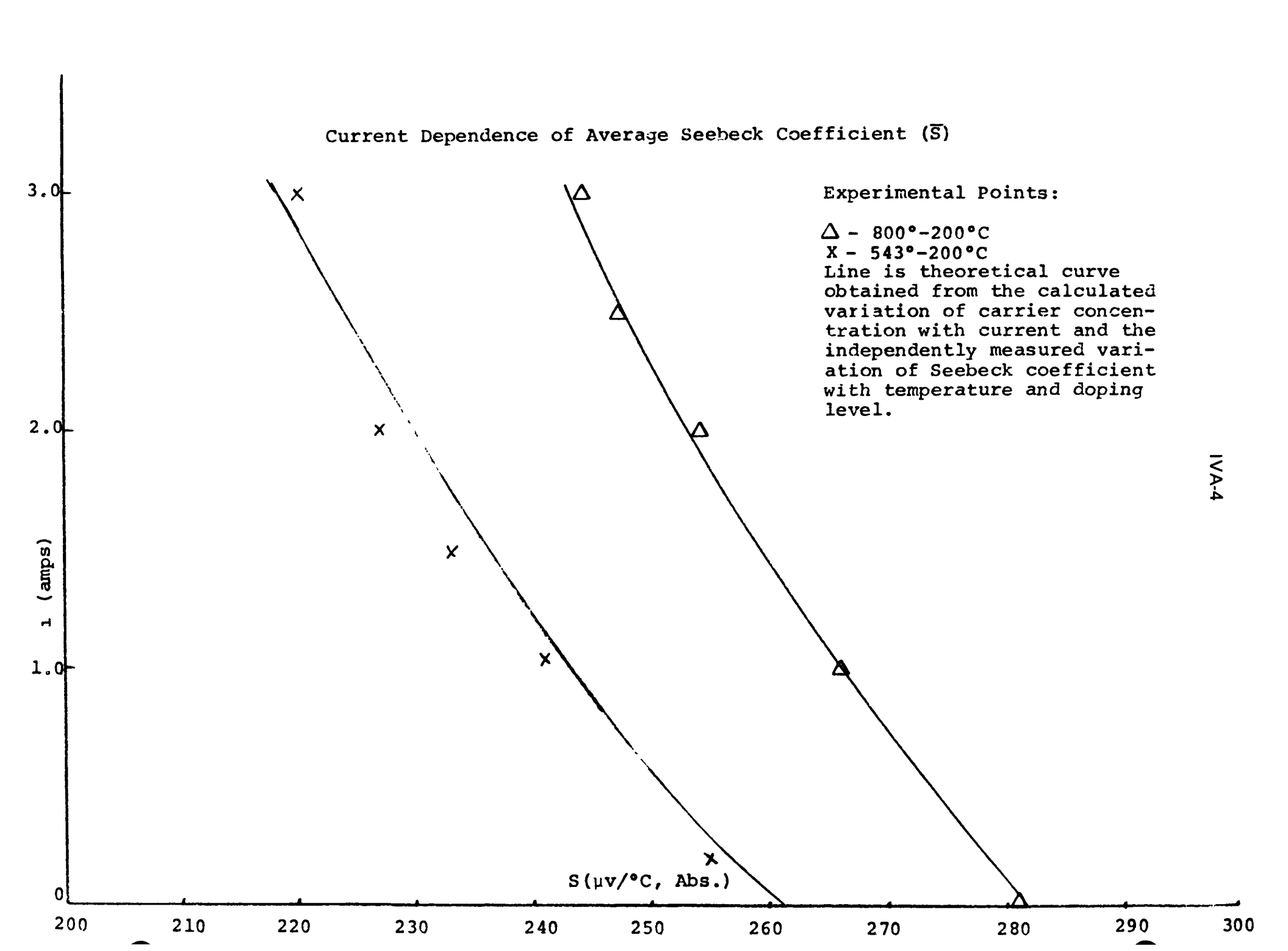
Current Dependence of Average Seebeck Coefficient ($\bar{S}$)
Experimental Points:
Δ - 800°-200°C
X - 543°-200°C
Line is theoretical curve obtained from the calculated variation of carrier concentration with current and the independently measured variation of Seebeck coefficient with temperature and doping level.
IVA-4
3.0
2.0
1.0
0
I (amps)
S(μv/°C, Abs.)
200
210
220
230
240
250
260
270
280
290
300

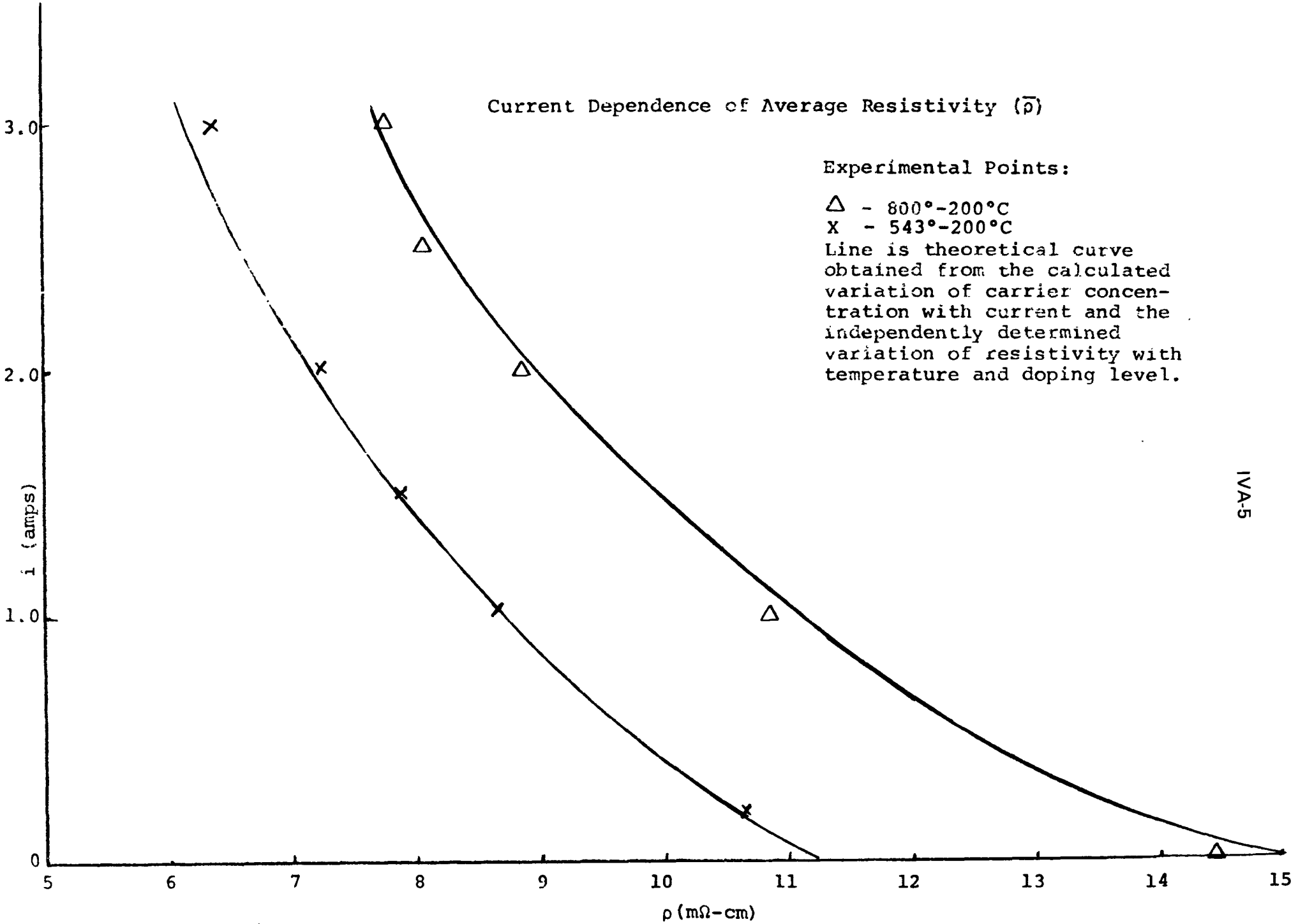
Current Dependence of Average Resistivity ($\bar{\rho}$)
Experimental Points:
△ - 800°-200°C
X - 543°-200°C
Line is theoretical curve obtained from the calculated variation of carrier concentration with current and the independently determined variation of resistivity with temperature and doping level.
i (amps)
3.0
2.0
1.0
0
5
6
7
8
9
10
11
12
13
14
15
ρ (mΩ-cm)

ATTACHMENT V

Grinding - Sintering Improvement Supporting Data

Figure 1 is an expansion of the graph given in Top Summary Report 120. The solid line represents the dependence of extraneous resistance on density followed by material produced in our current process. This curve is a linear regression fit to the data from P/S 107 - P/S 113. The circles represent data obtained in a reduced temperature sintering experiment, P/S 108, reported in Top Summary Report 120. Although the densification in this experiment was poorer so that in no case did the density approach the 98% density obtainable in the normal process, it is clear that the trend of extraneous resistance with density is much better than for the normal process. This indicates that if high densities can be achieved at the lower sintering temperature, very low extraneous resistance values would be attained. Also shown on this plot is one data point from the extreme case where the LTR material was ground directly instead of being cast into an RQC ingot. This avoided the large scale inhomogeneities observed in the RQC ingot, producing a very low value of extraneous resistance for its density, but densification of this material was very poor.

The second set of data reported originally in Top Summary Report No. 111, describes the particle size distribution obtained in the present grinding process. Since it is further observed that the present high speed grinding is ineffective due to the formation of a hard compact on grinding media and container walls, low speed grinding suggests itself as a means of obtaining more complete grinding and a better particle size distribution for a more sinterable power.

By preparing more sinterable powder, high density may be obtained at the lower sintering temperature, and therefore to produce low extraneous resistance elements.

LOW TEMPERATURE SINTERING

FIGURE 1.

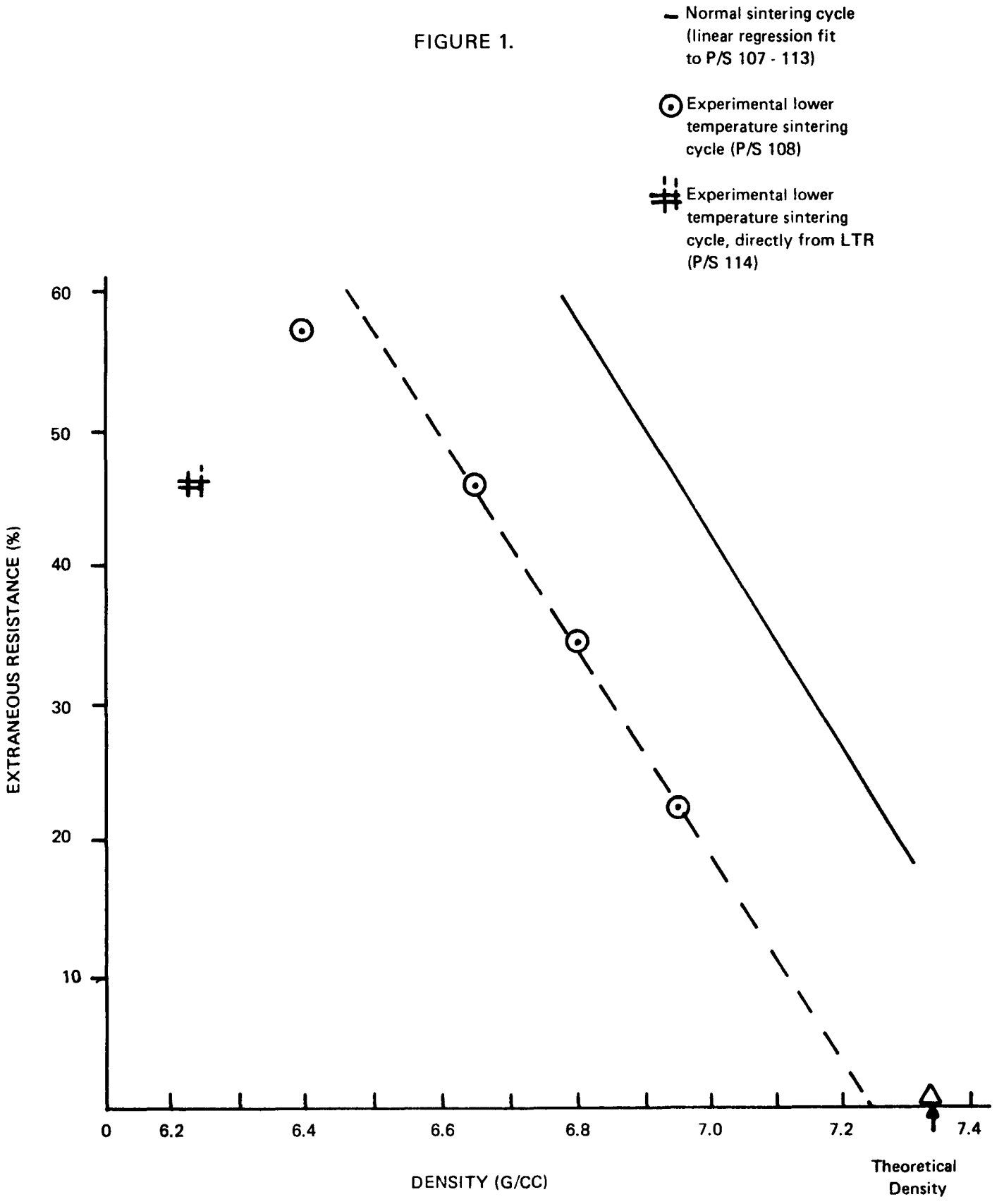

Work in the past month has become oriented to look at particlesize distribution in $GdSe_x$ powder. In Figure 1, A through C, are shown microstructures of a pressed pellet made from powdered N-2609 ingot. The powder was not sieved before pressing at 20,000 psi in the rebuilt die. It is immediately apparent from these photomicrographs that a very wide range of particle-size exists - - from about 300 μm down to 3 μm and probably less. Many of the large particles exhibit straight edges and a roughly rhombohedral symmetry, as would be expected from cleavage fracture of a cubic material. There is not much evidence of particle comminution during pressing, so we may tentatively assume that the pictures are representative of conditions in powder as-milled.

By dint of weighing and cutting photographs similar to Figure 1, A through C, it has been laboriously determined that the particlesize distribution is roughly:

18%	>	70 μm
12%	<	70, > 14 μm
28%	<	14, > 7 μm
42%	<	7 μm

Figure 2 is a plot of these data compared with a "typical" curve of dry-ground alumina, and a hypothetical distribution for a "typical" powder synthetically blended from 25 % coarse, and 75 % fine, powders (known to represent an optimum mixture for dense packing).

A couple of points are worth making with regard to Figure 2. First, it should be remembered that packing ability is merely a matter of relative particle geometry, whereas sinterability is a function of absolute particle size. In terms of broad generality, the further the curve is to the right of the graph, the more sinterable the powder; and the squarer the "knee" of the curve, the more likely is the powder to pack well. Hence it might be suggested that 2609 powder is somewhere intermediate between a "typical" sinterable powder which may not pack well, and a "typical" packable powder which may not (almost certainly would not) sinter well.

This seems to be roughly true, for 2609 powder only compacts to about 70 % theoretical density - - as opposed to approximately 90 % for highly packable powders ultrasonically blended - - and only seems to sinter reasonably well at around 95 % of its absolute melting point. It should be noted that specially prepared uranium oxide powders will sinter well at about 60 % of absolute melting point.

In practice, it is desirable to have a powder which packs well, thus exhibiting minimum shrinkage during firing, and more reproducible dimensions; on the other hand, it is essential to have good sinterability in order to reduce sintering temperatures and times, thereby minimizing oxidation and volatilization problems.

Figure 1. Photomicrographs of As-Pressed N-2609 Powder (Mag. x 145)

A

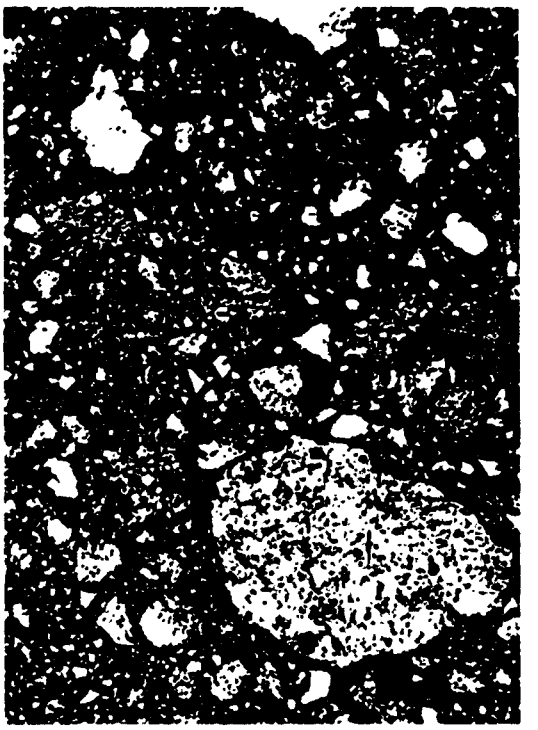

B

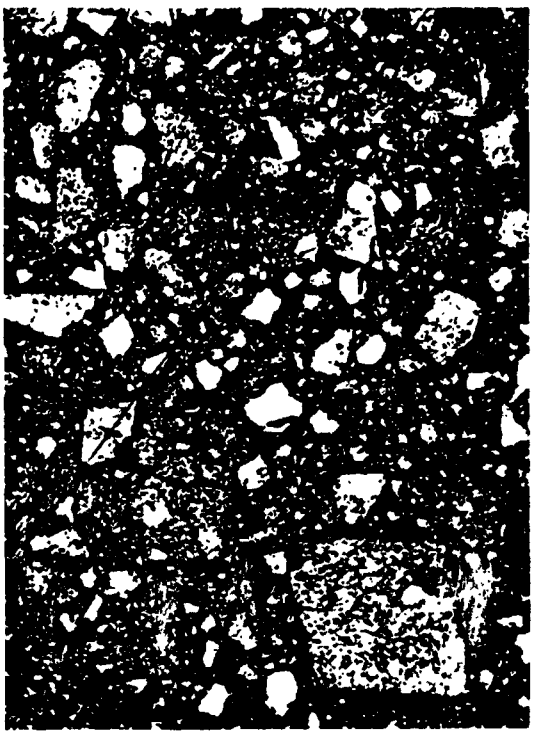

C

FIGURE 2. Particle Sizes of Powders

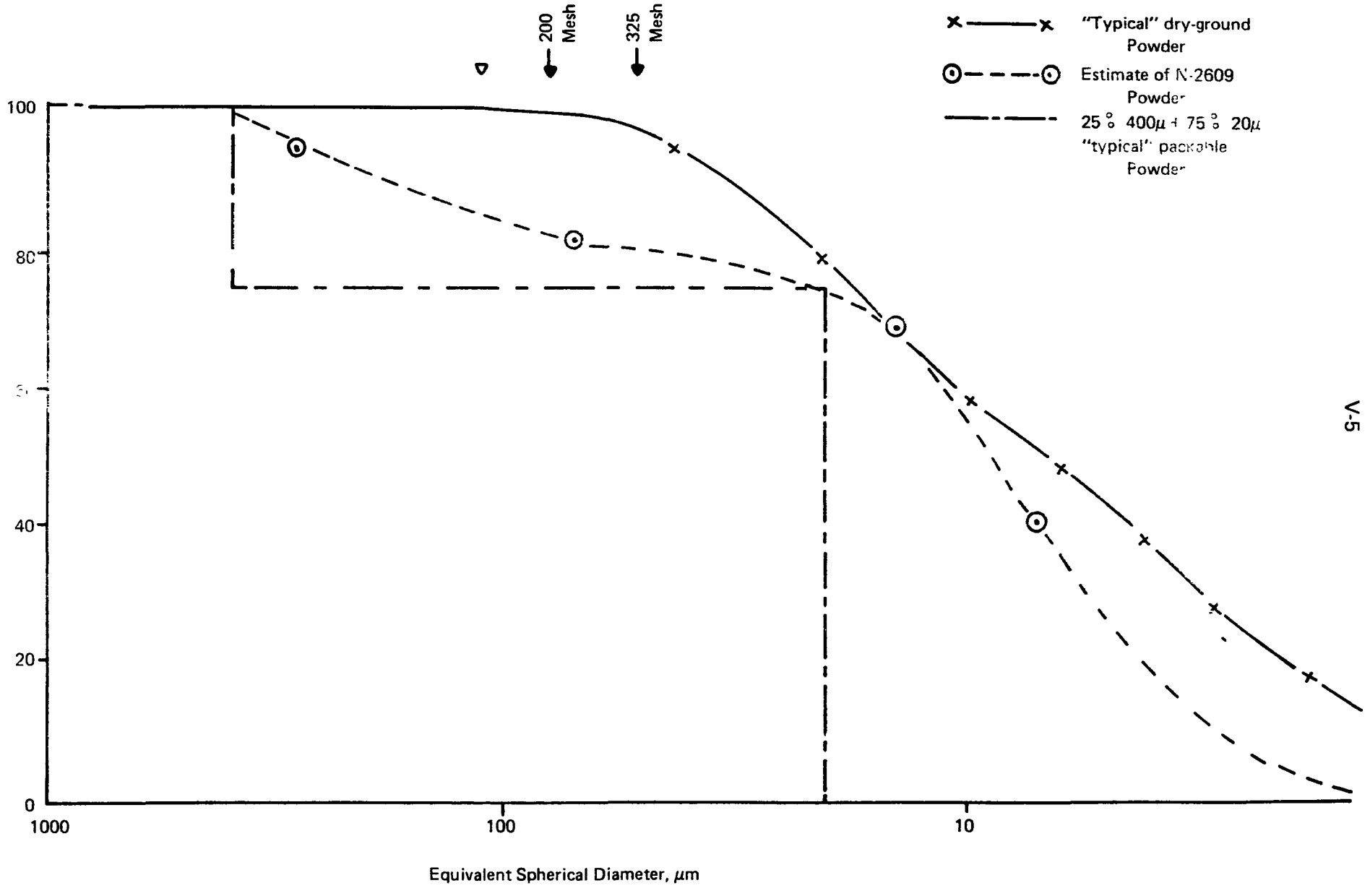

ATTACHMENT VI

The Effect of Thermal Expansion on the Operating Height of Springs

Objective:

To determine the change in spring height during heat-up.

Summary:

Two cases are treated: a full converter ring and an eighteen couple module. Components exposed to large temperature gradients are assumed to have linear temperature profiles and components exposed to small temperature gradients are assumed to be isothermal. Coefficiants of thermal expansion of all materials considered are treated as being independent of temperature. The findings are that for a full converter ring the springs are compressed about an additional .018 in. during heat-up, whereas for an eighteen couple module, they are compressed only about an additional .001 in.

Implications:

Eighteen couple modules should be over compressed about .017 inches during assembly in order to simulate actual conditions.

A. Full connector ring.

1. Estimation of change in stack height.
   Temp. of hot frame = 860 + 25 = 885°C
   ΔD Hot Frame = $(8.09 \bullet 10^{-6}/°C)$ (885 - 20) (8.117 in.) = + .057 in.
   Temp. of cold frame - 150 - 25 = 125°C
   ΔD cold frame = $(13.0 \bullet 10^{-6}/°F)$ (125 - 20°C) $(1.80°F/°C)$ (10.159 in.) = + .025 in.
   $\therefore$ Δ Stack height = ½ (.025 - .057) = - .016 in.
   $\therefore$ the stack height decreases by .016 in.

2. Estimation of change in spring height:

   a) N-Leg
      T Hot strap = ½(885 + 860) = 875
      Δ L Hot strap = $30 \bullet 10^{-7}/°F$ (873 – 20°C) $(1.80°F/°C)$ (.1 in.) = + .0005 in.
      Tn-leg = ½ (860 + 160) = 510
      Δ L N-Leg = $(10 \bullet 10^{-6}/°C)$ (510 - 20°C) (.3 in.) = + .0015
      Δ L cold strap, follower = $(10 \bullet 10^{-6}/°F)$ (150-20°C) $(1.80°F/°C)$ (.011 + .021 in.)
      = + .0001 Negligible
      Δ L BeO disc = $(5.5 \bullet 10^{-6}/°C)$ (150 - 20°C) (.030 in.) = .00002 - Negligible
      $\therefore$ Δ L spring = Δ Stack ht. – Σ Δ L's
      = - .016 – .0005 – .0015
      = - .018 in.
      $\therefore$ the operating N-Leg spring height decreases by .018 in. during heat-up in a full converter ring.

   b) P-Leg
      Δ L Hot strap = $(30 \bullet 10^{-7}/°F)$ (873 - 20) (1.80) (.068) = .0003 in.
      Δ L P-Leg = $(20 \bullet 10^{-6}/°C)$ (510 - 20) (0.30) = .0029 in.
      $\therefore$ Δ L spring = -.016 -.0003 -.0029
      = -.019
      $\therefore$ The operating P-Leg spring height decreases by .019 in. during heat-up in a full converter ring.

B. Eighteen couple module

1. Estimation of change in stack height.
   Temp. of hot frame = 885°C
   Δ L Hot frame = (8.09 - 10^{-6}/°C) (885 - 20) (1.250 in.) = .0087 in.
   Temp. of tantalum pins = ½ (885 + 125°C) = 505°C
   Δ L pins = (3.60 • 10^{-6}/°F) (505 - 20°C) (1.80) (3.22 in.) = .0101 in.
   $\therefore$ Δ Stack height = .0101 — .0087 = + .0014 in.
   $\therefore$ The stack height increases by .0014 in.

2. Estimation of change in spring height.
   a) N-Leg
      As before, Δ L Hot strap = .0005 in.
      Δ L N-Leg = .0015 in.
      $\therefore$ Δ L spring = .0014 - .0005 - .0015 = -.001 in.
      $\therefore$ The N-leg spring length decreases by .001 in. in an eighteen couple module during heat-up.
   b) P-Leg
      As before, Δ L Hot strap = .0003 in.
      Δ L P-leg = .0029 in.
      $\therefore$ Δ L spring = .0014 - .0003 - .0029 = -.002
      The P-leg spring length decreases by .002 in. in an eighteen couple module during heat-up.

C. A list of references cited for expansion coefficient data.

Material	Part	Source
POCO	Hot Frame	SR5 Report POB-64013, Feb. 28, 1978
Tatalum	18 Couple Module Pins	CRC Applied Engr. Science Handbook, 2nd Ed.
Molybdenum	Hot Straps	"
Aluminum	Outer Housing	Materials Eng'r. Materials Selector '78, Vol. 86, No. 6
Copper	Cold End Hardware	"
N-Leg	N-Leg	Internal
P-Leg	P-Leg	"

ATTACHMENT VII

Calculation of Stack Heights and Associated Leg Stresses in Converter

Objective:

The purpose of this report is to analyze the various modes of axial stresses on the thermoelectric legs in the SN-1 generator. (Prior to thermal expansion, sublimation or spring load relaxation)

Analysis will cover:

1. Range of stress at room temperature:
   a) in the overcompressed assembly stage.
   b) in the fully assembled stage.
2. Range of stress at operating temperature.

Conclusion

Table 3 summarizes the range of stresses on the legs for the various modes mentioned. The values given for stresses after heat-up may now be utilized as initial conditions in Figures 6 and 7 of the document to which this is attached.

ANALYSIS OF STATIC STRESSES

The initial stress on the legs is a function of spring force and insulation compliance.

Spring Force:

To determine the force applied to each leg by the spring, the following calculations were performed for each mode, using nominal, maximum and minimum values.

a) Determine spacing using the known values of the housing and POCO hot frame, under the appropriate conditions. (Shown in Table 1)

b) Add the individual components in the stack (shown in Table 2.)

c) Subtract this value from the appropriate spacing value in Table 1 to obtain the compressed spring length.

d) Subtract this compressed length from the free length of the spring to obtain the amount of spring compression.

e) Multiply this compression by the appropriate spring rate to obtain the spring force.

Insulation Compliance:

The initial spring force is reduced by the insulation compaction. With the use of an Instron Machine, this reduction of force has been determined to be 1.25 lbs.

The net stress applied to the legs is then determined by:

Stress = (Spring Force - Insulation Compliance)/Area of Leg

The following pages describe these calculations in detail. A summary of the room temperature and heat up stresses are summarized in Table 3.

SN-1 STACK HEIGHT CALCULATIONS

Three stages of stack height will be encountered by the thermoelectric ring.

1. Overcompressed spacing

   This describes the condition of the ring immediately prior to insertion into the housing. The amount of overcompression is .030" radially.

2. Fully assembled spacing

   This condition occures after rings have been completely assembled and released in the housing. The stress applied by the ring will cause the housing to deflect .0025 inches radially. This deflection is taken into account in the stack height calculations.

3. Operating Temperature Spacing

   This condition occures after SN-1 has been brought up to temperature and accounts for .020 radial expansion (thermal) of the POCO hot frame.

Table 1 lists the various stages of hot frame/cold frame spacing along with the tolerance range associated with each respective stage. The tolerance ranges are based on component tolerances taken from the design drawings.

Below is a sample calculation of the nominal overcompressed stack height:

Housing I.D. = $10.159 \pm .008$ inches

POCO across flats = $8.117 \pm .001$ inches

Spacing = (Housing I.D. – POCO O.D. (across flats)/2 – radial overcompression
= (10.159 – 8.117)/2 – .030
= .991 inches

INITIAL STRESS CALCULATIONS

Nominal: $\alpha_1 = \frac{1}{A\ nom}$ [Fsi nom – Fi nom]

Where Fsi nom = K nom. $[L_{FL}$ nom $- L_c$ nom]

Maximun: $\alpha_1 = \frac{1}{A\ min}$ [Fsi max – F_i]

Where Fsi max = K max $[L_{FL min} - L_{c\ min}]$

Minimum: $\alpha_i = \frac{1}{A\ max}$ [Fsi min – Fi]

Where Fsi min. = Kmin $[L_{FL\ max} - L_{c\ max}]$

VARIABLES

α_1 = Stress on leg
A = Cross-sectional area of leg (from leg spec's)
Fsi = Initial spring force
Fi = Insulation compliance force (initial = 1.25 lbs)
K = Spring constant (calculated from spring specifications)
L_{FL} = Spring free length (from spring spec's)
L_c = Spring compressed length (calculated from tables 1 & 2)

Examples of Stress Calculations for P-leg in overcompressed stage:

NOMINAL

From Tables 1 & 2

L_c = Stack height -- component height total

$L_c = .9910 - .5775$

$L_c = .4135$ inches

$Fsi = K [L_{FL} - L_c]$

$Fsi = 94.4 [.545 - .4135]$

$Fsi = 12.41$ lbs.

$$\sigma_i = \frac{1}{A} [Fsi - Fi]$$

$$\sigma_i = \frac{1}{.0547} [12.41 - 1.25]$$

$\sigma_i = 204$ lbs/in^2

MAXIMUM

$L_{c\,min}$ = Min. stack ht. - max. component ht. total

$L_{c\,min} = .9865 - .5915$

$L_{c\,min} = .3950$ inches

$Fsi\ max = K\ max [L_{FL\,min} - L_{c\,min}]$

$= 112.5 [.535 - .395]$

$= 15.75$ lbs.

$$\sigma i\ max = \frac{1}{A\ min} [Fsi\ max - Fi]$$

$$= \frac{1}{.0543} [15.75 - 1.25]$$

$\sigma i\ max = 267$ lbs/in^2

MINIMUM

$L_{c\,max}$ = max. stack ht -- min component ht. total

$= .9955 - .5645$

$= .431$

$Fsi\ min = K\ min [L_{FL\,max} - L_{c\,max}]$

$= 80 [.555 - .431]$

$= 9.92$ lbs.

$$\sigma i\ min = \frac{1}{A\ max} [Fsi\ min - Fi]$$

$$= \frac{1}{.0551} [9.92 \quad 1.25]$$

$\sigma i\ min = 157.4$ lbs/in^2

The remainder of the initial stress calculations will not be shown. The results are summarized in Table 3.

TABLE 1 Spacing Between Hot Frame O.D. and Cold Frame Segment O.D. (inches)

	NOMINAL	MAXIMUM	MINIMUM
Overcompressed Stack Heights (.030 overcompression for assembly)	.9910	.9955	.9865
Fully Assembled Stack Heights (with .0025 housing deflection)	1.0235	1.0280	1.0190
High Temperature (860/160°C) Stack Height (with .020 POCO expansion)	1.0035	1.0080	.9990

TABLE 2 – Summation of components in stack

N-Leg Stack Dimensions (inches)

COMPONENT	NOMINAL	MAXIMUM	MINIMUM
Pt. Hot End Foil	.0005	.0005	.0005
Hot Strap & Gimbal	.100	.101	.099
Ni Foil	.005	.006	.004
N-Leg Assembly	.305	.308	.302
Cold End Strap Assembly	.075	.081	.069
Twist Lock	.039	.041	.037
Cold Frame Assembly	.040	.042	.038
Tin Foil	.001	.001	.001
TOTAL	.5655	.5805	.5505

P-Leg Stack Dimensions (inches)

COMPONENT	NOMINAL	MAXIMUM	MINIMUM
Pt. Hot End Foil	.0005	.0005	.0005
Hot Strap	.068	.069	.068
P-Leg Assembly	.354	.357	.351
Cold End Strap Assembly	.075	.081	.069
Twist Lock	.039	.041	.037
Cold Frame Segment	.040	.042	.038
Tin Foil	.001	.001	.001
TOTAL	.5775	.5915	.5645

TYPICAL COUPLE HARDWARE

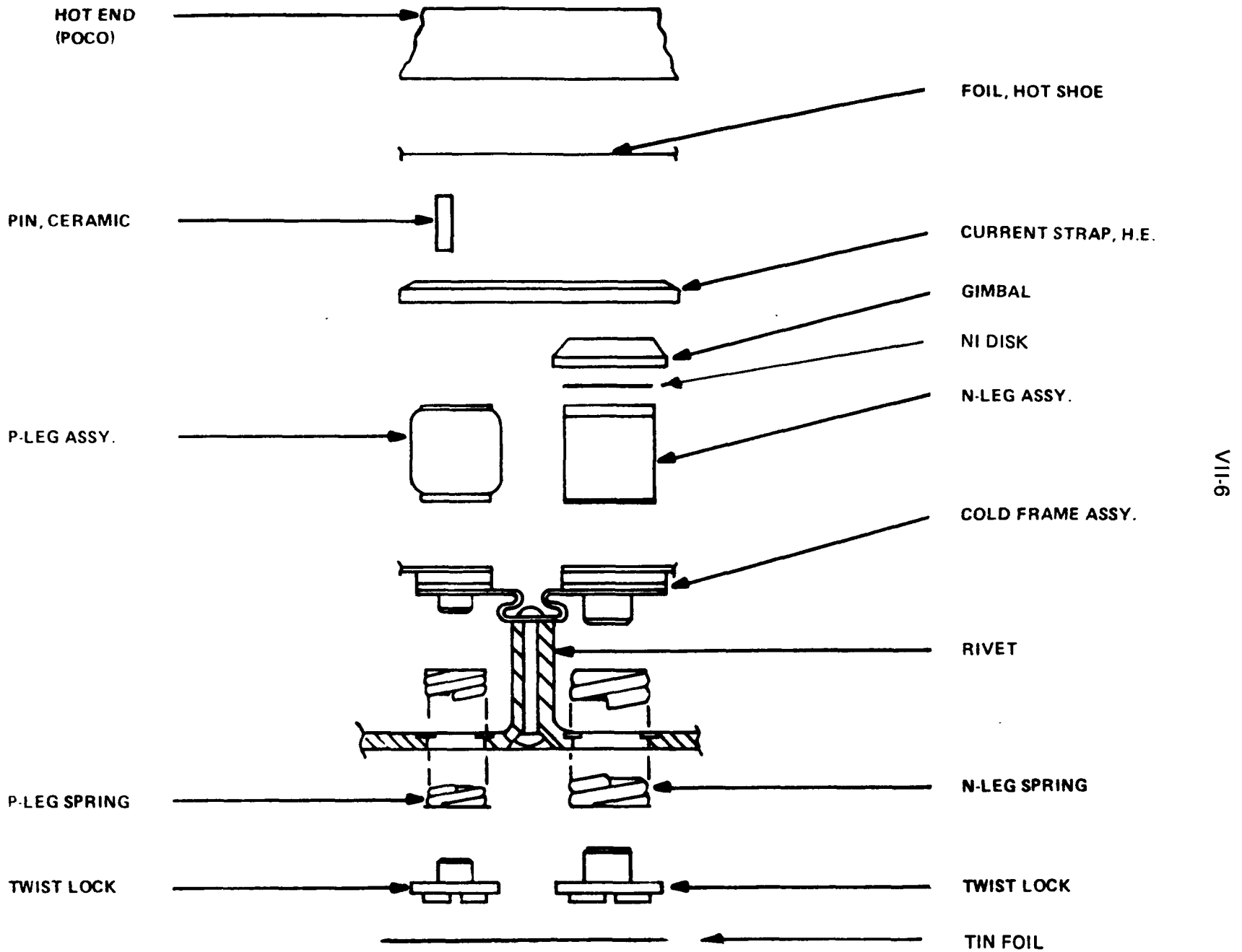

TABLE 3 – Initial Leg Stress Summary (PSI)

	P-LEG			N-LEG		
	NOM.	MIN.	MAX.	NOM.	MIN.	MAX.
Overcompressed State	204	157	267	384	284	515
Fully Assembled State	148	110	200	276	196	381
Heat-up State	182	139	241	341	250	464

ATTACHMENT VIII

S/N-1 Weight Analysis

ATTACHMENT VIII S/N-1 WEIGHT ANALYSIS

Objective:

- To analyze the component weights of the SN-1 thermoelectric rings.
- Use these weights to obtain a composite weight picture of the thermoelectric ring assembly.

Conclusion:

Based on the information shown in table 1, it can be seen than the actual weight of the thermoelectric ring assemblies for SN-1 will be 128/14.5 lbs. The design target was 16.0 lbs. As the stock of SN-1 components increases, this summary will be updated to assure accuracy.

Weight Analysis:

Two methods were used to derive the weights of the components listed in Table 1. In all cases where SN-1 component parts were available, samples from bonded stock were randomly selected and weighed. Whenever bonded stock components were not available, weight calculations were performed based on the material and dimensional properties shown in the appropriate SN-1 drawing. The method used for each component is noted in the table.

TABLE 1 – SN-1 WEIGHT SUMMARY

PART	NOM. UNIT WT.	QUANTITY/GEN.	NOM. TOTAL WT/GEN.	WEIGHT TOLERANCE
HOT FRAME	.8883*	2	1.780	1.560/1.850
FOIL, HOT SHOE	.0000357*	112	.004	.004/.007
CERAMIC PIN	.000089	336	.030	.028/1.031
STRAP, CURRENT, H.E.	.0100	168	1.680	1.613/1.747
GIMBAL	.00192	336	.644	.632/.659
Ni FOIL DISK	.000132	336	.044	.044/.045
P-LEG ASS'Y	.00583	336	1.960	1.940/1.990
N-LEG ASS'Y	.0062	336	2.090	2.070/2.120
COLD FRAME ASS'Y	.06805	56	3.811	3.783/3.822
P-SPRING	.0015	336	.504	.484/.518
N-SPRING	.0029	336	.974	.967/.988
P-TWIST LOCK	.00036	336	.122	.121/.123
N-TWIST LOCK	.00068	336	.228	.227/.229
TIN FOIL	.025*	2	.050	.040/.060
HiFi INSULATION	.006*	56	.316	.302/.330
MULTIFOIL PINS	.000045*	13	.0006	.0005/.0006
		GENERATOR TOTAL	14.238	13.816/14.520

* Based on calculations. Will be updated as weight measurements become available.

ATTACHMENT IX

Thermal Resistance of Cold End Hardware

ATTACHMENT IX: Thermal Resistance of Cold End Hardware

OBJECTIVE: To obtain a theoretical estimate of the temperature drop across the cold end hardware under operating conditions.

SUMMARY: One dimensional heat flow is assumed to occur throughout the hardware. All solder connections are assumed to provide 100% contact area. This model predicts a ΔT of 24.1°C between the cold strap and the base of the rail, which corresponds to a thermal resistance of 7.2°C/W.

1. Calculate R for one rail of one cold frame segment:

$R = (R^{A/L})^{-1}$

Refer to Fig. 1 for meanings of R_1, R_2, R_3, R_4, R_5

	R W/cm-k)	L_1 (cm)	L_2 (cm)	A (cm^2)	L (cm)	R (°C/W)
R_1	3.98	–	–	.456	.0267	.0147
R_2	.346	–	–	.456	.0102	.0646
R_3	2.30	–	–	.456	.0787	.0750
R_4	3.98	–	–	.456	.0254	.0140
R_5	.346	–	–	.350	.0051	.0413
R_6	3.98	–	–	.350	.0533	.0383
R_7	3.98	1.016	.0533	.0542	.794	3.68
R_8	.346	1.14	.356	.406	.005	.0356
R_9	1.71	2.11	.356	.750	1.02	.7953

$Re = R_1 + R_2 + R_3 + R_4 + R_5 + R_6 + R_7 = 3.93\,°C/W$

$$R_{tot} = R_9 + \left(\frac{R_8 + \frac{Re}{2}}{2} \right) = 1.80\,°C/W$$

2. Calculate heat flux through one rail of one cold frame segment:

$$Q \cong \frac{(1126\ \text{W/ring})}{(168\ \text{Couples/ring})} \times (2\ \text{Couples/rail}) = 13.4\text{W}$$

$\therefore$ Expected $\Delta T = QR = 24.1\ ^\circ\text{C}$

3. Now, what is the thermal resistance based on the heat flux through a single element:

$$R = \Delta T/Q = \frac{24.1\ ^\circ\text{C}}{3.35\ \text{W/Element}} = 7.19\ ^\circ\text{C/W}$$

This figure is an acceptable thermal resistance. (The goal is $7^\circ\text{C/W} \pm 3^\circ\text{C/W}$).

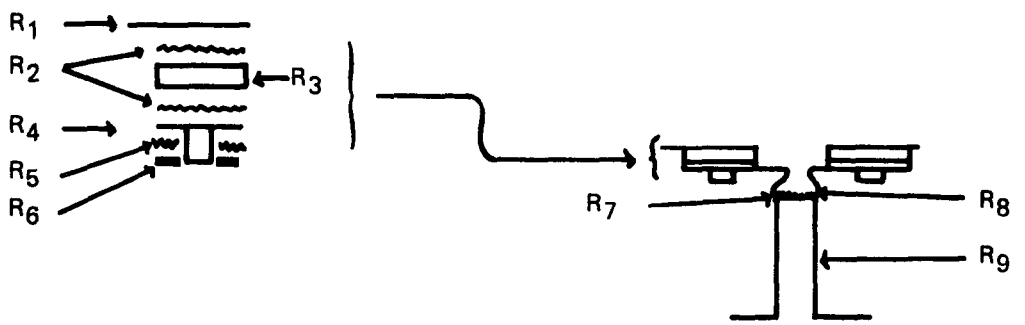

$$Re = \sum_{i=1}^{7} Ri$$

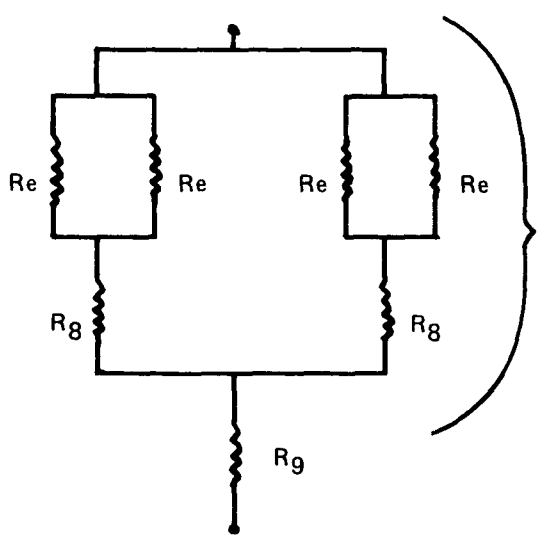

$$R_{tot} = R_9 + \left[\frac{R_8 + \frac{Re}{2}}{2} \right]$$

Cold End Hardware
One-Dimensional Heat Flow Model

FIGURE 1

ATTACHMENT X

Calculation of Bypass Heat Flow Within the S/N-1 Converter

ATTACHMENT X – Calculation of Bypass Heat Flow Within the S/N-1 Converter

Objective:

Calculate the bypass heat flow within the SN-1 converter including the stuffed Fiberfrax HiFi paper around the elements and the slurry/Astroquartz wrap on the P-elements.

Conclusions:

The bypass heat flow in the SN-1 converter is summarized as follows:

- Bypass in HiFi paper = 176 W(t)
- Bypass in slurry/Astroquartz wrap = 23 W(t)
- Total bypass in converter = 199 W(t)

This is a total of about 8.1% of the total heat input.

Calculation of Bypass

The calculation of the bypass in the HiFi paper is based on the following assumptions:

- Width of insulation for two (2) rings
  (from TES/3M Interface Drawing, No. SIG 116001)

= 2 [3.00 + 2(.12)] = 6.48 inches

- Average diameter of insulation

. Distance across POCO hot frame flats	= 8.117 inches
. Hot strap thickness x 2	= 0.136 inches
. 1/2 leg length x 2	= 3.300 inches
	8.553 inches

- Cut-outs for legs
  - . N-Leg Diameter = 0.315
  - . P-Leg Diameter (with .025 thick wrap) = 0.310
  - . 336 Couples

Heat Flow Area = $\pi(8.553)\ (6.48) - \pi/4\ [(.310)^2 + (.315)^2]\ 336$

$= 174.1 - 51.6 = 122.5\ in^2$

- Thermal conductivity of HiFi paper (15% compression) measurements at Dynatech R/D Co. at 0% compression and 30% compression are .015 and .013 BTU/hr-ft-°F respectively; therefore, the value of .014 BTU/hr-ft-°F will be used for 15% compression. The amount of compression of 15% was selected based on insulation compliance measurements performed at 3M.
- Assumed hot frame temperature = 860
- Assumed cold strap temperature = 160°C
- $Q_{Bypass\ (hiFi)} = K\ A\ \frac{\Delta T}{\Delta X}$

$$Q_{Bypass\ (hiFi)} = \frac{(.014)\ (122.5)\ (860 - 160)\ (12)\ (1.8)}{(144)\quad (0.3)\quad (3.413)} = 175.9\ W(t)$$

- Bypass in Wrap
  - . From Dynatech R/D Co. measurements

$$k_{wrap} = .030\ \frac{BTU}{hr\text{-}ft\text{-}^\circ F}$$

$$Q_{wrap} = \frac{336}{144}\ \frac{\pi}{4}\ (.310^2 - .260^2)\ (.030)\ \frac{(860 - 160)}{0.3}\ \frac{(12)\ (1.8)}{(3.413)} = 23.1\ W(t)$$

- Total converter bypass = 175.9 + 23.1 = 199 W(t)

ATTACHMENT XI

Environmental Test Levels for
TA and FA Testing

Objective: To describe in detail the severity of test environments that the RTG must be exposed to in order to qualify for its mission.

Implications: These specifications, taken from JPL's "Galileo Project Detail Specification for RTG's", set the test levels for all design verification testing as well as goals for the component designs themselves.

1. Introduction

It is of utmost importance to ensure that all delivered RTG units are flight worthy and capable of meeting mission requirements. The purpose of Type Approval (TA) and Flight Acceptance (FA) testing is to prevent un-flight worthy equipment from being accepted for use in the mission. Whereas 3M will not be responsible for conducting the formal certification tests, the environmental test levels established in the TA and FA specifications represent survivability goals to be designed for. This report describes TA and FA testing. Any statements appearing in quotation marks are taken from JPL's "Galileo Project Detail Specification for RTG's Environmental Design and Test Requirements".

2. TA and FA Testing

"FA tests are performed on all (delivered) RTG units. The tests are intended to simulate conditions expected during actual ground handling, launch and space operation ... (and) are required for formal certification of flight acceptability of spacecraft equipment". TA tests, on the other hand, "are intended to establish confidence that the design is qualified for its designated flight mission by verification of design (safety) margins in the flight equipment". All TA tests are to be run on a non-flight RTG which is in every respect identical to the flight RTG's.

JPL Galileo Project personnel are to be invited to witness all tests and review test equipment and data. Any unit to be either TA or FA tested must at the outset meet the BOL performance requirements described in JPL's "Galileo Project Detail Specification for RTG Requirements". Figure 1 represents a brief list of the most important specifications. Any deterioration in performance of any test unit which prevents operation at specified output levels is to be considered a failure.

JPL has specified tolerances within which all environments must be controlled. All relevant quantities have been compiled and are shown in Figure 2.

3. A List of Environmental Tests

3A. Spin Velocity and Spin Rate: This environmental test will be used only in TA testing. Two (2) tests will be applied: one with the RTG principle axis parallel to the spacecraft z-axis (stored configuration) and one with the RTG principle axis normal to the spacecraft z-axis (deployed configuration), Specifications for spin rate and spin arm appear in Figure 3.

3B. Acoustic: The TA acoustics test consists of a field of 149 db with a duration of three (3) minutes. The sound pressure profile specification is discretized into 1/3 octive bands as shown in Figure 4. The FA test consists of a field of 143 db with a duration of one (1) minute. The FA sound pressure profile appears in Figure 5. For both tests, the RTG "is to be rigidly attached to the mounting fixture using the attachment points for the RTG/spacecraft mounting interface".

3C. Vibration: Vibration tests fall into two (2) categories, low-frequency random input and high-frequency random input. Low-frequency random vibration testing will only be conducted during TA testing. The spectral density level to be used will be determined by JPL "on the basis of a defined heat source damping factor as provided by DoE". The possible signatures are shown in Figure 6. The RTG is to be exposed to the chosen signal for twenty (20) seconds along all three (3) axes.

High frequency random vibration testing will be conducted during both TA and FA testing. During TA testing, the RTG is to be exposed to the signal described in Figure 7 for three (3) minutes along all three (3) axes. During FA testing, the RTG is to be exposed to the signal described in Figure 8 for one (1) minute along all three (3) axes.

3D. Pyrotechnic Shock: For TA testing, three (3) shocks having the spectrum shown in Figure 9, are to be applied to the RTG mounting structure in both directions along all three (3) axes. This is a total of eighteen (18) shocks. The waveform shown in Figure 9 is assumed to be "an exponentially decaying complex sinusoid with an approximate decay time of 7 ms". Pyrotechnic shock tests will not be performed during FA testing.

3E. Thermal Vacuum: During TA testing, the RTG is to be exposed to an environment of less than or equal to 10^{-5} torr for a minimum of seven (7) days. Installation of the RTG in the vacuum chamber will be such that it "is not exposed to abnormal hot or cold surfaces and assures operation of the heat pipes." "The RTG internal pressure shall be representative of normal flight conditions." The same will be a part of FA testing.

3F. Mass Properties: As part of TA and FA testing, the mass, center of mass and moments of inertia about the axes of the RTG unit "shall be determined with sufficient accuracy to verify the criteria" described in the RTG requirements specification.

3G. Magnetic Properties: During both TA and FA testing, the RTG "will be exposed to a magnetic field not to exceed 50 Gauss", and to a "peak demagnetizing field of 40 Gauss." The duration of exposure to the magnetic field will be that amount required to determine the effect, if any, on the ability of the RTG to retain performance at acceptance levels.

3H. Nuclear Radiation: Neutron and gamma radiation flux levels will be checked for compliance with the RTG requirements specification on all RTG units.

FIGURE 1

BOL Output Requirements

1.	Converter Weight:	$\leq$ 16.0 lbs
2.	Operating Conditions	
	a. Hot Junction Temperature:	860°C
	b. Cold Junction Temperature:	160°C
	c. Cold Frame:	$\geq$ 135°C
	d. Output Voltage:	30.0 $\pm$ .5 V (.179 V per couple)
	e. Output Power:	$\geq$ 217 W (0.646 W per couple) after projection to 1000 operating hours

FIGURE 2

Relevant Test Measurement Tolerances

1.	Temperature:	± 2°C
2.	Spin Velocity, Spin Rate:	± 10% on acceleration level + 30% on gradients across the test article
3.	Random Vibration Spectral Shape:	Measured in bands no more than 25 Hz wide, Spectral Density spectra with ± 1.5 db
4.	Random Vibration Wideband Level:	± 1 db (true RMS) of that specified
5.	Acoustic Test Overall Level:	± 1 db (true RMS) of that specified
6.	Frequency:	± 5% or 1 Hz, whichever is greater
7.	Shock Spectrum:	± 3 db or ± 5% of the maximum shock spectrum level achieved, whichever is greater
8.	Time:	5%

FIGURE 3

RTG Spin Details

Spin Event	Spin Rate (RPM)	Spin* Arm (M)	Axis/SC Spin Axis (+Z) (0)	Spin Duration (S)	Centripetal Acceleration (G)
IUS Burn	70	1.35	3.5 ± 3	900	7.40
Cruis	5	3.71	90 ± 5	**	0.10
JOI	30	3.71	90 ± 5	5×10^3	3.73
Orbit	5	3.71	90 ± 5	3×10^6	0.10

* From S/C spin axis to cg of RTG

** Combined with obrbit time

Figure 4 Type Approval Level Acoustic Sound Pressure Levels

1/3 Octave Band Center Frequency	Sound Pressure Level [dB ref 20 x 10^{-6} Newton/m^2 (2×10^{-4} dyne/cm^2)]
32	126
40	128
50	130
63	131.5
80	133.5
100	134.5
125	136
160	137
200	137.5
250	138
315	138.5
400	138.5
500	138
630	137.5
800	137
1000	136
1250	135.5
1600	134
2000	133
2500	132
3150	130.5
4000	129
5000	128
6300	126.5
8000	125
10000	124
Overall	149
Duration	3 minutes

Figure 5 Flight Level Acoustic Sound Pressure Level

1/3 Octave Band Center Frequency Hz	Sound Pressure Level [dB ref 20 x 10^{-6} Newton/m^2 (2 x 10^{-4} dyne/cm^2)]
32	120
40	122
50	124
63	125.5
80	127.5
100	128.5
125	130
160	131
200	131.5
250	132
315	132.5
400	132.5
500	132
630	131.5
800	131
1000	130
1250	129.5
1600	128
2000	127
2500	126
3150	124.5
4000	123
5000	122
6300	120.5
8000	119
10000	118
Overall	143
Duration	1 minute

FIGURE 6 Low Frequency Random Vibration
(Alternative to Type Approval Slow Swept Sine)

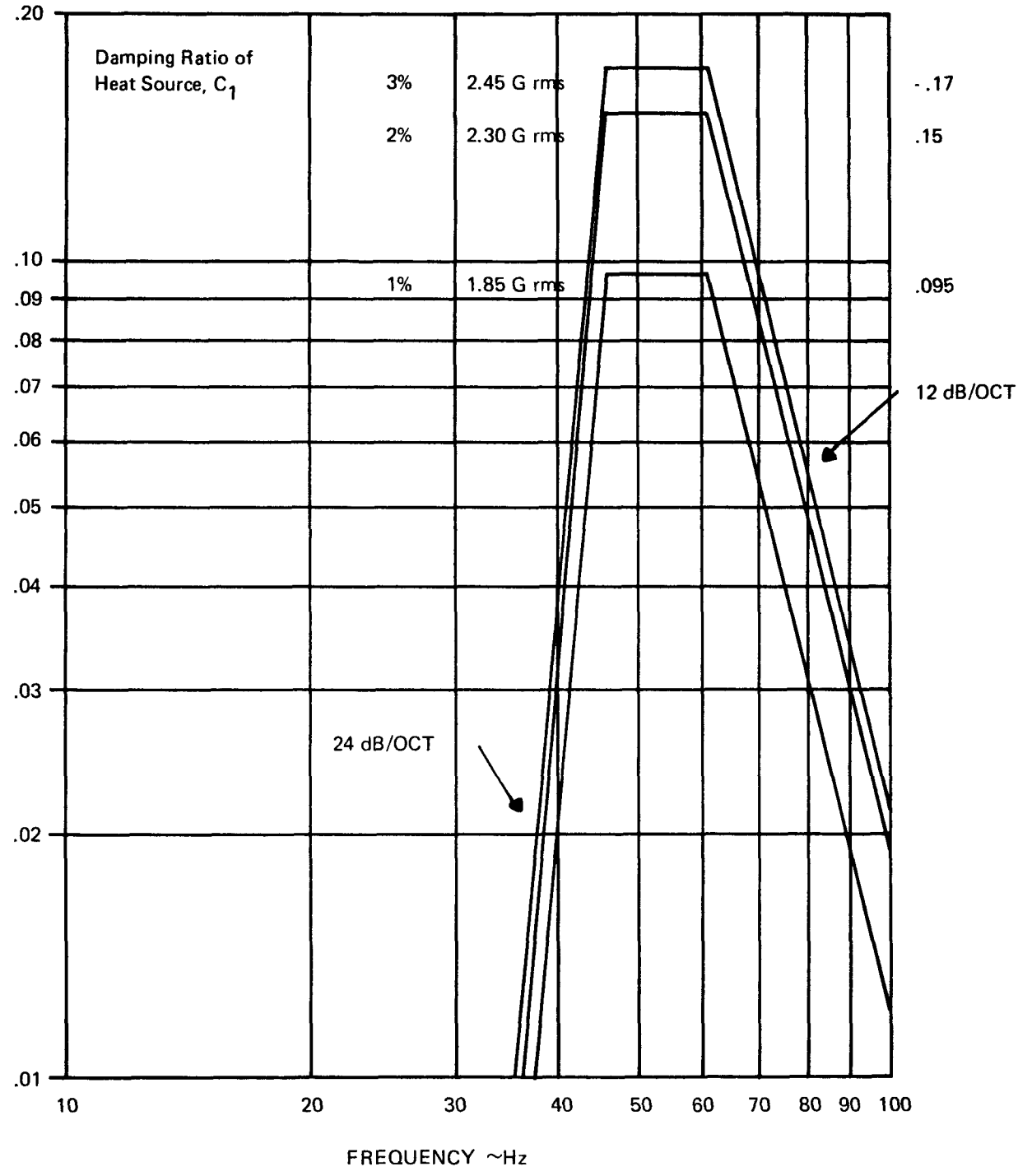

Figure 7 Type Approval Level Random Vibration Spectrum

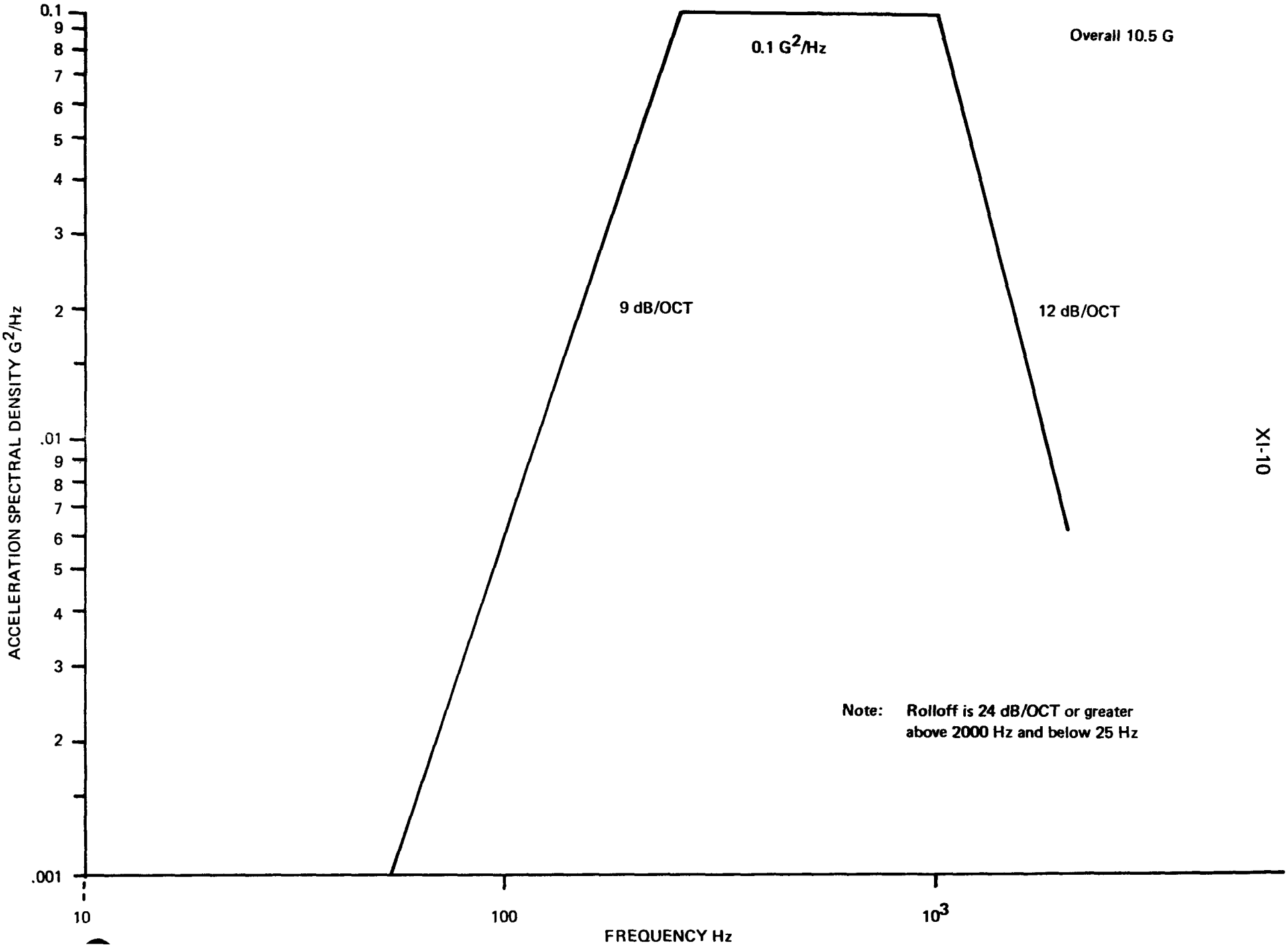

FIGURE 8 Flight Level Random Vibration Spectrum

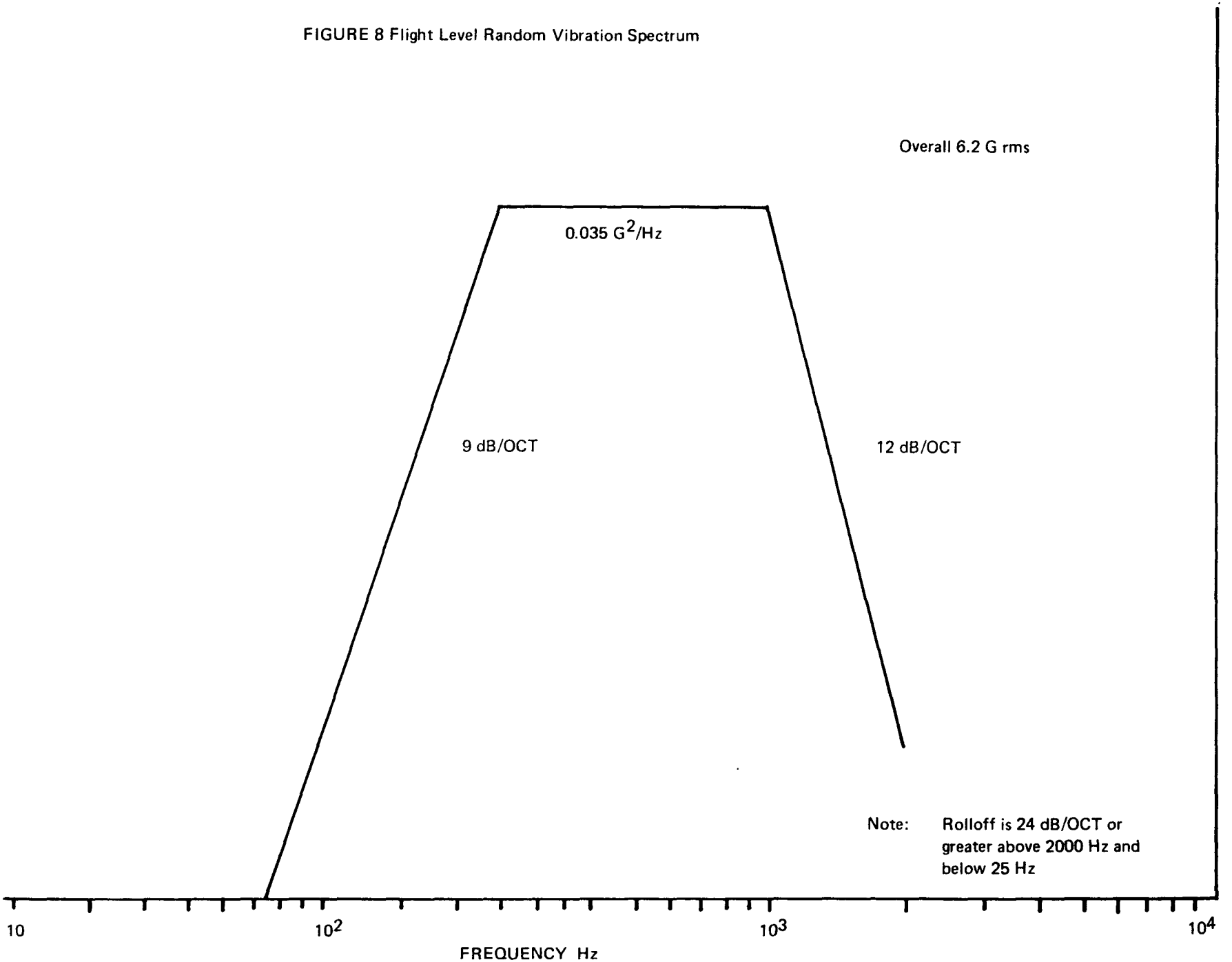

FIGURE 9 Pyrotechnic Shock Response Spectrum

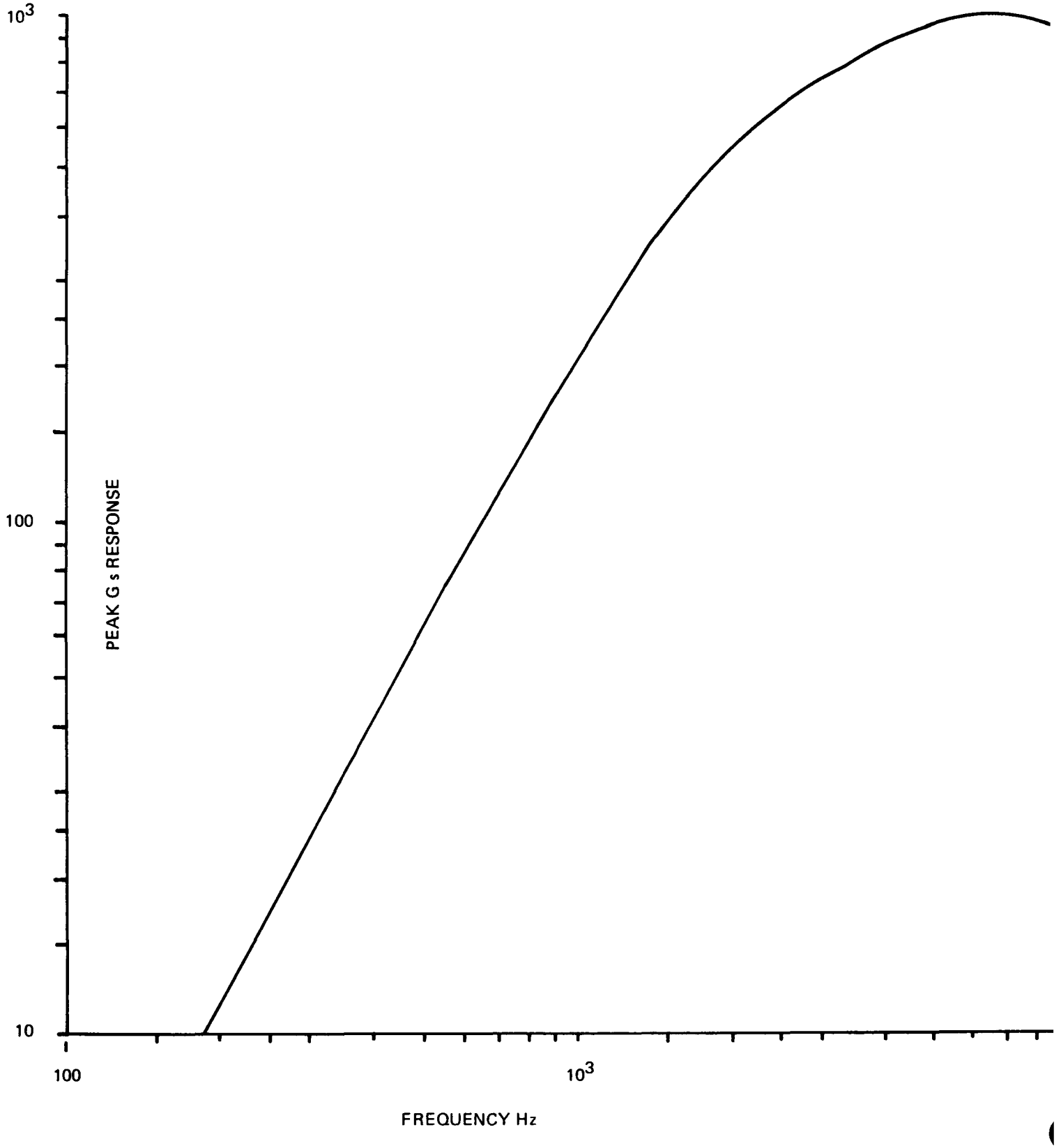

ATTACHMENT XII

Angular Misalignment of Hard P-Legs

ATTACHMENT XII – Angular Misalynment on N and P Legs.

Objective

In order to fully determine the consequences of non-uniform stress loading on the thermoelectric legs, it is necessary to evaluate the extent of possible angular misalignment. One of the primary causes of misalignment is the parallelism tolerance of the stack components. By analyzing these component tolerances, we can determine the maximum angular misalignment of the legs.

Summary

As shown in the analysis, the maximum leg misalignment is 4.8° for the P-Leg and 4.7° for the N-Leg.

The stress effects caused by the N-leg misalignment are considerably reduced with the use of the gimbal in the hot shoe.

The results of this analysis will be incorporated into tests which have been defined to determine the effects of leg misalignment on sublimation and N-leg cracking.

Analysis

The following table lists the maximum variation in parallelisms of the mating faces of each component in a leg stack.

	VARIATION IN FACE PARALLELISM	
COMPONENT	P	N
Hot shoe	.001	.001
Gimbal	Not Applicable	.004
Leg Assembly	.006	.006
Cold Strap Ass'y	.003	.003
Spring	.004	.004
Twist Lock	.004	.004
Cold Frame	.004	.004
TOTAL	.022	.026

These variations were obtained from the tolerance specifications of the respective design prints with the exception of the cold strap assembly. This assembly is solder bonded. Measurements were made on completely soldered assemblies and the maximum variation in thickness across the leg-mating surface was used.

The total variations listed represent the maximum stack height difference across the face of a leg. This correlates directly with angular misalignment as follows:

$$\Theta = \arctan\left(\frac{V}{D}\right)$$

Where Θ = angular misalignment
V = total variation
D = diameter across face of leg

$$\therefore \Theta_{P\text{-}Leg} = \arctan\left(\frac{.022}{.264}\right)$$

$$\Theta_{P\text{-}Leg} = 4.8°$$

$$\Theta_{N\text{-}Leg} = \arctan\left(\frac{.026}{.315}\right)$$

$$\Theta_{N\text{-}Leg} = 4.7°$$

ATTACHMENT XIII

Converter Materials Chemical Compatability and Outgassing Requirements Assessed for GDS

CONVERTER MATERIALS CHEMICAL COMPATIBILITY & OUTGASSING REQUIREMENTS ASSESSED FOR GDS

3M NO. 2331-0464

February 28, 1977

THIS REPORT IS SUBMITTED TO SATISFY THE
REQUIREMENTS OF MILESTONE NO. 51,
FEBRUARY 1977

UNDER

CONTRACT No. EY-76-C-02-2331 .*000

WITH THE

UNITED STATES ENERGY RESEARCH & DEVELOPMENT ADMINISTRATION

PREPARED BY	REVIEWED BY	APPROVED BY
R.B. ERICSON	W.C. MITCHELL	E.F. HAMPL, JR. PROGRAM MANAGER

MINNESOTA MINING & MANUFACTURING COMPANY
PIONEERING LABORATORY
ELECTRICAL PRODUCTS GROUP
ST. PAUL, MINNESOTA 55101

TABLE OF CONTENTS

LIST OF FIGURES

LIST OF TABLES

INTRODUCTION

The objective of the studies described in this report was to assess the chemical compatibility and outgassing requirements for GDS. To provide a data base for this assessment, data were obtained in the following three areas:

- Isothermal chemical compatibility of converter components
- Compatibility with reactive gas species
- Outgassing of insulations

Potentially several intercomponent reactions, either solid-solid or gas-solid, can occur within the converter section of the GDS. Since previous experiments had indicated no major bulk reactions, the compatibility studies described in this report were designed to detect surface reactions with high sensitivity, and to determine outgassing rates of the converter thermal insulations.

The evaluation of data from the areas studied showed that the materials tested for use in GDS were compatible and that the thermal insulations could be processed so as to minimize gas-solid reactions with the thermoelectric materials.

Previous material selections and storage/handling of processed materials recommendations for the GDS converter have been substantiated by these studies. In addition, the Min-K SiO_2/TiO_2 type thermal insulation was found to be acceptable.

SECTION 1

EXPERIMENTAL RESULTS

1.1 ISOTHERMAL CHEMICAL COMPATIBILITY

1.1.1 Purpose of Study

This study was done to ascertain interactions between materials, extent of these interactions, and finally the effect these interactions might have on material compatibility.

1.1.2 Description of Test Equipment

This method involved sealing previously outgassed samples in an appropriate geometrical array, under Research Grade Xenon, in cleaned and outgassed quartz tubes and soaking for 500 and 1000 hours at 900°C and 850°C respectively. Since the objective was to determine compatibility of materials and not of impurities/contaminants, the isothermal compatibility candidate materials were individually outgassed and stored in sealed mason jars. These jars contained activated molecular sieves and a helium or argon atmosphere. At an appropriate time, a sample was removed from its mason jar, under a helium/activated molecular sieve atmosphere, and loaded into a cleaned and outgassed quartz tube. Figure 1-1 illustrates the experimental apparatus used for the evacuation/backfilling/seal-off operations.

1.1.3 Test Matrix

The test matrix for this isothermal chemical compatibility series is summarized in Table 1-I.

1.1.4 Test Results

The results from the various post-test analytical evaluation techniques are detailed in Table 1-II. The following summarizes these results:

	Material	Results
I	TPM-217	
	A. Tantalum - proximity	Compatible through 850°C
	B. Molybdenum - proximity	Compatible through 850°C

	Material	Results
C.	Pt-3008 - proximity	Compatible through 850°C
D.	Fiberfrax H-Blanket - contact	Compatible through 850°C
II.	$GdSe_{1.49}$	
A.	Min K-1800TE - proximity	Compatible through 900°C
B.	Min K-1800TE - contact	Compatible through 900°C
C.	Fiberfrax H-Blanket - contact	Compatible through 900°C

Because of sealoff problems, no direct compatibility determination for Fiberfrax 660 AH HiFi was made in this series. However, because of similarities in main constituents, outgassing characteristics, and trace impurity levels as well as previous compatibility test results, Fiberfrax 660 AH HiFi is considered to be compatible. This conclusion will be justified experimentally.

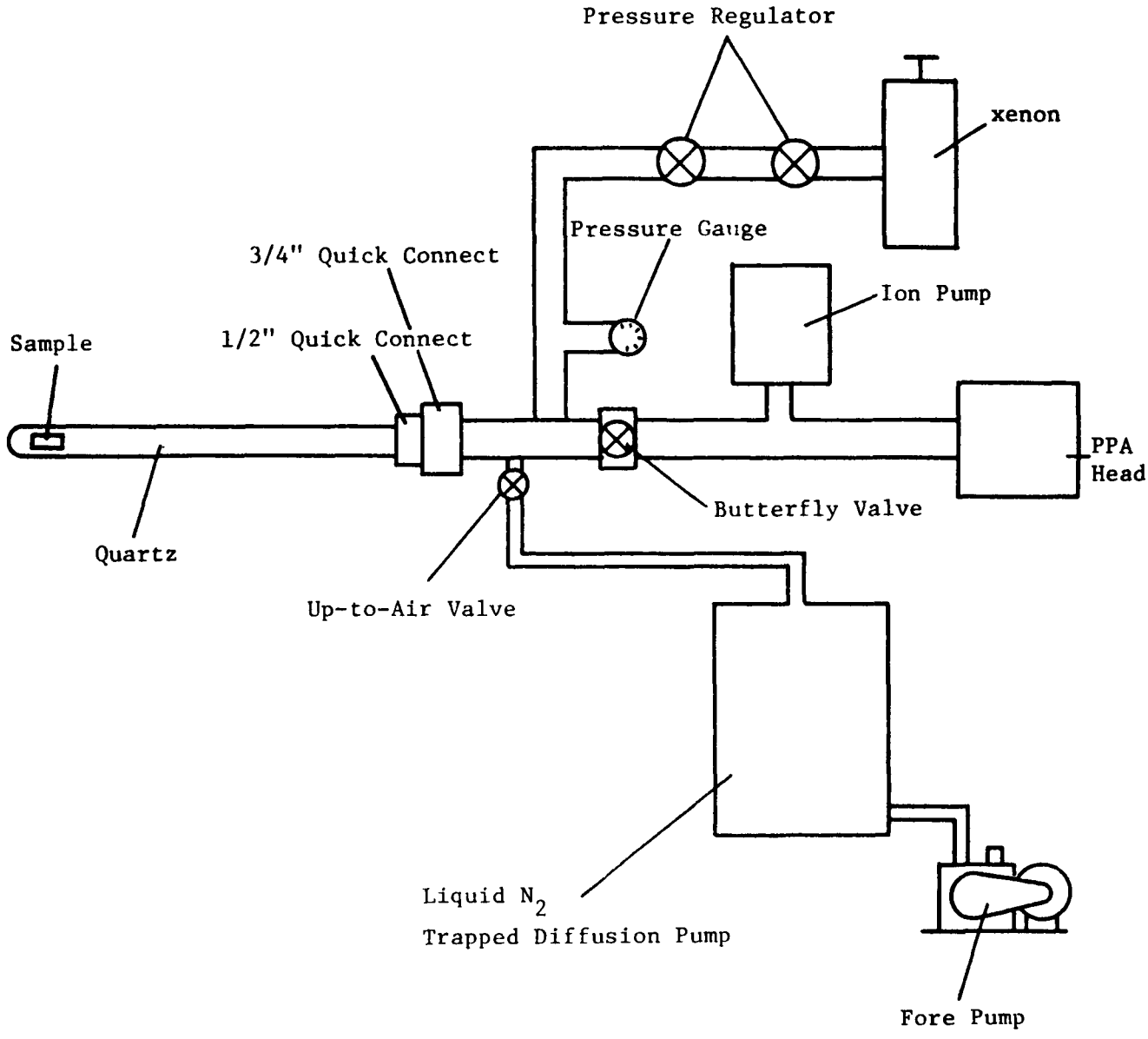

Figure 1-1. Isothermal Chemical Compatibility Backfill/Sealoff Apparatus

TABLE 1-I. TEST MATRIX FOR ISOTHERMAL CHEMICAL COMPATIBILITY SERIES

I. MATERIALS

A. TPM-217 (outgassed at 850°C/1 hr./vacuo)

1. Pt-3008, Mo, Ta (proximity): outgassed at 950°C/18 hours/vacuo

2. Fiberfrax H-Blanket, Fiberfrax 660 AH HiFi paper (contact): outgassed at 950°C/18 hours/vacuo

B. $GdSe_x$ (As Cast)

1. Min K 1800TE (proximity): outgassed at 1000°C/40 hrs/vacuo

2. Min K 1800TE, Fiberfrax H-Blanket, Fiberfrax 660 AH HiFi paper (contact): outgassed at 1000°C/40 hrs/vacuo

II. PARAMETERS

A. Temperatures

1. 850°C

2. 900°C

B. Test Duration

1. 1000 hours

2. 500 hours

C. Cover Gas

1. Research Grade Xenon

D. Containment Ampoule

1. Cleaned and outgassed quartz

III. ANALYTICAL EVALUATION TECHNIQUES

A. Emission Spectroscopy (ES): This is a technique useful for identifying trace (ppm) amounts of active impurities.

TABLE 1-I. TEST MATRIX FOR ISOTHERMAL CHEMICAL COMPATIBILITY SERIES - Continued

B. Mass Spectroscopy (MS): This is a technique useful for identifying volatile species.

C. Infrared Spectroscopy (IR): This is a technique useful for identifying organic structures.

D. Electron Beam Microanalyzer (EBM): This is a technique useful for identifying in situ inclusions, secondary phases, and interface diffusion parameters.

E. Electron Spectroscopy Chemical Analysis (ESCA) and Ion Scattering Spectroscopy (ISS): These techniques are useful for identifying outermost surface components, structure and depth of diffusion into bulk.

F. X-Ray Diffraction (XRD): This is a technique useful in identifying the structure of a material.

G. Seebeck Coefficient (S): This is a technique useful for obtaining carrier concentration levels in T/E materials.

H. Leco Carbon (Leco): This is a combustion technique for obtaining total carbon concentrations.

TABLE 1-II. TEST RESULTS FROM ISOTHERMAL CHEMICAL COMPATIBILITY SERIES

SYSTEM	OBSERVATIONS/RESULTS
I. TPM-217 ($Cu_{1.97}Ag_{0.03}Se_{1+y}$)	
A. Tantalum - Proximity (850°C/1000 hrs./Xenon)	TPM-217: The element appeared as pre-test. The post-test Seebeck coefficient was 254 μv/°C abs. which is within one standard deviation from the mean for the parent non-tested batch material.
	Tantalum: The surface was only slightly darkened. ISS analysis indicated trace selenium on the surface diminished into the background after sputter etch removal ($\sim$100-200Å). The selenium level was about four times the minimal detection level.
B. Molybdenum - Proximity (850°C/1000 hrs./Xenon)	TPM-217: The element appeared as pre-test. The post-test Seebeck coefficient was 251 μv/°C abs. which is within one standard deviation from the mean for the parent non-tested batch material.
	Molybdenum: The surface was only slightly darkened. ISS analysis indicated trace selenium present to 1600Å into the sample. Metallurgically, the selenium layer was estimated to be less than 0.5 μm thick. Hence a bound of 1600-5000A diffusion into the Mo for the vapor transported selenium. This reaction rate is insignificant for the mechanical integrity of molybdenum components: for a seven-year mission, less than 1% of the hot strap would react at this rate.

TABLE 1-II. TEST RESULTS FROM ISOTHERMAL CHEMICAL COMPATIBILITY SERIES - Continued

SYSTEM	OBSERVATIONS/RESULTS
C. Pt-3008 - Proximity (850°C/1000 hrs./Xenon)	TPM-217: The element appeared as pre-test. The post-test Seebeck coefficient was 249 μv/°C abs. which is within one standard deviation from the mean for the parent non-tested batch material. Pt-3008: The tensile specimen appeared as pre-test. ORNL tensile test data indicated little difference between the control Pt-3008 and the TPM-217 exposed to Pt-3008 with respect to yield strength, ultimate tensile strength, and elongation:

	Proximity Sample	Control Pt-3008
Yield Strength	24.8	27.2
UTS	46.2	51.8
Elongation	15.4	18.4

In addition, selenium was not detected by ORNL Auger analysis in the interior nor on

TABLE 1-II. TEST RESULTS FROM ISOTHERMAL CHEMICAL COMPATIBILITY SERIES - Continued

SYSTEM	OBSERVATIONS/RESULTS
	the exterior of the proximity Pt-3008 [1] However, silicon was detected in the interior of the control Pt-3008.
D. Fiberfrax Hi-Fi Blanket - Contact (850°C/1000 hrs./Xenon)	TPM-217: The element appeared as pre-test. The post-test Seebeck coefficient was 249 μv/°C abs. which is within one standard deviation from the mean for the parent non-tested batch material.
	H-Blanket: The H-Blanket appeared as pre-test. ES Analysis indicated only that trace TPM-217 particles were on the sample of the H-Blanket in contact with the TPM-217. No other selenium was detected in the H-Blanket.
E. Fiberfrax 660 AH Hi-Fi Paper - Contact (850°C/1000 hrs./Xenon)	The sample was totally destroyed because of improper seal-off.
F. TPM-217 Control (850°C/1000 hrs./Xenon)	The sample was totally destroyed because of improper seal-off.

[1] Phone Conversations - J. Keiser ORNL/R. Ericson 3M Co. 2/4/77 and 3/2/77. The Control Pt-3008 was subjected to the same thermal cycles as the Pt-3008/TPM-217.

TABLE 1-II. TEST RESULTS FROM ISOTHERMAL CHEMICAL COMPATIBILITY SERIES - Continued

SYSTEM	OBSERVATIONS/RESULTS
II. $GdSe_{1.49}$	
A. $GdSe_{1.49}$ Controls (900°C/500 hrs./Xenon)	$GdSe_{1.49}$: One control appeared to be only thermally etched whereas the second had a trace surface layer over about one-half its surface. Metallurgical/EBM analysis of this two μm layer indicated Gd_2Se0_{3-4}. This surface layer corresponds to $\sim$0.2 mg of oxygen. ESCA analysis indicated Si, C, and 0 contaminants on the surface. These contaminants most likely originate from back-streaming vacuum pump oil.
3. Min-K 1800TE - Proximity (900°C/500 hrs./Xenon)	$GdSe_{1.49}$: A faint lace-like pattern was detected on a portion of the surface. There was not a detectable reaction nor penetration. In addition, there was a trace surface layer over the entire surface. Metallurgical/EBM analysis of this four μm layer indicated Gd_2Se0_{3-4}. This surface layer corresponds to $\sim$0.4 mg of oxygen. ESCA analysis indicated Si, C, and 0 contaminants on the surface of the elements. These contaminants were also present in the control, probably originating from back-streaming of vacuum pump oil.
	Min-K 1800TE: There was a color change from pre-test light blue to dark navy blue. ES analysis of the test insulation indicated the same impurity distribution as pre-test insulation. In addition, MS and IR analyses of the as received insulation revealed trace volatile oxygenated hydrocarbons. Furthermore, Leco carbon analysis indicated 0.10% within the as received insulation.

TABLE 1-II. TEST RESULTS FROM ISOTHERMAL CHEMICAL COMPATIBILITY SERIES - Continued

SYSTEM	OBSERVATIONS/RESULTS
	Note: The color change is probably caused by carbon from either thermal cracking of the intrinsic oxygenated hydrocarbons within the insulation and/or back-streaming vacuum pump oil, reducing the TiO_2 opacifier.
C. Min-K 1800TE - Contact (900°C/500 hrs./Xenon)	$GdSe_{1.49}$: Observations and analytical evaluation results are identical to the Min-K 1800TE - Proximity test. The trace Gd_2Se0_{3-4} surface layer was 4 and 8 μm for two specimens and corresponded to 0.8 and 1.6 mg. oxygen respectively.
	Min-K 1800TE: Observations and analytical evaluation results are identical to the Min-K 1800TE - Proximity test.
D. Fiberfrax H-Blanket - Contact (900°C/500 hrs./Xenon)	$GdSe_{1.49}$: There was a trace surface layer over the entire surface. Metallurgical/EBM analysis of this four μm layer indicated Gd_2Se0_{3-4}. This surface layer corresponds to 0.8 mg. of oxygen. ESCA analysis indicated Si, C, and O contaminats on the surface of the element. Again, the presence of these same contaminants in the control indicates vacuum pump back-streaming as the source.
	H-Blanket: Very sooty appearance over entire surface of insulation. When the sooty insulation was heated in air, the sooty color disappeared. This observation suggests a carbon deposit on the surface of the insulation. Leco carbon analysis confirmed this - 0.21% wt. on the sooty insulation vs 0.02% wt. on as received insulation. In addition, MS and IR

TABLE 1-II. TEST RESULTS FROM ISOTHERMAL CHEMICAL COMPATIBILITY SERIES - Continued

SYSTEM	OBSERVATIONS/RESULTS
	analyses of the as received insulation revealed trace volatile oxygenated hydrocarbons. ES analysis of the test insulation indicates the impurity distribution as pretest insulation. Note: The sooty appearance of the insulation most likely is caused by vacuum pump oil backstreaming. The Si, C, O contaminants on the surface of the element most likely originate from the same source.
E. Fiberfrax 660 AH Hi-Fi Paper - Contact (900°C/500 hrs./Xenon)	$GdSe_{1.49}$: There was a moderate to heavy brownish-tan surface deposit over the entire element. Metallurgical/EBM analysis of the 150 μm surface layer indicated Gd_2SeO_{3-4}. This surface layer corresponds to about 30 mg. of oxygen. Since selenium was detected on both the seal-off side and air side of the quartz tube seal-off, it is clear that an air leak produced the oxygen surface reaction in this sample. It is noteworthy that the oxygen was restricted to a surface layer and did not diffuse into the sample. Figure 1-2 shows a clearly defined surface layer adjacent to a columnar phase. Metallurgical/EBM analysis of this phase indicated $GdSe_{1.8}$. Hence, selenium from the surface has diffused into the bulk $GdSe_{1.49}$ a maximum of 600 μm and reacted to form $GdSe_{1.8}$. In the previously discussed $GdSe_{1.49}$ compatibility cases, insufficient free selenium was available from the surface reaction of $GdSe_{1.49}$ with oxygen to diffuse and react with bulk $GdSe_{1.49}$. Figure 1-2 also shows a

TABLE 1-II. TEST RESULTS FROM ISOTHERMAL CHEMICAL COMPATIBILITY SERIES - Continued

SYSTEM	OBSERVATIONS/RESULTS
E. Fiberfrax 660 AH Hi-Fi Paper - Contact (Cont'd)	a clearly defined surface layer without the columnar $GdSe_{1.8}$ phase on one of these $GdSe_{1.49}$ compatibility samples. ESCA analysis indicated C and O contaminants on the surface of the $GdSe_{1.49}$; a shift in the electron energy toward a higher electronegativity for the Gd-Se-C-O peaks which indicate Gd-Se-O and C-O type of compounds. These are formed as a result of the air leak and vacuum pump oil back-streaming. Hi-Fi: Brownish-tan deposit on the insulation directly contacting the element. MS and IR analyses of the as received insulation revealed trace volatile oxygenated hydrocarbons. Furthermore, Leco analysis on the as received insulation indicated 0.14-0.17% wt. total carbon.

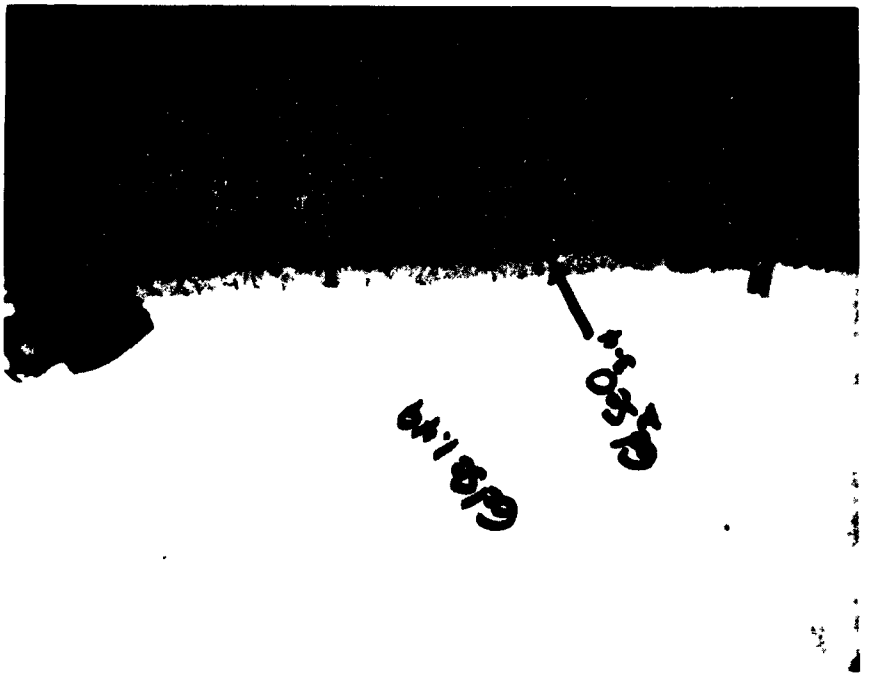

$GdSe_x$/Fiberfrax H-Blanket
900°C/500 hrs./Xenon
750x

$GdSe_x$/Fiberfrax 660 AH HiFi Paper
900°C/500 hrs./Xenon
75x

Figure 1-2. Surface Layer Contaminants - Isothermal Chemical Compatibility Series

1.2 REACTIVE GAS TESTING

1.2.1 Purpose of Study

Previous experiments have shown the following gas-thermoelectric material reactions can occur within the converter section of the GDS:

$$3/2(O_2) + Gd_2Se_3 \rightarrow Gd_2O_3 + 3\langle Se\rangle \qquad \Delta G = -147 \text{ k-cal/mol}$$

$$3(H_2O) + Gd_2Se_3 \rightarrow Gd_2O_3 + 3(H_2) + 3\langle Se\rangle \qquad \Delta G = -23 \text{ k-cal/mol}$$

$$3/2(CO_2) + Gd_2Se_3 \rightarrow Gd_2O_3 + 3/2C + 3\langle Se\rangle \qquad \Delta G = -28 \text{ k-cal/mol}$$

$$3(CO) + Gd_2Se_3 \rightarrow Gd_2O_3 + 3\,C + 3\langle Se\rangle \qquad \Delta G = -72 \text{ k-cal/mol}$$

$$2(O_2) + Gd_2Se_3 \rightarrow Gd_2SeO_4 + 2\langle Se\rangle \qquad \Delta G = \text{not known}$$

The large free energies of reaction imply that these reactions are thermodynamically possible for any partial pressure of the reactive gases practically attainable in a generator. The limitation on the reactions are entirely kinetic, depending on the availability of the gas species and the solid state diffusion into the Gd_2Se_3.

Because of kinetic limitations, the effect of the above reactions on thermoelectric performance is strongly influenced by the test conditions: the effect of oxygen in an isothermal closed tube at high temperature, the effect of air at room temperature, and the effect of oxygen on an element operating ingradient all differ.

For an element soaked isothermally in a sealed tube with a known amount of oxygen, the effect of the oxygen can be calculated by assuming that the selenium freed by the surface oxidation of the gadolinium selenide dopes the element. Thus, 0.3 mg. of oxygen is calculated to reduce the carrier concentration of a standard $GdSe_{1.48}$ element by 10%, increasing the resistivity by 10% and the Seebeck Coefficient by 7 μv/°C. This effect has been observed experimentally: a sealed tube sample soaked 89 hours at 800°C reacted with 1.8 mg. of oxygen to produce a 42 μv/°C increase in Seebeck Coefficient. Chemical and metallurgical analyses of gadolinium selenide elements exposed to oxygen in an isothermal sealed tube also substantiates the model of a surface reaction with oxygen and a diffusion of the liberated selenium into the bulk. On lightly oxidized samples, the oxygen is visible as a distinct surface layer of composition Gd_2SeO_{3-4} attached to the normal bulk composition. In a heavily oxidized element, the surface oxide layer was 150 μm and was followed by a 600 μm oxygen-free layer of $GdSe_{1.8}$. Since alteration of bulk thermoelectric properties requires that the selenium liberated diffuse into the bulk element, the isothermal sealed tube condition represents the most conservative estimate for the tolerable limit for oxygen exposure. Only in this case is all the selenium liberated by oxidation constrained to rereact and diffuse into the element.

For an element exposed to air at room temperature, the reaction with oxygen and water, according to the above equations, has been found to be extremely rapid but self-limiting. If the surface of an element is abraded in air, the resistive oxide surface film forms so rapidly that no reduction in contact resistance can be produced. Only by removal of the surface oxide layer in inert atmosphere (e.g., by sputtering or grinding under kerosene) can the contact resistance be reduced. The formation of the thin oxide surface layer is observed to be accompanied by formation of a thin deposit of free selenium, as it should be according to the above equations. The reaction at room temperature, although very rapid is strongly restricted to the surface by diffusion kinetics. Elements stored at room temperature have surface films undetectable by optical microscopy, which puts an upper bound of $<1\ \mu m$ on the reaction zone. Sputter contacting experiments put an upper bound of $<0.1\ \mu m$ on the thickness of the high resistance oxide layer formed at room temperature.

For an element operated ingradient with oxygen, the effect of the oxygen on thermoelectric properties is greatly reduced from the isothermal sealed tube value by two mechanisms: only a fraction of the gas which impinges on the element surface reacts (accommodation coefficient) and the selenium formed on the surface is free to diffuse away from the surface rather than into the bulk material. As a result, the isothermal sealed tube experiments place a very conservative upper bound on the tolerable oxygen level.

This reactive gas study was initiated to ascertain contaminant gas tolerance limits, under simulated module conditions, for the thermoelectric materials and to define the diffusion coefficient and accommodation coefficient for the oxygen absorption/reaction process.

1.2.2 Description of Test Equipment

This method involved ingradient operation of a selenide couple, in the geometric array shown in Figures 1-3 and 1-4, with a 4 amp load current, T_h 850°C/T_c 150°C thermal gradient, and oxygen partial pressure levels of 10^{-2}, 10^{-4}, 10^{-6} torr.

The legs were brought to operating temperature conditions and allowed to seat-in before the contaminant gas was introduced. In this way, the effect of seat-in and initial property variation can be separated from the contaminant gas effect on Seebeck and resistance. In addition, a temporary decrease in Seebeck of approximately 1 $\mu v/°C/day$ has been occurring in ingradient tests of N-legs because of annealing, Gd doping, or phase change. The test duration was short enough that this effect could be isolated.

1.2.3 Test Matrix

The test matrix for this reactive gas testing series is summarized in Table 1-III.

1.2.4 Test Results

This study is still continuing and results will be periodically updated. The primary result from the first contaminant gas experiment using oxygen was that no appreciable change in thermoelectric performance occurred which could be attributed to the oxygen exposure.

The total exposure history is summarized in Table 1-IV and depicted in Figure 1-5. The total exposure to oxygen was 0.301 torr-hour, which would be equivalent to an exposure level of 5×10^{-6} torr for seven years.

Analytical evaluation of the thermoelectric elements to determine diffusion and accommodation coefficient data is in progress and will be reported in a future Reactive Gas Testing update.

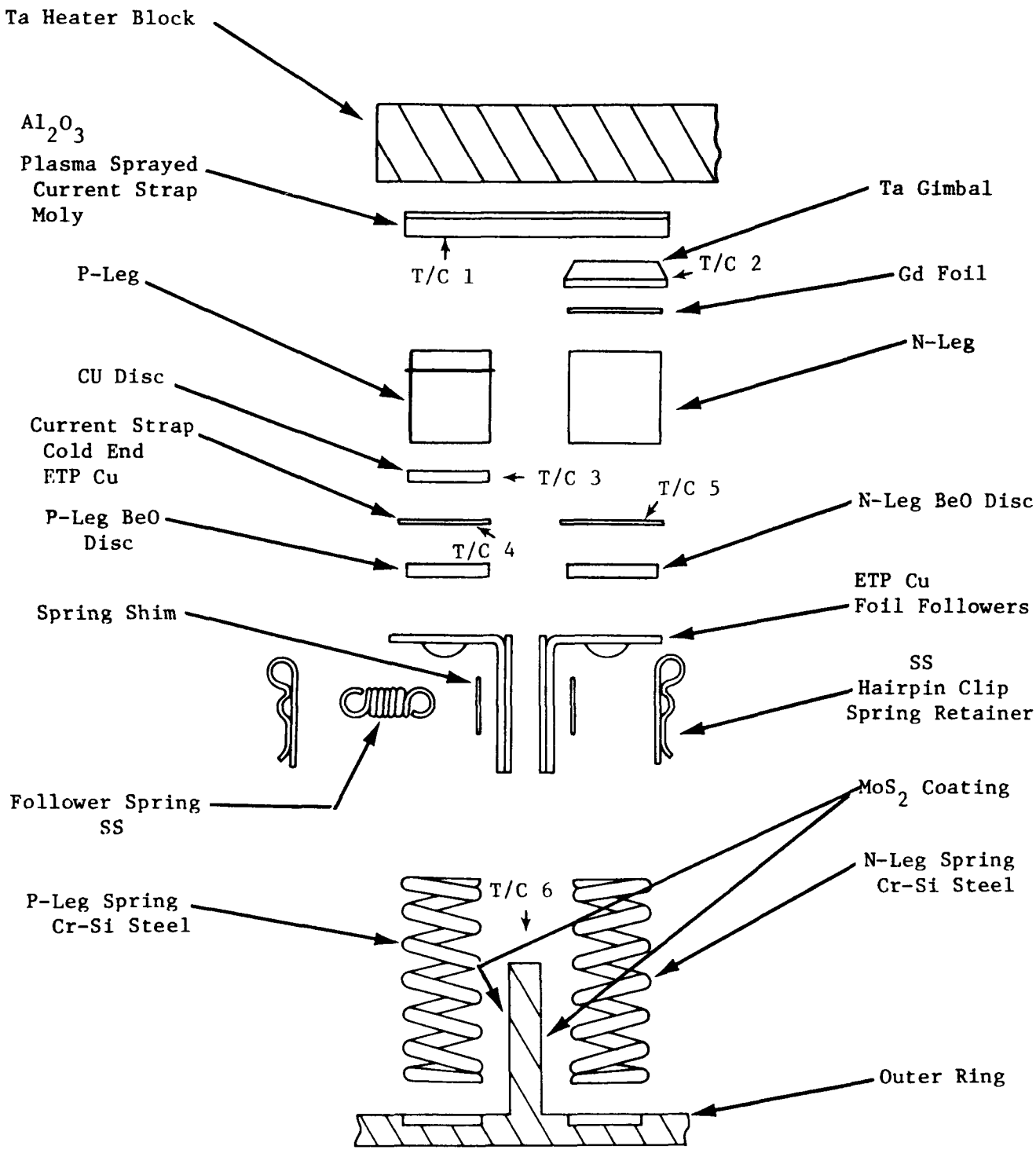

Figure 1-3. Reactive Gas Test - Couple Assembly and Thermocouple Location

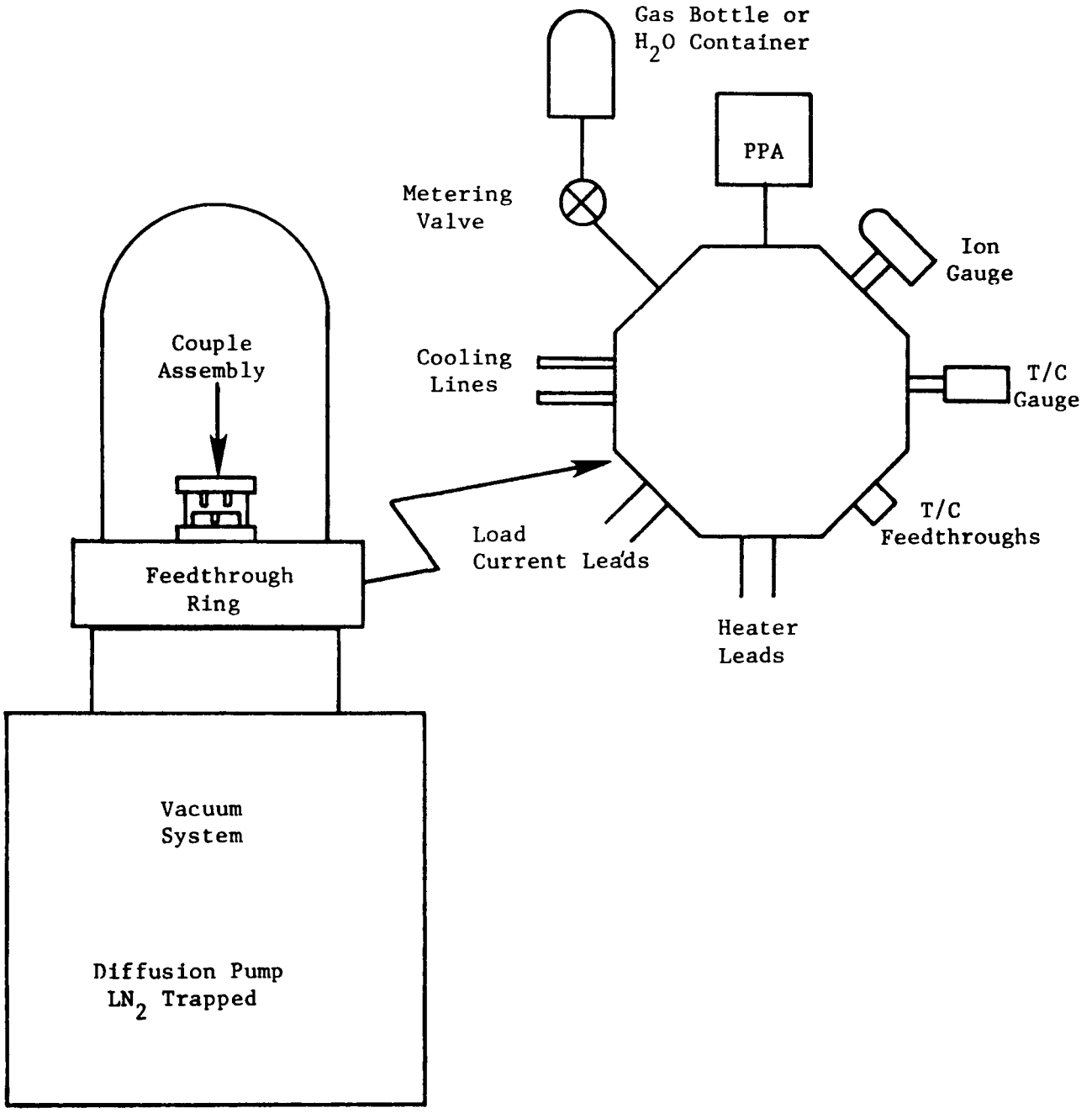

Figure 1-4. Schematic of Reactive Gas Test Assembly

TABLE 1-III. TEST MATRIX FOR REACTIVE GAS TESTING SERIES

I. MATERIALS

(As shown in Figure 1-3)

II. PARAMETERS

A. Thermal Gradient

1. T_h 850°C/T_c 150°C

B. Test Duration

1. 8 - 30 hours @ each partial pressure level

C. Contaminant Gas and Partial Pressure Level

1. O_2
   a. 10^{-2} torr
   b. 10^{-4} torr
   c. 10^{-6} torr
2. H_2O
   a. 10^{-2} torr
   b. 10^{-4} torr
   c. 10^{-6} torr
3. CO
   a. 10^{-2} torr
   b. 10^{-4} torr
   c. 10^{-6} torr

TABLE 1-III. TEST MATRIX FOR REACTIVE GAS TESTING SERIES - Continued

II. PARAMETERS - (Continued)

4. CO_2

a. 10^{-2} torr

b. 10^{-4} torr

c. 10^{-6} torr

III. ANALYTICAL EVALUATION TECHNIQUES

A. Neutron Activation Analysis (NAA): This is a technique useful for non-destructively determining trace levels of impurities in materials.

B. Ingradient Seebeck & Resistivity: These are techniques which give carrier concentration data on T/E materials.

C. ESCA/ISS: These techniques are useful for identifying outermost surface components, structure and depth of diffusion into bulk.

TABLE 1-IV. TEST PERFORMANCE FROM TIME STABLE CONDITIONS WERE ACHIEVED

TIME (HRS)	T_h (°C)	T_c (°C)	ENVIRONMENT	PRESSURE (Torr)	S_n (μv/°C)	R_n (mΩ)	Sp(μv/°C)	Rp(mΩ)
0	763	147	H_2O,N_2	9×10^{-8}	183.0	25.6	255.6	16.1
5	853	172	H_2O,N_2	5×10^{-8}	194.8	27.9	277.4	21.2
6	856	190	H_2O,N_2	5×10^{-8}	195.1	29.6	267.8	15.8
7	860	190	H_2O,N_2	5×10^{-8}	195.4	31.6	268.1	15.9
8	861	189	H_2O,N_2	5×10^{-8}	195.0	31.7	268.2	16.0
24	861	189	H_2O,N_2	4×10^{-8}	195.3	31.3	268.0	16.4
26	857	185	O_2	1×10^{-6}	198.4	31.7	272.8	17.3
27	858	185	O_2	1×10^{-6}	196.9	31.6	266.9	16.3
28	865	186	O_2	1×10^{-6}	197.7	31.8	267.9	16.4
29	863	187	O_2	1×10^{-6}	198.5	38.7	270.6	16.9
30	867	186	O_2	1×10^{-6}	197	38.7	268	16.4
31	869	186	O_2	1×10^{-6}	198	39.1	268	16.5
32	868	185	O_2	1×10^{-6}	198	39.2	268	16.5
33			H_2O,N_2	2.5×10^{-8}				

TABLE 1-IV. TEST PERFORMANCE FROM TIME STABLE CONDITIONS WERE ACHIEVED - Continued

TIME (HRS)	T_h (°C)	T_c (°C)	ENVIRONMENT	PRESSURE (Torr)	S_n (μv/°C)	R_n (mΩ)	Sp(μv/°C)	Rp(mΩ)
49	861	186	$H_2O.N_2$	2.5×10^{-8}	199	39.2	268	16.2
50	852	184	O_2	1×10^{-4}	196	39..	266	16.0
51	848	183	O_2	1×10^{-4}	197	39.4	266	15.9
52	849	184	O_2	1×10^{-4}	195	39.4	267	15.9
53	846	183	O_2	1×10^{-4}	196	39.7	267	16.0
54	846	183	O_2	1×10^{-4}	196	39.8	267	15.8
55	847	183	O_2	1×10^{-4}	196	40.0	267	15.8
56	848	184	O_2	1×10^{-4}	197	4 .5	266	15.8
57			$H_2O.N_2$	1×10^{-7}				
72	845	182	$H_2O.N_2$	1×10^{-7}	198	39.9	266	16.0
74	836	182	O_2	1×10^{-2}	196	40.0	265	15.7
75	838	184	O_2	1×10^{-2}	197	40.4	266	15.7
76	840	183	O_2	1×10^{-2}	196	40.6	265	15.8
77	836	182	O_2	1×10^{-2}	197	40.7	266	15.9

TABLE 1-IV. TEST PERFORMANCE FROM TIME STABLE CONDITIONS WERE ACHIEVED - Continued

TIME (HRS)	T_h (°C)	T_c (°C)	ENVIRONMENT	PRESSURE (Torr)	S_n (μv/°C)	R_n (mΩ)	Sp(μv/°C)	Rp(mΩ)
78	842	184	O_2	1×10^{-2}	197	40.9	265	15.8
79	842	183	O_2	1×10^{-2}	197	41.1	267	16.0
80	841	183	O_2	1×10^{-2}	198	41.4	266	16.0
81			O_2	1×10^{-2}				
96	837	183	O_2	1×10^{-2}	197	41.9	264	15.9
101	837	183	O_2	1×10^{-2}	197	42.0	265	16.1
103	662	193	O_2	1×10^{-2}				

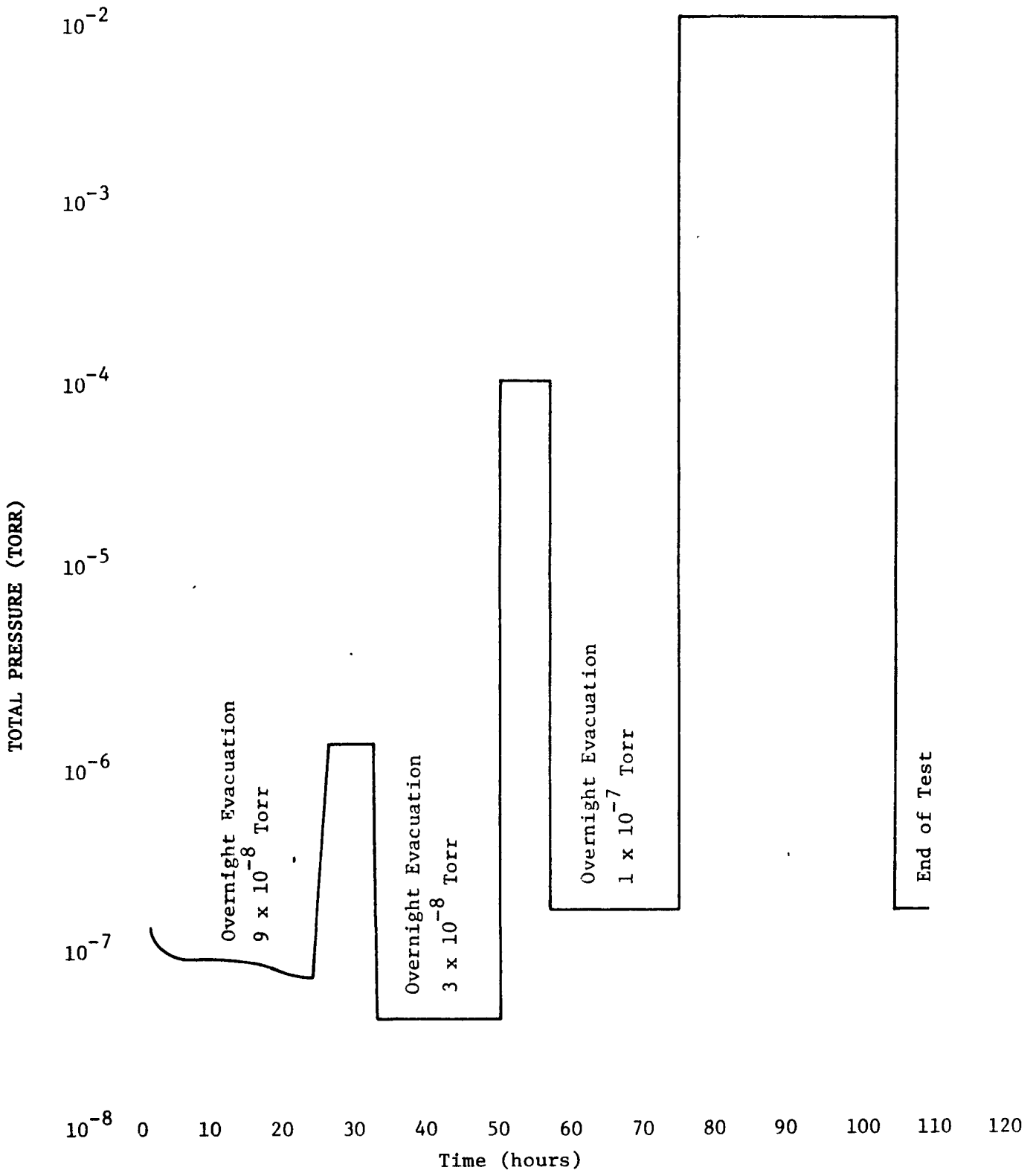

Figure 1-5. Oxygen Exposure History

1.3 OUTGASSING

1.3.1 Converter Thermal Insulations

1.3.1.1 Purpose of Study

This study was done to determine the outgassing rates and the storage/handling conditions for the converter thermal insulations.

1.3.1.2 Description of Test Equipment

Outgassing studies on thermal insulations were done in a laboratory experimental outgassing apparatus diagrammed in Figure 1-6. The insulations were processed by vacuum outgassing the as received materials to 100°C above the expected peak operating temperatures for times of 18-40 hours. After this initial processing, an upper limit on the residual outgassing of the material was determined using a partial pressure analyzer. The insulation was then exposed to air for 7-24 hours at 27-56% RH, stored in argon for 216-1400 hours, and then reprocessed. During this reprocessing, the outgassing rates were monitored at each thermal plateau to determine the total material outgassing. Tables 1-V, 1-VI and 1-VII describe the overall outgassing scheme used for these studies. Figure 1-7 illustrates the outgassing flow diagram.

Scale-up outgassing studies were done in an outgassing apparatus diagrammed in Figure 1-8 and described in Table 1-VIII. The insulation was processed by a dual processing technique: 1) air bake-out at 800°C for 15-18 hours; 2) vacuum outgassing at 1000°C until the monitored pressure is of the same magnitude as that achieved in the smaller laboratory experimental outgassing apparatus. The reason for a dual outgassing scheme is that MS, IR and Leco analyses indicated the as received thermal insulations contained 0.02-0.17% wt. volatile oxygenated hydrocarbons which are not removed by vacuum outgassing. Since these analytical results were not available until completion of the laboratory experimental outgassing studies; this process differs from the above laboratory experimental one.

1.3.1.3 Test Matrix

The test matrix for the thermal insulation outgassing studies is summarized in Table 1-IX.

1.3.1.4 Test Results

The results from these thermal insulation outgassing studies are summarized in Tables 1-X and 1-XI and Figures 1-9 and 1-10.

In addition to these data, the following experimental observations were made:

Carbon deposits detected on quartz walls of laboratory experiment series during 1000°C/40 hr processing of both Min-K and Fiberfrax materials.

A color change, off-white to light-blue, was observed for Min-K experiments. This color change can be attributed to a reduction of TiO_2 by the previously discussed (Isothermal Chemical Compatibility Section) intrinsic oxygenated hydrocarbon contaminants within Min-K insulation. Titania can react with carbon as follows:

TITANIA REACTIONS WITH CARBON

($T°_C$ = 930)

1. $TiO_2 + C \rightarrow Ti + CO_{2(g)}$ $\quad \Delta G = 77.3$ K-cal, $P_{CO_2} = 7 \times 10^{-12}$ torr

2. $TiO_2 + C \rightarrow TiO_{(s)} + CO(g)$ $\quad \Delta G = 24.4$ K-cal, $P_{CO} = 3 \times 10^{-2}$ torr

3. $2\ TiO_2 + C \rightarrow 2\ TiO_{(s)} + CO_2(g)$ $\quad \Delta G = 59.5$ K-cal, $P_{CO_2} = 1 \times 10^{-8}$ torr

4. $2\ TiO_2 + C \rightarrow Ti_2O_{3(s)} + CO(g)$ $\quad \Delta G = 12.7$ K-cal, $P_{CO} = 4$ torr

5. $4\ TiO_2 + C \rightarrow 2\ Ti_2O_{3(s)} + CO_{2(g)}$ $\quad \Delta G = 34.8$ K-cal, $P_{CO_2} = 4 \times 10^{-4}$ torr

6. $3\ TiO_2 + C \rightarrow Ti_3O_{5(s)} + CO(g)$ $\Delta G = 14.1$ K-cal, $P_{CO} = 2$ torr

7. $6\ TiO_2 + C \rightarrow 2\ Ti_3O_{5(s)} + CO_{2(g)}$ $\Delta G = 37.5$ K-cal, $P_{CO_2} = 1 \times 10^{-4}$ torr

Thermodynamic values taken from Metallurgical Thermochemistry by O. Kubaschewski, Pergamon Press, 1967.

The significance of the gaseous partial pressure levels is that, if in a LCHPG they were lower than the above values, titania would react with carbon at 930°C.

STABILITY OF TITANIA IN ABSENCE OF CARBON

($T_{°C} = 930$)

1. $2\ TiO_2 \rightarrow 2\ TiO + O_{2(g)}$ $\Delta G = 153.2$ K-cal, $P_{O_2} = 1 \times 10^{-25}$ torr

2. $4\ TiO_2 \rightarrow 2\ Ti_2O_3 + O_2\ (g)$ $\Delta G = 129.7$ K-cal, $P_{O_2} = 2 \times 10^{-21}$ torr

3. $6\ TiO_2 \rightarrow 2\ Ti_3O_5 + O_{2(g)}$ $\Delta G = 132.5$ K-cal, $P_{O_2} = 6 \times 10^{-22}$ torr

Thermodynamic values taken from Metallurgical Thermochemistry by O. Kubaschewski, Pergamon Press, 1967.

The reaction most likely, according to Johns-Manville Research Center, Denver, Colorado, to produce this color change is the $TiO_2 \rightarrow Ti_2O_3$ or Ti_3O_5 reaction and not a $TiO_2 \rightarrow TiO_{2-x}$. ② To eliminate the carbon contaminant (colloidal graphite mold release) which originates during the molding operation, an 800°C/15-24 hour air bake-out was recommended. A preliminary experiment to verify this was attempted in which the air baked-out insulation was then vacuum processed as per the aforementioned laboratory experimental method. The insulation did not exhibit the off-white to light blue color transition as observed when only vacuum processing was done.

② Phone Conversation: John Pallo, JM/R. Ericson, 3M 2/24/77.

Laboratory Experimental Verses Scale-Up:

The experimental outgassing times for the vacuum processing was in good agreement with the calculated value. ③ The following shows this agreement:

	Experimental		Calculated
	Lab Exp.	Lab Scale-Up	Lab Scale-Up
Fiberfrax H-Blanket	40 hours	140 hours	110 hours

In addition, calculations of the time necessary to reach uniform temperature within a level insulation indicates seven hours at 1000°C. ④ Hence, the above processing time should be adequate for converter requirements.

1.3.2 Components Other Than Thermoelectric Element Insulations

1.3.2.1 Purpose of Study

This study was done to determine the outgassing rates of the components other than thermal insulations in the GDS Converter Section.

1.3.2.2 Description of Test Equipment

The outgassing studies in this section were identical to those described in 1.3.1.1. Thermal Insulations with the exception that these components were not subjected to reprocessing after an air/argon exposure.

1.3.2.3 Test Matrix

The test matrix for this series is summarized in Table 1-XII.

1.3.2.4 Test Results

The results from these outgassing studies are summarized in Table 1-XIII. For comparison purposes, the thermal insulation data are also listed.

---

③ S. Dushman, "Scientific Foundations of Vacuum Techniques," John Wiley, & Sons, 1962, p. 94.

④ P. Schneider, "Conduction Heat Transfer," Addison-Wesley Inc., 1955, p. 249.

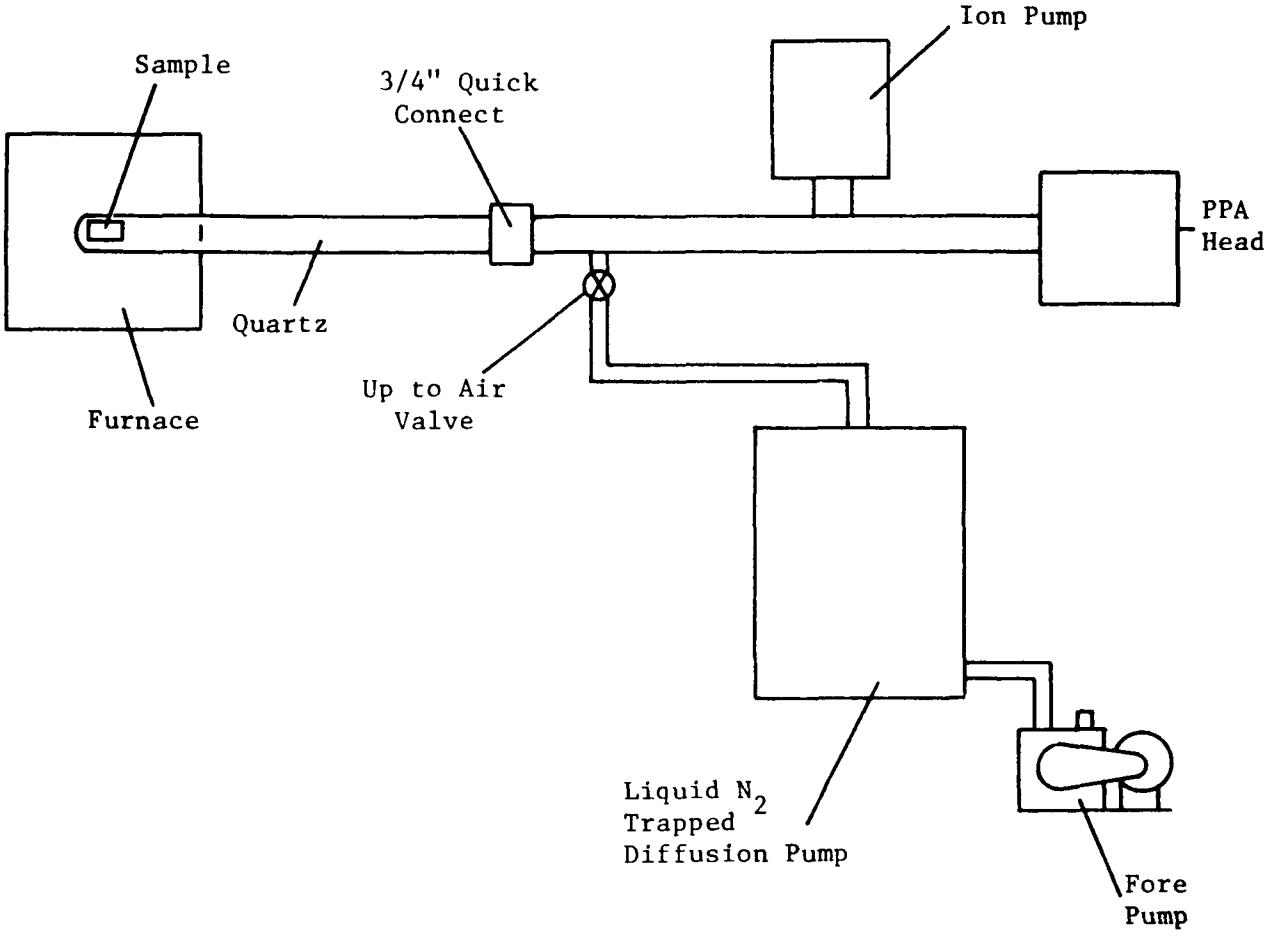

Figure 1-6. Laboratory Experimental Outgassing Apparatus

TABLE 1-V. OUTGASSING STUDY: PROCEDURE I

Experimental Conditions for Outgassing Data Base

Cycle (1) Initial processing of material to temperature A;

(2) Determination of maximum outgassing of processed material at temperature B;

(3) Outgassing rate of stored material during simulated module processing from ambient to temperature C.

GDS

MATERIAL	A	B	C
Fiberfrax HiFi Paper	1000°C	900°C	900°C
Fiberfrax H-Blanket	1000°C	900°C	900°C
Min-K 1800TE	1000°C	900°C	900°C
Min-K 1400TE	950°C	850°C	850°C

TABLE 1-VI. OUTGASSING STUDY: PROCEDURE II - INITIAL PROCESSING & RESIDUAL OUTGASSING OF PROCESSED MATERIAL

PARAMETERS:

Temperature - Initial processing: Ambient to 950°C or 1000°C

Materials - Fiberfrax H-Blanket
Fiberfrax 660 AH HiFi Paper
Min-K 1800TE
Min-K 1400TE

Schedule	Temperature Cycle °C	Elapsed Time Hours	Conditions
A. Material Processing	Ambient to 950° or 1000	2.5	Dynamic vacuum - LN_2 trapped diffusion pump
B. Material Processing	950° or 1000° Soak	18 or 40	Dynamic vacuum - ion pump
C. Material Processing	950°→850° or 1000°→900°C	0.6	Dynamic vacuum - ion pump
D. Pressure Equilibration	850° or 900°C	3-4	Dynamic vacuum - ion pump
E. Residual Outgassing Measurement	850° or 900°C	2-3	Static vacuum ion pump off
F. Cool-Down	850° or 900°→ ambient	6-7	Dynamic vacuum ion pump

TABLE 1-VII. OUTGASSING STUDY: PROCEDURE III - OUTGASSING RATES OF STORED MATERIAL

PARAMETERS:

Temperature - Ambient to 850° or 900°C in six heat up cycles

Materials - Fiberfrax 660 AH HiFi Paper
Min-K 1800TE
Min-K 1400TE

Schedule	Temperature °C	Elapsed Time Hours	Conditions
A. System Evacuation	Ambient	18-22	Dynamic vacuum - ion pump
B. Heat Up Cycle 1	Ambient-100	1	Dynamic vacuum - ion pump
C. Heat Up Cycle 2	100-200	1	Dynamic vacuum - ion pump
D. Heat Up Cycle 3	200-400	1	Dynamic vacuum - ion pump
E. Heat Up Cycle 4	400-600	1	Dynamic vacuum - ion pump
F. Heat Up Cycle 5	600-800	1	Dynamic vacuum - ion pump
G. Heat Up Cycle 6	800-850 or 900	18	Dynamic vacuum - ion pump

OUTGASSING FLOW DIAGRAM

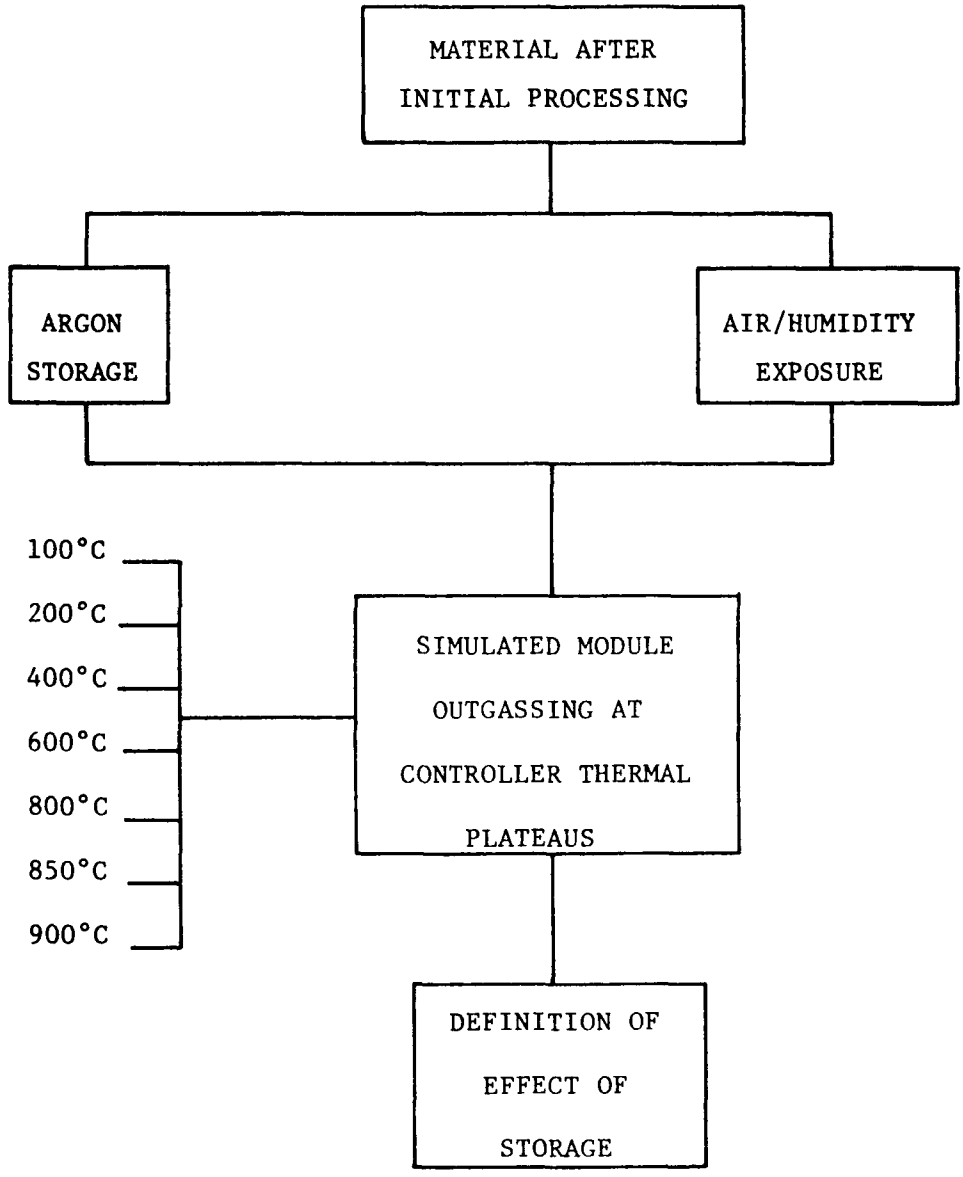

Figure 1-7. Outgassing Flow Diagram

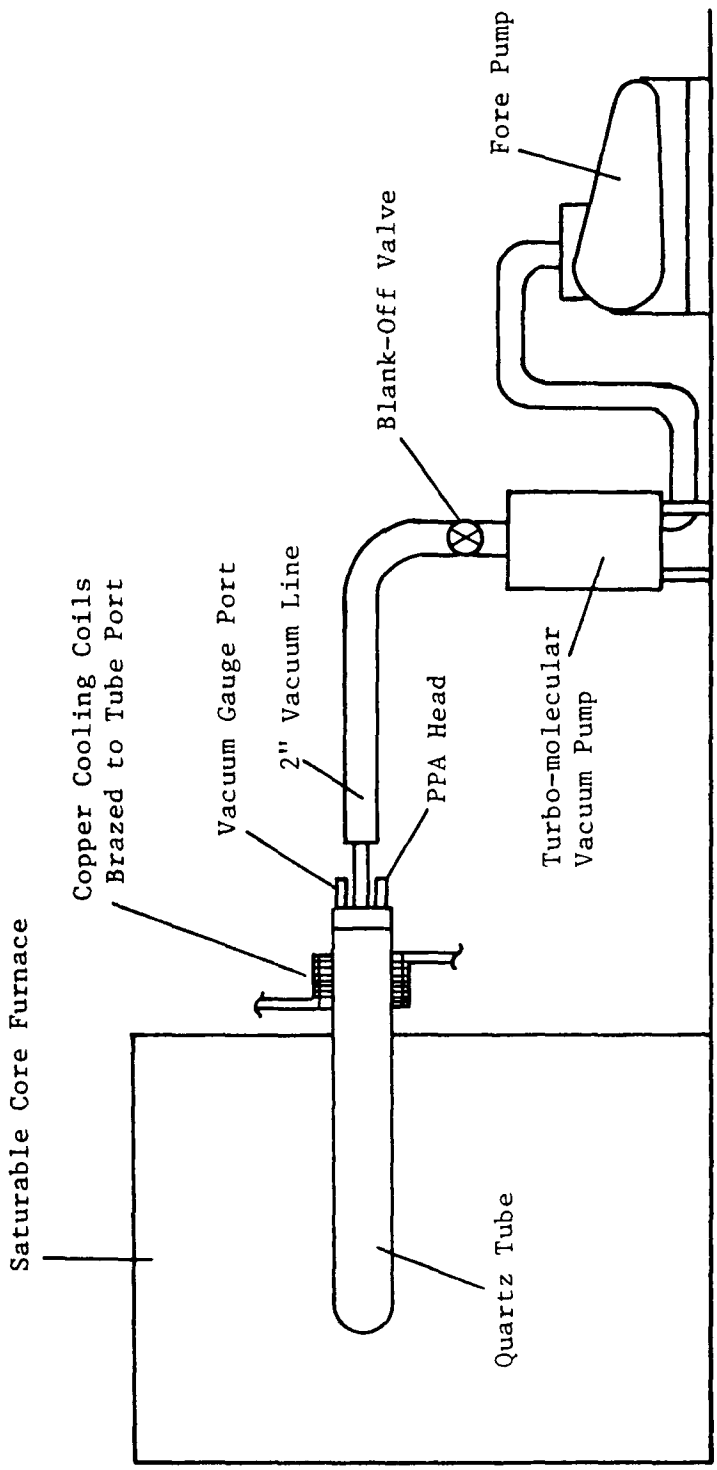

Figure 1-8. Outgassing Scale-up Apparatus

TABLE 1-VIII OUTGASSING SCALE-UP: PROCEDURE

Experimental Conditions for Outgassing Scale-Up Data Base:

Cycle (1) Initial air processing of material to Temperature A

(2) Vacuum processing of material to Temperature B

	A		B		
Material	Temp.	Residence Time	Temp.	Residence Time	Final Processing*
Fiberfrax H-Blanket	800°C	17 hrs.	1000°C	140 hrs.	10^{-7} torr range @ 1000°C 10^{-8} torr range @ ambient

*Laboratory Experimental Unit pressure at 1000°C was low 10^{-7} torr range.

TABLE 1-IX. TEST MATRIX FOR THERMAL INSULATION OUTGASSING STUDIES

I. MATERIALS

A. Laboratory Experimental Series: Initial Processing

1. Min-K 1400TE
2. Min-K 1800TE
3. Fiberfrax H-Blanket
4. Fiberfrax 660 AH Hi-Fi Paper

B. Laboratory Experimental Series: Simulated Module Outgassing After Storage

1. Min-K 1400TE
2. Min-K 1800TE
3. Fiberfrax 660 AH Hi-Fi Paper

C. Laboratory Scale Up Series

1. Fiberfrax H-Blanket

II. PARAMETERS

A. Temperatures

1. Initial Processing

a. 950°C

b. 1000°C

c. 800° (scale-up dual scheme)

TABLE 1-IX. TEST MATRIX FOR THERMAL INSULATION OUTGASSING STUDIES - Continued

II. PARAMETERS (Continued)

2. Simulated Module Outgassing

a. 850°C

b. 900°C

B. Test Duration

1. Laboratory Experimental Series

a. Initial processing 21-44 hours

b. Module simulation 44 hours

2. Laboratory Scale-Up Series

a. Air bake-out 17 hours (overnight)

b. Vacuum processing ~140 hours

C. Atmosphere

1. Laboratory experiment series - vacuum (10^{-7} - 10^{-8} torr)

2. Laboratory Scale-up series

a. Air

b. Vacuum (10^{-7} - 10^{-8} torr)

D. Equipment

1. Laboratory Experiment Series - See Figure 1-6

2. Laboratory Scale-Up Series - See Figure 1-8

TABLE 1-IX. TEST MATRIX FOR THERMAL INSULATION OUTGASSING STUDIES - Continued

III. ANALYTICAL EVALUATION TECHNIQUES

A. Leco Carbon (Leco) - This is a combustion technique for obtaining total carbon concentration.

B. Mass Spectroscopy (MS) - This is a technique useful for identifying volatile species.

C. Partial Pressure Analyzer (PPA) - This is essentially a MS technique and is useful for rapidly obtaining relative distribution of volatile species to mass 100.

D. Electron Beam Microanalyzer (EBM) - This is a technique useful for identifying minute deposits on reaction vessels, etc.

TABLE 1-X. WEIGHT OF OXYGEN OUTGASSED
(mg/Couple)*

***7 hour exposure was at 58% RH and 70°F

24 hour exposure was at 27% RH and 70°F

	Argon Storage**		Air Exposure***	
	1400 hours	216 hours	1400 hours argon +7 hrs.	24 hours
I. 850°C Converter Hot Junction Temperature				
A. Min-K - 1400TE:				
1. Outgassed during processing to 850°C in 22 hour cycle	1.34	-	2.38	-
2. Maximum residual outgassing at 850°C for 22 hrs to 7 yrs.	0.05	-	0.09	-
3. Total possible outgassing	1.39	-	2.47	-
II. 900°C Converter Hot Junction Temperature				
A. Min-K - 1800TE:				
1. Outgassed during processing to 900°C in 22 hr cycle	-	1.59	-	4.10
2. Maximum residual outgassing at 900°C for 22 hrs to 7 yrs.	-	0.10	-	0.05
3. Total possible outgassing	-	1.69	-	4.15

TABLE 1-X. WEIGHT OF OXYGEN OUTGASSED - Continued
(mg/Couple)*

	1400 hours	216 hours	1400 hours argon +7 hrs.	24 hours
II. 900°C Converter Hot Junction Temperature (Continued)				
B. Fiberfrax HiFi 660 AH 1/32" paper:				
1. Outgassed during processing to 900°C in 22 hr cycle	-	0.24	-	0.97
2. Maximum residual outgassing at 900°C for 22 hrs to 7 yrs.	-	0.06	-	0.01
3. Total possible outgassing	-	0.30	-	0.98

*Assuming 7.5 grams of insulation per couple and summation of 18, 28, 32, and 44 mass numbers normalized to oxygen

**1400 hour storage - argon purity unknown whereas 216 hour storage argon purity was 99.7% with 0.3% H_2O (Samples were exposed to this argon atmosphere but had molecular sieve getter also)

TABLE 1-XI. TOTAL OXYGEN OUTGASSED AS A FUNCTION OF THERMAL TREATMENT (mg/Couple)*

Sample Description	RT-100°C	100-200°C	200-400°C	400-600°C	600-800°C	800-850°C	800-900°C
Min-K 1800TE 24 hr air and 27% RH	0.6	0.6	0.8	1.2	0.5		0.4
Min-K 1800TE 216 hr argon	0.2	0.2	0.2	0.6	0.2		0.2
Min-K 1400TE 1400 hr argon + 7 hr air 56% RH	0.1	0.7	0.5	0.7	0.2	0.1	
Min-K 1400TE 1400 hr argon	0.08	0.2	0.3	0.5	0.2	0.07	
Fiberfrax 660AH HiFi 1/32" paper 24 hr air and 27% RH	0.2	0.1	0.6	0.02	0.01		0.04
Fiberfrax 660AH HiFi 1/32" paper 216 hrs argon	0.04	0.02	0.08	0.02	0.01		0.06

*Assuming 7.5 grams insulation per couple and summation of 18, 28, 32, and 44 mass numbers normalized to oxygen.

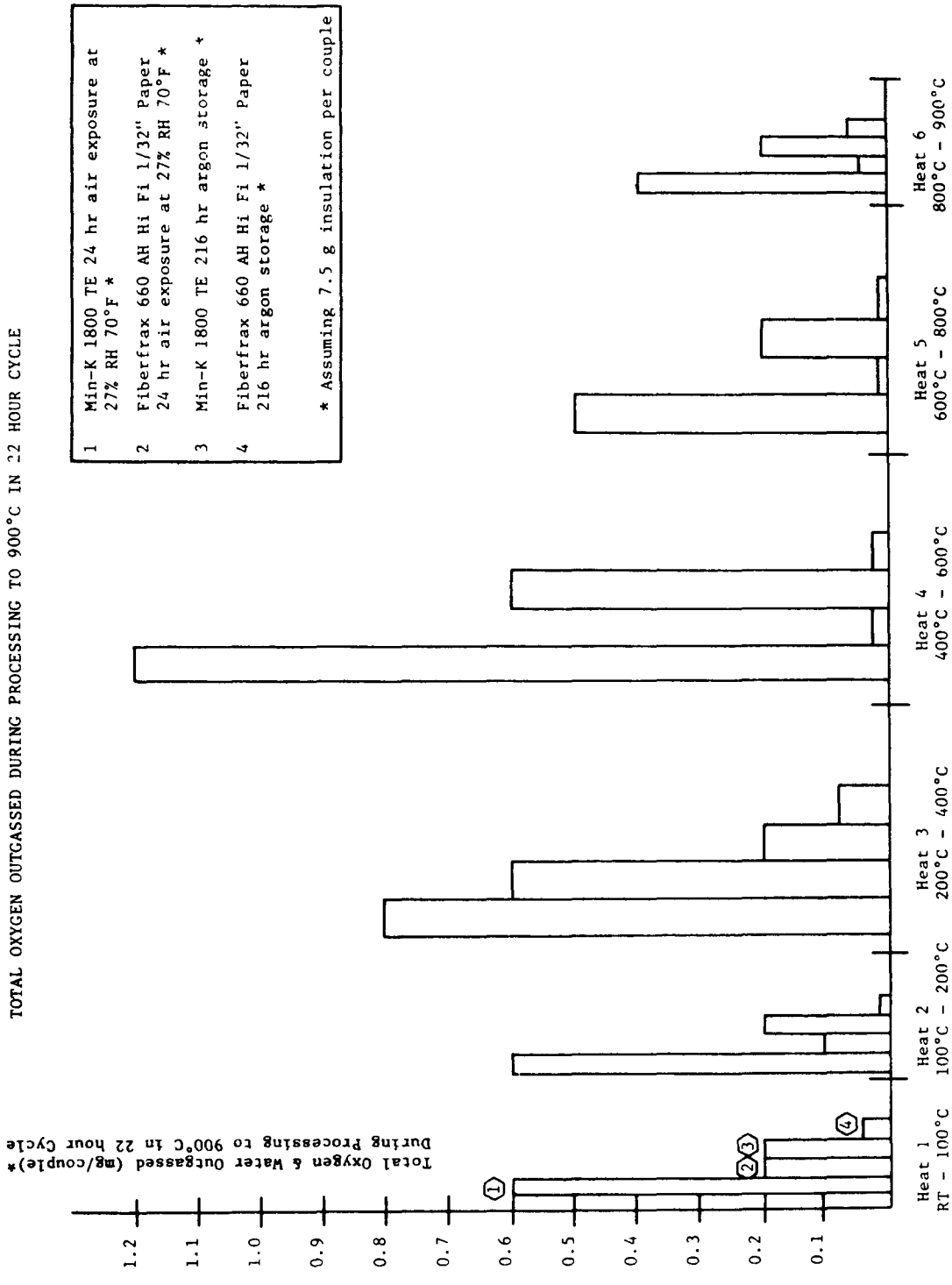

Figure 1-9. Total Oxygen & Water Outgassed From Pre-Processed Insulations Which Had Different Storage Histories

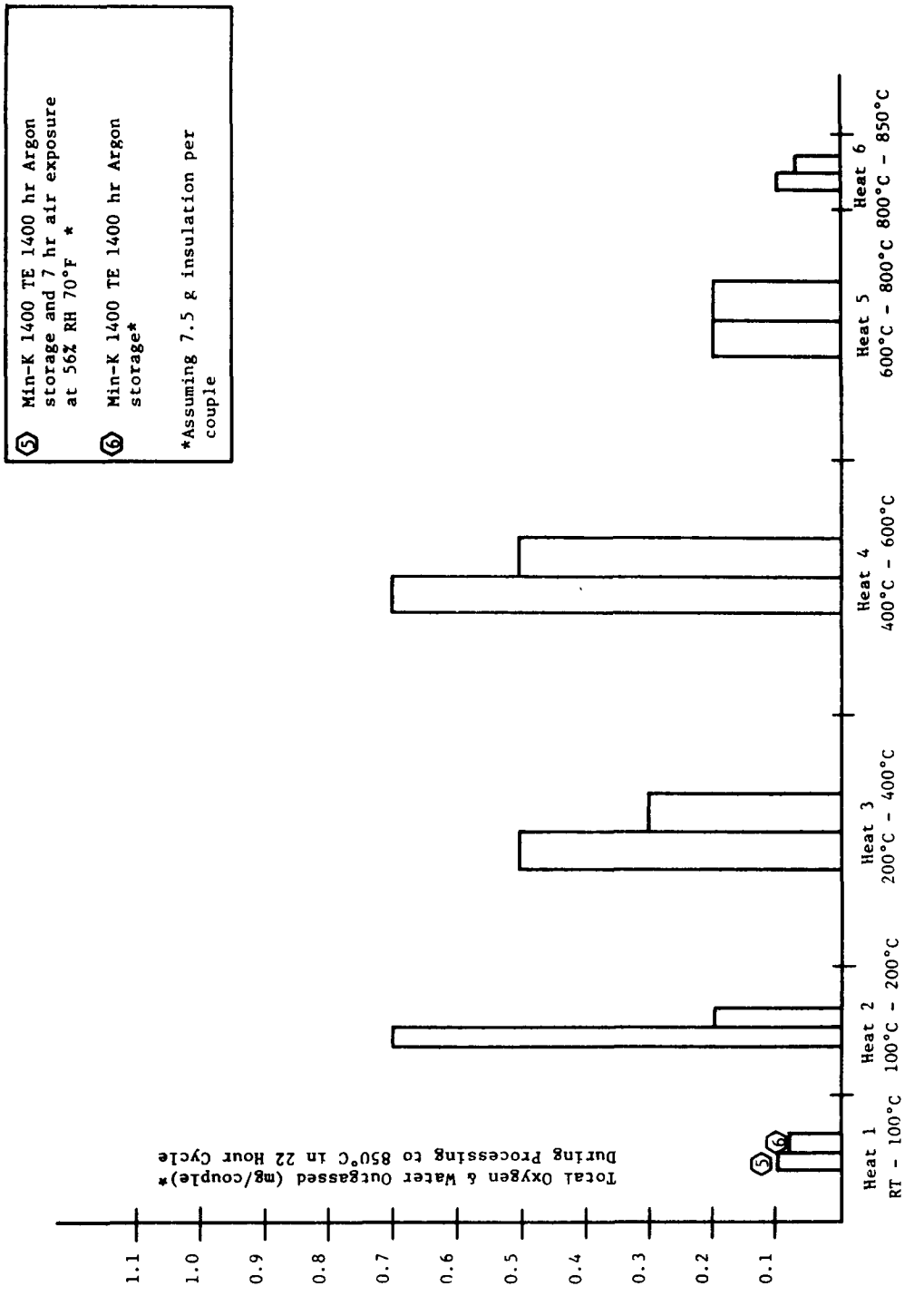

Figure 1-10. Total Oxygen & Water Outgassed From Pre-Processed Min K-1400TE Which Had Different Storage Histories

TABLE 1-XII. TEST MATRIX FOR COMPONENTS OTHER THAN T/E ELEMENT INSULATIONS

I. MATERIALS

A. Carb-I-Tex 500 Carbon/Carbon Composite

B. Molybdenum

C. Tantalum

D. Alumina

E. Pt-3008

F. Cotronics 360

II. PARAMETERS

A. Temperature

1. 950°C

B. Test Duration

1. ~ 21 hours

C. Atmosphere

1. Vacuum (10^{-7} - 10^{-8} torr)

D. Equipment

1. See Figure 1-6

III. ANALYTICAL EVALUATION TECHNIQUES

NOTE: See 1.3.1.3 Table 1-IX.

TABLE 1-XIII. OUTGASSING RATES OF INSULATIONS & OTHER COMPONENTS

Conditions: T = 850°C; Static Vacuum

Materials processed at 950°C in vacuum for 16-18 hours

MICROGRAMS OF OUTGASSED MATERIAL/GRAM OF MATERIAL/YEAR

Component	Min-K 1400TE	Fiberfrax HiFi 660AH	Fiberfrax H-Blanket*	Carb-I-Tex	Molybdenum	Tantalum	Alumina	Pt-3008
Mass 18	2	0.4	0.3	<0.004	0.04	0.004	0.2	0.006
28	300	100	200	75	0.1	0.02	15	2
32	< 0.1	< 0.002	< 0.01	< 0.006	< 0.001	<0.0002	< 0.01	<0.0003
44	1	0.6	0.8	1	< 0.002	<0.0004	< 0.01	<0.0004

Note: Cotronics 360 was not included because of severe outgassing throughout the experiment. This outgassing was caused by decomposition of a hydrocarbon binder in the Cotronics 360. Preliminary outgassing in air prior to vacuum outgassing indicated that this problem could be circumvented.

*Bake-out at 950°C twice that of others.

1.3.3 Summary of Results

Since carbon was detected in all of the insulations, see Section 1.3.1.4 Test Results, and since the carbon-TiO_2 interaction appears responsible for the off-white to light blue color change in Min-K without an air bake-out, an air bake-out prior to vacuum processing thermal insulations is recommended.

The residual outgassing rates for Min-K 1400TE, 1800TE, and Fiberfrax HiFi Paper insulations after independent processing through 17 and 40 hour cycles to 1000°C were less than 0.1 mg. per element for the mass of insulation in the GDS converter. This residual outgassing rate is below the most conservative threshold (0.3 mg./element) for affecting the thermoelectric behavior of the element.

After initial processing, the Min-K and Fiberfrax Paper data indicate that the quantity of oxygen and water outgassed is a function of air exposure time and percent relative humidity and independent of initial processing temperatures and times. The quantity of oxygen and water outgassed after argon exposure is independent of length of argon exposure as well as of initial processing temperatures and times.

The data indicate that the total quantity of oxygen and water outgassed from processed insulation exposed to air is about a factor of two-three higher than that stored under an argon environment.

The data indicate that the oxygen and water outgassed in a processed and stored insulation reaches a maximum during the 400-600°C cycle of the simulated module processing.

The total weight of outgassed reactive gases is of the order of magnitude to produce observable effects on the N-elements. However, through careful processing of the module and operation of a getter, the available outgassed material which actually reacts with the element should be at a safe level. The presence of the xenon cover gas, and the fact that only a portion of the insulation is at the maximum temperature should also decrease the outgassing rates.

As Table 1-XIII clearly shows, the magnitude of the quantity of outgassed species from materials other than thermal insulations is minor compared to that outgassed from the thermal insulations.

SECTION 2

ASSESSMENTS OF REQUIREMENTS FOR GDS

2.1 COVER GAS REQUIREMENTS FOR GDS ASSEMBLY

To insure maximum reliability, 3M recommends:

- After final processing at 3M, the thermoelectric module will be shipped in a hermetic enclosure with less than 50 ppm water and oxygen.
- Non-thermoelectric components in the converter cavity will be processed and then stored in atmospheres with less than 50 ppm water and oxygen.
- Final assembly of the GDS to take place in an atmosphere with less than 50 ppm water and oxygen.

These trace level limitations on water and oxygen exposure after initial processing of the insulation and module are important in that the amount of insulation in the non-module area is about thirty times that in the module area. Thus, most of the reactive gas load to which the hot thermoelectric elements will be exposed during processing of the assembled generator will come primarily from the non-module insulations. To reduce this reactive gas load, it is important that the non-module insulation be properly preprocessed, and that assembly of the generator be performed in a controlled atmosphere. A second consideration is that since the effective pumping speed for the assembled generator will be much slower than for the converter module alone at 3M, low quantities of potential outgassing species become important in reducing the generator pump-down time as well as the hot element exposure to reactive gas.

2.2 DETAILED OUTGASSING PROCEDURE FOR THE SEALED CONVERTER SECTION

Based on the data in this report and on experience with processing of selenide test modules, 3M recommends:

Equipment:

- A partial pressure analyzer,
- Module evacuation ports and vacuum manifold sufficient to provide at least 40 liter/second pumping speed for the module. (Two one inch ports, two inches long would have a conductance of 40 liter/second),
- Bakeable vacuum manifold, turbomolecular vacuum pumps, and xenon backfill system capable of 10^{-8} torr ultimate blanked off pressure,
- Cold end heaters and controllers.

Temperature/Time Cycle for Assembled GDS Converter Section:

- Heat converter isothermally to 150°C at a rate such that partial pressures of H_2O and O_2 remain below 5×10^{-5} torr in interior of thermoelectric module,
- Maintain cold end at 150°C and heat hot end at a rate such that partial pressures of H_2O and O_2 remain below 5×10^{-5} torr in interior of thermoelectric module,
- Estimate temperature/time cycle from outgassing data for processed insulation (Figures 1-9 and 1-10) and conductance of non-thermoelectric module.

2.3 SUMMARY OF RECOMMENDED AND ALTERNATE MATERIAL SELECTIONS FOR THE GDS CONVERTER SECTION

The recommended material selections for the converter section of the GDS are outlined in Table 2-I. The selections were made after reviewing literature data and conducting chemical compatibility and outgassing experiments.

TABLE 2-I. MATERIAL SELECTION FOR GDS CONVERTER MODULE

Component	Material	Reason for Selection
Outer ring and rails	2024 Al, sliding surface of rail plated with electroless nickel	Lightweight, strong and hard surface for sliding interface
N- and P-Leg Springs	Cr-Si Steel, AISI 9254	High temperature strength
Follower Spring	302 Stainless Steel	Fabricability and strength
Hairpin Clip, Spring Retainer	300 Series Stainless Steel	Fabricability and strength
Spring Shim	ETP Copper	Compatibility with follower
Foil Follower, Body	ETP Copper	Bondable to BeO and capability of yielding at bend (provides additional cold end mobility)
Foil Follower, Wear Surface	Cr Copper	Minimizes friction and galling problems with sliding interface
Cold End Insulator Discs	BeO (metallized)	Electrically insulating, bondable and high thermal conductivity
Cold End Current Strap	ETP Copper	High electrical conductivity, bondable, chemically compatible with cold end disc
P-Leg Cold End Disc	ETP Copper	Bondable and chemically compatible with P-Leg
Hot End Electrodes	W-25 Re Foil for TPM-217 Sputter Coated W for $GdSe_x$	Chemically compatible with T/E materials up to and including 1000°C
N-Leg Hot End Compliant Foil	Gadolinium	Malleable, reacts with $GdSe_x$ to form various $GdSe_x$ compositions which are not electrically deleterious.

TABLE 2-I. MATERIAL SELECTION FOR GDS CONVERTER MODULE - Continued

Component	Material	Reason for Selection
Hot End Gimbal	Tantalum	Good mobility with the current strap; high temperature strength; ingradient module tests at 800°C have indicated Ta to be compatible with T/E materials. Ingradient and Isothermal compatibility tests at 800°C under xenon have shown Ta to be compatible with T/E materials.
Hot End Current Strap	Molybdenum with plasma sprayed Al_2O_3	Good mobility with the gimbal; high temperature strength; ingradient module tests at 800°C have indicated Mo to be compatible with T/E materials, e.g., M-1 thru M-6. Isothermal compatibility tests at 850°C under xenon have shown Mo to be compatible with the T/E materials.
Hot and Cold End Thermocouples	Pt/Pt-10% Rh	Ease of fabrication; thermocouples remain in calibration after long term exposure to TPM-217 and selenium atmospheres.
	W/W-Re	Compatible with TPM-217 materials.
Hot End Spacer	POCO AXF-Q1 Graphite	High temperature strength/weight ratio; (Note: Outgassing and isothermal chemical compatibility experiments are being planned for this material.)
Thermal Insulation	1. Min-K SiO_2/TiO_2 Series	
	Min-K 1400TE (outgassed) 1800TE (outgassed)	Low thermal conductivity; chemically compatible with T/E materials.
	2. Fiberfrax Series	
	H-Blanket and HiFi 660 AH paper (outgassed)	Low thermal conductivity, chemically compatible with T/E materials.

2.4 RECOMMENDATIONS FOR NON-MODULE COMPONENTS: OUTGASSING, STORAGE AND HANDLING

The following equipment and procedures are recommended for the outgassing and storage of non-module components and insulations:

Equipment:

- Turbo pump,
- Vacuum furnace capable of operation to 1000°C at 10^{-7} torr,
- Partial pressure analyzer.

Temperature/Time Cycle:

- Initial bake of insulation at 800°C for 24 hours in air,
- Vacuum outgassing at 1000°C until a residual outgassing rate of 1 x 10^{-6} torr-liter per g-sec is obtained,
- Cool to ambient and transfer to storage chamber in inert atmosphere (less than 50 ppm water and oxygen).

Storage and Handling:

- Store and handle in inert atmosphere (less than 50 ppm water and oxygen).

As stated in Section 2.1 Cover Gas Requirements for GDS Assembly, the principal reactive gas load in the converter section comes from non-thermoelectric module components, and it is important that these materials be properly processed and stored to reduce reactive gas outgassing.

In addition to the normal high vacuum outgassing, the analytical results described in Section 1, 1.3.1.4 Test Results and 1.3.1.5 Summary of Test Results, dictate the further recommendation that prior to vacuum outgassing, the insulations be baked out in air to remove intrinsic oxygenated hydrocarbon contaminants.

The outgassing characteristics of Cotronics 360, Carb-I-Tex 500 carbon/carbon composite, and Pt-3008 have been assessed in addition to the thermal insulations. The outgassing procedure was identical to that for the thermal insulations. However, the Cotronics 360 material had an exceedingly high outgassing rate; the origin of which was found to be thermal cracking of the organic binder. In order to process this material properly, a dual outgassing procedure involving an air bake-out prior to vacuum outgassing is recommended. A word of caution here is that this air bake-out may affect such things as mechanical strength and thermal conductivity.

ATTACHMENT XIV

Load Relaxation in Springs

Objective:

To describe efforts geared towards isolating the source of the load relaxation problem observed in several modules.

Summary:

Post test evaluation of M-7 springs brought to light a significant problem. Throughout the course of its 20,000 hour test duration the springs experienced an almost complete loss of load. Several experiments have been initiated in an effort to characterize the problem and from there move to a solution.

Presently, the following is known:

1. Steel springs are being subjected to chemical attack in module envorinments This reaction accelerates the relaxation rate.
2. A likely containment is selenium vapor. Tests indicate that the reaction, whatever it is, occurs at internal locations and not just at the surface.

Efforts are in progress to determine:

1. Where exactly the reaction is occuring, and what the reaction is.
2. How the reaction affects mechanical properties.
3. What spring materials can survive the module environment without excessive relaxation.

A. Description of the spring environment.

All module springs are exposed to a vacuum environment. There is selenium vapor present. The concentration of selenium is determined by the temperature level which for the springs is roughly 150°C. The stress levels in the springs are moderately high. The corrected p–leg spring stress is 74.0 ksi, and the corrected N-leg spring stress is 107 ksi.

This is how the corrected stress is computed for a typical N-leg spring:

Wire Dia. = .056" ≡ d Mean Dia. = .226" ≡ D → C≡ $\frac{D}{d}$ = 4.036

OD = .282"

Applied force - 23.4 lbs ≡ F, force at operating condition

$$K \equiv \frac{4C-1}{4C-4} + \frac{615}{C} = 1.399$$

$$t = \frac{8KFD}{\pi d^3} = \frac{8\,(1.399)\,(23.4)\,(.226)}{\pi\,(.056)^3} = 107.3 \text{ ksi}$$

B. The Problem

A compilation of module spring relaxation data appears in Fig. 1. In the course of 20,000 hours of exposure, M-7 springs experienced an almost complete loss of load due to excessive relaxation. The behavior was far in excess of existing load relaxation vs. time literature for the same material under similar loading and similar temperatures. Other module springs accounted for in Fig 1 though not as bad as M-7, had load relaxations greater than what the literature indicated. The two fundimental differences in environment between the modules and the literature were that module springs were in a vacuum and that present in the vacuum environment was selenium vapor. (Tests conducted in the literature took place in air).

C. Efforts to isolate the source of the problem

1. Load Relaxation tests

A series of load relaxation tests is in progress. The test plan is described in Fig. 2 and the results of the air tests are shown in Fig. 3. Results from the vacuum and Selenium tests run thus far appear with the module data shown in Fig 1. Air data is in acceptable agreement with the literature, and the vacuum and selenium data is in good agreement with module data. These results indicate a contamination problem.

2. Dip tests

An experiment was devised to try and determine whether the contamination problem is a surface phenomenon. The test plan is shown in Fig 4. The springs were dipped a total of four times. With each additional dip, significant weight losses were observed. Also, no change in free length was detected, and force measurements successively decreased with each dip. These results indicate that the problem is not associated with a surface phenomenon.

3. X-Ray Flourescence tests

A number of springs were analyzed for selenium content with X-ray floerescence. This test was only semi-guartitative which means that reliability of the data is to some exlent in question. The results show that there is unquestionably selenium present, but that there is no observable correlation of selenium content with time.

4. Metallographic and Microhardness

A list of springs tested appears in Fig. 5. All springs were sectioned and polished and then subjected to microhardness profile tests using the Kroop Indent with a 300 g load. Following the microhardness test, they were submitted for metallography analysis. These tests are complete, but the results are still being analyzed. These tests results should help define where the contamination is occuring.

5. Auger analysis

Those springs described in Fig 5 that are marked with an asterisk will be submitted for Auger analysis in order to measure selenium concentration profiles through them. This also should give some indication of where the reaction is occuring.

6. Program at Oak Ridge Nat'l Lab.

A program has recently begun at Oak Ridge National Lab in the metals and ceramics division aimed at supplementing 3M's efforts. Among other things, they will be conducting M-5 spark tests for surface concentrations, and additional metallographic analysis.

7. Search for new spring materials.

New materials are being sought after for evaluation of compatability with module environments. Relaxation tests will be run and will be immediately followed by the full gamet of chemical tests described above. Experimental springs are in the process of being designed and fabricated right now. Materials being investigated include Tungsten-Rhenion, Inconel x-750 and MP35N.

D. Summary

Test results obtained thus far indicate the following:

1. That steel springs are being subjected to chemical attack in module environments
2. That the attack occurs not only at the surface but throughout the cross-section.
3. That after a large exposure time, the effect on the springs can be devastating, and that even for short exposure times relaxation rates are dramatically accelerated.

Test results to be obtained should show

1. Where the reaction is occuring
2. The effect of the reaction on mechanical properties
3. What is the selenium reacting with
4. What materials can survive the module environments without excessive relaxation

FIGURE 1
A COMPILATION OF MODULE SPRING RELAXATION DATA

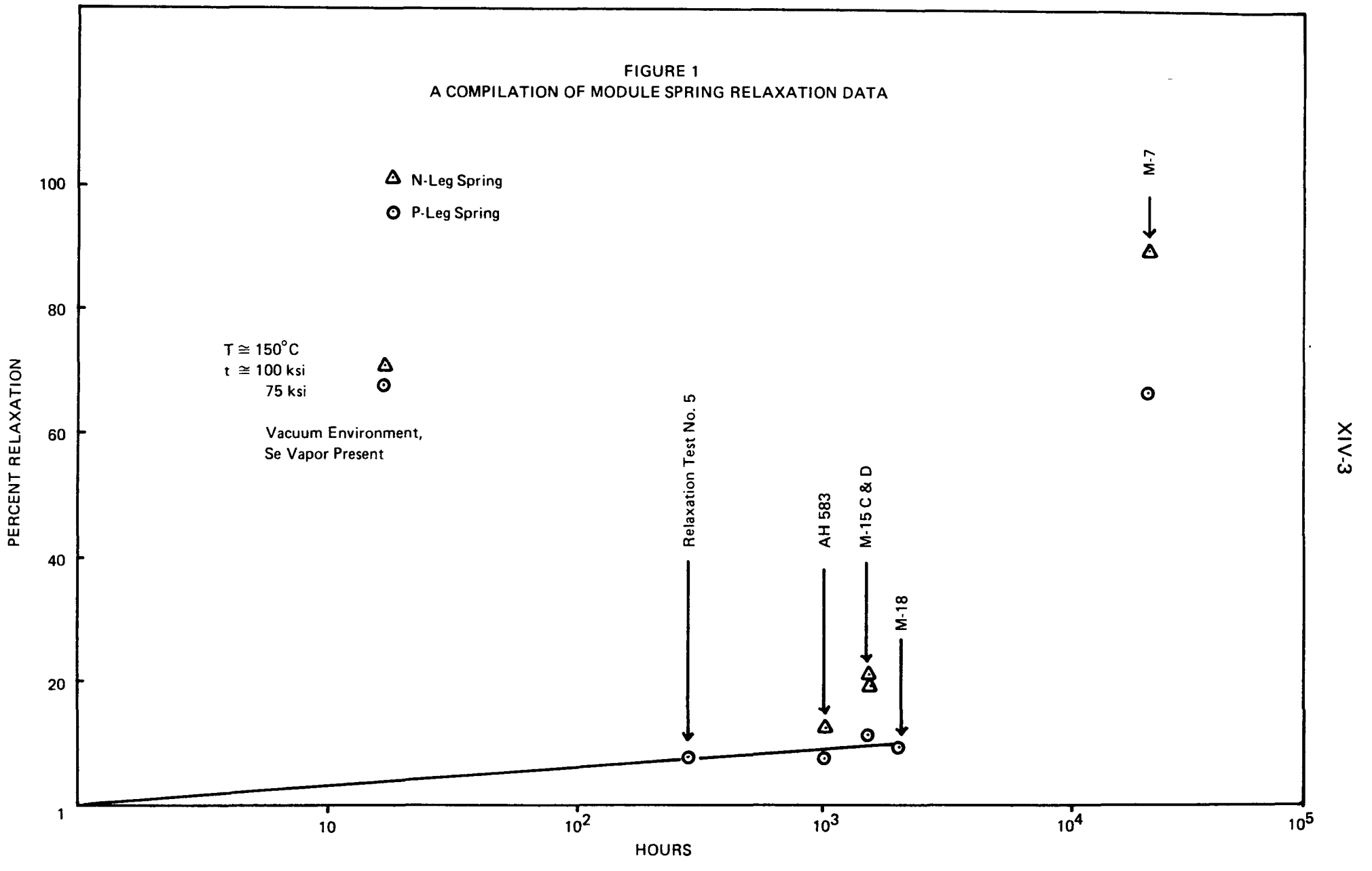

FIG. 2 COUPLE HARDWARE SPRING LOAD RELAXATION TEST PLAN

TEST NO.	NO. OF SPRINGS	SPRING MAT'L.	TYPE OF SET	ENVIRONMENT	TEMP. (°C)	DEFLECTION (IN)	COMPLETION DATE
1.	6	ASTM A401 Cr-Si	NONE	AIR	150	.465	11/23
2.	6	302 St. St.	NONE	AIR	150	.465	11/23
3.	6	17-7 PH St. St.	ROOM TEMP.	AIR	150	.465	11/23
4.	6	17-7PH St. St.	HIGH TEMP. (450° F)	AIR	150	.465	11/23
5.	6	ASTM A401 Cr-Si	NONE	VACUUM, Se	180	.465	11/23
6.	6	17-7 PH St. St.	ROOM TEMP.	VACUUM, Se	180	.465	11/23
7.	12	ASTM A401 Cr-Si	NONE	"	150	.500	12/28
8.	6	17-7 PH St. St.	ROOM TEMP.	"	150	.435	12/28
9.	6	17-7 PH St. St.	HIGH TEMP.	"	150	.435	12/28
10.	12	ASTM A401 St. St.	NONE	VACUUM	200	.500	1/15
11.	6	17-7 PH St. St.	ROOM TEMP.	VACUUM	200	.435	1/15
12.	6	17-7 PH St. St.	HIGH TEMP.	VACUUM	200	.435	1/15

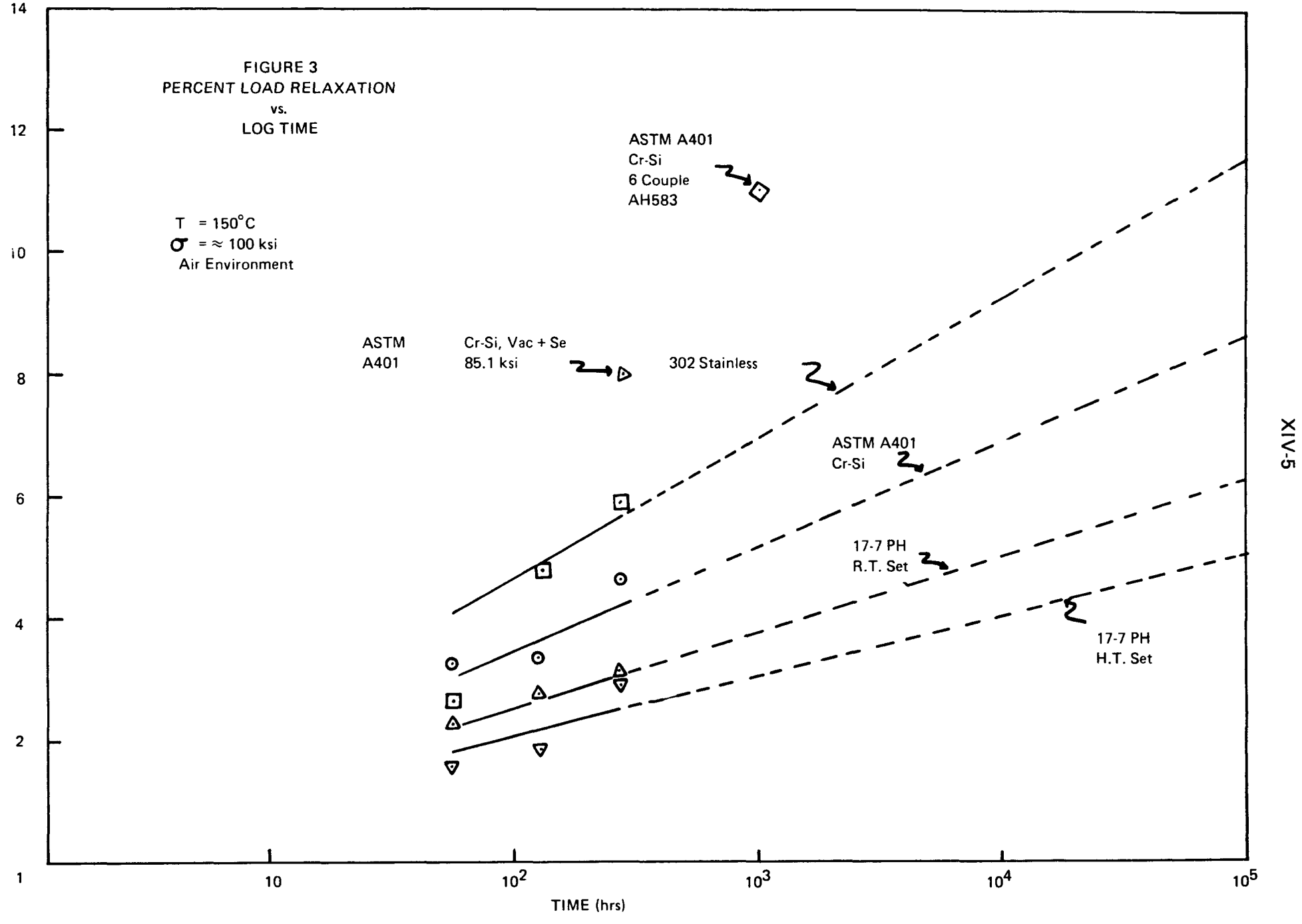
FIGURE 3
PERCENT LOAD RELAXATION
vs.
LOG TIME
T = 150°C
σ = ≈ 100 ksi
Air Environment
ASTM A401
Cr-Si
6 Couple
AH583
ASTM
A401
Cr-Si, Vac + Se
85.1 ksi
302 Stainless
ASTM A401
Cr-Si
17-7 PH
R.T. Set
17-7 PH
H.T. Set
14
12
10
8
6
4
2
1
10
10^2
10^3
10^4
10^5
TIME (hrs)

TEST PLAN FOR DIP EXPERIMENT
FIGURE 4

Spring Descriptions:

1. 17.7 PH, N-leg spring, previously unused
2. Cr-Si, N-leg spring, previously unused
3. 17-7 PH, N-leg spring, previously used in a vacuum + Se vapor relaxation test.
4. Cr-Si, P-leg spring, previously used in a vacuum + Se vapor relaxation test.
5. M-7, N-leg spring (Cr-Si)
6. M-7, P-leg spring (Cr-Si)

TEST PROCEDURE:

1. Make a set of mechanical measurements
   a. Free length
   b. Force at same specified deflection
   c. Weight
2. Dip springs for 5 seconds in a 50% HNO_3 solution. Immediately following the dip, rinse in running water then de-ionized water, and then methanol.
3. Repeat the mechanical measurements
   Repeat the cycle either until a significant change occurs or until it is obvious that any scale that may have been present is no longer there.

FIGURE 5
A LIST OF SPRINGS TO BE TESTED METALLOGRAPHICALLY
AND FOR MICROHARDNESS PROFILES

1. Cr-Si, previously unused
2. M-7, N-Leg
3. M-7 P-Leg
4. M-15C, N-leg
5. M-15C, P-leg
6. M-18, P-leg
7. AH583, N-leg
8. AH583, P-leg
9. Cr-Si, relaxation tested in air
10. M-5, N-leg
11. M-5, P-leg
12. Cr-Si, previously relaxation tested in vacuum + Se vapor
13. 17-7 PH, previously relaxation tested in air
14. 17-7 PH, previously relaxation tested in vacuum + Se vapor
15. 17-7 PH, previously unused.

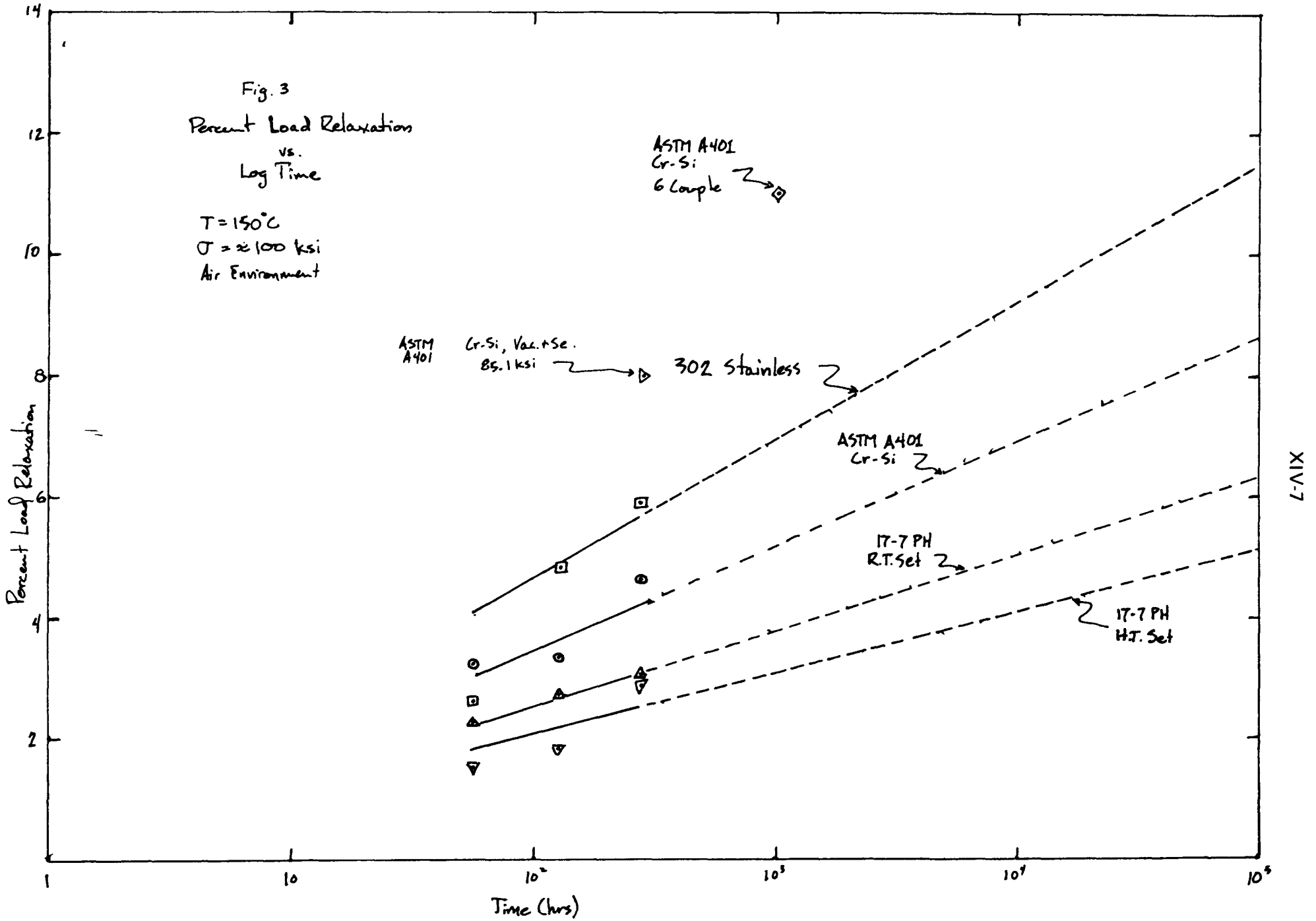
Fig. 3
Percent Load Relaxation
vs.
Log Time
T = 150°C
σ = ≈100 ksi
Air Environment
ASTM A401
Cr-Si
6 Couple
ASTM
A401
Cr-Si, Vac. +Se.
85.1 ksi
302 Stainless
ASTM A401
Cr-Si
17-7 PH
R.T. Set
17-7 PH
H.T. Set
Percent Load Relaxation
Time (hrs)
14
12
10
8
6
4
2
1
10
10²
10³
10⁴
10⁵

ATTACHMENT XV

Dynamic Behavior of a Converter Ring

Objective:

To describe efforts geared towards characterizing dynamic behavior of a converter ring.

Introduction:

In order to be able to predict dynamic response, resonant frequencies and damping coefficients must be known. This report describes efforts geared towards determining these quantities.

There are six relevent quantities: resonant frequency and damping coefficient for each of the three types of motion described in Fig. 1. Of these, only one has been predicted analytically. The experiment for verifying the prediction and determining the other five numbers is a direct measurement test that incorporates all current design facets.

Results from these tests will be used as input data for a mathematical model that will be generated with the use of ANSYS, a finite-element structural analysis program.

A. Determination of Resonant Frequencies in a Converter Ring.

1. Calculation in transverse direction (ref. fig. 1). Treat a single ring.

K_n = 260 lbs/in.

K_p = 94.4 lbs/in.

K for 6 couple $\equiv K_6 = 6[k_n + K_?] = 2126$ lbs/in.

K for half of converter $\equiv K_h = K_6 \left[1 + \sum_{i=1}^{?} 2\,\mathrm{Cos}^2(\Theta_{i-1} + 12.86°)\right]$, $\Theta_o = o$

$= 7.00\, k_6$

$- 14{,}890$ lbs/in.

K for entire converter $\equiv K_T = 2K_4 =$ 29.780 lbs/in.

Lumped mass of a single ring = 7.10 lb_m

$$\therefore W_n = \sqrt{\frac{(29{,}780\ \text{lbf/in.})\ (12\ ^{\text{in}}/_{\text{ft}})\ (32.2)\ ^{\text{lbm}}/_{\text{slug}}}{(7.10\ \text{lbm})}} = 1273\ /\text{s} = 203\ \text{Hz.}$$

Note that spring and damping behavior of hardware has been neglected. Also, transverse spring constants of the springs have been neglected.

2. Calculation in longitudinal and Torsional directions

Resonant Frequencies for both torsional motion and longitudinal motion will be measured directly. Refer to section C for details.

B. Determination of Damping coefficients

Damping coefficients in all three directions of interest will be measured directly. See Section C for details.

C. Description of Experimental apparatus for measuring resonant frequencies and damping coefficients.

A sketch of the apparatus appears in Fig. 2. It consists of two opposing 6 couple assemblies separated by a dummy hot frame. The hot frame is supported only by the two 6-couples and is therefore "floating" with respect to the outer housing. It's mass has been scaled down from a full ring proportionately to the No. of 6-couples and it has been instrumental with 3 acceterometers, one for each major direction of motion.

A sudden displacement of the hot frame with respect to the outer housing will be imposed by suddenly dropping the apparatus a short distance onto a hard surface. The natural response of the system will then be examined by feeding the outputs of the accelerometers into an oscilloscope equipped with a digital memory unit. The decay rate and frequency of the natural response will be measured.

FIGURE 1
TYPES OF MOTION

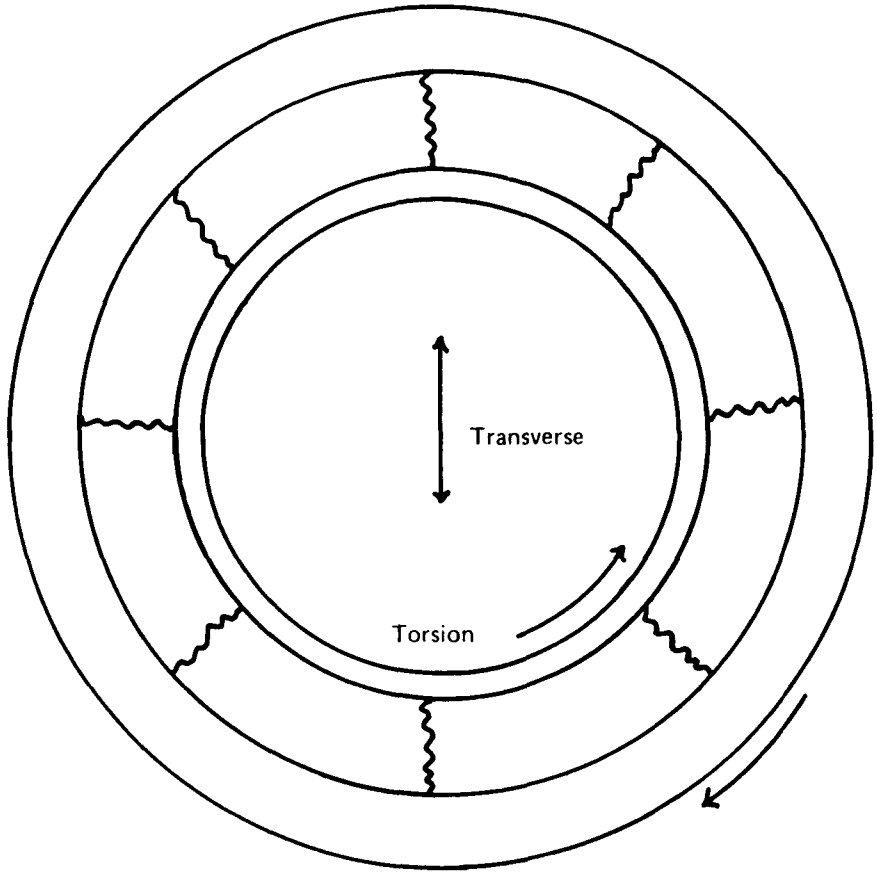

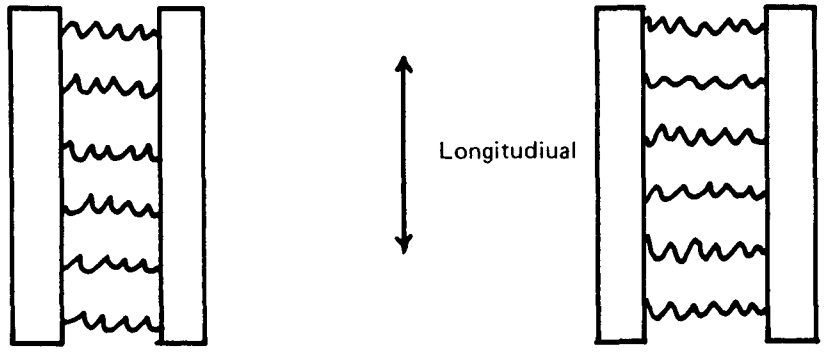

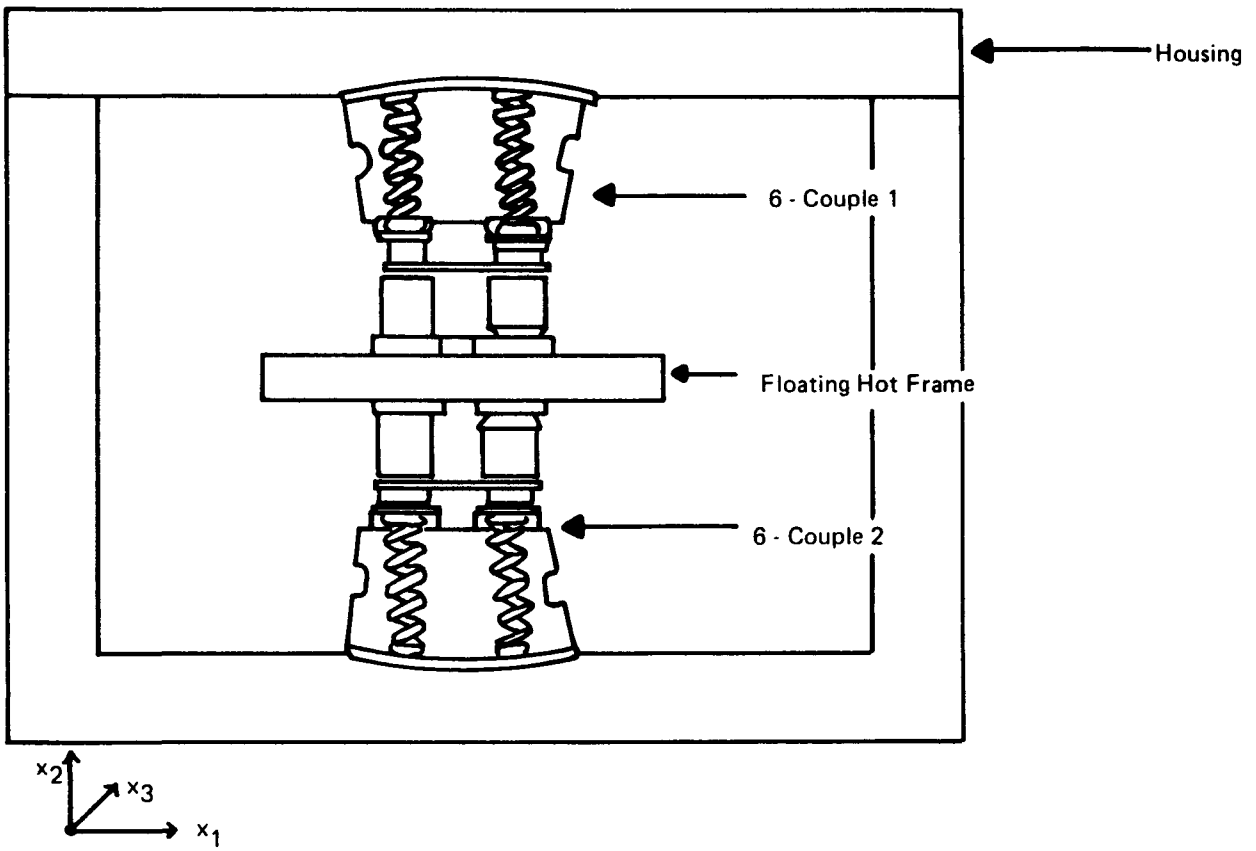

NOTE: Acceterometers are installed to measure along x_1, x_2 and x_3 axes.

x_1 corresponds with torsional motion

x_2 corresponds with transverse motion

x_3 corresponds with longitudiual motion

SKETCH OF APPARATUS FOR MEASURING RESONANT FREQUENCIES AND DAMPING COEFFICIENTS

FIGURE 2

ATTACHMENT XVI

Finite Element Stress Analysis of N-Legs

Objective:

The identification of the stresses the N-leg is subjected to, and a brief description of a computer program being written for stress analysis of the element.

Conclusion:

To date the analysis hasn't been completed, but it appears that the cracking is caused by a composite of different stresses, although the mechanical stresses due to off-loading could be sufficient in themselves to cause cracking in the element. Until the results are obtained from the stress analysis program any conclusions are speculation.

Introduction:

With the discovery of cracked N-legs in recent module there has been a lot of interest in determining more concisely the stresses present in a N-leg. In order to obtain an accurate picture of the stress distribution it is important to identify all possible modes of stress.

Therefore, this document will list the types of stresses that occur in the N-leg and outline a finite element stress program for analysis of the stress distribution.

Types of Stresses

1. Thermal stresses from axial ΔT (steady state)
2. Thermal stresses from radial ΔT (steady state)
3. Thermal stresses from temperature transients
4. Mechanical stresses from off-loading
5. Non-uniform contact creating non-uniform thermal and current flow paths.

Outline of Finite Element Program

The computer program is being written using the finite element method. In the finite element method the leg is divided into small sections and a system of stress equations is written for the sections and solved to yield the stress distribution. All of the above mentioned modes of stress will be taken into account in this program.

The program will have the ability to change the initial loading condition and thus simulate off loading and non-uniform contact. The effect of actual operating axial temperature distributions will be evaluated for various temperature and current conditions. These temperature distributions will be obtained from the thermoelectric couple evaluation computer program. Estimates of radial temperatures will be made based on differences between thermoelectric element and thermal insulation temperature distributions.

ATTACHMENT XVII

A Summary of Results From the Module
Vibration Testing Program as of November, 1978.

1. Background

Over the last four (4) months, there has been an active effort geared towards evaluating the durability of a module in a dynamic environment. This effort has been proceeding under two (2) programs, a multi-couple module test program and a single couple test program, both of which have yielded useful information. This report contains descriptions of the test procedures, the results, and future efforts.

2. Multi-Couple Test Program

a. Description

M12A was an eighteen-couple module that was vibrated during the week of June 26, 1978 at Environ Labs in Bloomington, MN. A sketch of the module layout is shown in Figure 1 and the intended test procedure is listed in Figure 2. Due to the loss of the Xe atmosphere, the test was terminated after vibration of the X-axis.

M12A was heated and operated at 3M for 500 hours as planned, but due to problems with fuse blow-outs, the hot end temperature was held at 700°C. A brief graphical summary is shown in Figure 3. Figure 4 shows how performance at Environ Labs compared with the initial heatup. The total resistance and the open circuit voltage were used as measurements of the degree of degradation and the closed circuit voltage (a continuous record) was used as an instantaneous indicator of performance.

The purpose of the sine-sweeps was to determine how effectively the module housing could transmit the signal from the vibrator to the converter. The source signal was measured by a control accelerometer attached to the vibrator. Two (2) accelerometers on the housing measured the transmitted signal and distortion due to off-axis vibration, respectively. The results of the X-axis sine-sweeps are shown in Figures 5 and 6. There is one sweep per accelerometer on the housing, since

the equipment at Environ is instrumented for only one accelerometer other than the control.

Figure 7 displays the random vibration signal specification. In an attempt to sustain the converter through 3 axis vibrations, the random vibration sequence in step 2 of the procedure was set at .5x of this specification.

Figure 8 shows the signal output from the random vibrator, and Figure 9 shows a record of the total closed circuit voltage during the X-axis vibration.

b. Discussion

Due to the premature shutdown of M12A, it wasn't possible to obtain as much information as planned. Even so, there is information to be had from the results that were obtained.

The data summary for the heatup at 3M shows a slight increase in resistance after the heater failures (5-10%) which is not uncommon and which generally improves with additional seat in. It is assumed that this increase has no bearing on the dynamic behavior of the system. Figure 4 shows that the performance at Environ Labs is comparable to what was seen at 3M. The cyclic behavior at Envron is attributable to the use of non-regulated power for the cartridge heaters. It is assumed again that this has no bearing on the dynamic behavior of the converter.

Figures 5 and 6 show that the converter housing distorted the signal by a significant amount. An important implication of this is that the converter was vibrated at higher energy levels than what the control accelerometer indicated. Most of the distortion was caused by the vibration of the processing valve (3" bellows) which formed a large cantilever limb jutting out from the side of the housing.

Throughout the 2g sine-sweeps, converter performance remained stable. No measurable degradation occurred. For the random vibration sequence, there was a one minute build up period. Once the vibrator reached full power, the three minute sequence officially started. At just under the three minute mark on the X-axis, the stainless steel tube connecting the backfill valve to the housing snapped at a weak spot that was caused by excessive heating during welding. Up to this time, no change in behavior could be measured. As the atmospheric air diffused into the chamber, the closed circuit voltage began dropping fairly rapidly, indicating an increase in resistance (reference Figure 9). The module was held at temperature for about thirty minutes before the cooling sequence was initiated.

The module was returned to 3M and partially disassembled for inspection. There was evidence of oxidation at the hot end of the N-legs, but the converter was sufficiently intact to make the prospect of a re-test encourageing. Unfortunately, outgassing of water from the legs during storage at room temperature under vacuum destroyed the legs irreparably.

c. Conclusions and Future Plans

Converter performance was stable (i.e. there was no measurable degradation) during the 2g sine-sweeps (10 min) and during four minutes of random vibration, three of which were at greater than .5x of specifications. The failure that cut the test short was a failure of the housing and not of the converter.

The converter housing has been modified to alleviate the signal distortion problem and to eliminate the possibility of recurring loss of atmosphere in future tests.

The next multi-couple vibration test is scheduled for December 1978. The converter for that test will contain reference design hardware, and the test procedure will be the same as for M12A.

3. Single Couple Test Program

a. Description

The single couple vibration testing program was initiated in the first trimester of 1977. As a consequence of the design, a massive heater block was free to vibrate, thereby exaggerating the severity of the test and causing premature failures. Some design modifications were made and the test program reinstated in mid 1978. A sketch of the current apparatus is shown in Figure 10. Since the design modifications were made, three (3) tests have been run. Throughout the course of these experiments, the test procedure has been refined to the point where no further changes are seen for future tests. This procedure is listed in Figure 11. Any deviations from this list in the first three tests will be described in the text of this report.

b. Discussion

The first test was run on 6/23/78. Sliding follower hardware was used, and the test was run in an Argon atmosphere. The module was not processed at 850-150°C. Due to excessive heat losses, the hot and cold end temperatures were only 500-110°C. The first test was run in an open circuit configuration. Resistance was measured directly across the power output leads. Resistances in this test were abnormally high, with a beginning of test value of 950 mΩ (hot) and an end of test value of 1250 mΩ (hot). This increase occurred gradually throughout the course of the test, which lasted about 10 hours. An example of an interesting observation is shown in Figure 12. The resistance was stable for lower frequencies. However, as the frequency was increased, a threshold g level was ultimately reached above which the resistance would fluctuate wildly. When the excitation was stopped, the fluctuations would also stop, and the resistance would recover immediately to its previous stable value. This behavior was observed during the vibration of each axis. The smallest threshold g level was approximately 10. The source of this behavior is not known. The source of the gradual increase in resistance appears to be an oxide layer that formed on the gimbal, and the high resistance appears to have been caused by oxidation on the hot side of the N-leg (reference Figure 13), and not from cracking.

The second test was run on 8/8/78. As in test 1, sliding follower hardware was used, and the test was run in Argon. Again, the module wasn't processed at high temperature. Certain modifications to the module were made between tests 1 and 2 in an attempt to cut down heat losses, but despite the effort, the hot and cold end temperatures were once again 500-110°C. Unlike the first test, test 2 was run with a load current. Resistance measurements were made indirectly in the normal way by measuring I, E_{oc}, and E_{cc} (i.e. $R = (E_{oc} - E_{cc})/I$). The closed circuit voltage was monitored continuously with a strip chart recorder to give an indication of instantaneous performance. There were once again indications of

a steady gradual increase in resistance with time, though it was less pronounced than in the first test. (The resistance increased 13% between the first and second axes in test 1 compared to 7% in test 2). Also, there was once again evidence of a recoverable resistance increase during vibration (ref. Figure 14). This behavior was, as in test 1, found to begin at about 10 g's. Figure 15 displays another significant observation which occurred at the 20 g level during the vibration of both axes. Shortly after this behavior emerged during the second axis, the closed circuit voltage dropped abruptly to zero, signaling a failure. (The voltage didn't recover and so the test was terminated before vibration of the third axis). Disassembly after the test uncovered what we believe to be the cause of the disturbance. The P-leg had shuffled across the follower, leaving only about 10% of the cross sectional area in contact between the cold and hot end current straps. This was something that hadn't occurred in the first test, which wasn't taken above the 10 g level. It appears that the shuffling action was induced by relative motion of the graphite spacer with respect to the cold block. As in test 1, couple resistance was extremely high, the cause being oxidation on the hot side (ref. Figure 16), and not cracking.

Test three was also run with sliding follower hardware. Further modifications to the module permitted higher operating temperatures (750-200°C) for this test. The data taken for test 3 is more complete than the previous two, and a graphical summary appears in Figure 17. The results of this test are much more encouraging than those of the other two. Total resistance was much lower for this test, ranging between 40 and 50 mΩ. No gradual resistance increase were detected. In fact, no severe changes in resistance or open circuit voltage occurred throughout the test. The sudden decrease in both open circuit voltage and resistance at the very end of the test was the result of a heater fuse blow out and is therefore of no consequence. At 12:10 (ref. Figure 17), the open circuit voltage decreased and the resistance increased. This frequency was 50 cps (21.5 g). This would tend to indicate an increase in the contact resistance at the hot end induced by the high degree of excitation.

The hot end thermocouple data is questionable, since what appears to be a rapid increase in temperature at 9:20 AM and a rapid decrease at 11:50 AM have little or no effect on the open circuit voltage.

c. Conclusions and Future Plans

The results of the first three single couple vibration tests indicate that both N and P legs can endure a severe dynamic environment (20 g's) intact. The high resistances seen in the first two tests, caused by oxidation on the hot end of the N-legs, seem to have been done away with by the high temperature outgassing prior to the test and/or the switch to a Xenon atmosphere, which may be more pure. Evidence of P-leg motion found in test 2 indicates a need to secure the P-legs in place. This problem is currently being addressed.

Examination of the modules upon disassembly showed that all hardware was intact. There was no evidence of shorting across either the hot or cold end electrical insulators, and the followers, springs, etc., survived unscathed. Thermal insulation appeared to be in good shape also. So far, all tests have been run with sliding follower hardware. All future tests will be run with compliant follower hardware.

Test No. 3 showed that it's possible for a module to survive an intense dynamic environment (20 g's) without significant degradation. The ability to do so is of course dependant on the quality of assembly. A recoverable drop in converter performance during dynamic loading was an unexpected finding. The agreement on this behavior in the results of tests 1 and 2 indicates that there is a potential stability problem at g levles of 10 or greater.

4. Conclusions

The first four (4) vibration tests have shown no fundamental problems with the converter designs. They have brought to light a few problems that deserve and are receiving attention. The single couple program has provided the most notable finding, those being P-leg motion and recoverable degradation of performance. All in all, results thus far show reason for optimism. Hopefully, the remainder of these programs will help to further isolate problems to be solved.

Peter B. Hagerty

PBH/ac

Fig. 1

M-12A CONFIGURATIONAL DRAWING

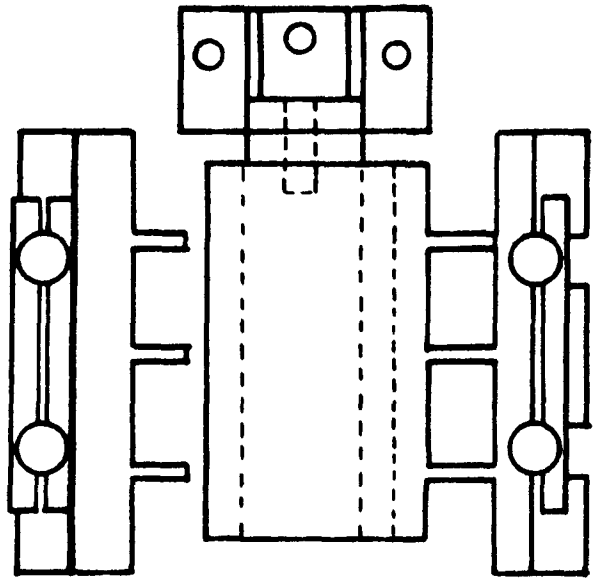

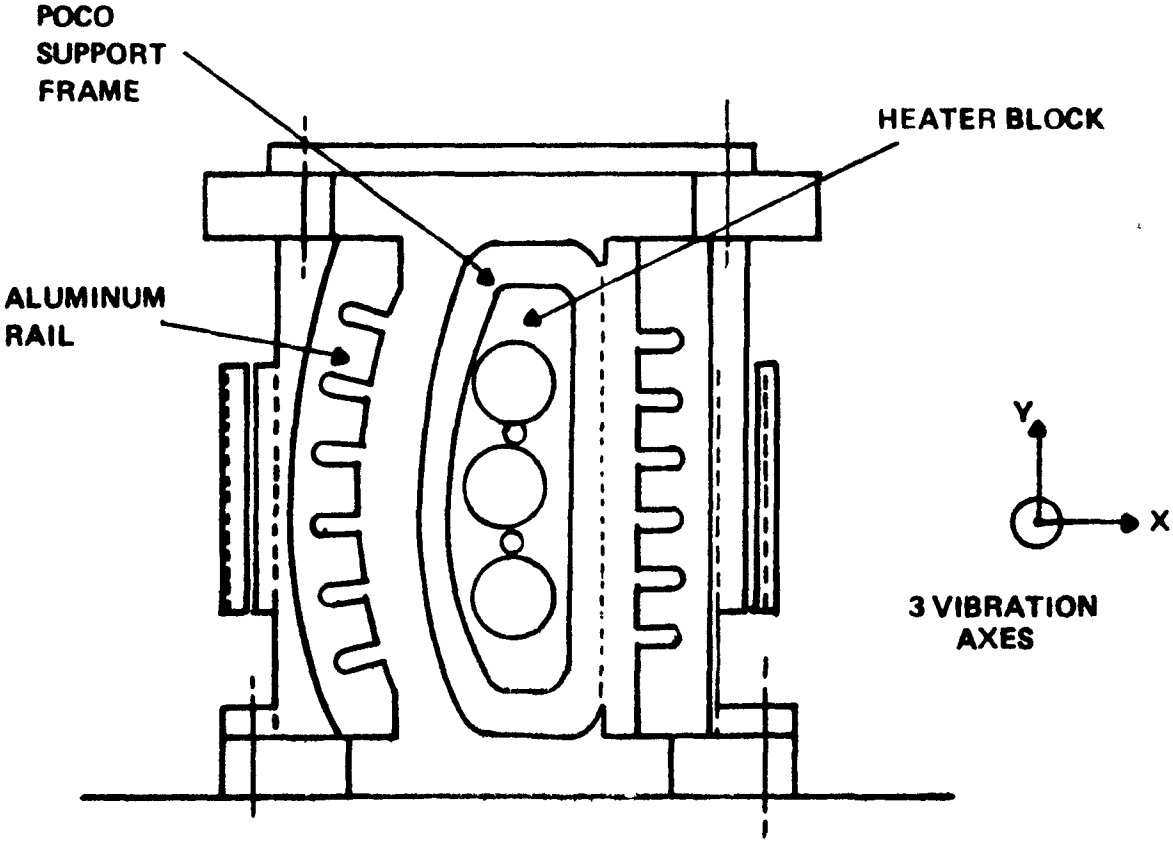

FIGURE 2

TEST PROCEDURE FOR MODULE M12A

1. Operate module in 3M labs at 900-150°C for 500 hours prior to the vibration test.

2. For x, y then z axes:

   - Sinusoidal sweep at 2g's, 20-2000 cps.
   - Random vibration at .5x of specifications, 3 minutes duration.

3. For z-axis only:

   - Random vibration at 1.0x, 1.5x, 2.0x,..... until failure, 3 minutes duration at each level.

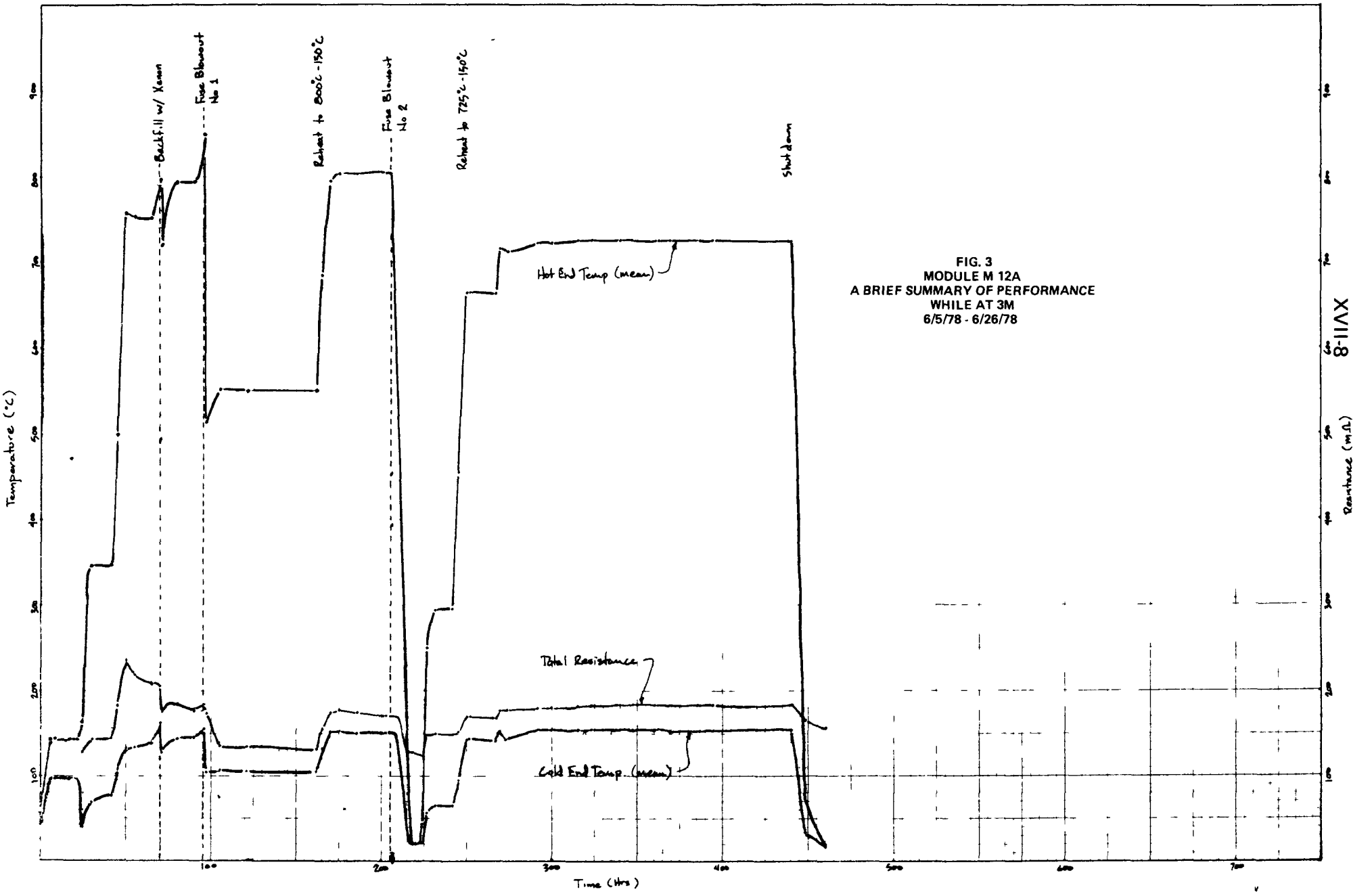

FIG. 3
MODULE M 12A
A BRIEF SUMMARY OF PERFORMANCE
WHILE AT 3M
6/5/78 - 6/26/78

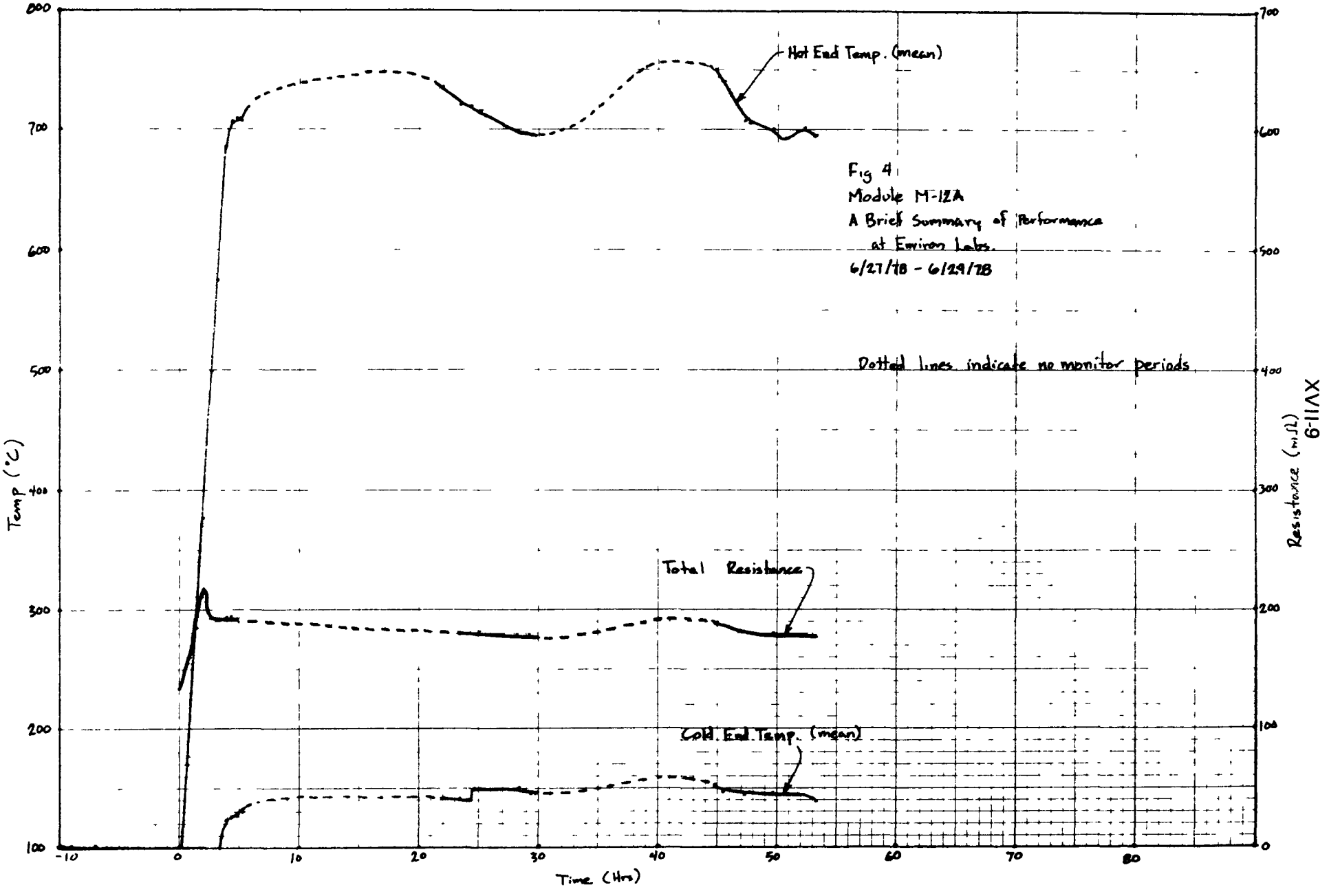

Fig 4
Module M-12A
A Brief Summary of Performance
at Environ Labs.
6/27/78 - 6/29/78

Dotted lines indicate no monitor periods

6-11-XVII-9

K•Σ LOGARITHMIC 3 x 5 CYCLES
KEUFFEL & ESSER CO. MADE IN U.S.A.

46 7522

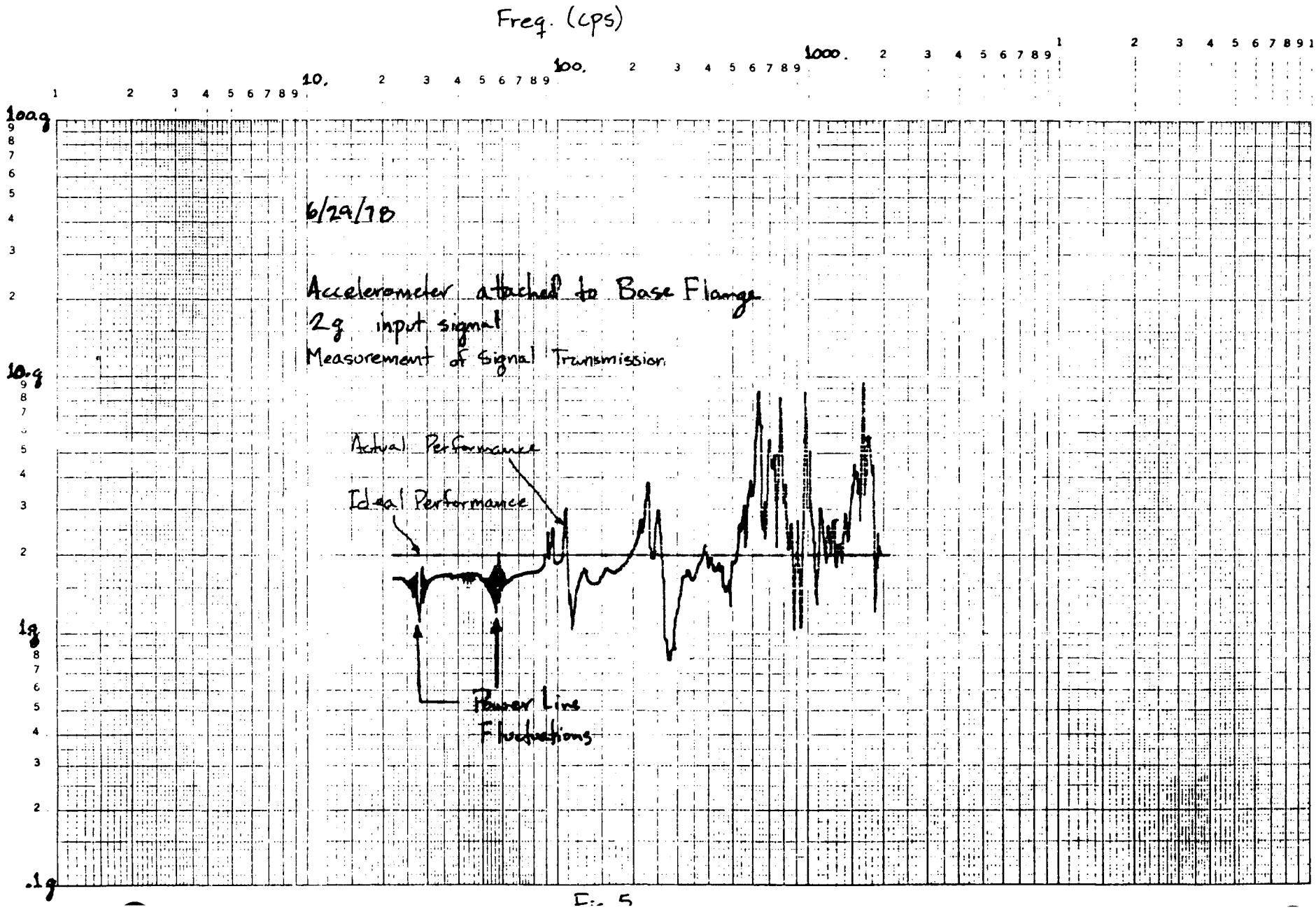

Fig. 5

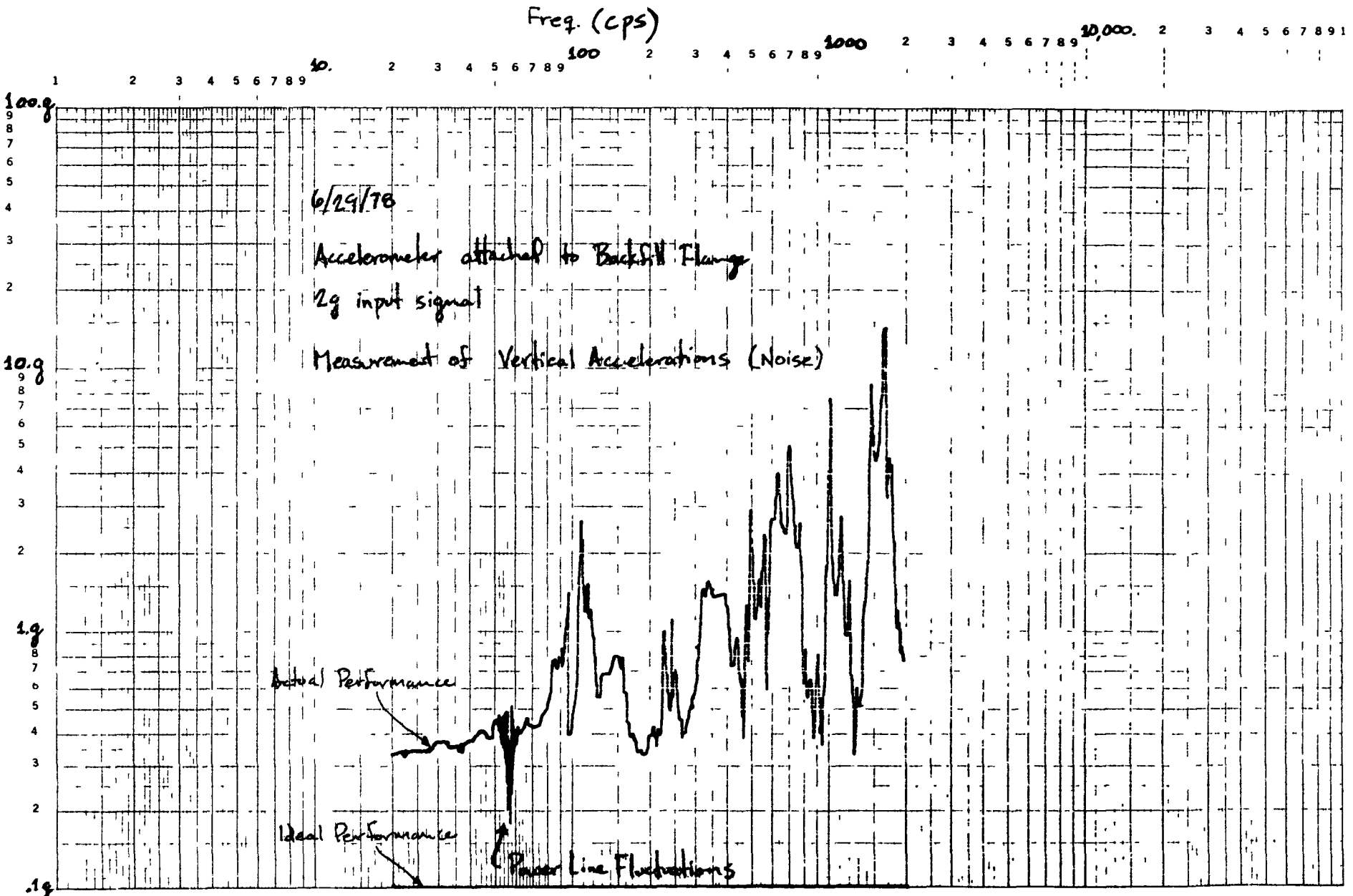
Freq. (cps)
10.
100
1000
10,000.
100.g
10.g
1.g
.1g
6/29/78
Accelerometer attached to Backshell Flange
2g input signal
Measurement of Vertical Accelerations (Noise)
Actual Performance
Ideal Performance
Power Line Fluctuations

Fig. 6

Fig. 7

NOMINAL RANDOM VIBRATION SPECIFICATION FOR M-12 TEST

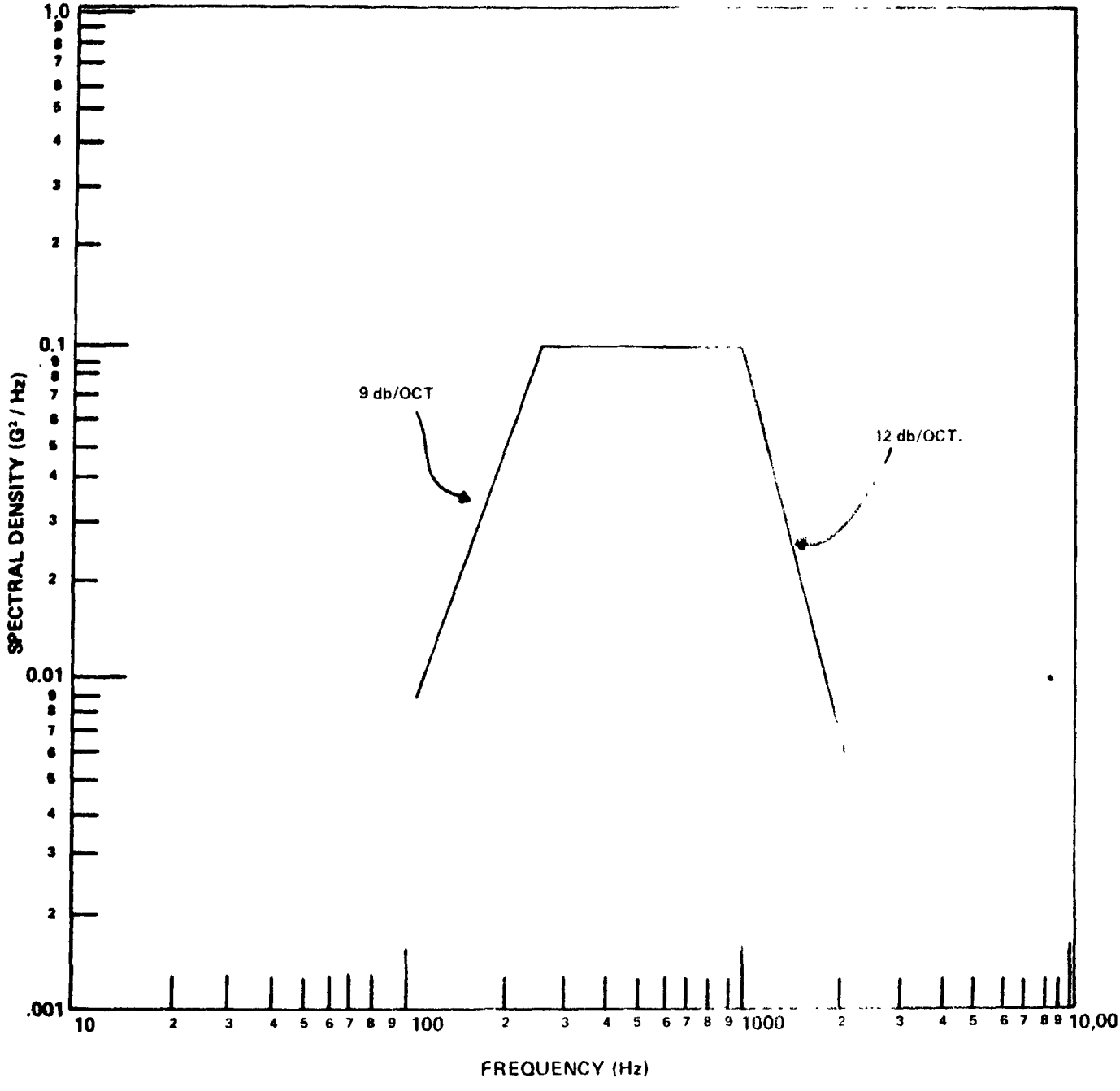

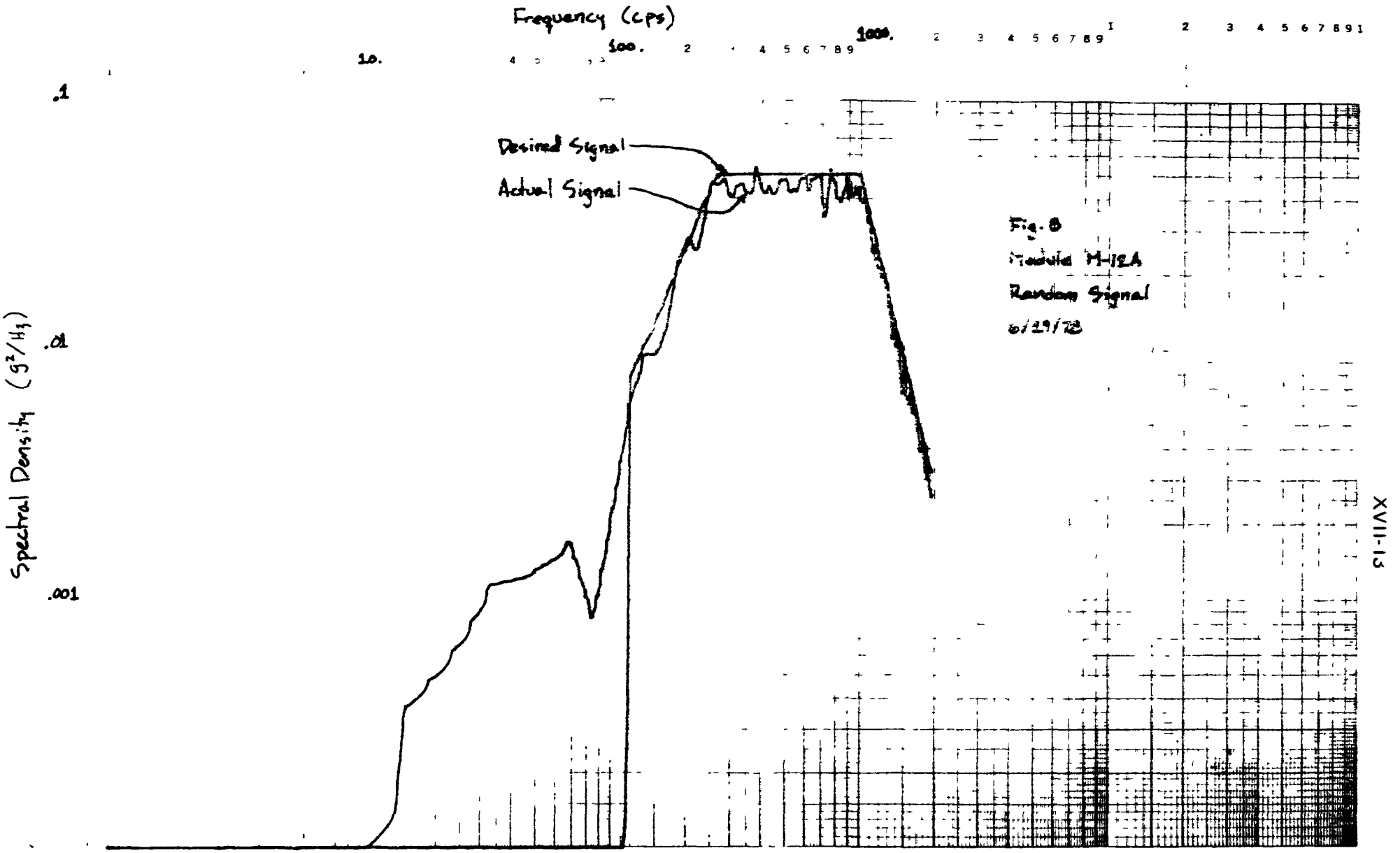
Frequency (cps)
10.
100.
1000.
.1
.01
.001
Spectral Density (g²/Hz)
Desired Signal
Actual Signal
Fig. 8
Module M-12A
Random Signal
6/29/72

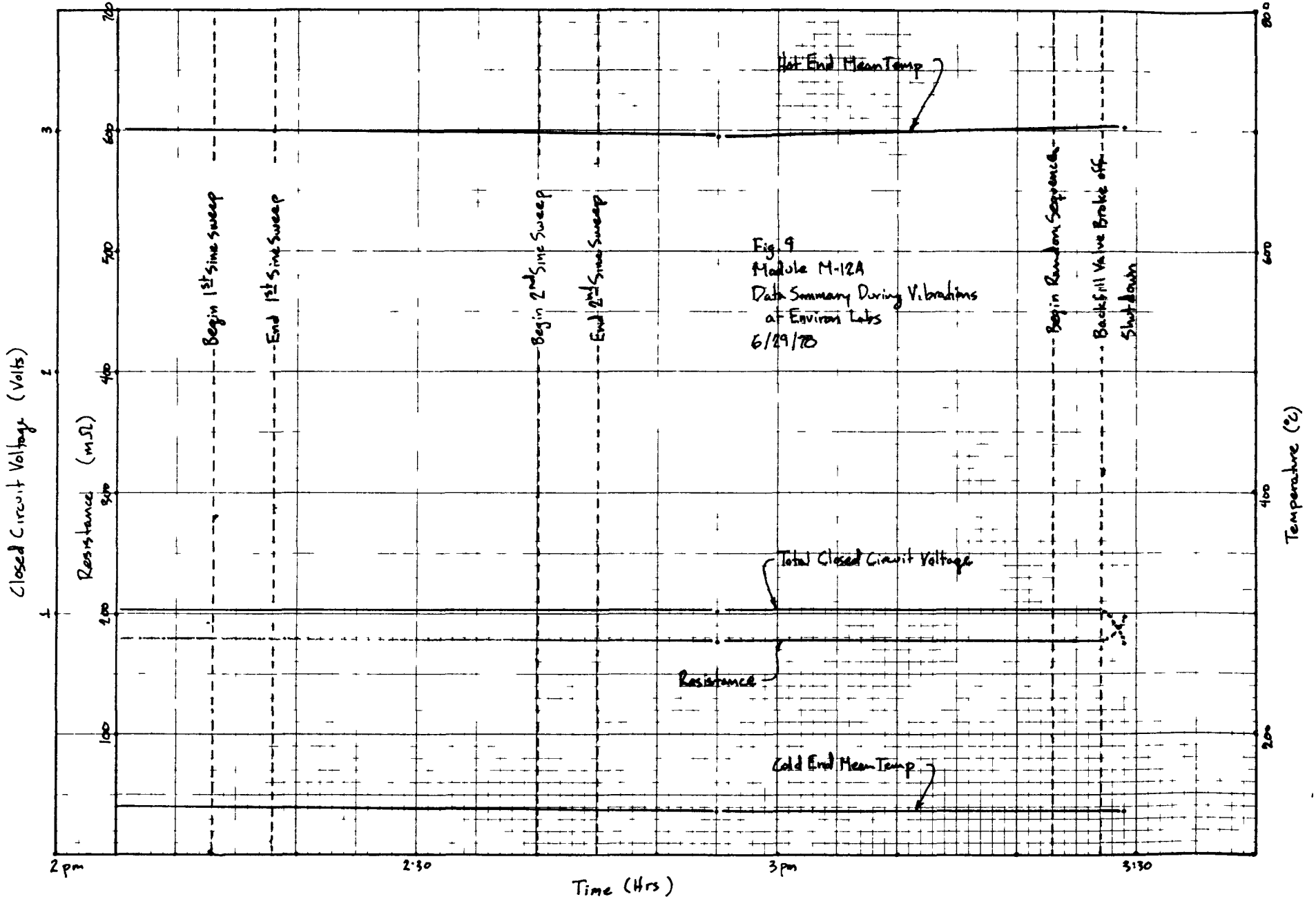

Fig. 9
Module M-12A
Data Summary During Vibrations
at Environ Labs
6/29/70

Fig. 10

SINGLE COUPLE VIBRATION TESTING PROGRAM

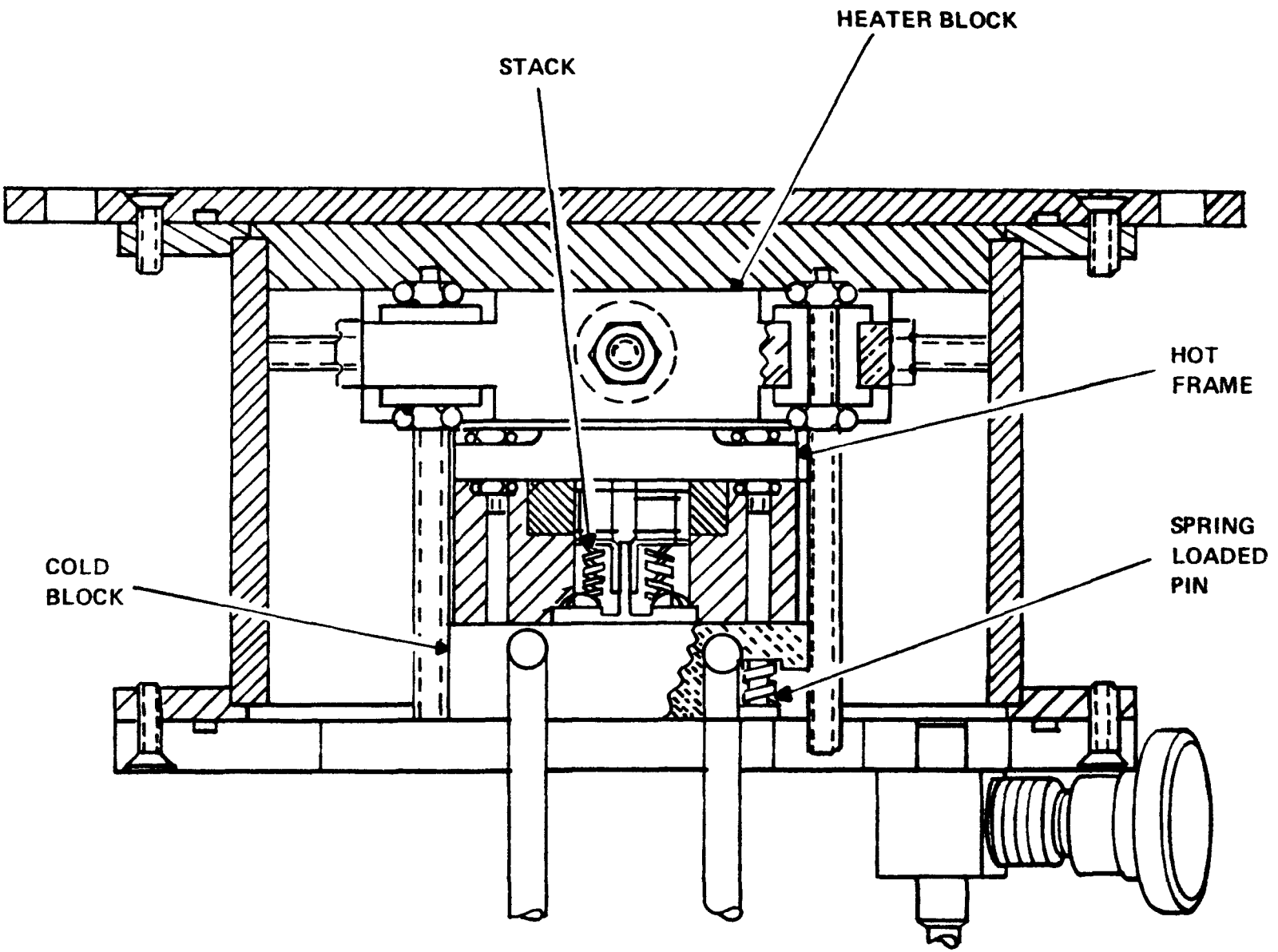

FIGURE 11

Single Couple Vibration Test

Procedure

1. Assemble the module, taking care to use standard assembly techniques and checks.

2. Evacuate the housing to 10^{-8} torr. Process the module at 850-150°C under vacuum. Then cool to room temperature.

3. Backfill the module with Xenon to a pressure of +5 psig.

4. Heat the module to 850-150°C on the vibration machine at a rate of 100-150°C/hr., continually monitoring all temperatures and electrical behavior.

5. Once the module is at temperature, the test can begin. The following will be done for the axes parallel to the rail, perpendicular to the rail, and parallel to the axes of the legs:

   a. Vibrate the module for a minimum of five (5) minutes at .125" peak to peak amplitute, and at each of the following frequencies: 10,20,30,40,50,60 Hz. If significant degradation occurs at a frequency less than 60 Hz, stop there. If the degradation is recoverable, proceed to the next axis. If it's irreversible, terminate the test.

   b. During the vibration, continously monitor the total closed circuit voltage with a strip chart recorder, and make regular checks on the temperatures and electrical behavior (once or twice per frequency setting). The current flow should be maintained at a constant value throughout the test.

6. Cool the module down at the rate of 100-150°C/hr.

7. Carefully disassemble the module, taking care to note any significant observations.

FIG 12
SINGLE COUPLE VIBRATION TESTING PROGRAM
TEST NO 1 6/23/78

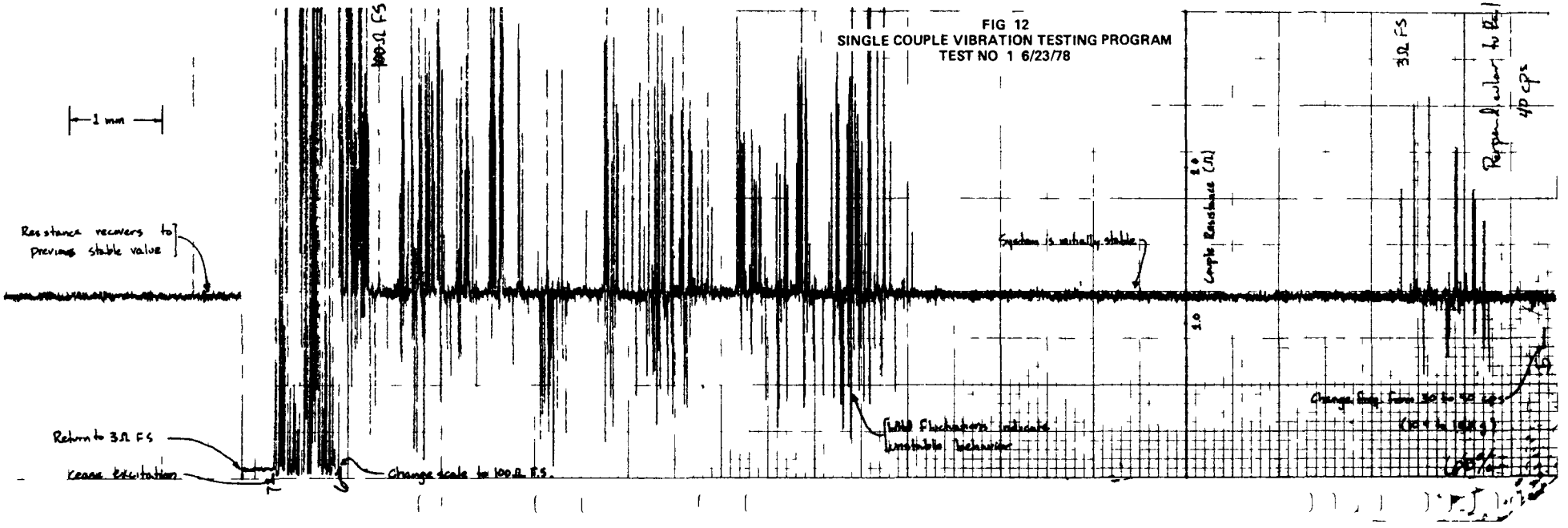

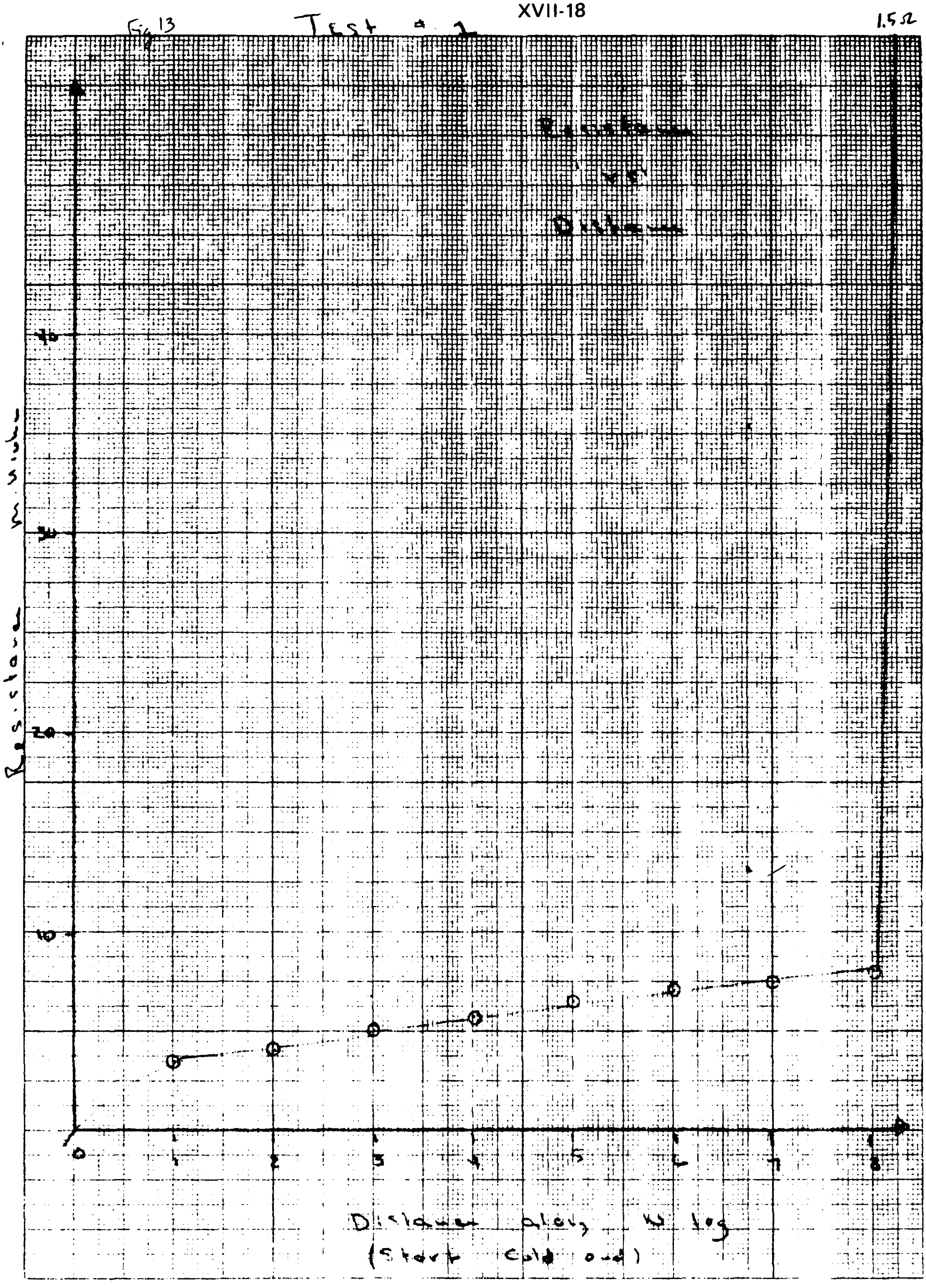
Fig 13
Test # 2
1.5Ω
40
30
20
10
0
1
2
3
4
5
6
7
8
Distance along the log
(Start cold end)

Fig. 14
Single Couple Vibration Program
Test. no 2, 8/8/78

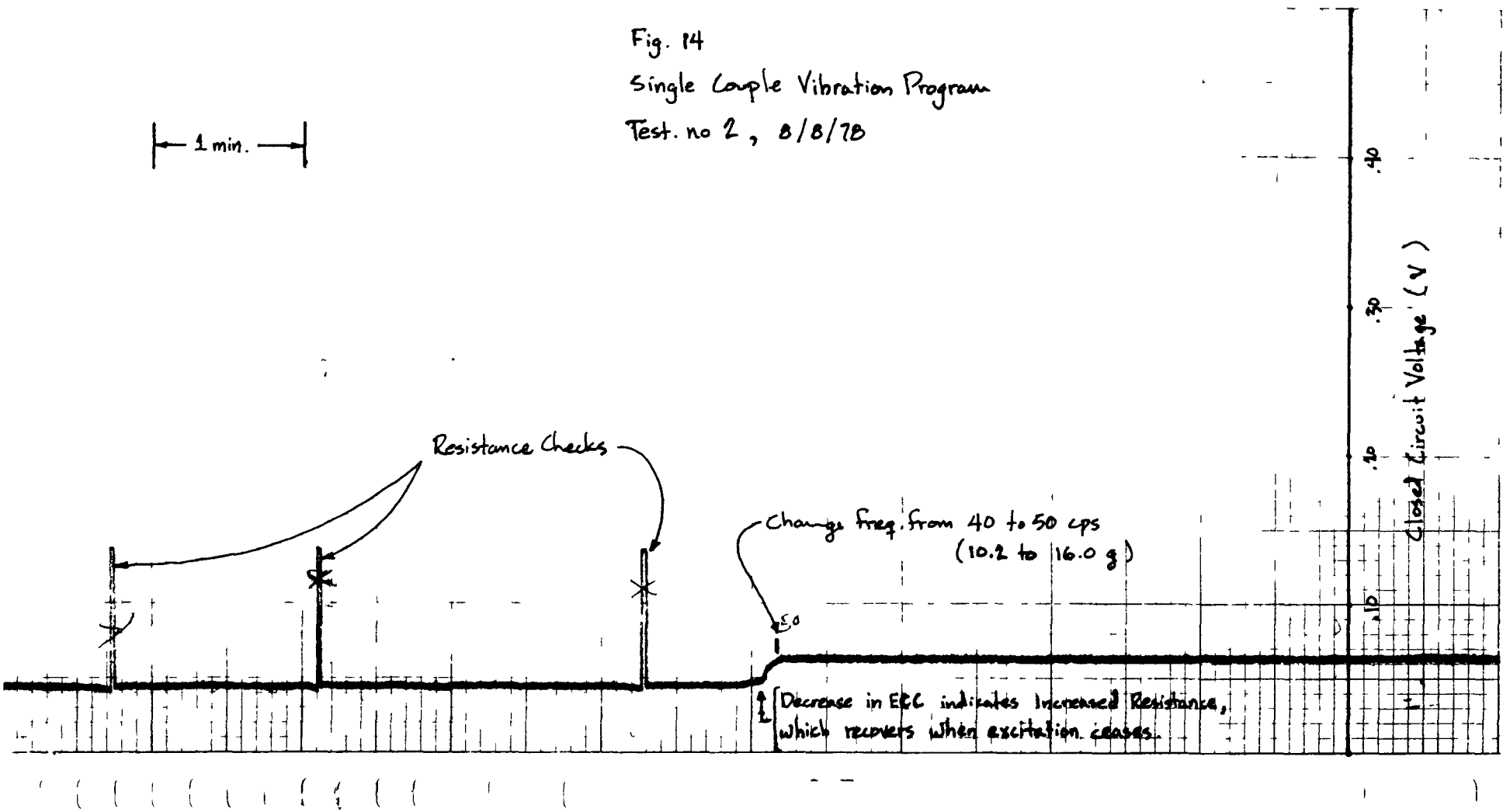

Fig. 15
Single Couple Vibration Testing Program
Test No. 2 , 8/8/78

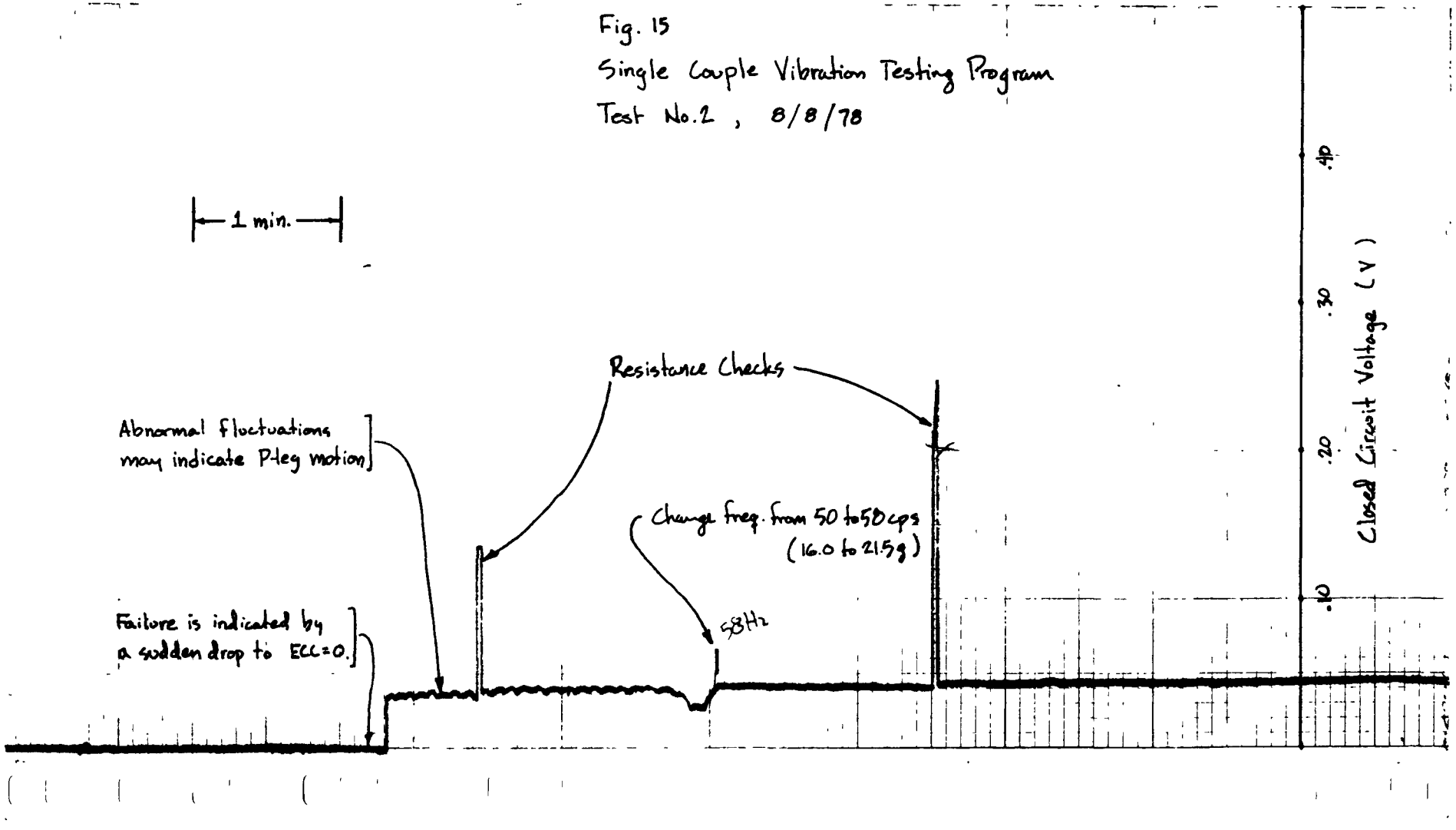

Fig. 16

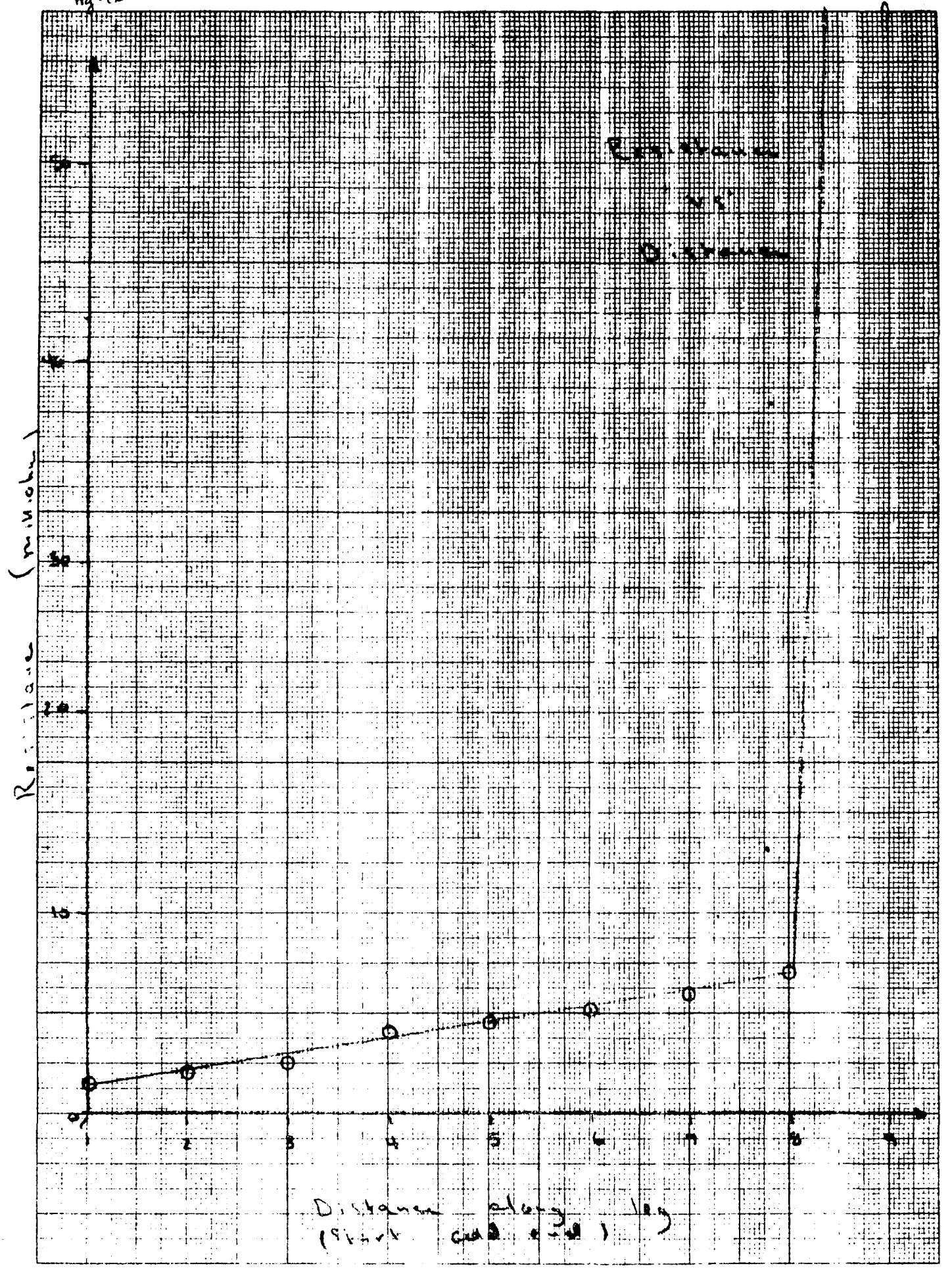

Fig. 17 A Summary of Results from Single Couple Test no. 3

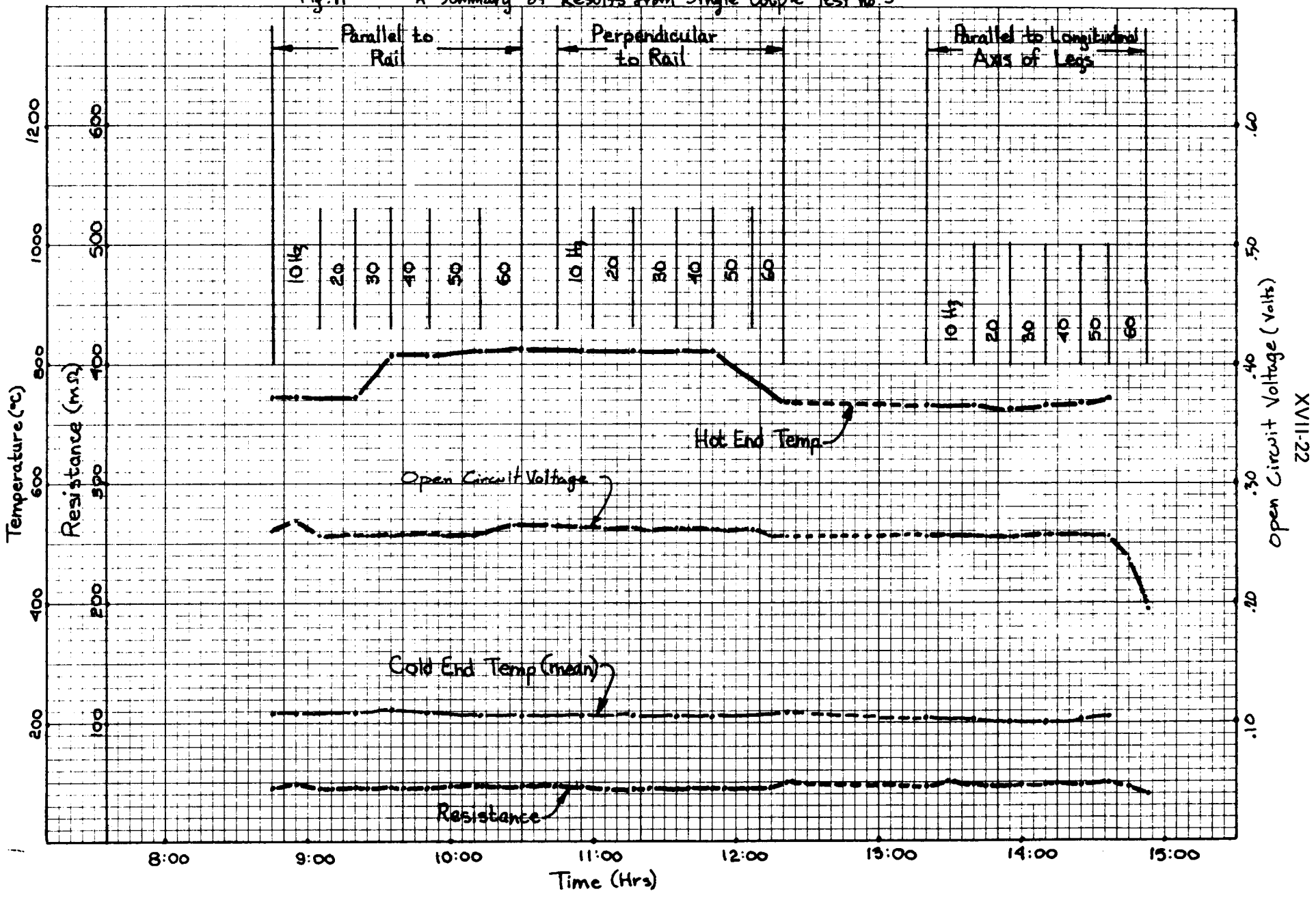

ATTACHMENT XVIII

Converter Materials Compatibility and Removal of IHF Assessed for GDS-II

INTRODUCTION

The objective of the studies in this report was to assess the chemical compatibility and outgassing requirements for GDS-II. GDS-II was intended to be a single-ring generator of the type of GDS-I, but it was to include flight system components. This generator has subsequently been removed from the program. To provide a data base for this assessment, data were obtained in the following areas:

- Isothermal chemical compatibility of GDS-II components
- Update of compatibility with reactive gas species
- Outgassing of converter components and GDS-I

Midway into these studies, a program change was instituted: GDS-II was to be replaced by several 18-couple flight system type converters. As a result of this change, the converter materials compatibility and IHF removal assessment was reoriented toward preliminary flight system type converters.

SECTION 1

EXPERIMENTAL METHODS AND RESULTS

The basic test methods used for these studies were similar to those described previously.[1] The test matrices for the extended studies described in this report are listed in Tables 1-I and 1-II. The test results are discussed in this section, arranged by test method.

Isothermal Chemical Compatibility (Sealed Ampoule)

A sketch of the test configuration for this series is shown in Figure 1-1. The results from this study are detailed in Table 1-III and are summarized below:

	Material	Results
I.	P-TPM-217-$Cu_{1-x}Ag_xSe$	
	A. Bare and Poco encapsulated iridium (proximity)	Analytical evaluation underway at ORNL
	B. Bare and Poco encapsulated Pt-3008 (proximity)	Analytical evaluation underway at ORNL
II.	N-TPM-217-$GdSe_x$	
	A. Min-K 1800TE (contact)	Compatible through 900°C
	B. HiFi 660AH (contact)	Compatible through 900°C
	C. Poco AXF-Q1 (proximity)	Compatible through 900°C
	D. Poco AXF-Q1 wrapped in HiFi (proximity)	Compatible through 900°C
	E. Poco AXF-Q1 wrapped in Min-K 1800TE (proximity)	Compatible through 900°C

These results are consistent with those previously reported.[2]

---

[1] "Converter Materials Chemical Compatibility and Outgassing Requirements Assessed for GDS," Milestone No. 51 report on Contract EY-76-C-02-2331, 3M No. 2331-0404 (2/28/77).

[2] Ibid., p. 1-1 and 1-2.

The following conclusions are drawn from the data in Table 1-III.

1. Neutron Activation, Auger, and metallurgical analyses on the $GdSe_x$ samples show the total increase in oxygen content of the $GdSe_x$ samples is confined to a thin surface film.

2. A water cycle reaction, initiated from adsorbed water on the quartz ampoule walls, is responsible for generating the oxygen content observed in the Gd_2SeO_2 surface film on the $GdSe_x$ samples. The reaction cycle for the water is

$$Gd_2Se_3 + 2H_2O \rightarrow Gd_2SeO_2 + 2H_2 + 2Se$$
$$SiO_2 + H_2 \rightarrow SiO + H_2O$$

This cycle results in the transport of oxygen from the SiO_2 to the $GdSe_x$. Substantiation for this mechanism comes from the following:

- Thermodynamic and rate of evaporation calculations for the $SiO_2 + H_2 \rightarrow SiO + H_2O$ reaction indicate an oxygen content consistent with the observed levels reported in Table 1-III.
- Metallurgical and ESCA analyses of M-5 and reactive gas test $GdSe_x$ legs did not indicate the aforementioned Gd_2SeO_2 surface film.
- The quartz tubes from this study were partially devitrified, whereas quartz tubes from similar sealed ampoule tests containing a Ti-Zr getter did not devitrify. In addition, $GdSe_x$ elements from the getter series did not have the Gd_2SeO_2 film.
- Dynamically pumped isothermal chemical compatibility quartz tubes did not devitrify nor was there any Gd_2SeO_2 film on the outer surfaces of the $GdSe_x$ material.

The water cycle requires a closed system to retain the hydrogen which comes in only from the initial water. Under flight system conditions (dynamic vacuum), the hydrogen would be removed and the cycle broken. Alternatively, the cycle can be broken by a hydrogen getter, as seen in the test series with Ti-Zr getter.

3. Auger analysis of the outer surface of the $GdSe_x$ samples in contact with and in proximity to HiFi 660AH showed iron and sodium only diffused to a depth of <10A. Consequently, these impurities are not considered to be harmful to the $GdSe_x$ performance. However, the trace amounts of sodium and/or sodium component being

vapor transported from the HiFi may affect other generator components. In particular, the effects this sodium has on either iridium or Pt-3008 must be ascertained before a system compatibility statement can be made.

4. Selenium did not diffuse from the TPM-217 into the Poco AXF-Q1 encapsulation crucibles.

5. The effect of selenium from P-TPM-217 on the mechanical integrity of Pt-3008 and iridium cannot be defined until analytical evaluation at ORNL is completed.

6. Portions of the Cab-O-Sil(R) component in the Min-K 1800TE insulation appear to have sintered at 900°C. In contrastto this observation, however, Min-K 1800TE blocks or sleeves used om ingradient experiemnts have shown minute localized indications of Cab-O-Sil(R) sintering at only the hot face surfaces.

Isothermal Chemical Compatibility (Knudsen Cell - Mass Spectrometer)

The results from this study are as follows:

- For the Poco/fibrous insulations and the Poco/fibrous insulations/Pt-3008 system, SiO and CO were detected initially at 920°C.

  The most probable reactions occurring are:

  (1) $SiO_2 + C \rightarrow SiO_g + CO_g$ $\quad \Delta G_{930°} = 63.3$ k cal.

  (2) $SiO_2 + 3C \rightarrow SiC_5 + 2CO_g$ $\quad \Delta G_{930°} = 47.6$ k cal.
  $P_{CO} = 4 \times 10^{-2}$ torr
  $P_{SiO} = 5 \times 10^{-5}$ torr

  The thermodynamics favor the formation of SiC which should inhibit further reaction. Experimentally, the evolution of SiO appears to decrease rapidly when held at 1200°C, indicating that the SiC reaction is occurring. However, it was noted that in ingradient experiments using Fiberfrax H-Blanket around Poco heater blocks at a temperature of 975°C for 1000 hours, SiC was not detected.

- For the Poco/fibrous insulations/$GdSe_x$ systems, SiO, CO, SeSi, Se and Se_2 were detected at 920°C. The $GdSe_x$ from these tests had a surface film similar to those from the sealed ampoule tests. The most probable additional reactions are:

  $$Gd_2Se_3 + 2SiO \rightarrow Gd_2SeO_2 + 2SeSi$$

  $$Gd_2Se_3 + 2CO \rightarrow Gd_2SeO_2 + 2C + 2Se$$

- For all systems, water was not detected above 200°C.

- For the Poco/HiFi 660AH and Poco/HiFi 660AH/Pt-3008 systems, vapor species of iron and sodium were not detected up through 1300°C at the maximum mass spectrometer sensitivity setting. Since sodium and iron were detected by Auger analysis on the outer surface of the sealed ampoule $GdSe_x$ samples in contact with or proximity to HiFi 660A, this result is surprising.

- Surface grain boundary Auger analysis of the Pt-3008 samples from the Poco/fibrous insulations/Pt-3008 did not reveal any foreign impurities.

Reactive Gas Testing (Update)

The effect of atmospheres on the performance of couples continues to be investigated in a series of reactive gas couple tests. Neutron activation analysis for oxygen uptake has been completed on an element run in 10^{-2} torr oxygen atmosphere (this test was reported in Milestone No. 51, "Converter Materials Chemical Compatibility and Outgassing Requirements Assessed for GDS"). The measured oxygen pickup was only 0.16mg after a total oxygen exposure of 0.30 torr-hour (10^{-6}, 10^{-4}, 10^{-2} torr for 103 hours). The test conditions, results, and conclusions for this test along with an extended water vapor tests are summarized in Table 1-IV.

The effect of oxygen doping on thermoelectric generator performance has been calculated under the following assumptions:

1. The temperatures are assumed to remain at 900°/150°C. In reality, if oxygen uptake were to occur in a generator with a fixed size heat source, the temperatures would increase because the power changes more rapidly than the efficiency for the proposed doping mechanism.

2. The doping mechanism assumed was suggested by the analyzed composition and microstructure of heavily oxidized samples and is as follows:

   a. $\alpha(0) + GdSe_{1.485} \rightarrow (1-\frac{2\alpha}{3})\ GdSe_{1.485} + \frac{\alpha}{3}\ Gd_2SeO_3 + \beta(Se)$

   b. $\beta(Se)$ diffuses into bulk

   $$(1-\tfrac{2\alpha}{3})GdSe_{1.485} + \beta(Se) \rightarrow (1-\tfrac{2\alpha}{3})GdSe_{(1.485\ +\ y)}$$

Other degradation mechanisms involving oxygen are possible, including oxidation of the gadolinium contact at the hot end of the N-leg. For the purpose of this calculation, however, only the above mechanism is considered.

The resultant effect of this oxygen doping on thermoelectric properties (S, ρ, K) and on generator performance properties are shown in Table 1-V and 1-VI.

The variable voltage columns in Table 1-VI result from permitting the voltage to vary as Seebeck coefficient varies by always adjusting for maximum efficiency current. The constant voltage columns assume constant voltage regulation of some sort (common in spacecraft power conditioning). A plot of the performance for the variable voltage is shown in Figure 1-2.

Outgassing (Carbon Retention)

Processing experiments were performed to remove the carbon impurity in Min-K 1800TE.

The carbon contaminate in/or on Min-K 1800TE after an 800°C air bake-out was found to be 0.07% wt. Thus, air processing is about 40% effective. Figure 1-3 illustrates the percent carbon versus time and temperature during air bake-out.

Outgassing (No-Load Shrinkage)

Preliminary no load shrinkage data were obtained on six (6) Min-K 1800TE blocks after 800°C/16 hours air bake-out and 1000°C/48 hours vacuum outgassing. Three (3) blocks were a nominal 1-1/4" x 1-1/4" x 1/2" with two (2) 0.290" holes drilled completely through.

The conditions and results of this non-load shrinkage test were:

Conditions:

Block - 1-1/4" x 1/2" with two 0.290" diameter holes

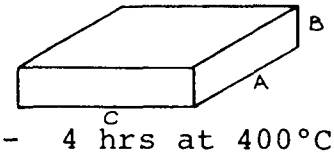

Heat Treatment - 4 hrs at 400°C Air
- 12 hrs at 800°C Air
- 48 hrs at 1000°C Vacuum 10^{-7} torr

Results:

Percent Shrinkage

	After Air	After Air + Vacuum
a.	-.16 ± .49	- .22 ± .48
b.	-.18 ± .75	- .53 ± .49
c.	-.78 ± 1.01	-1.4 ± .70

Holes did not change dimensionally.

Outgassing (Adsorption/Desorption)

The rate of gas adsorption of a 1-1/4" x 1/4" x 1/2" block of Min-K in various atmospheres was measured. After processing of the insulation in accordance with the procedure given in Milestone

Two points can be made from Figure 1-2:

1. The level of 0.3 mg/couple produces an acceptably small degradation in efficiency.

2. The performance varies continuously with oxygen contamination, rather than dropping abruptly at the 0.3 mg/couple level.

Using the measured oxygen uptake of the element, the changes in Seebeck coefficient and resistivity were calculated according to this model and found to be consistent with the measured values.

The 0.16 mg of oxygen actually picked up by the element is four orders of magnitude lower than the amount of oxygen available calculated from the partial pressure and time. This indicates that only a small fraction of the available oxygen will react with the N-legs during generator processing and operation.

This study will continue and results will be periodically updated.

Report No. 51, weight gain was measured on an analytical balance. This rate data is plotted in Figure 1-4. As anticipated, the weight gain in the argon atmosphere glove box was significantly less than in air, and the weight gain in air increased with humidity. The rate of weight gain in air was extremely rapid, reaching one-half of its asymptotic value within 10 minutes of exposure.

The effect of block thickness on Min-K 1800 gas adsorption was also studied in a similar manner, with the data plotted in Figure 1-5. It was anticipated that the fractional weight gain of the block with the higher surface to volume ratio would be higher if diffusion into the bulk Min-K were a significant limiting factor. In fact, measurement showed the opposite effect. It is concluded that inhomogeneity of the Min-K block material is more significant than block size effects per se.

A series of adsorption/desorption experiments were run on Min-K 1800TE to verify the reversibility of adsorption/desorption. These experiments were run on the CRL TGA on minute powdered samples and also in air using an analytical balance on large Min-K 1800TE block samples. All samples were processed, as per Milestone Report No. 51, prior to initiating the adsorption/desorption experiments. The results are tabulated in Tables 1-VII and 1-VIII. The data reported in Table 1-VII show that within the accuracy of the experiment, the adsorption/desorption cycles are reversible. The data summarized in Table 1-VIII shows that 27% of the adsorbed gas can be removed by processing at room temperature, and 43% by processing at 120°C.

Outgassing
(Module Processing - Components)

Manufacturing Standard Instructions 2003 and 2004 for outgassing thermal insulations and Poco graphite parts used in thermoelectric modules were issued. These are shown as Tables 1-IX and 1-X, respectively.

Outgassing
(Module Processing - GDS-I)

Employing the MSI's for outgassing the thermal insulations and Poco graphite parts contributed to the successful processing of GDS-I as per Milestone Report No. 51. Details of the processing are described in MSI 2001, "Thermoelectric Module Outgassing and Heat-Up Procedure." This MSI is shown as Table 1-XI.

TABLE 1-I

TEST MATRIX FOR CHEMICAL COMPATIBILITY

I. Sealed Ampoule

A. Materials:

1. TPM-217
   - Bare and Poco AXF-Q1 encapsulated iridium (proximity) 6
   - Bare and Poco AXF-Q1 encapsulated Pt-3008 tensile specimens (proximity) 8
   - Controls 18

2. $GdSe_x$
   - Min-K 1800TE (contact) 8
   - HiFi (contact) 8
   - Poco AXF-Q1 (proximity) 6
   - Poco AXF-Q1 wrapped in HiFi (proximity) 5
   - Poco AXF-Q1 wrapped in Min-K 1800TE (proximity) 4
   - Controls 17

B. Parameters

1. Temperature - 900°C
2. Test Duration - 1000 and 1500 hours
3. Atmospheres - Static vacuum (10^{-7} torr at seal off) and Xenon
4. Containment Ampoule - Cleaned and outgassed quartz
5. Thermal Insulation and Poco Pretreatment - Outgassed as per 3M MSI's 2003 and 2004.

C. Analytical Evaluation

1. Emission Spectroscopy
2. Electron Beam Microanalyzer
3. Surface Analyses (Auger ESCA)
4. Scanning Electron Microscopy
5. Visual Microscopy
6. X-ray Diffraction
7. X-ray Fluorescence Spectrometry
8. Seebeck and Resistivity Measurements
9. Physical Testing

II. Mass Spectrometer/Knudsen Cell

A. Materials:

Poco AXF-Q1
- Min-K 1800TE
- HiFi 660AH

TABLE 1-I (cont.)

TEST MATRIX FOR CHEMICAL COMPATIBILITY

- Min-K 1800/Pt-3008
- HiFi/Pt-3008
- Min-K 1800/$GdSe_x$
- HiFi/$GdSe_x$
- $GdSe_x$

B. Parameters

1. Temperature - Ambient to 1300°C
2. Test Duration - 2-12 hours
3. Atmosphere - Dynamic vacuum 10^{-6} torr
4. Containment Cell - Poco AXF-Q1
5. Poco and Thermal Insulation Pretreatment - Poco outgassed at 2000°C in mass spectrometer. Thermal insulation outgassed as per 3M MSI 2003.

C. Analytical Evaluation

1. Insitu in Mass Spectrometer
2. Electron Beam Microanalyzer
3. Surface Analyses (Auger)

TABLE 1-II

TEST MATRIX FOR OUTGASSING

I. Min-K 1800 Update

   A. Carbon Removal

   B. No-load Shrinkage

   C. Adsorption/Desorption

II. Converter Processing

   A. Thermal Insulations

   B. Poco AXF-Q1

   C. GDS-I

TABLE 1-III

TEST RESULTS FROM ISOTHERMAL CHEMICAL COMPATIBILITY - SEALED AMPOULE SERIES

System	Observations/Results
I. TPM-217 ($Cu_{1.97}Ag_{0.03}Se_{1+y}$)	
A. Bare and Poco AXF-Q1 encapsulated Iridium - proximity (900°C/1500 hrs/ 10^{-7} torr at seal-off)	TPM-217: The elements were slightly thermally etched. The post-test Seebeck coefficients averaged 253 μv/°C abs. which is within one standard deviation from the mean for the parent non-tested batch material. Poco AXF-Q1: Microprobe analysis did not show selenium diffusion into the Poco bulk mpr pm tje sirface. Iridium: Auger analysis for presence of selenium on surface and in/on grain boundaries and metallurgical analysis for structural changes are underway at ORNL. Microprobe analysis identified trace black deposits on bare iridium as TPM-217, not selenium.
B. Bare and Poco AXF-Q1 encapsulated Pt-3008 - proximity (900°C/1500 hrs/ xenon)	TPM-217: The elements appeared as pretest. The post-test Seebeck coefficients averaged 248 μv/°C abs. which is within one standard deviation from the mean for the parent non-tested batch material. Poco AXF-Q1: Microprobe analysis did not show selenium diffusion into the Poco bulk nor on the surface.

TABLE 1-III (cont.)

I. B. (cont.)		**Pt-3008:** The tensile specimens appeared as pre-test. Ultimate tensile strength, yield strength, elongation, Auger analysis for presence of selenium on surface and in/on grain boundaries and metallurgical analysis for structural changes are underway at ORNL.
C.	TPM-217 Controls (900°C/1500 hrs/ 10^{-7} torr at seal-off)	**TPM-217:** The elements were slightly thermally etched. The post-test Seebeck coefficients averaged 254 μv/°C abs. which is within one standard deviation from the mean for the parent non-tested batch material.
D.	TPM-217 Controls (900°C/1500 hrs/ xenon)	**TPM-217:** The elements appeared as pretest. The post-test Seebeck coefficients averaged 255 μv/°C abs. which is within one standard deviation from the mean for the parent non-tested batch material.
E.	Pt-3008 Controls Bare and Poco AXF-Q1 encapsulated (900°C/1500 hrs/xenon)	**Pt-3008:** The tensile specimens appeared as pre-test. Ultimate tensile strength, yield strength, elongation, and metallurgical analysis for structural changes are underway at ORNL. **Poco AXF-Q1:** The encapsulating crucibles appeared as pre-test.
II. $GdSe_{1.49}$		
A.	Min-K 1800TE-contact (900°C/1000 hrs/ 10^{-7} torr at seal-off)	**$GdSe_{1.49}$:** A greyish-white surface coating was detected on all four test samples. Auger, microprobe and metallurgical analyses of this

TABLE 1-III (cont.)

II. A. (cont.)

surface layer indicated Gd_2SeO_2.

In addition, neutron activation analysis for total oxygen in conjunction with the above techniques showed the oxygen to be localized in the surface layer. The relationship between the film thickness, the bulk oxygen as measured by NAA, and the bulk oxygen calculated as Gd_2SeO_2 is given below:

	Thickness (μm)	Oxygen Content (mg) NAA Bulk Analysis	Calc. A/m/m
1.	23	4.3	4.1
2.	17	3.4	3.0

Min-K 1800TE: There was a color change from pre-test light blue to a dark navy blue. Previous investigations have shown the as received Min-K 1800TE to contain 0.10-0.14%wt carbon (see footnote 1, p. 1-9).

Recent investigations, discussed in the outgassing/reactive gas section, show intrinsic carbon removal by thermal treatment in air to be only 40% effective. The color change is most likely caused by the residual carbon in or on the Min-K 1800TE reducing the TiO_2 component. This color change is not observed in ingradient tests; only the hot face area turns dark blue.

TABLE 1-III (cont.)

II. A. (cont.)

The Cab-O-Sil(R) component of the Min-K 1800TE insulation appears to have partially sintered throughout the entire Min-K 1800TE samples. This observation is in contrast to ingradient tests wherein only the hot face area appears to have any sintered Cab-O-Sil(R) material.

B. Min-K 1800TE-contact (900°C/1000 hrs/xenon)

$GdSe_{1.49}$: Observations and analytical evaluation results are identical to the Min-K 1800TE static vacuum tests. The relationship between the film thickness, NAA oxygen content and the Auger/metallurgical/microprobe data for two of the four test samples is:

	Thickness (μm)	Oxygen Content (mg) NAA Bulk Analysis	Oxygen Content (mg) Calc. A/m/m
1.	13	2.2	2.3
2.	20	3.5	3.4

Min-K 1800TE: Observations and analytical evaluation results are equivalent to the Min-K 1800TE static vacuum tests.

TABLE 1-III (cont.)

II. C. Min-K 1800TE/Poco AXF-Q1/proximity (900°C/1000 hrs/10^{-7} torr at seal-off)

$GdSe_{1.49}$: Observations and analytical evaluation results are identical to the Min-K 1800TE tests listed in A and B. The relationship between the film thickness, NAA oxygen content and the Auger/metallurgical/microprobe data for one of the two test samples is:

Thickness (μm)	Oxygen Content (mg)	
	NAA Bulk	Calc. A/m/m
17	3.8	3.4

Min-K 1800TE: Observations and analytical evaluation results are equivalent to the Min-K 1800TE tests listed in A and B.

Poco AXF-Q1: ESCA analysis underway at ORNL.

D. Min-K 1800TE/Poco AXF-Q1/proximity (900°C/1000 hrs/xenon)

$GdSe_{1.49}$: Observations and analytical evaluation results are identical to the Min-K 1800TE tests listed in A, B, and C.

The aforementioned surface film on these samples was discontinuous. Consequently, an estimate of the oxygen content was not done.

Min-K 1800TE: Observations and analytical evaluation results are equivalent to the Min-K 1800TE tests in A, B, and C.

Poco AXF-Q1: ESCA analysis underway at ORNL.

TABLE 1-III (cont.)

II. E. Fiberfrax 660AH HiFi Paper-contact ($900°C/1000$ hrs/10^{-7} torr at seal-off)

$GdSe_{1.49}$: The surfaces of both the elements were mottled. Auger, microprobe and metallurgical analyses of these surfaces indicated Gd_2SeO_2. As with the Min-K 1800TE series, NAA analysis showed the oxygen to be localized in this surface layer.

The relationship between the film thickness, NAA oxygen content and the Auger/metallurgical/microprobe data for these elements is:

	Thickness (μm)	Oxygen Content (mg) NAA Bulk Analysis	Calc. A/m/m
1.	10	2.7	2.0
2.	10	3.0	2.0

Auger analysis showed trace iron and sodium only on the outer surfaces of the test samples.

Fiberfrax HiFi: Slight grey appearance uniformly distributed on surface of insulation. This grey material is selenium which was released from the surface of the $GdSe_{1.49}$ during the oxygen reaction.

II. F. Fiberfrax 660AH HiFi Paper-contact (900°C/1000 hrs/xenon)

$GdSe_{1.49}$: Observations and analytical evaluation results for these two samples are identical to the Fiberfrax 660AH HiFi test samples in E. The relationship between

TABLE 1-III (cont.)

II. F. (cont.)

the film thickness, NAA oxygen content and the Auger/metallurgical/microprobe data for one of these elements is:

Thickness (μm)	Oxygen Content (mg) NAA Bulk Analysis	Oxygen Content (mg) Calc. A/m/m
7	1.4	1.3

Fiberfrax HiFi: Observations and analytical evaluation results are equivalent to the Fiberfrax HiFi in E.

G. Fiberfrax 660AH HiFi Paper/Poco AXF-Q1-proximity (900°C/1000 hrs/10^{-7} torr at seal-off)

$GdSe_{1.49}$: The surfaces of the three elements were mottled and darkened. Other observations and analytical evaluation results are identical to those in E and F. The relationship between the film thickness, NAA oxygen content and the Auger/metallurgical/microprobe data for these samples is:

	Thickness (μm)	Oxygen Content (mg) NAA Bulk Analysis	Oxygen Content (mg) Calc. A/m/m
1.	7	1.4	1.3
2.	10	1.4	1.7
3.	10	2.8	1.7

Fiberfrax HiFi: Observations and analytical evaluation results are similar to the Fiberfrax HiFi in E and F.

TABLE 1-III (cont.)

		Poco AXF-Q1: ESCA analysis underway at ORNL.
H.	Fiberfrax 660AH HiFi paper/Poco AXF-Q1 proximity (900°C/1000 hrs/xenon)	$GdSe_{1.49}$: Observations and analytical evaluation results for the two samples are equivalent to those in E, F, and G. The relationship between the film thickness, NAA oxygen content and the Auger/metallurgical/microprobe data for one of these samples is:

Thickness (μm)	Oxygen Content (mg)	
	NAA Bulk Analysis	Calc. A/m/m
7	1.6	1.5

Fiberfrax HiFi: Observations and analytical evaluation results are similar to the Fiberfrax HiFi in G.

Poco AXF-Q1: ESCA analysis underway at ORNL.

I. Poco AXF-Q1-proximity (900°C/1000 hrs/10^{-7} torr at seal-off)

$GdSe_{1.49}$: The surfaces of both the elements were mottled and greyed. Other observations and analytical evaluations were equivalent to those in C, D, G and H. The relationship between the film thickness, NAA oxygen content and the Auger/metallurgical/microprobe data for one of these samples is:

TABLE 1-III (cont.)

		Thickness (μm)	Oxygen Content (mg) NAA Bulk Analysis	Oxygen Content (mg) Calc. A/m/m
		10	1.8	1.7
	Poco AXF-Q1: ESCA analysis is underway at ORNL.			
J.	Poco AXF-Q1-proximity (900°C/1000 hrs/ xenon)	$GdSe_{1.49}$: The surfaces of the four elements were slightly darkened. Visual microscopy did not detect a Gd_2SeO_2 surface film on any of these samples. As a result, the relationship between film thickness, NAA oxygen control and Auger/metallurgical/ microprobe data could not be determined for this sample.		
	Poco AXF- Q1: ESCA analysis is underway at ORNL.			
K.	$GdSe_{1.49}$ Controls (900°C/1000 hrs/ 10^{-7} torr at seal-off)	$GdSe_{1.49}$: The surfaces of the two elements were matted. Auger, microprobe and metallurgical analyses of this surface layer indicated Gd_2SeO_2. In addition, neutron activation analysis for total oxygen in conjunction with the above techniques showed the oxygen to be localized in the surface film. The relationship between the film thickness, NAA oxygen content and the Auger/ metallurgical/microprobe data for two of these samples is:		

TABLE 1-III (cont.)

	Thickness	Oxygen Content (mg) NAA Bulk Analysis	Oxygen Content (mg) Calc. A/m/m
1.	11	1.7	1.9
2.	6	1.4	1.0

L. $GdSe_{1.49}$ Controls (ambient temp./ 1000 hrs/10^{-7} torr at seal-off)

$GdSe_{1.49}$: Both the elements were as pretest. Visual microscopy did not detect a Gd_2SeO_2 surface film. However, using a 1 μm upper bound for visual microscopy on both of these samples, relationship between film thickness, NAA oxygen content and Auger/metallurgical/microprobe data was found to be:

	Thickness (μm)	Oxygen Content (mg) NAA Bulk Analysis	Oxygen Content (mg) Calc. A/m/m
1.	<1	0.2	<0.2
2.	<1	0.2	<0.2

M. $GdSe_{1.49}$ controls (900°C/1000 hrs/ xenon)

$GdSe_{1.49}$: The surfaces of the three elements were darkened. Other observations and evaluation results are equivalent to those in L. The film thickness, NAA oxygen content, and Auger/ metallurgical/microprobe data on two of three samples was found to be:

	Thickness (μm)	Oxygen Content (mg) NAA Bulk Analysis	Oxygen Content (mg) Calc. A/m/m
1.	<1	0.3	0.2
2.	<1	0.3	0.2

TABLE 1-III (cont.)

N. $GdSe_{1.49}$ controls (ambient temp./1000 hrs/xenon)	$GdSe_{1.49}$:	The two elements were as pretest. All other observations and evaluation results are identical to those in L.

TABLE 1-IV

Reactive Gas Ingradient Test Measurements

Conditions:

	Oxygen	Water Vapor
Time - 103 hours operation at 850°/150°C		314 hours operation at 850°/100°C
Pressure - 10^{-6}, 10^{-4}, 10^{-2} torr		10^{-6}, 10^{-4}, 10^{-2} torr
Total Exposure - 0.30 torr-hour		3.0 torr-hour

Results:

	Oxygen	Water Vapor
•	Oxygen pickup by $GdSe_x$ - 0.16 mg	--
•	ΔS increased 3 μv/°C	ΔS linear to 1.3 torr-hour (similar to oxygen test)
•	ΔR increased 7%	ΔR linear to 1.3 torr-hour then ΔR accelerated
•	Slight oxidation of gadolinium hot end contact	Severe oxidation of gadolinium foil, heater block and tantalum gimbals
•	ESCA analysis indicated cleaner surface than for isothermal compatibility sealed ampoule/xenon cover gas control elements.	--

Conclusions:

- Electrical changes consistent with Oxygen Doping Mechanism

Property	Measured*	Predicted From 0.16 mg Pickup
ΔS	+3	4
ΔR	+7%	4%

- Oxygen Pickup Four Orders of Magnitude Below Available Oxygen

*Difference between averages at 30-32 hrs, before 10^{-4} torr O_2 exposure, and average between 96 and 101 hrs at end of test, corrected for changes in temperature.

TABLE 1-V

Effect of Oxygen Doping on Thermoelectric Properties

Weight of Oxygen Uptake (mg)	$S\mu$ (<μv/°C,Abs)	($m\Omega$-cm)	K(mw/cm-°C)
0.0	213	10.26	5.22
0.3	220	11.12	5.13
0.6	227	12.24	5.03
0.9	235	13.57	4.94
1.2	244	15.30	4.85
1.5	255	17.44	4.75
1.8	267	20.40	4.66
2.1	281	24.48	4.57

TABLE 1-VI

Effect of Oxygen Doping on Thermoelectric Properties

Weight of Oxygen Uptake (mg)	Variable Voltage			Constant Voltage Regulator		
	V(volts)	P_o(w)	η_{TE}(%)	V(volts)	P_o(w)	η_{TE}(%)
0	29.1	259	12.6	29.1	259	12.6
0.3	29.6	255	12.5	29.1	256	12.5
0.6	30.1	249	12.3	29.1	252	12.3
0.9	30.7	243	12.2	29.1	247	12.2
1.2	31.3	235	12.0	29.1	239	12.0
1.5	32.1	227	11.7	29.1	231	11.7
1.8	32.9	215	11.4	29.1	219	11.3
2.1	33.9	201	10.9	29.1	205	10.7

TABLE 1-VII

Adsorption/Desorption Experiments: Min-K 1800TE

Sequence	ΔW $\frac{mg\ H_2O/N_2/O_2}{g\ Min\text{-}K\ 1800TE}$	
I. Min-K 1800TE Block: 1-1/4" x 1/4" x 1/2"	(Processed and not stored prior to adsorption/desorption experiments)	
A. Adsorption		
1. Air: 42% R H (41 hrs)	+3.0	
2. Air: 52% R H (40 hrs)	+3.8	
3. Glove Box Argon (330 hrs)	+1.3	
B. Desorption: Vacuum (22 hr at ambient temp)	-0.7	
C. Adsorption: Air (42% R H) (0.5 hr)	+0.5	
D. Desorption: Vacuum (96 hr at ambient temp)	-0.2	
E. Adsorption: Air (42% R H) (1 hr)	+0.4	
F. Desorption: Vacuum (16 hr at ambient temp)	-0.5	
G. Adsorption: Air (42% R H) (1 hr)	+0.6	
H. Desorption: Vacuum (22 hr at 120°C)	-1.4	
I. Adsorption: Air (42% R H) (6.5 hr)	+1.0	
J. Desorption: Vacuum (113 hr at 120°C)	-0.9	
K. Adsorption: Air (42% R H) (3 hr)	+1.1	
II. Min-K 1800TE Powder	(Processed and stored in Argon for about 150-350 hours prior to desorption/adsorption experiments)	
A. Desorption: Vacuum (∿2 hr ambient to 845°C)	-5.0	
B. Adsorption:		
1. Air: R H* (16 hr)	+10.5	
2. Argon: Lab cylinder (16 hr)	+ 4.0	
C. Desorption: Vacuum (∿7 hr ambient to 845°C)		
1. After air 16 hr	-10.8	
2. After Argon 16 hr	-3.5	
D. Adsorption:		
1. After ∿7 hr vacuum desorption of 16 hr air experiment Argon exposure (system suspected of leaking air)	+10.5	
2. After ∿7 hr vacuum desorption of 16 hr argon experiment air exposure	Appeared to parallel Argon exposure of (1)	

*Unknown

TABLE 1-VIII

Desorption: Min-K 1800TE
(Summation)

Conditions:

Sample - 1-1/4" x 1-1/4" x 1/2" Block

Atmosphere Exposure - 42% R H Lab Air

Contaminant Loading - 3.0 mg/g Min-K 1800

Desorption Cycle - Ambient temperature, 10^{-7} torr, and 22 hours

Results:

	Remaining Contaminant Loading (mg/g Min-K 1800)	% Removal
Ambient Temperature	2.2	27
120°C	1.7	43

3M COMPANY

ELECTRICAL PRODUCTS GROUP
PIONEERING LABORATORY

MANUFACTURING STANDARD INSTRUCTIONS

Issue Date 9/27/77 MSI 2003

Revised _____ Page 1 of 2

TITLE: Outgassing Procedure for Thermal Insulation used in Thermoelectric Modules

APPLICABLE DOCUMENTS

1.0 SCOPE

This specification covers the outgassing procedure for removing gaseous and volatile impurities from thermal insulation used in thermoelectric modules.

2.0 EQUIPMENT

The equipment required to perform the outgassing procedures noted herein includes:

2.1 Quartz Tube - Clear fused quartz heavy wall commercial tubing capable of operating at 10^{-7} - 10^{-8} torr at a maximum temperature of 1050°C.

2.2 Vacuum System - This system includes:

2.2.1 Bakeable Vacuum Manifold - Stainless steel elbows, tubing, valving, and vacuum tube port.

2.2.2 Turbomolecular Vacuum Pump - Capable of ultimate pressure of 10^{-8} - 10^{-7} range.

2.2.3 Forepump - Capable of evacuating total system to 10^{-4} torr.

2.3 Furnace and Controller - Capable of sustained closed loop controlled operation at 1100°C.

2.4 Water Cooling Source and Drain - Capable of providing cooling for the vacuum tube port and turbopump.

2.5 Storage Container - Capable of being evacuated to 10^{-4} torr and holding activated molecular sieves gettering material.

2.6 Ion Gauge and Controller - For measuring pressure in vacuum system.

Originator	Engineer	Materials	Quality	MFG
Robert B. Emerson 9/27/77	9/27/77	Robert B. Emerson 9/27/77	9/27/77	9/27/77

FORM 15807-PWO

2.7 Temperature Measurement Device - Pt-10% Rh T/C and readout equipment.

3.0 MATERIALS

3.1 The thermal insulations covered by this specification include:

3.1.1 Min-K 1400 TE and 1800 TE.

3.1.2 Fiberfrax H-Blanket.

3.1.2 Fiberfrax 660AH HiFi Paper.

4.0 METHOD

4.1 Air Bake-out - The following thermal insulations are baked out in air accordingly:

4.1.1 Min-K and 1800 TE and HiFi Paper - Load clean insulation into quartz or high purity Al_2O_3 trays.

- o Heat to 400°C ± 10°C and hold for 4-6 hours.
- o Increase heat to 800°C ± 10°C and hold for 16-18 hours.
- o Furnace cool and transfer to quartz tube.

4.2 Vacuum Outgassing - Each of the previous listed thermal insulations are vacuum outgassed accordingly:

- o Weigh the total quantity of insulation to be processed.
- o Assemble quartz tube into the vacuum furnace system.
- o Evacuate system until turbomolecular pump can be started.
- o Start turbomolecular pump and continue evacuating at ambient temperature for a minimum of 2 hours.
- o Heat up system at such a rate that the pressure is $\leq 1 \times 10^{-4}$ torr.
- o Vacuum outgas at 100°C above the expected peak temperature insulation is to reach in the thermoelectric module until a residual outgassing rate of $\leq 1 \times 10^{-6}$ torr-liter/g-sec. is obtained,

$$\left(\text{i.e. } \frac{\text{torr-liter}}{\text{g-sec}} = \frac{(\text{Pressure in torr}) \times (\text{Speed of Pumping System at Point of Pressure Measurement})}{\text{Wt. of Insulation in grams}}\right.$$

- o Furnace cool to ambient and quickly transfer, in air, to the storage container.

5.0 DISPOSITION

- o Indentify material with part number, intended use, processing MSI, operating initial and date, on QC OK Limited Acceptance Tag.
- o Record and initial date of removal, of pieces, from storage container.
- o Handle only with appropriate gloves and not with bare hands.

Issued 9/27/77 RA Francis 9/27/77 John Ford 9/27/77

TABLE 1-X

3M COMPANY

PIONEERING LABORATORY
ELECTRICAL PRODUCTS GROUP
ST. PAUL, MINNESOTA

ENGINEERING CHANGE NOTICE
ECN NO. _____
SHT. 1 **OF** 1 **SHTS.**

Specification or Drawing Title	Rev.	Spec. or Dwg. No.
Outgassing Procedure for Poco Graphite		MSI 2004

Change Requested By	Date	Mat'l. Disposition	Effective:
R. B. Ericson	3/27/78		3/27/78

Reason for Change

Adding Cleaning Spec. and Additional Processing Spec.

Description of Change

1. Add heat tape to the equipment section, 2.8.

2. Section 4.1 becomes section 4.2; modify this section to include heating of manifold with heat tape.

3. The new section, 4.1, is as follows:

   4.1 Equipment: Prior to Assembly:

   - The quartz tube is degreased with Trichloroethylene, washed with Alconox/hot water, tap water rinsed, distilled water rinsed and hot air dried.
   - The vacuum manifold is degreased with Freon.
   - The "O" rings are degreased with Freon and re-greased with a light coating of Corning Silicone Vacuum Grease.

Other Parts or Drawings Affected

None

E. C. O. APPROVAL		DATE	E. C. N. APPROVAL		DATE
DSN.	D. Thulemeyer	3/30/78	DSN.		
MFG.	J. Bostrom	4/5/78			
~~QA.~~					
~~REL.~~	J. C. Dall	3-29-78			
MAT'L.	Robert B. Ericson	4/4/78			
PROG.	R. D. Pufahl	4-4-78			

ECN NO.

FORM 16521-PWO

3M COMPANY

ELECTRICAL PRODUCTS GROUP
PIONEERING LABORATORY

MANUFACTURING STANDARD INSTRUCTIONS

Issue Date 9/27/77 MSI 2004

Revised 4/5/78 Page 1 of 3

TITLE: Outgassing Procedure for Poco Graphite Hot Frame and Heater Block Pieces

APPLICABLE DOCUMENTS

1.0 Scope

This specification covers the outgassing procedure for removing adsorbed gaseous impurities from Poco AXF-Q-1 hot frame and heater block pieces.

2.0 Equipment

The equipment required to perform the outgassing procedures noted herein includes:

2.1 Quartz Tube

Clear fused quartz heavy wall commercial tubing capable of operating at 10^{-7} - 10^{-8} torr at a maximum temperature of 1050°C.

2.2 Vacuum System

This system includes:

2.2.1 Bakeable Vacuum Manifold

Stainless steel elbows, tubing, valving, and vacuum tube port.

2.2.2 Turbomolecular Vacuum Pump

Capable of ultimate pressure of 10^{-8} - 10^{-7} range.

2.2.3 Forepump

Capable of evacuating total system to 10^{-4} torr.

2.3 Furnace and Controller

Capable of sustained closed loop controlled operation at 1100°C.

Originator	Engineer	Material's	Quality	
T B Evenson 4/4/78	D Ahlgren 3/31/78	K B Evans 4/4/78	Mitchell 3/29/78	

FORM 15807-PWO

3M COMPANY ELECTRICAL PRODUCTS GROUP PIONEERING LABORATORY	MANUFACTURING STANDARD INSTRUCTIONS Issue Date _____ MSI 2004 Revised _____ Page 2 of 3

TITLE:

APPLICABLE DOCUMENTS

2.4 Water Cooling Source and Drain

Capable of providing cooling for the vacuum tube port and turbopump.

2.5 Storage Container

Capable of being evacuated to 10^{-4} torr and holding activated molecular sieves gettering material.

2.6 Ion Gauge and Controller

For measuring pressures in vacuum system.

2.7 Temperature Measurement Devices

Pt-10% Rh T/C and readout equipment.

2.8 Manifold Heating Devices

Heat tapes capable of heating processing manifold to 75°C.

3.0 Material

The Poco graphite material covered by this specification is AXF-Q-1.

4.0 Method

4.1 Equipment Preparation Prior to Assembly:

- The quartz tube is degreased with Trichloroethylene, washed with Alconox/ hot water, tap water rinsed, distilled water rinsed, and hot air dried.
- The vacuum manifold is degreased with Freon®.
- The "O" rings are degreased with Freon® and regreased with a light coating of Dow Corning Silicone Vacuum Grease.

Originator	Engineer	Materials	Quality	

FORM 15807-PWO

3M COMPANY ELECTRICAL PRODUCTS GROUP PIONEERING LABORATORY	MANUFACTURING STANDARD INSTRUCTIONS Issue Date _____ MSI 2004 Revised _____ Page 3 of 3

TITLE:

APPLICABLE DOCUMENTS

4.2 Vacuum Outgassing

The Poco AXF-Q-1 hot frame and heater block pieces are vacuum outgassed accordingly:

- Weigh each piece to be processed.
- Assemble quartz tube into the vacuum and furnace system.
- Evacuate system until turbopump can be started.
- Start turbomolecular pump and continue evacuating at ambient temperature for a minimum of 8-16 hours.
- Turn on heater tapes (50% on Variac) on manifold, heat to 75°C ± 25°C.
- Heat up system at such a rate that the pressure is $\leq 1 \times 10^{-4}$ torr.
- Vacuum outgas at 1000°C ± 50°C for 1 ± 1/4 hour or 800°C ± 50°C for 4 + 1/2 hour.
- Furnace cool to ambient temperature, turn off heat tapes and quickly transfer, in air, to storage container.

5.0 Disposition

- Identify material with part number, intended use, processing MSI, operator initial and date, on QC OK Limited Acceptance Tag.
- Record and initial date of removal of pieces from storage container.
- Handle only with appropriate gloves and not with bare hands.

Originator	Engineer	Materials	Quality	

3M COMPANY ELECTRICAL PRODUCTS GROUP PIONEERING LABORATORY	MANUFACTURING STANDARD INSTRUCTIONS Issue Date Aug. 17, 1977 MSI 2001 Revised Oct. 28, 1977 Page 1 of 5

TITLE: Thermoelectric Module Outgassing and Heat-Up Procedure

APPLICABLE DOCUMENTS

Reference: Manufacture Flow Plan

1.0 Scope

This document describes the method required to process a completely assembled module to remove undesirable foreign materials such as water, oil, entrapped air, etc., without damaging the module in any way.

2.0 Materials

2.1 Freon® TF Solvent (Trichloro-Tri Fluoro Ethane)

2.2 Kaydry Disposable Towels (lint free) or equivalent

3.0 Apparatus

3.1 A turbo-molecular vacuum pump with a speed of at least 450 liters/sec.

3.2 Flexible heater tape with a rating of at least 100 watts/foot.

3.3 Ion vacuum gauge and controls.

4.0 Assembly

4.1 The processing fixture consists of stainless steel pipe with standard vacuum flanges. The flanges are welded to pipe and are connected with copper gaskets and 5/16" bolts.

4.2 Clean the inside of the processing fixture with Freon® and disposable towels. Caution should be exercised to ensure that the inside of flanges or pipes is not touched with bare hands. The oil and minerals from the skin will contaminate the flange surface.

4.3 Assemble processing fixture without converter. Leak check the assembly by external Helium spraying method, for any detectable leak when connected to the MS-12 mass spectrometer leak detection or partial pressure analyzer set to indicate a 1×10^{-9} maximum sensitivity.

Date and Initial ______________ ______________

Originator	Engineer	Materials	Quality	MFG
Robert L. Smith	Joseph Hoffman 11/15/77	Robert B. Evans 11/3/77	D.A.Wald 11-3-77	J. Bratman 11/3/77

3M COMPANY ELECTRICAL PRODUCTS GROUP PIONEERING LABORATORY	MANUFACTURING STANDARD INSTRUCTIONS Issue Date Aug. 17, 1977 MSI 2001 Revised Oct. 28, 1977 Page 2 of 5

TITLE:

APPLICABLE DOCUMENTS

5.0 Processing Method

5.1 Connect turbo-molecular pump to the roughing valve on the module manifold. The line to the module system should be cleaned with Freon.®

5.2 Connect cooling lines, apply water cooling.

5.3 Inspect for water leaks. _____

5.4 Turn water off and connect air cooling.

5.5 Evacuate the module at room temperature until the pressure reaches 5×10^{-6} torr.

Time _____ Active Torr Reading _____

5.6 PPA Data and Leak Check

a. Leak check the assembly, by spraying the exterior with Helium, and checking for any detectable leak when connected to the PPA set to indicate a 1×10^{-9} maximum sensitivity.

Initial and Date _____

b. Take a PPA scan between mass numbers 1 to 100 as Engineering data.

5.7 Apply heat tapes to the outside of the module fixture and the manifold. There should not be more than a 3 inch gap on all round surfaces. Attach a thermocouple to the outside of the processing container in a representative location with fiberglass tape, put a pad of insulation over the thermocouple with fiberglass tape.

5.8 Inspect for placement of heat tape and thermocouple. _____

Originator	Engineer	Materials	Quality	

FORM 15807-PWO

3M COMPANY

ELECTRICAL PRODUCTS GROUP
PIONEERING LABORATORY

MANUFACTURING STANDARD INSTRUCTIONS

Issue Date Aug. 17, 1977 MSI 2001

Revised Oct. 28, 1977 Page 3 of 5

TITLE:

APPLICABLE DOCUMENTS

5.9 Apply power to the heat tapes and the hot end heaters to heat the entire thermopile to 129°-139°C. The heating rate should be such that the pressure in the system does not rise above 5×10^{-5} torr. Alternate heating and air cooling may be necessary to avoid going over this pressure. The thermocouples to be monitored are: The hot and cold frame temperatures, one cold junction temperature and the processing container temperature.

Actual Readings:

Time	Temperatures			Processing	
	Hot Frame	Cold Frame	Cold Junction	Container	Torr
_____	_____	_____	_____	_____	_____
_____	_____	_____	_____	_____	_____
_____	_____	_____	_____	_____	_____
_____	_____	_____	_____	_____	_____
_____	_____	_____	_____	_____	_____
_____	_____	_____	_____	_____	_____

5.10 Continue to evacuate the thermopile and processing container 129°-139°C until at least a vacuum of 5×10^{-6} torr is reached.

Actual Reading _____ Inital and Date _____ Time _____

5.11 Take a PPA scan between mass numbers 1 to 100 to check for impurities.

Partial pressure upper limits of various impurities are:

Originator	Engineer	Materials	Quality	

FORM 15807-PWO

3M COMPANY

ELECTRICAL PRODUCTS GROUP
PIONEERING LABORATORY

MANUFACTURING STANDARD INSTRUCTIONS

Issue Date Aug. 17, 1977 MSI 2001

Revised Oct. 28, 1977 Page 4 of 5

TITLE:

APPLICABLE DOCUMENTS

AMU	Partial Pressure (Torr)
2	6.0×10^{-7}
12	5.0×10^{-8}
18	5.0×10^{-7}
28	6.0×10^{-7}
32	3.0×10^{-8}
41	9.0×10^{-7}
43	9.0×10^{-7}
44	8.0×10^{-7}

All other peaks should be below 4×10^{-7} torr.

5.12 Prepare system for heat up; maintain the hot frame temperature at 129°-139°C during this preparation stage.

a. Turn off heat tapes.

b. Air cool the cold frame to 40°-60°C.

Data

Hot Frame °C	Cold Frame °C	Cold Junction °C	Pressure Torr
_____	_____	_____	_____
_____	_____	_____	_____
_____	_____	_____	_____

Originator	Engineer	Materials	Quality	

FORM 15807-PWO

3M COMPANY ELECTRICAL PRODUCTS GROUP PIONEERING LABORATORY	MANUFACTURING STANDARD INSTRUCTIONS Issue Date Aug. 17, 1977 MSI 2001 Revised Oct. 28, 1977 Page 5 of 5

TITLE:

APPLICABLE DOCUMENTS

c. Turn water flow to minimum and switch to water cooling.

6.0 Heat Up

6.1 Heat up the module hot end by using the rate program on the computer to slowly bring the hot end temperature up without exceeding a pressure of 5×10^{-5} torr. The cold end temperature must be adjusted to its nominal value manually during the heat-up process.

(Note: Maximum rate of temperature change is 100°C/hour)

Computer "Rate Program" constants:

Maximum Hot Temperature _____ Channel No. _____ Initial Voltage _____

Ohms. _____ Sample Period-Sec. _____ Temp. Rate - Deg./min. _____

Start In Process	Date	Time	Temp. (°C)	Vacuum Torr	Remarks
At Temp.					

Originator	Engineer	Materials	Quality	

Figure 1-1

SKETCH OF AMPOULE USED FOR
MULTICOMPONENT COMPATIBILITY SERIES

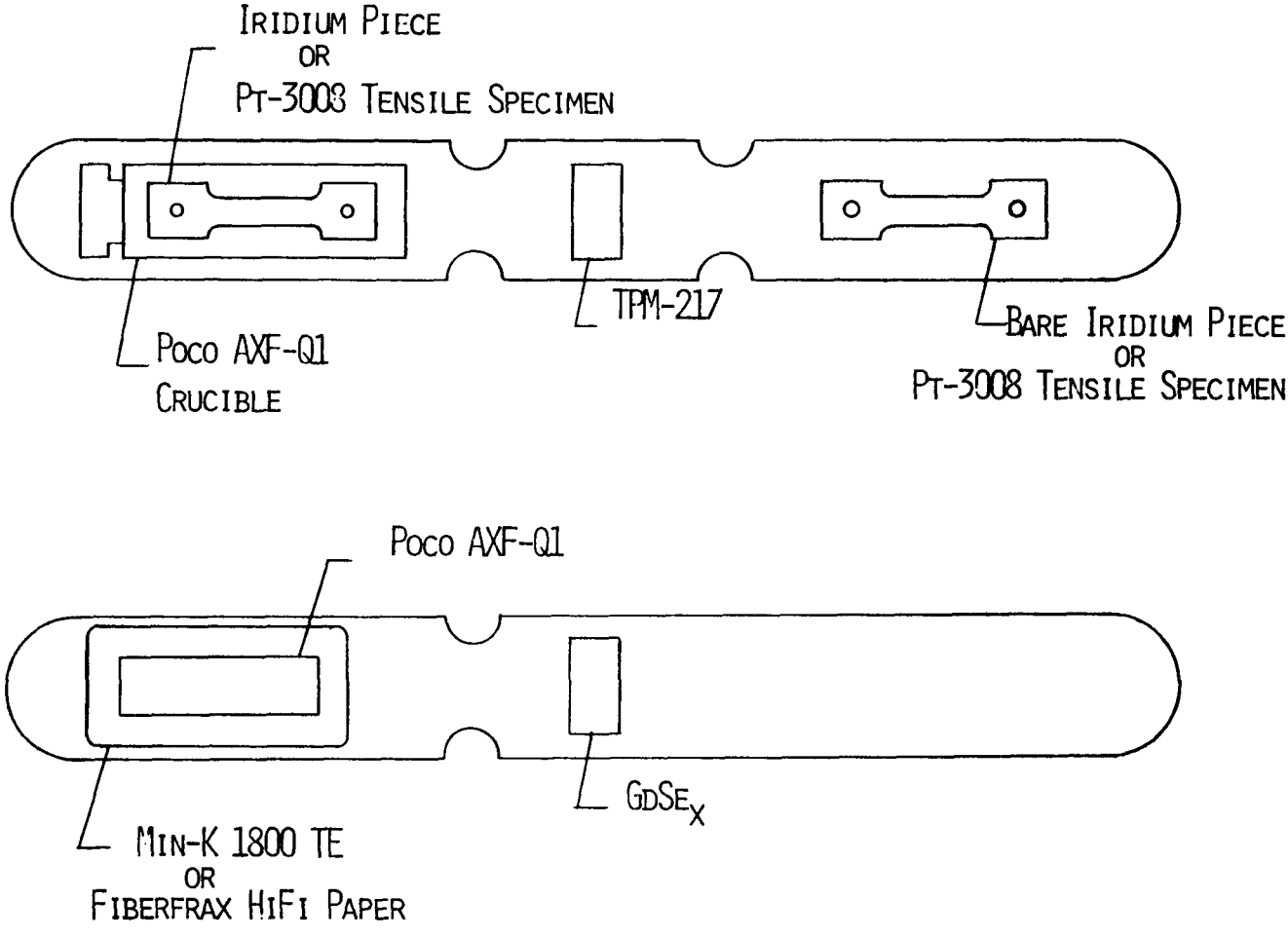

Figure 1-2

PERFORMANCE VERSUS OXYGEN UPTAKE

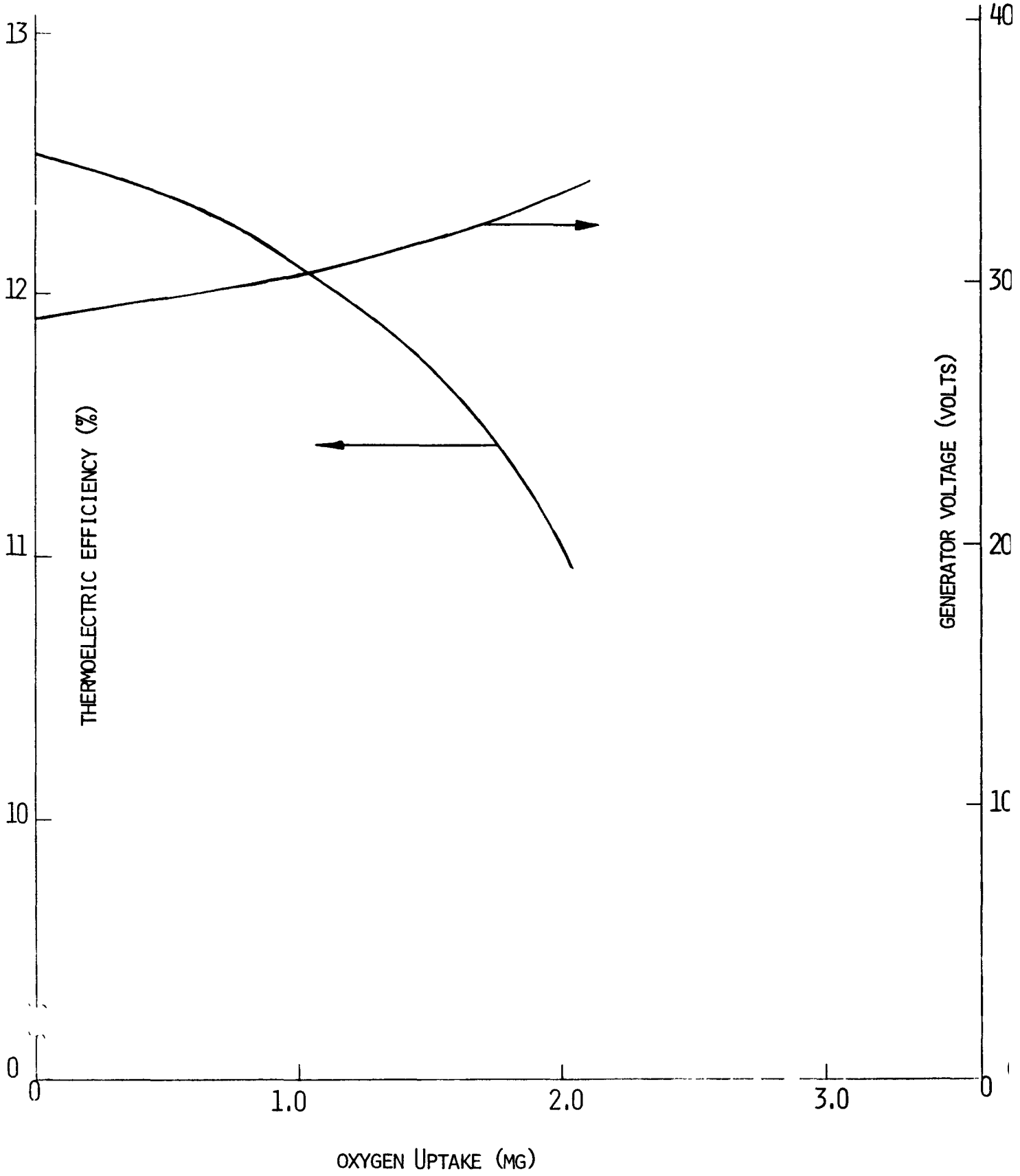

Figure 1-3 Min-K 1800 TE
% Carbon versus Time and Temp.

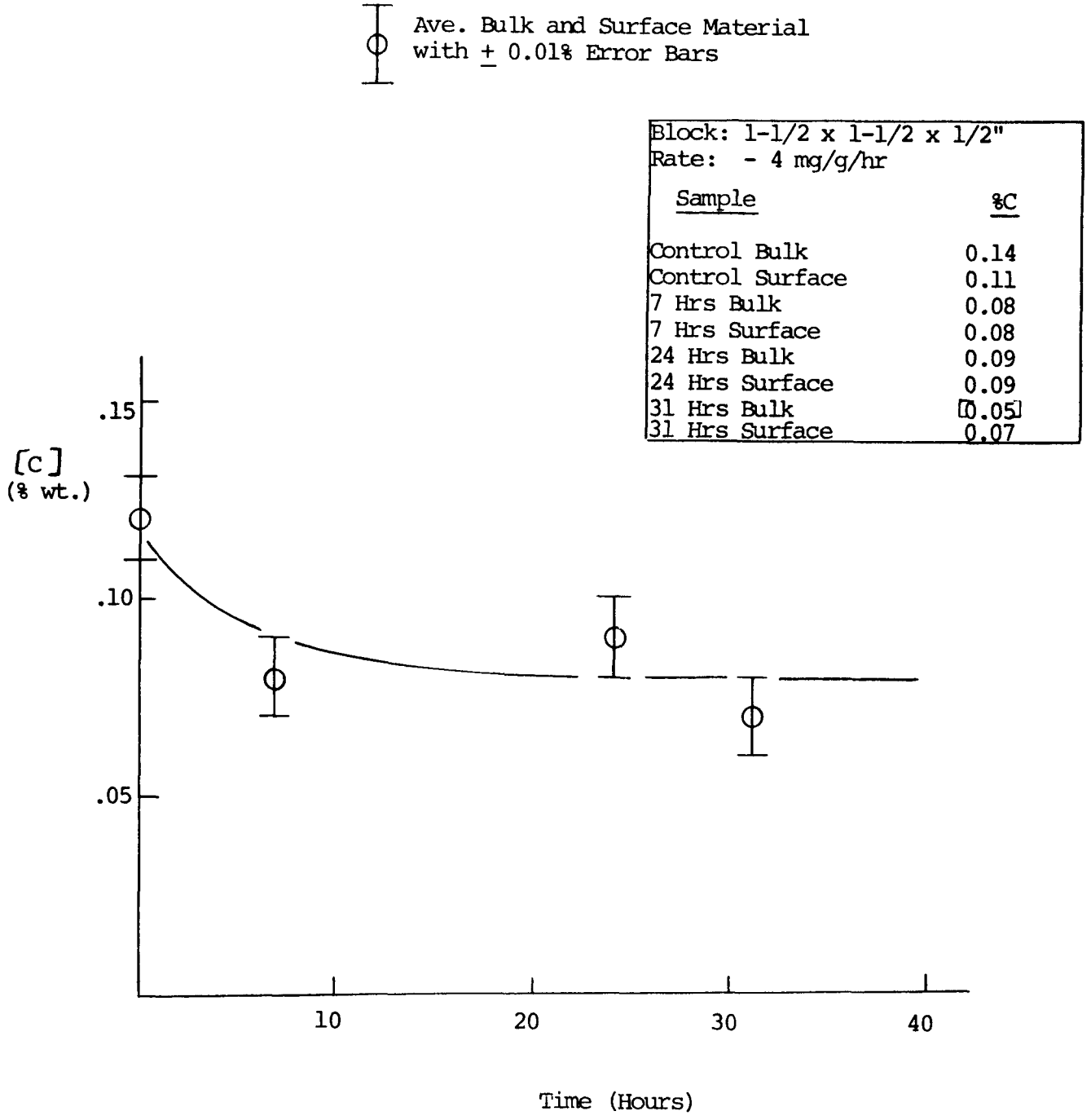

Figure 1-4 ADSORPTION: MIN-K 1800TE IN VARIOUS ATMOSPHERES

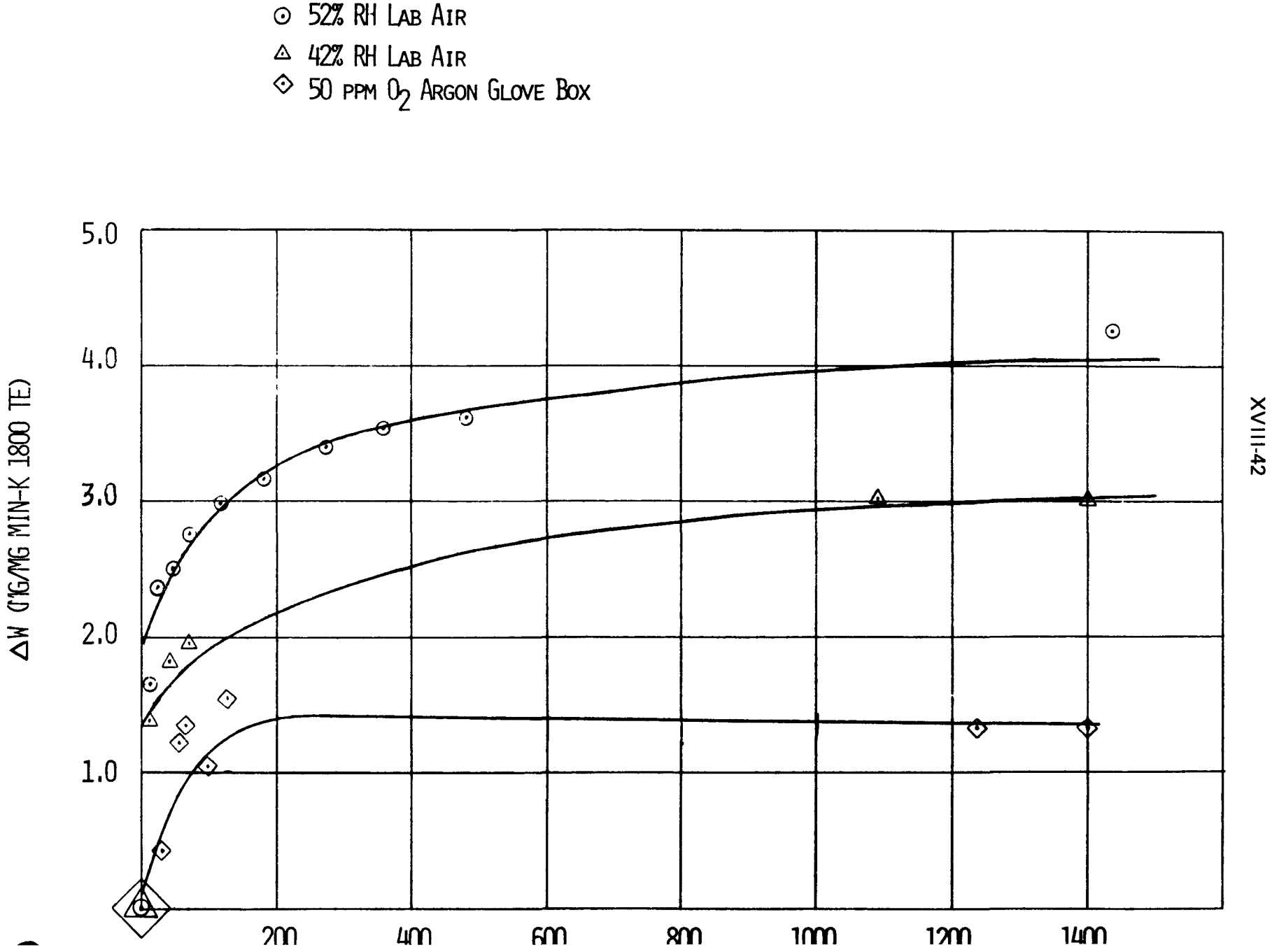

Figure 1-5 ADSORPTION: CONTAMINATION PICKUP AS A FUNCTION OF GEOMETRY (42% LAB AIR)

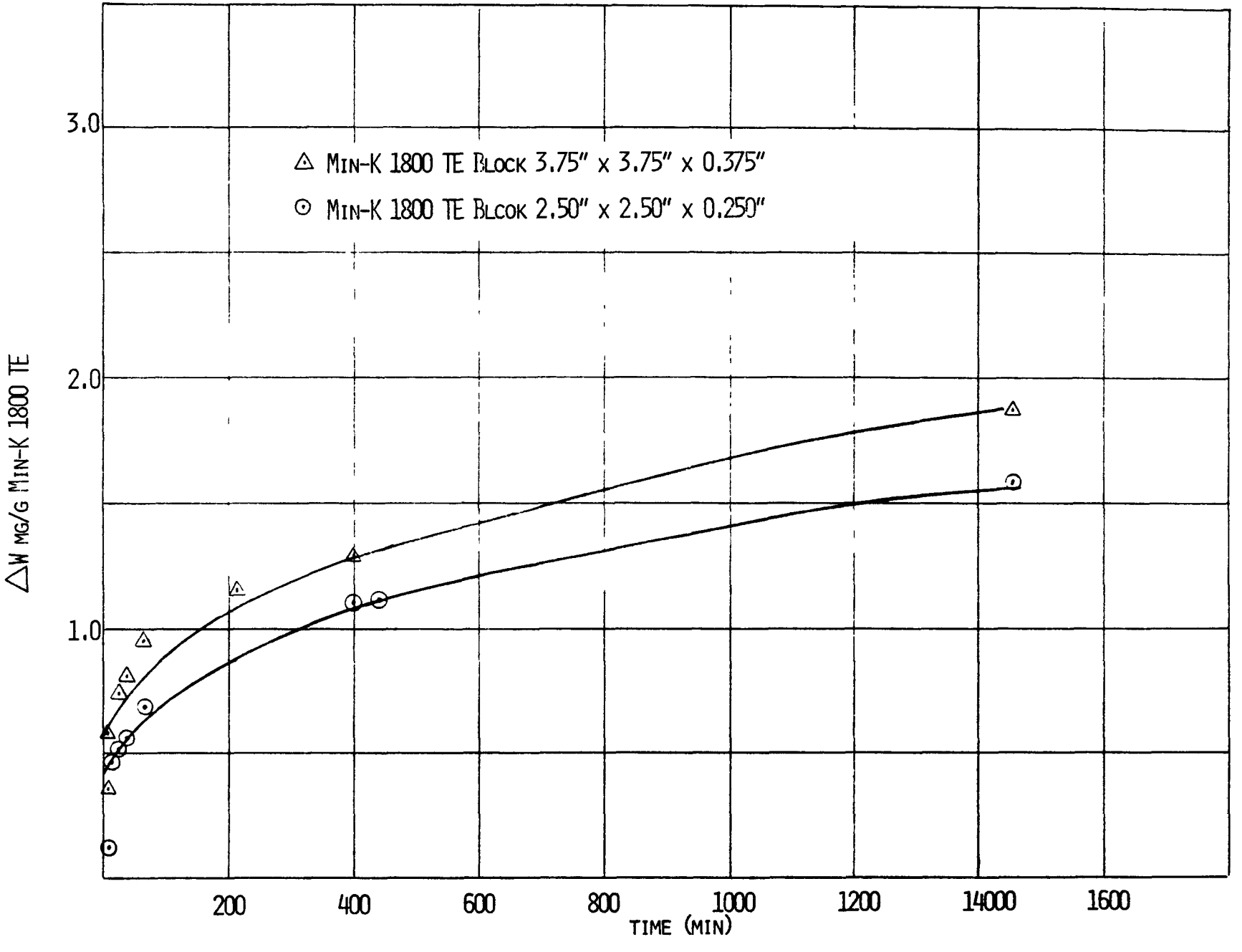

SECTION 2

ASSESSMENTS OF REQUIREMENTS FOR PRELIMINARY FLIGHT SYSTEMS

Cover Gas Requirements for Flight System Assembly

The requirements for flight system assembly are the same as assessed for GDS and described previously.[3]

Outgassing Procedure for the Sealed Converter Section

The recommended procedure for outgassing the sealed converter section is as described in 3M MSI 2001 "Thermoelectric Module Outgassing and Heat-Up Procedure," Section 1, Table 1-XI.

Assessment of IHF Removal on System Compatibility

Post-test analytical evaluation of the iridium/TPM-217 compatibility tests outlined in Section 1 Sealed Tube Chemical Compatibility are underway at ORNL. These tests were designed to determine effect of selenium on the mechanical stability of bare and Poco encapsulated iridium. At this time, an assessment of this effect can not be made.

ERDA IHS Gas Tap and LASL Thermodynamic Analysis of MHW data show that reactive gases should not be generated within the FSA and consequently not contaminant the converter section.[3-4]

---

[3] "Converter Materials Chemical Compatibility and Outgassing Requirements Assessed for GDS," Milestone No. 51 Report on Contract No. EY-76-C-02-2331, 3M No. 2331-0404 (2/28/78).

[4] "Thermodynamic Analysis of MHW Space Electric Power Generator," R. A. Kent, LASL Report LA-5202-MS on Contract W-7405-Eng. 36, March 1973.

[5] "IHS Gas Tap Data," ERDA Memo J.S. Griffo to J. J. Lombardo, July, 18, 1977.

ATTACHMENT XIX

Computation of the Maximum Stress in the Graphite Hot Ring

Objective:

To ensure an acceptable safety factor in the design of the hot ring.

Summary:

An estimate of the maximum stress in the graphite hot ring was determined by the following procedure:

1) Treat one-half of a ring
2) Neglect facets and pinholes (treat as a hemi-cylinder) and solve for reaction forces. These reactions correspond to the internal compressive stress in the system.
3) Using this stress as the applied stress, calculate the maximum stress using a concentration factor that is obtained from standard graphs available in the literature.

The result obtained indicates that Omax = 3279 psi. Since the compressive strength of graphite AFX-Q1 is 22,000, there is a safety margin of 6.7 inherent in the design.

1. Calculate engineering stress (neglect holes and facets). The applicable free body diagram appears in Fig. 1.

   Cross-sectional area = 3.00 in x .230" = .690 in^2

   $F_6 = 6\ (23.4) + 6(8.5) = 191.4$ lbs.

   $F_{RT} = F_{R1} + F_{R2}$

   $F_{RT} = F_6 \left[1 + \sum_{i=1}^{7} 2 \cos (\Theta_{i-1} + 12.86°)\right], \Theta_o = o°$

   $= 7.88\ F_6$

   = 1508 lbs

   From symetry, $F_{R1} = F_{R2} = \frac{1508}{2} = 754$ lbs.

   $\therefore \sigma_e = \frac{754 \text{ lbs}}{.690 in^2} = 1093$ psi

2. Account for pin-holes through assignment of a stress concentration factor. Various graphs appearing in "Stress Concentration Factors" by Peterson, Wiley Interscience, 1974 were used in arriving at a rough estimate of 3. See Fig. 2 for pin-hole layout.

   $\therefore$ Estimated maximum stress in Graphite hot ring = 3(1093) = 3279 psi

3. Compare w/ Compressive strength of AFX-Q1 Graphite (POCO)

   Temp = 22,000 psi

   $\therefore$ Estimated safety margin = $\frac{22000}{3289} = 6.71$

FIGURE 1

Free Body Diagram for Calculating
Engineering Stress in Ring

Use one-half of the ring and neyhert facets and pin-holes:

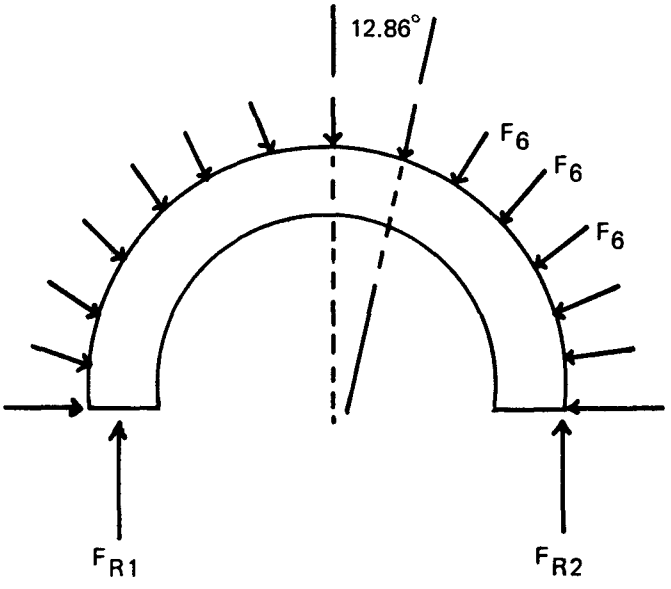

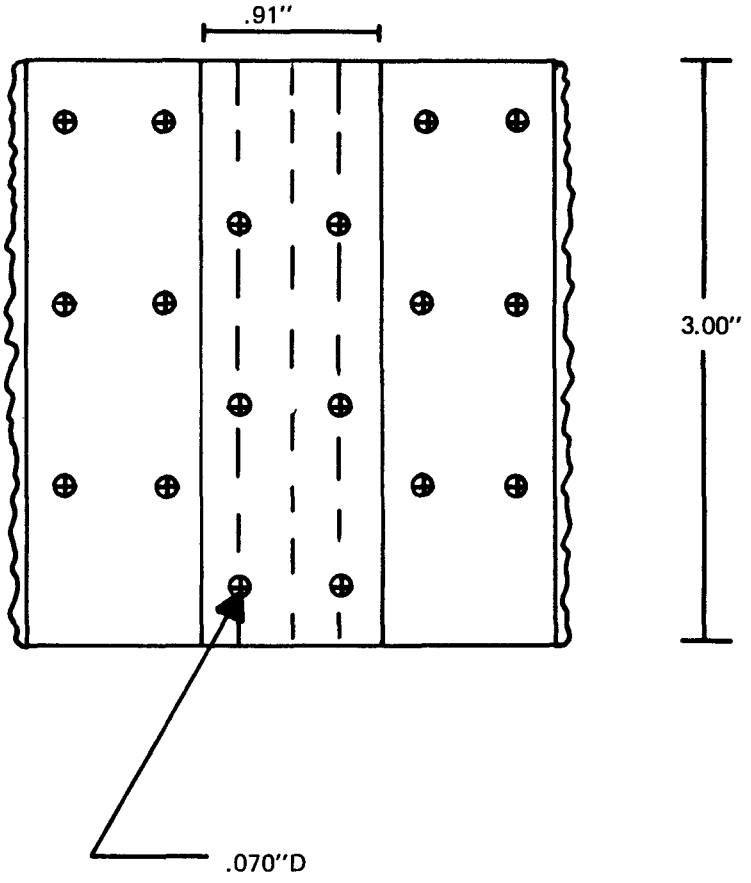

PIN HOLE LAYOUT
FIGURE 2

ATTACHMENT XX

Thermal Resistance for Flat Copper Follower Cold End Hardware

Introduction

The reference design for the thermoelectric convertor for the Selenide Isotope Generator (SIG) includes a compliant spring/follower system which permits couple mobility during thermal expansion, and has the potential for relatively low thermal resistance. In this report, the basic concept will be described and an analytical model will be presented which predicts the thermal resistance of the cold end hardware for slightly different configurations.

Test results on this hardware in couple configurations and multi-couple module configurations are also described herein for several values of a number of parameters including cover gas, interface material, load pressure, etc.

Analytical Model

The basic configuration of the hardware is shown in Figure 1. A thermal model of this hardware has been devised and is shown in Figure 2. The number of nodes is not large, but a side calculation on the effect of number of nodes on the results indicated that nine (9) nodes is a good number to use for reasonable accuracy (5%) and ease of calculation. The thermal resistance of each of the heat transfer paths are easily calculated. The metal conduction resistances are evaluated assuming thermal conductivities for copper and aluminum to be 201 and 109 BTU/hr-ft-°F, respectively. The contact conductance between the copper follower and the aluminum rail is assumed to be 350 BTU/hr-ft^2-°F and is based on experiments described in Appendix A. This value is also consistent with results reported in Ref. 1.

A number of cases were evaluated using the model and the results are summarized in Table I. The values of contact coefficient shown in the table are based on the results shown in Appendix A.

As such, they represent a potential which can be achieved if the flatness is as good as in the experiment described in Appendix A. The width and thickness for the GDS-1 reference design are 0.35 and 0.032 m., respectively. The effect of increasing the width is shown to be fairly significant. The maximum width (point of adjacent follower contact) would be 0.54 inches for the present SIG design. Thus, a width of 0.50 inches would probably be the maximum possible width, with 0.45 inches width being a much more likely width for systems after GDS-1.

The value of $Q = 3.8$ W(t) at which ΔT is calculated, is the heat flow across a follower/rail interface for the GDS-1 reference design assuming a 10% module efficiency (including only the part of bypass heat loss going through the followers).

The situation which is most representative of the GDS-1 design is the case assuming vacuum values. Even though a xenon cover gas is used, the effect on overall thermal contact conductance is small because of the relatively low thermal conductivity of xenon. Thus, the expected value of ΔT at the cold end of GDS-1 is approximately 40°C. Increasing the follower width to 0.5 inches would decrease the cold end ΔT to 25°C.

Experimental Methods and Results

A number of tests have been performed on single couples using standard cold end hardware for various conditions. These test data will be reported in this section. In addition, recent modules which have been tested have yielded information on the cold end thermal resistance.

Couple Tests

The configuration for the complete tests are shown in Figure 1. All thermocouple bead locations were covered with insulation to minimize radiation and convection errors. An attempt was made to insulate around the couple, although the bypass heat transfer was still significant. This was evidenced by the scatter in the data, expecially for cover gas testing. The results of this test program are shown in Table I. Measurements were made in three environments, namely, vacuum, xenon and argon. The effect of various interface materials applied to rail and/or follower on thermal contact resistance was also investigated. These materials are used primarily to reduce the friction in the sliding interface between the rail and follower.

The results are displayed in Table II in chronological order. In Table III, a summary of mean values for similar types of tests are shown to permit a better evaluation of trends. The following conclusions result from an evaluation of Tables II and III:

1. There is considerable variation between tests with supposedly identical conditions.
2. There is significant variation between follower No. 1 and No. 2 in the same test.
3. Although the mean values influence improvements in the expected direction for cover gas testing, the scatter in the data (and the scarcity of data) do not justify the use of anything other than vacuum data for GDS-1 predictions.
4. There appears to be a small degradation of thermal contact resistance as the result of using low friction interface materials.

Analytical Prediction of Thermal Contact Resistance

Follower Width (in.)	Follower Thickness (in.)	Cover Gas	Contact Pressure (psi)	Contact Conductance (BTU/hr-ft^2-°F)	R(°C/W)	ΔT(Q= 3.4W) (°C)
0.35	0.032	Vacuum	50	350	10.5	36
0.35	0.032	Argon	50	700	7.0	24
0.45	0.032	Vacuum	50	350	7.7	26
0.45	0.032	Argon	50	700	5.2	18
0.50	0.032	Vacuum	50	350	6.5	22
0.50	0.032	Argon	50	700	4.4	15
0.35	0.100	Vacuum	50	350	9.2	32
0.35	0.100	Argon	50	700	5.7	20
0.45	0.100	Vacuum	50	350	6.7	23
0.45	0.100	Argon	50	700	4.1	14

Summary of Lightweight Flat Follower Thermal Resistance Data for Couple Tests
(Contact Pressure = 45 psi Unless Otherwise Indicated, 2024 Electroless Nickel Plated Cold Frame, Chromium Copper Followers, Follower contact surface dimensions = 0.45 x 0.45 in. unless otherwise indicated)

			Follower No. 1				Follower No. 2			
Environment	Follower Interface Material	Rail Interface Material	$T_{Current\ Strap}$ (°C)	$T_{Cold\ Frame}$ (°C)	Q_{TE} (W)	R_T (°C/W)	$T_{Current\ Strap}$ (°C)	$T_{Cold\ Frame}$ (°C)	Q_{TE} (W)	R_T (°C/W)
Vacuum(4)	None	None	--	--	--	--	209	196	2.6	5.0
Vacuum	None	None	202	188	2.2	6.4	200	188	2.6	4.6
Vacuum	None	None	153	144	2.4	3.8	162	144	2.6	6.9
Xenon	None	None	153	130	2.5	9.2	151	130	2.8	7.5
Argon	None	None	151	128	2.5	9.2	147	128	2.7	7.0
Vacuum	None	None	149	139	2.4	4.2	154	139	2.7	5.6
Argon	None	None	153	130	2.5	9.2	149	130	2.7	7.0
Vacuum	MoS_2	MoS_2	124	109	1.6	9.4	119	109	1.8	5.6
Vacuum	MoS_2	MoS_2	150	133	2.4	7.1	144	133	2.5	4.4
Xenon	MoS_2	MoS_2	166	157	2.4	3.8	157	157	2.5	0.0
Argon	MoS_2	MoS_2	166	156	2.4	4.2	154	156	2.6	--
Vacuum	MoS_2	MoS_2	151	138	2.2	5.9	148	138	2.3	4.4
Xenon	MoS_2	MoS_2	149	112	2.5	14.8	143	112	2.7	11.5
Vacuum	MoS_2	MoS_2	151	97	2.0	26.9	148	97	2.4	21.5
Vacuum	MoS_2	MoS_2	213	184	2.8	10.3	215	184	2.8	11.0
Vacuum	None	None	162	111	3.1	17.0	152	111	3.1	13.2
Vacuum	None	None	173	151	3.0	7.3	186	151	3.0	11.8
Vacuum	MoS_2	None	163	113	3.0	16.5	156	113	3.1	14.6
Vacuum	MoS_2	None	169	146	3.0	7.6	181	146	3.0	11.8
Vacuum	MoS_2	None	150	116	3.1	11.0	174	116	3.0	19.5
Vacuum	MoS_2	None	148	116	3.1	10.4	166	116	3.0	19.6
Vacuum	MoS_2	None	189	157	2.9	10.9	187	157	2.9	10.2
Vacuum	MoS_2	None	184	172	2.9	4.1	207	172	2.8	12.4
Vacuum	MoS_2	None	146	134	3.1	3.8	175	134	3.0	8.4
Vacuum	$CbSe_2$	$CbSe_2$	153	128	3.1	8.1	148	128	3.1	6.5
Vacuum	$CbSe_2$	$CbSe_2$	180	138	3.0	14.1	183	138	3.0	15.2
Vacuum	$MoSe_2$	None	145	122	3.1	10.6	163	122	3.0	16.8
Vacuum	$MoSe_2$	None	146	121	3.1	11.3	162	121	3.0	16.9
Vacuum(1,5)	MoS_2	None	153	126	3.1	9.6	166	126	3.1	13.0
Vacuum(5)	None	None	150	120	3.1	9.7	148	120	3.1	9.0
Vacuum(3)	None	None	145	121	3.1	7.7	144	121	3.1	7.4
Vacuum(2,3)	None	None	146	125	3.1	6.7	147	125	3.1	7.0

(1) This test was left on for approximately 72 hours and no significant change in thermal resistance was observed.
(2) This test had an extension spring force of 13 lb. rather than the nominal value of 7 lb. used on the other tests.
(3) These tests had a thermocouple on back of follower rather than on cold current strap as for previous tests.
(4) Only one of the followers was instrumented.
(5) Followers were width (0.35 inch) of GDS-1. Special care was exercised to maintain flatness.

Trends in Thermal Resistance Couple Testing

Condition	Thermal Resistance (°C/W) Mean	Standard Deviation	No. of Points
Argon Cover Gas	6.1	± 3.5	6
Xenon Cover Gas	7.8	± 5.3	6
Vacuum	10.5	± 5.2	47
Vacuum, No Interface Material	8.0	± 4.0	13
Vacuum, MoS_2 Interface Material	11.2	± 5.8	26

5. There does not appear to be a significant difference between the thermal resistance for tests with MoS_2 on both rail and follower, or follower alone.

6. There is no significant difference between thermal resistance characteristics of MoS_2 or $MoSe_2$, but both appear to be better than $CbSe_2$ interfacial material.

7. Followers of the type that went into M-11 (better control on flatness, etc.) appear to have better thermal resistance characteristics than the previous followers. Thus, a stringent control of surface flatness will be instituted for subsequent follower assemblies.

8. There is a significant, but not overwhelming effect, of extension spring force on thermal resistance indicating that a fair amount of thermal resistance is contained in metallic conduction rather than interfacial conduction.

Module Thermal Resistance Data

During a recent module testing, data has been obtained on the thermal resistance of cold end hardware. Temperature measurements on the cold end current strap, and the rail (cold frame), have permitted an assessment of thermal resistance. The quantitative evaluation of thermal resistance is difficult, however, because the heat flow across the follower/rail interface is difficult to estimate. The heat throughput is estimated based on the measured power output /couple and the calculated efficiency (calculated using measurements of Seebeck coefficient and resistance). Thus, heat throughput for one element is thus given by:

$$Q = 0.5 \frac{Po}{couple} \frac{100}{\eta} - 1$$

Nine-Node Thermal Model of Cold End Hardware

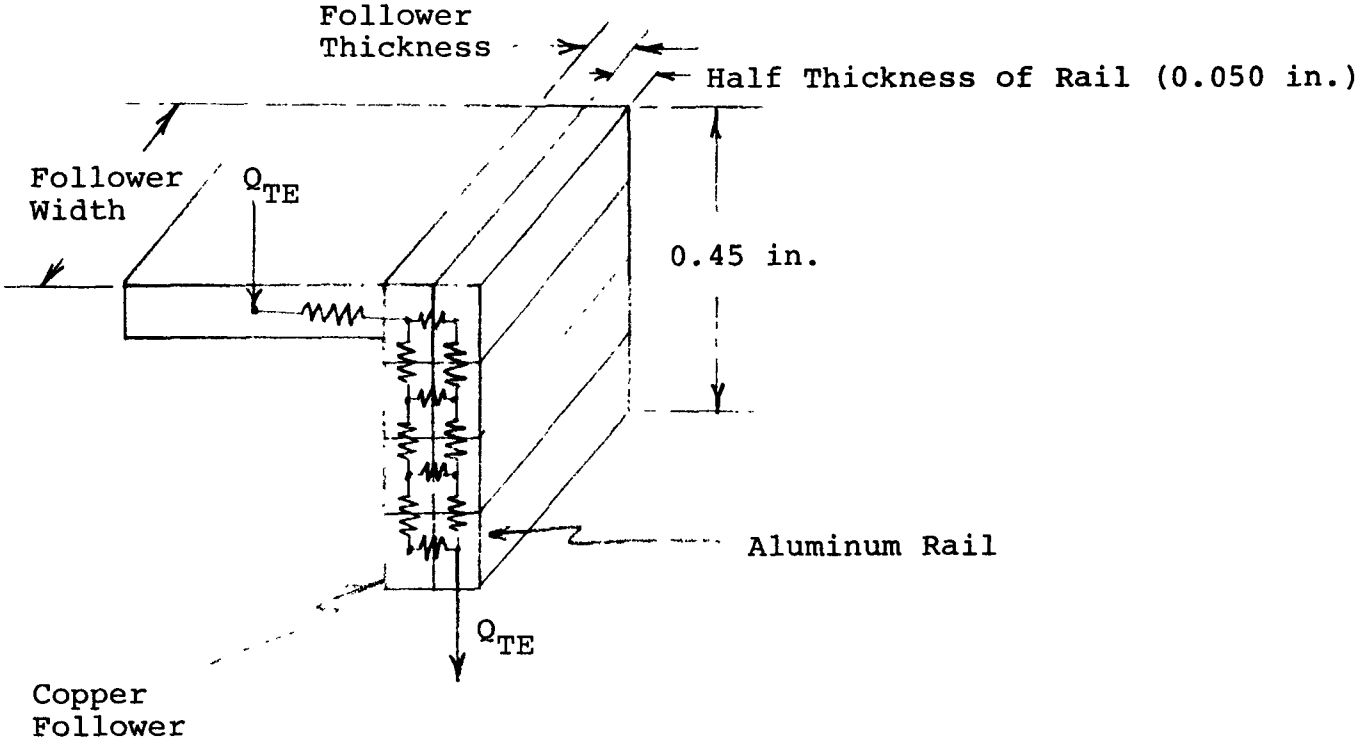

This method of estimating Q tends to underestimate the throughput since it neglects any bypass heat which flows across the interface. In that sense, the thermal resistance values determined in module testing are conservative.

A summary of module performance, including cold end thermal resistance data, is contained in Table IV. The thermal resistance for modules M-8 through M-11 appears to be higher than in M-6 and M-7. This is probably because the rail thermocouple is at the bottom of the rail in the later modules and near the top for M-6 and M-7.

In general, the thermal resistance measured in modules is higher than that measured in couples (20°C/W compared to 10°C/W). In addition to the aforementioned difficulty in estimating throughput, this difference is primarly due to the deviations from flatness caused during the assembly of modules in large arrays. It has been shown that flatness is an important parameter and assembly techniques are currently being developed and implemented which will permit better control of follower flatness.

Conclusions

This report summarizes the results to date of an ongoing investigation to measure and improve the thermal resistance of thermoelectric cold end hardware. An analytical model predicts values of thermal resistance (10°C/W) which are consistent with results measured in couple tests. Thermal resistance values measured in modules are higher (20°C/W), primarily because of follower waviness caused during assembly. These waviness effects will be mitigated by a modification of assembly methods.

References

(1) A.M. Clausing and B.T. Chao, "Thermal Contact Resistance in a Vacuum Environment," J. Heat Transfer, May 1965, pp. 243-251.

Module Cold End Thermal Resistance Data

	Time (Hrs)	No. of Couples	P-Leg Dia. (in)	Follower Thickness (in)	Follower Width (in)	Interfacial Material	Cover Gas	$T_{Hot\ Strap}$ (°C)	$T_{Cold\ Strap}$ (°C)	$T_{Cold\ Frame}$ (°C)	ΔT_{Leg} (°C)	ΔT_{CS-CF} (°C)	Q*	R_C (°C/W) $= \frac{T_C - T_{CF}}{Q}$
M-6	510	10	0.292	0.100	0.45	None	Vac	811	198	152	613	46	3.0	15.3
	4060							788	198	157	590	41	2.8	14.8
M-7	525	10	0.292	0.032	0.45	None	Xe	854	125	75	729	50	3.7	13.5
	9160							863	128	82	735	47	3.7	12.7
M-8	520	36	0.292	.032	0.45	None	Xe	861	141	69**	720	72	3.4	21.2
	4523							837	159	84**	678	77	3.1	24.8
M-9	450	2	0.292	.032	0.45	MoS_2	Xe	848	152	77**	696	75	3.2	23.3
	3745							858	147	74**	711	73	3.5	21.0
M-10A	540	18	0.292	.032	0.45	MoS_2	Xe	867	156	75**	711	81	3.3	24.5
	2510							856	160	79**	696	82	3.3	24.9
M-11	450	54	0.260	.032	0.35	MoS_2	Xe	859	150	95**	709	55	2.9	18.9
	710							847	153	97**	694	59	2.8	21.0

* $Q = 0.5 \left(\frac{P_O}{Couple} \right) \left(\frac{100}{\eta} - 1 \right)$

** At bottom of rail

APPENDIX A

MEASUREMENT OF CONTACT RESISTANCE BETWEEN COPPER AND ALUMINUM

A series of experiments were undertaken to determine the thermal contact resistance across an aluminum copper interface. Measurements were obtained at different load pressures in a cover gas (Ar) and a vacuum environment. The test fixture is shown schematically in Figure A-1. Both the followers and the cold frames were quite massive to minimize internal gradients. The entire experiment was well insulated to minimize bypass heat losses. The heat transfer through the interface was obtained from the temperature measurements on the heat flux meter. The results of the test are shown in Figure A-2. The contact conductance is plotted as a function of contact pressure. The value of h = 350 BTU/hr-ft^2-°F is obtained for vacuum at 50 psi contact pressure.

Figure A-1. Square Follower Configuration

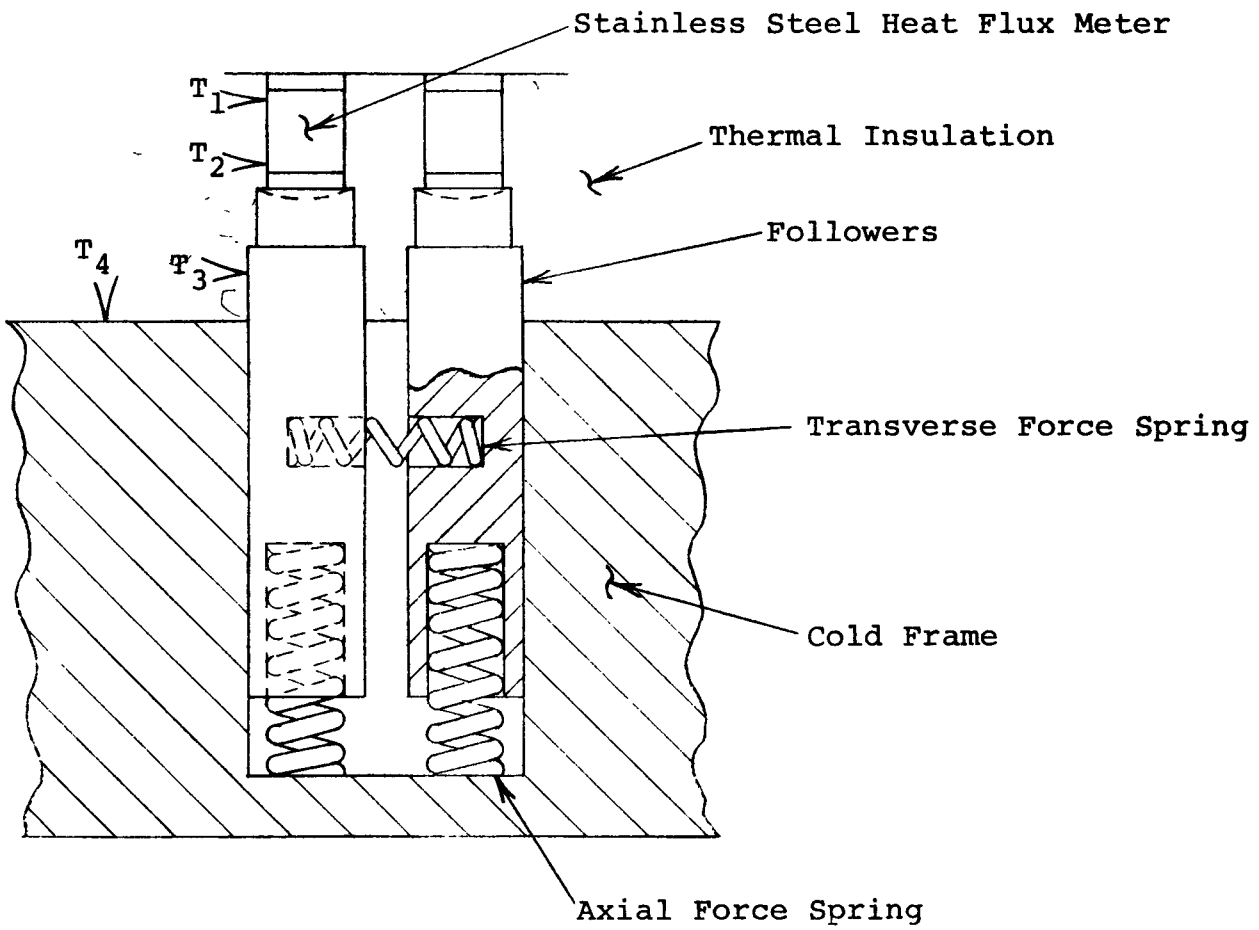

Figure A-2. Effect of Contact Pressure on Thermal Conductance

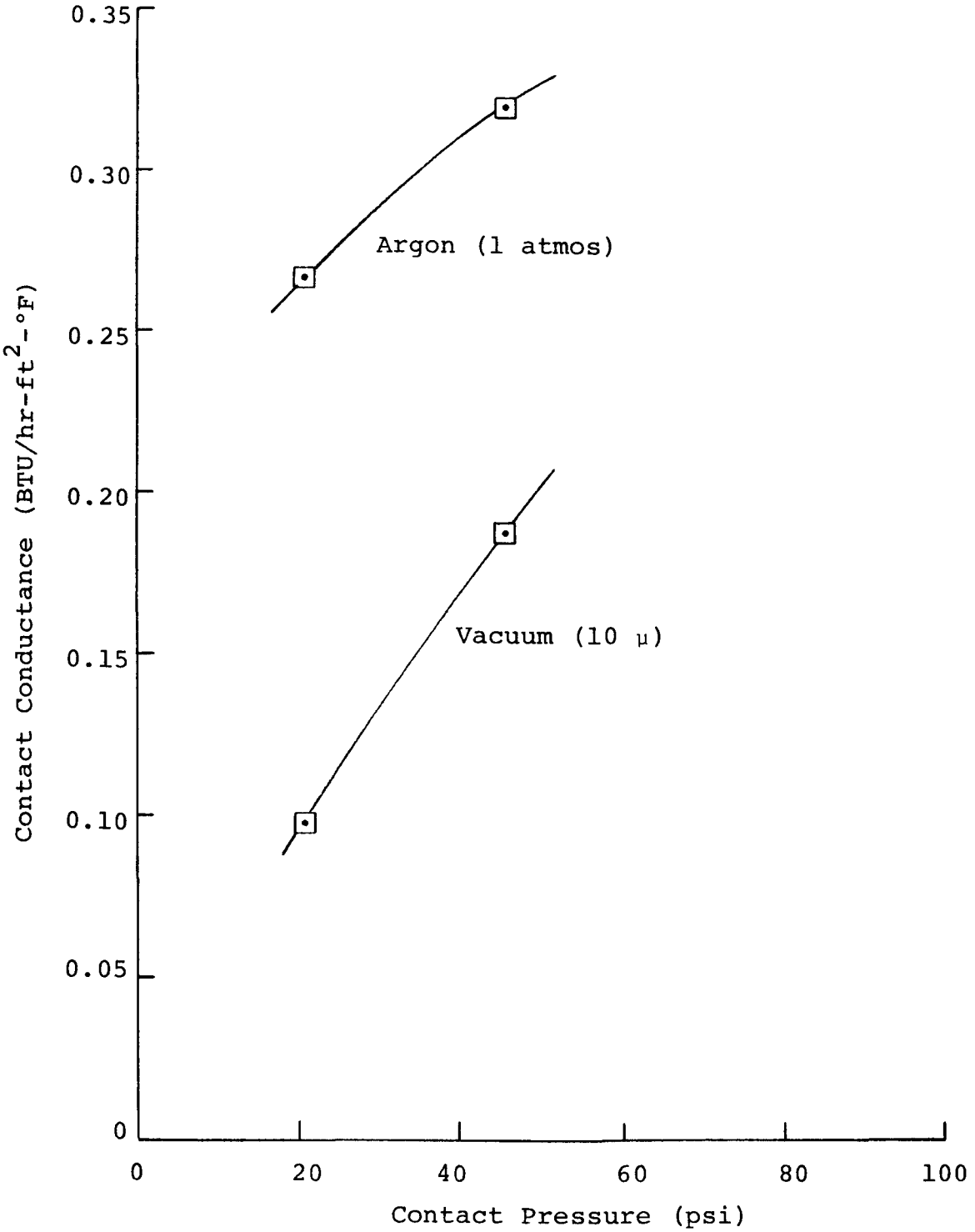

[redacted]